TOTAL BODY NITROGEN BY PROMPT NEUTRON ACTIVATION ANALYSIS USING CALIFORNIUM-252

Alison Mackie

Thesis submitted for the degree of Ph.D.
University of Edinburgh
1988

DECLARATION

This thesis is my composition, excepting such assistance as is herein acknowledged. All verbatim extracts are in *italic* and distinguished by quotation marks and the sources of information specifically acknowledged. The report has not been submitted for any previous degree application. The work, of which this report is a record, was carried out by me over a four year period from August 1983. The technical details for the construction and the building of the clinical apparatus was the work of Messrs. L. Mackie, H.J. Easton and J.M. Watt of the Mechanical Workshop. Mr. G. Kelly constructed the pneumatic delivery system, Mr. W. Duvall contributed to the electronic control systems and Mr. C. Ferrington developed all data analysis software.

Alison Mackie

INDEX

ABSTRACT

Many diseases are accompanied by wasting with a consequent loss of protein. The establishment of nutritional status in such patient groups would enable the efficacy of management regimens to be evaluated. The nutritional model adopted will be a compromise between its useful complexity and the practicality of measuring each compartment. The advantages of the four compartment model (protein, water, minerals and fat) adopted for this thesis, over simpler two compartment (fat and fat free mass) models are discussed.

Protein is related to nitrogen by the universally accepted multiplicative factor of 6.25. Prompt neutron activation analysis (NAA) $\{^{14}N(n,\gamma)^{15*}N\}$ has been shown to be superior to delayed NAA $\{^{14}N(n,2n)^{13}N\}$ for the measurement of protein. These advantages are in respect of : specificity of reaction product; number of interfering reactions; uniformity of combined activation/detection sensitivity; radiation dose for a given precision and cost of apparatus. Furthermore, only the prompt technique is feasible for studies involving the critically ill. Additionally, radio-isotopic neutron sources can be used and the advantages of Californium-252 (^{252}Cf) over alternative sources are discussed. The disadvantage of the prompt technique is the high count rate at the detectors, caused by the simultaneous irradiation and detection of the subject.

A consequence of the high count rate during the protein measurement is pulse pile-up, which leads to spectrum distortion and has been identified as the principal contributor to the nitrogen background.

Consideration has been given to the characteristics of the pulse processing system to minimise this pile-up. The combination of source and detector shielding materials has been determined empirically by minimising the nitrogen background. Comparison has been made of alternative unilateral and bilateral irradiation/detection geometries for prompt NAA and the latter chosen for construction of clinical apparatus. The apparatus enables the in-vivo measurement of total body protein by prompt NAA using ^{252}Cf with a precision of ±3%, from a 40 minute scan for a whole body dose equivalent of 0.18mSv.

Techniques for predicting the nitrogen background from a subject spectrum are presented. Calibration of the apparatus to convert a nitrogen:hydrogen counts ratio to a mass ratio and the continued requirement for recalibration as the ^{252}Cf decays is discussed. The prompt technique requires total body nitrogen to be calculated from the nitrogen:hydrogen mass ratio by the independent estimate of total body hydrogen. A circularity in the relationships used enables this estimate to be made by measuring total body water by an isotope dilution technique. Finally, data from a study on normal subjects is presented and prediction equations generated for total body nitrogen based on anthropometrics. The results are compared with findings from other centres.

INTRODUCTION

INTRODUCTION

Neutron activation analysis is a technique which enables measurement of elemental composition non-invasively. The technique has been used to measure many elements besides nitrogen including calcium, phosphorus and cadmium.

The feasibility of using the delayed method of analysis for nitrogen (protein) measurement {$^{14}N(n,2n)^{13}N$} was first demonstrated by Palmer et al (80) in 1968. The first patient measurements were reported in 1971 by another group (Cohn et al, 24). Since then the technique has been applied at many other centres. However, major limitations of the delayed technique were being increasingly recognised. The reaction has a high threshold energy, necessitating a fast neutron generator or cyclotron, with a correspondingly high radiation dose to the subject. Attenuation of the neutron beam in tissue results in poor penetration with depth and generates a poor activation uniformity through the body; resulting in the phenomenon of "surface nitrogen measurement". Additionally, the measurement suffers many interferences to the nitrogen peak from reactions with other body elements, particularly oxygen.

An alternative prompt technique {$^{14}N(n, \gamma)^{15*}N$} was first used to measure total body nitrogen in 1972 (Biggin, 10). The prompt technique has many advantages over the delayed technique. Since a thermal neutron reaction is involved radioisotopic neutron sources can be used, so reducing the patient dose. The thermalisation of fast neutrons within the body provides a source of reaction neutrons

deep within tissue. The activation uniformity with depth is therefore better than that of the delayed technique. The 10.8 MeV gamma ray produced in the reaction is specific to nitrogen and so the reaction has few interferences. The major disadvantage of the technique is the high count rate at the detectors imposed by the requirement for simultaneous irradiation and detection.

^{241}Am-Be and ^{238}Pu-Be radioisotopic neutron sources, both having a mean neutron energy of around 5 MeV, have been used for the prompt measurement of nitrogen. However, Morgan et al (76) have suggested that Californium-252 (^{252}Cf), with a mean neutron energy of 2.3 MeV, may have advantages over alternative radioisotopic neutron sources. The advantages arise because of the lower mean energy of the neutron output of ^{252}Cf, which ensures a greater thermal neutron flux per unit dose to the patient as well as reducing shielding requirements for the detectors. Additionally, ^{252}Cf neutron sources have a smaller physical size per neutron output compared with alternative radioisotopic sources , which enables more effective collimation and eases the pneumatics of the delivery system. The major disadvantage of ^{252}Cf is its 2.65 y half-life, which would require a decreasing source-to-skin distance with time if the same precision of measurement were to be maintained for a fixed irradiation period.

The absolute determination of nitrogen mass from nitrogen counts would require corrections for the effect of body habitus on the composite sensitivity (combined activation and detection) uniformity. However, Vartsky et al (96) showed that the nitrogen:hydrogen counts ratio was much less dependent on body habitus than the nitrogen

counts alone. This is because both the nitrogen and hydrogen signal depend on thermal neutron reactions, and the cross-sections for the capture reactions vary in the same manner with neutron energy for the two elements. Body hydrogen was therefore recommended as an internal standard for converting the detected gamma ray counts to an absolute mass of nitrogen.

The work undertaken in this thesis was to design and build apparatus for the measurement of whole body nitrogen by prompt neutron activation analysis, using Californium-252 neutron sources. The neutron sources were previously purchased for work involving the measurement of part body calcium by a delayed technique. The requirement for simultaneous irradiation and detection introduces the need to optimise the spectroscopy system to handle the high count rates anticipated and to minimise the extent of pulse pile-up. Alternative irradiation/detection geometries were to be investigated to enable a decision concerning the design of the clinical apparatus. In addition it was intended to compare the advantages of the prompt technique over the delayed technique, involving use of the Medical Research Council cyclotron. Time permitting it was hoped to be able to complete a study on normal subjects to enable evaluation of the measurement procedure.

CHAPTER 1

CHAPTER 1

REVIEW OF COMPARTMENTAL ANALYSIS OF BODY COMPOSITION

1.1 Compartmental Analysis

The human body is a very complex mixture of many components. The model of body composition which one adopts is therefore a compromise between the useful complexity and the practicality of the methods which must be adopted in order to measure each of those compartments.

1.1.1 Nutritional Model

For nutritional purposes the body can be considered to consist of four compartments, namely:-

i) **WATER**	**FAT**	BODY CELLS	
ii) **PROTEIN**	**FREE**	EXTRACELLULAR FLUID	
iii) **MINERALS**	**MASS**	EXTRACELLULAR SOLIDS (skeleton, collagen, etc.)	
iv) **FAT**			

where the fat free mass is the sum of all of the compartments with the exclusion of fat. Protein and fat are separately identified because of the different nutritional values of each. There exists a second energy store in the body, other than fat, that of glycogen (body carbohydrate). Strictly speaking this separation would be advantageous in energy balance studies since the two have different calorific values. However, glycogen represents less than 1% of the fat free mass in normals and in wasting illness prior to parenteral nutrition could be negligible. Its exclusion from the nutrition model would therefore make little difference, whilst its inclusion

would make the model unnecessarily complicated. Additionally, there is no available direct in-vivo measurement for glycogen.

Since wasting illness involves the depletion of the patient's energy stores whilst undergoing gross body composition distortion, monitoring of the patient's body composition by this four compartment model would assist in patient management. Use of the model requires the independent measurement of at least three of the compartments. Total body water can be easily measured by an isotope dilution technique. However, until the application of in-vivo neutron activation analysis (NAA) by Palmer et al (80) in 1968 protein could not be measured absolutely. Protein is related to total body nitrogen by the universally accepted multiplicative factor of 6.25. A measure of nitrogen by NAA is therefore a measure of protein. The importance of the protein compartment in patients has been recognised for a long time, although it was not possible to measure it absolutely. It was only possible to determine whether or not a patient was in positive or negative balance by laborious calculation of intake and losses. These balance studies required the constant supervision of a patient for a number of days in a Metabolic Ward and the technique is subject to large errors (Beisel, 9). Unfortunately, a knowledge of a patient's protein balance would not help in the compartmental model since the absolute mass of protein is required. Reference Man (55) contains 2790 g of bone ash and 630 g of extra-skeletal minerals; 245 g of extra-skeletal phosphorus, 140 g potassium, 100 g sodium, 95 g chlorine and 50 g of other elements. The element sulphur is not included in the mineral compartment since it is largely included in the protein compartment. The major

fraction of the mineral compartment is the bone mineral ash. This could be measured directly by delayed neutron activation analysis of calcium, which bears a fixed relationship to bone mineral ash (Bigler et al, 11). Alternatively, the bone mineral ash could be estimated from prediction equations (Nelp et al (77), Cohn et al (25)) based on parameters not expected to change in wasting disease. Beddoe et al (5) have demonstrated that the total mineral compartment represents 6.22% by weight of the fat free mass in normal individuals so enabling an estimate of the mineral compartment if the fat free mass can be estimated. In the critically ill prediction equations,relating the mineral compartment to body size parameters, generated from data on normals have been used (5). However, the model for nutrition can only be used if three of the four compartments can be measured or estimated with acceptable accuracy; the fourth compartment then being determined as the difference of the sum of the three measured compartments from body mass. There still exists no direct method of measuring total body fat, though efforts are being made at Leeds (Kyere et al, 62) to relate a carbon measurement from fast neutron inelastic scatter gamma rays to an estimate of fat. Indirect estimates of fat relying on relationships with skinfold thickness at different sites have been suggested (Durnin et al, 40), though these methods have frequently been shown to be grossly inaccurate in patients suffering wasting illness (Streat et al, 89).

In essence, before the establishment of in-vivo neutron activation analysis techniques it was not possible to use this four compartment model for nutritional studies. In consequence, a simpler two

compartment model of body composition was used; fat free mass and fat. Several methods, each making different a priori assumptions, have been advanced for the measurement of this inhomogenous compartment the fat free mass.

To add further complication to this compartmental analysis it is important to consider the fat free mass, not only as the sum of water, protein and minerals, but alternatively as the sum of the body cells, extracellular fluid and extracellular solids. This concept of the fat free mass has been shown on the right hand side of the nutritional model.

There now follows a brief synopsis of the methods advanced for the delineation of body composition into its fat free and fat compartments.

a) Fat Free Mass from Densitometry

Total body fat can be calculated by underwater weighing to determine body density. The density is calculated using Archimedes' principle with a correction being made for lung volume. The estimation of fat from density alone is founded upon broad generalisations. It requires the assumption that all adults are identical in composition except for individual differences in their proportions of fat; that is that there are fixed relationships between water, protein and minerals in the lean body. The studies of Fidanza, Keys and Anderson cited by Keys and Brozek (60) indicate a remarkable uniformity in the density of human fat irrespective of the site from which it is taken.

While the density of human fat seems well established, the reliability of the numerical values of the densities of protein and mineral (also from biopsy studies) cannot be argued with great confidence (48,18). Proteins are known to differ in density and the value used of 1.340 g cm^{-3} is an average for fully hydrated protein in vitro. Whether or not it is the correct average for human protein in vivo has not been demonstrated. The same reservation applies to the density of mineral of 3.0 g cm^{-3}. However, the densities of lean and fat tissue are assumed to have known fixed values (density of fat, d_f = 0.90 g cm^{-3} and density of fat free tissue, d_l = 1.1 g cm^{-3}) (84). The mass of fat can then be calculated from the relationship:-

$$\frac{M}{D} = \frac{m_l}{d_l} + \frac{m_f}{d_f}$$

where M, m_l and m_f are the total body, lean tissue and fat tissue masses respectively. D, d_l and d_f are the corresponding density values.

Manipulation of this equation and substitution of $(M - m_f)$ for m_l yields the relationship:-

$$\frac{m_f}{M} = \frac{d_l d_f}{D(d_l - d_f)} - \frac{d_f}{(d_l - d_f)}$$

Substitution of the assumed densities of lean and fat tissue results in the equation:-

$$m_f = M \times \left[\frac{4.95}{D} - 4.50\right] \quad \text{- (Siri,84)}$$

The fat free mass can then be calculated as $(M - m_f)$.

Since the technique involves underwater weighing of the subject it is

not a practical option for measurements of the critically ill. Additionally, the technique assumes that the fat free mass has a constant density. It is well known that after major trauma and sepsis patients undergo radical changes in body composition involving losses of protein and fat and very rapid accumulation of water. It is widely believed that increases in total body water are predominantly associated with the extracellular fluid, although the extent of the initial intracellular water gain is not known. These changes alter the ratios of the protein, water and mineral compartments and have a consequent effect on the density of the fat free mass; this density in patients suffering gross distortion of their body composition will not be the same as that derived for normals and used in the equation of Siri (84) for predicting total body fat. In consequence, the relationship is good when used to apportion body mass to the lean and fat compartments for populations similar to those from which it was derived (normals), but should be used with caution in other population groups. Additionally it has been shown that even if experimental error in measuring the body density is very small there will still be an uncertainty in the estimate of total body fat of $\pm$ 3.8% body weight (84). For a 70 kg man containing 13.5 kg of fat this would mean an error in the fat measurement of approximately $\pm$ 20%. This error is primarily because of normal variability in body constituents, but also because of the uncertainty in attempting to establish the compositions of adipose tissue and reference man lean tissue that are true averages for the category of subjects measured.

b) Fat Free Mass from Skinfold Anthropometry

Durnin and Womersley (40) generated regression equations from data on 481 normal subjects (209 males and 272 females) aged 16 to 72 years, to relate skinfold thickness at four sites (biceps, triceps subscapular and supra-iliac skinfold) to body density. Equations were generated of the regression of the logarithm of the sum of the four skinfolds on body density, as determined from underwater weighing. Separate equations for sex and five different age groups (17-19, 20-29, 30-39, 40-49, 50+) were presented. The sex difference was considered to reflect the greater proportion of body fat content situated internally in women. This is also one reason postulated for the change in the regression equation with age; the proportion of internal fat deposits increasing with age. A second reason is that skinfold compressibility may become greater in older people. The available evidence, however, suggests that the converse is true (references cited by Durnin, 40). Once obtained the body density can be substituted into the densitometry equation to predict fat and consequently fat free mass. Unfortunately, there was a large biological component of the residual error in the original regression of density against sum of skinfold thickness. This requires studies on small groups of patients to be considered with extreme caution, if done at all, taking proper consideration of the effect of biological components on the precision of the results. Furthermore, the distribution of subcutaneous and internal fat deposits may change in wasting disease, and the accurate measurement of skinfolds may be impaired by oedema.

c) Fat Free Mass from Total Body Water

Fat free mass can be estimated from total body water (TBW) assuming a constant hydration coefficient of the fat free mass of 0.732. The relationship is:-

$$FFM(kg) = \frac{TBW(l)}{0.732} \qquad \text{(Pace et al,79)}$$

This relationship was assumed given the constancy of the total body water: fat free mass ratio in six mammalian species, where the ratios were calculated from chemical analysis of the whole animals. 0.732 was the mean hydration coefficient of 10 independent investigations, the range being 0.699 in the dog to 0.763 in the rabbit.

The total body water of an individual can be measured by an isotope dilution technique by the administration of a known activity of tracer. After a suitable period to allow the isotope to equilibrate with the water compartment a plasma sample is taken. A urine collection is made up to this time which enables the total body water to be calculated from a knowledge of the plasma activity and the activity lost through the urine.

Problems with this model arise through the biological variation in normal healthy adult individuals along with the uncertainty in reference body composition and the error associated with the total body water measurement. The standard deviation of the estimate of body fat has been calculated by Siri (84) to be $\pm$ 3.5% body weight. The normal range of hydration coefficients in freshly isolated tissues varies from 0.704 to 0.779 (Allen et al, 1). However, in

disease the range of hydration coefficients is even greater; being as low as 0.67 in dehydrated patients and as high as 0.85 in overhydrated, oedematous patients (Moore et al, 74). Such overhydration is common in wasting illness and would lead to an overestimation of the fat free mass. Any deviation from this 0.73 hydration coefficient would lead to errors in the calculated fat free mass and hence fat. In short, the validity of the total body water method for estimating fat free mass rests upon the same assumptions as are inherent in the densitometric method; briefly, that gross body composition is constant for all humans with the same proportion of adipose tissue and that the reference body is a true average whose composition is known.

d) Fat Free Mass from Total Body Water and Body Density

A reduction in the standard deviation, due to biological variation, of a total body fat estimate to $\pm$ 2% body weight has been shown to be possible using independent measurements of body water and density (84). This is because the method requires the fewest assumptions concerning interrelations between constituents. The formulation of the method is derived directly from two fundamental equations, namely:-

$$1 = f + w + p + m$$

where f, w, p, and m are the fractional weights of fat, water, protein and mineral respectively.

and

$$\frac{1}{D} = \frac{f}{d_f} + \frac{w}{d_w} + \frac{p}{d_p} + \frac{m}{d_m}$$

where D, d_f, d_w, d_p and d_m are the densities of the body and of the

compartment indicated by the suffix.

One additional relationship is needed to complete the system, but it may be any assumption one chooses to introduce that relates two or more of the constituents by means of a constant. A relationship which reduces the biological variability can therefore be chosen. Siri (84) chose to relate mineral to protein by the relationship $m = Kp$. The value of K rests on rather meagre data for humans. The direct analysis of five cadavers by several investigators, cited by Keys and Brozek (60), yielded values varying from 0.290 to 0.527. Siri chose to put $K = 0.35$, which corresponds to total mineral of about 7% of the fat free mass. However, the exact value of k does not need to be known since it was shown to introduce little error into the estimate of fat.

Combining the equations and substituting assumed values for the densities yields:-

$$m_f = M \left[\frac{2.118}{D} - 0.780\, w - 1.354 \right]$$

This technique suffers the same objections as that of the densitometric technique because of the impossibility of underwater weighing of the critically ill intensive care patient. However, the technique has advantages over those involving density or water alone; firstly the biological variation is much reduced and secondly the technique is strictly valid when changes in hydration occur.

e) Fat Free Mass from Total Body Potassium

Relationships have been generated from the regression of total body potassium (TBK) on fat free mass in normals estimated from a variety of methodologies. Values for the coefficients in males and females have been calculated from a summary of the literature given by Boddy et al (16), together with the values obtained from Womersley et al (102) and Delwaide et al (38b). The data were then re-analysed by omitting data greater than one standard deviation from the mean. This gave 15 references for males and 11 for females. The mean relationships are :

$$FFM(kg) = \frac{TBK(g)}{2.533} \quad \text{-for men}$$

$$FFM(kg) = \frac{TBK(g)}{2.253} \quad \text{-for women}$$

Total body potassium can be measured in a whole body counter where the 1460 KeV gamma rays from naturally occurring ^{40}K in the body are counted. Since the measurement is non-invasive and involves no radiation risk to the patient (an advantage if repeat measurements are envisaged) the estimation of the fat free mass from potassium would be attractive for those patient groups for which these relationships hold.

As has been previously mentioned expansion of the extracellular water is believed to be a common occurence in wasting illness (Moore et al, 75). In the presence of oedema therefore the TBK/FFM ratio used will be too large, and the fat free mass calculated will be underestimated. Since the independent estimate of the fat free mass was based on the mean of anthropometric and total body water

estimates the technique is subject to the large errors inherent in each of these techniques, which include a large biological variation (see b) and c) above). Whilst group results should be reasonable in normals there is a considerable margin of error in estimating individual values. Additionally, these relationships should not be extended to other populations, such as patients in whom there are potassium disturbances specific to disease processes. In particular, the two compartment model (fat and fat free mass) cannot be applied to the phenomena involved in potassium changes with age (Anderson, 3).

f) Fat Free Mass From BIA and TOBEC

Recent years have seen two new commercial technologies: bioelectrical impedance analysis (BIA) and total body electrical conductivity (TOBEC). Both technologies measure impedance - in the case of BIA the tissue impedance to current flow applied at the skin surface and in the case of TOBEC the impedance to current flow in an external electromagnetic coil. Both techniques utilise the good conductivity of ions in the fat free mass excluding extracellular solids compared with the poor conductivity of fat and extracellular solids. Effectively a volume is determined by normalising the impedance by the subject height. This volume has been related to the TBW compartment. Impedance measurements have been shown to correlate extremely well with TBW measured by dilution techniques (Cunningham, 37). However if the same relationships as used for TBW measurements are used to relate this measurement to the fat free mass then the techniques will be subject to the same biological variation inherent

in the assumption of a constant hydration coefficient, and to increasing errors as the hydration coefficient departs from this "normal" value in wasting illness.

The problem so far has been that the fat free mass has too many components. At its conception in 1915 by Dubois and Benedict the "fat-free" mass was conceived as the oxidising protoplasmic mass which might reasonably be regarded as containing a reasonably homogenous cellular mass responsible for energy exchange, oxygen consumption and the metabolic, chemical or mechanical work achieved by the organism. No mention was originally made of that large component of the fat free mass that actually requires very little oxygen, the skeleton (10.3% by weight of the fat free mass in health). This concept was superceded in 1941 by the "lean body" mass (Behnke, 8) which was envisaged as a constant density heterogenous tissue compartment that included the whole body except neutral fat and included between 2 and 10% "essential lipid". Both of these terms, the fat free mass and the lean body mass, are presently used interchangeably and refer simply to the mass of body tissue excluding fat. The cortical bone of the skeleton has a much higher density than normal tissue. Consequently, in severe wasting disease as fat and muscle are depleted and the skeleton looms larger and larger in the "lean body" mass, so that density rises. The constancy of the "lean body" mass as a reference for density or compositional ratio has been lost. Additionally, the members of the extracellular tissue solids, the skeleton, tendon, fascia, collagen, elastin and dermis, use almost no oxygen and require no calories. Yet they are still in the "fat-free" mass occupying an increasing proportion of the total

mass as the body wastes. It is clear that the "lean body" mass and "fat-free" mass have become meaningless in terms of chemical composition, density, or, most importantly, in homogeneity of energetics. The "fat-free" or "lean body" mass then can be seen to be of little use as a reference for nutritional studies since it is too complex a compartment to be adequately defined by any one measurement. Additionally, since the "fat-free" or "lean body" mass includes the extracellular water, that component most commonly believed to change in wasting illness, then changes in its size may be of no nutritional interest since it may simply be reflecting changes in fluid overload.

Garrow (45) has argued that strictly speaking the terms "lean body mass" and "fat-free mass" are not quite synonymous. Body weight may be considered to be the sum of the lean body mass and adipose tissue, or alternatively of the fat free mass and fat. If adipose tissue were pure fat the terms would be synonymous; but adipose tissue is about 83% fat, 2% protein and 15% water. The fat free mass has therefore been used throughout this thesis to avoid any confusion.

1.1.2 Metabolic Model

Left with the failings of the fat free mass to represent a chemically or energetically homogenous mass, because of its inclusion of both the body cells and the extracellular supporting structures, Moore et al (74) suggested the concept of the "body cell mass" in 1963. The body cell mass was defined as:-

"The cellular mass of the body is a pure culture of living cells. It is that component of body composition containing the oxygen-exchanging, potassium-rich, glucose-oxidising, work- performing, tissue. This we refer to as the body cell mass (BCM). It is that entity with which one is primarily concerned in the consideration of the working, energy-metabolising portion of the human body in relation to its supporting structures. In any anthropometric consideration of the energy conversion of foodstuffs, oxygen requirement, carbon dioxide production or work performance the body cell mass is the basic reference entity."

The body cell mass consists of the cellular components (minus their bathing extracellular tissue) of all the body's tissues. Included are the sparsely populated cells of tendon, dermis, skeleton, fascia, cartilage, periarticular structures, collagen and elastin; these are all cells that contain potassium and perform chemical work. They are measured by their potassium content and must be considered a component of the body cell mass even though their main feature is the synthesis of a large mass of surrounding extracellular material (bone, tendon, collagen, elastin). The small cellular population of obesity tissue is likewise included in the body cell mass. Also included are the red blood cells.

Moore et al proposed estimating the body cell mass by measuring the total exchangeable potassium by an isotope dilution technique. This technique is no longer necessary with the advent of whole body counters, as already discussed. Total body potassium was suggested for the measurement of the body cell mass since virtually all potassium is intracellular. The derivation of the body cell mass makes several assumptions, namely:-

i) That cell protein is one quarter of the cell mass such that

$$BCM(g) = 4 \times 6.25 \times ICN(g)$$

where ICN is intracellular nitrogen and 6.25 is the universally accepted multiplicative factor for relating nitrogen to protein mass. This factor will vary with individual proteins.

ii) That the cellular N/K ratio is constant at 3 mEq K/g N.

$$BCM(g) = \frac{4 \times 6.25}{3} \text{ TBK } (mE_q)$$

Therefore $BCM(g) = 8.33 \text{ TBK } (mE_q)$

or $BCM(kg) = 0.213 \text{ TBK}(g)$

Whilst the assumptions in i) are reasonably well established the assumption in ii) of a constant intracellular N/K ratio has yet to be verified in wasting disease.

The BCM is highly dependent on changes in cellular hydration since changes in intracellular water (ICW) are normally accompanied by changes in TBK which in turn alters the cellular ratio of N/K. Consequently, an increase in cellular hydration would result in an overestimation of the BCM. Increases in total body water (TBW) are common in many wasted diseases; although the expansion is largely associated with the extracellular water (ECW), changes in the ICW are not so well established. However, Hill et al (53) demonstrated an increase in both ICW and ECW in 25 surgical patients after two weeks of total parenteral nutrition. Muscle biopsies before and after treatment showed no change in the cellular N concentration but did show a significant increase in the K concentration - illustrating a change in the cellular N/K ratio. Similarly, Cohn et al (33) demonstrated an elevated TBW in 15 renal patients after one year of maintenance haemodialysis. The increased TBW was normally

partitioned between the intra- and extracellular phases but will presumably have changed the cellular N/K ratio. In contrast, Cohn et al (32) demonstrated from muscle biopsies that the cellular N/K ratio in 4 wasting cancer patients was not significantly different from that in 4 normals. Similarly, Cohn et al (27) showed that the cellular N/K ratio of a patient losing weight post-surgically was maintained, as determined from muscle biopsies. Additional support for the existence of a constant cellular N/K ratio even in wasting disease is presented in the work of H. James et al (56). In her model total body nitrogen (TBN) was considered in three compartments, the intracellular compartment (70% of TBN in normals) and two extracellular compartments (30% of TBN in normals). The intracellular nitrogen (ICN) was assumed proportional to TBK and the extracellular nitrogen (ECN) was considered to be in the compartments:-

1) Highly fibrous tissue (bone, skin, tendons, ligaments) assumed proportional to anthropometrics (shoulder width x height^2); and

2) Low concentration irregular connective tissues (within adipose tissue and between and around muscle, nerves, blood vessels, organs and glands) which was assumed proportional to the body weight minus the body cell mass.

The study included 29 normals and 81 patients (suffering from Crohn's disease, malabsorption syndrome, cancer, chronic renal failure, diabetes mellitus, endocrine disorders). Multiple regression analysis of the data yielded an equation with a very small constant

term and a constant for the term in TBK equivalent to the known cellular N/K ratio determined from muscle biopsies in normals. A consequence of the good fit of the model even to wasted patient data was evidence that the cellular N/K ratio was constant in patient groups and equivalent to that in normals. However, many studies have been reported where TBN and TBK change disproportionately during depletion and repletion (57, 71, 73, 21, 68, 53, 50, 101). This is not surprising when one considers that 30% of TBN in normal subjects is extracellular and considered to be resistant to wasting. However, if the cellular N/K ratio remained constant throughout disease then the absolute changes in mass of TBN and TBK could be expected to occur in the cellular N/K ratio. This has often not been the case, with changes in TBK not being followed by changes in TBN, or vice versa. This is evidence in support of a changing cellular N/K ratio in wasting disease.

The difficulties with the body cell mass as the index of the size of the "metabolic engine" arise because of its dependence on intracellular water. An increase in intracellular water (ICW) would increase the size of the BCM compartment since ICW is one of its components. However, increases in the ICW may not necessarily affect the calculation of the BCM if the absolute mass of intracellular potassium has not followed a change in the ICW. However, potassium is believed to follow changes in ICW so as to maintain a constant concentration in solution. Such a phenomenon would infer that changes in the cellular hydration coefficient, away from the normal value, would lead to changes in the cellular N/K ratio. Such a change would invalidate the relationship used to calculate the body

cell mass. Evidence has been presented which suggests that the cellular N/K ratio does change in certain disease states, whilst other evidence would suggest that this is not the case. This uncertainty suggests that care should be exercised when interpreting the result of a body cell mass calculated for a wasted patient. Despite these drawbacks the body cell mass as an index of the state of health of the tissue is thought to be more resistant to errors of calculation in disease than the alternative, the fat free mass. This is because the expansion of total body water observed in many wasting illnesses is associated principally with the extracellular phase.

1.1.3 A Place for Total Body Nitrogen Measurements

The calculation of the body cell mass from potassium relies upon assumptions made about the relationship between potassium and intracellular nitrogen (ICN) and also upon that between ICN and the cell mass. The uncertainty in these relationships associated with the presence of wasting illness could be circumvented if a measurement of the intracellular nitrogen could be made directly. Indeed, when an estimate of the "metabolic engine" is required, intracellular nitrogen is the most appropriate "yardstick". This is because the energy storage molecules (adenosine triphosphate molecules (ATP)), the multi-enzyme complex which constitutes the electron transport chain responsible for the generation of an ATP molecule and the proton channel which pumps the protons generated at points along this electron transport chain out of the mitochondrion by active transport, all contain nitrogen. Additionally, the membrane proteins of cells and organelles are essential for

maintaining function and integrity. Furthermore the nucleotides responsible for replication also contain nitrogen. Hence the activities of energy production, replication and biosynthesis are associated with intracellular nitrogen which constitutes approximately 70% of total body nitrogen (TBN). The remainder of total body nitrogen is extracellular and is associated with the fabric molecules (connective tissue, collagen, keratin, elastin, etc.). Consequently, intracellular nitrogen represents the metabolic engine better than does potassium.

As well as being the best index for the metabolic model of body composition, nitrogen also enables the nutritional model to be realised in terms of its four compartments. This nutrition model would gain if total body protein could be further sub-divided in terms of intra- and extracellular protein. This modification would be advantageous since the extracellular protein, being associated with the supporting structures is known to have a very slow rate of turnover and therefore is believed to remain essentially intact during the wasting process. This component of the total protein compartment is therefore only of interest in helping to establish the intracellular protein compartment.

The procedure of neutron activation analysis relies upon the interaction of nitrogen with neutrons. Consequently, the method makes no distinction between intra- and extracellular nitrogen but measures the total body nitrogen compartment. The development of in-vivo neutron activation analysis techniques for the measurement of nitrogen enabled the four compartment nutrition model of body

composition to be realised. Additionally, if the extracellular nitrogen component can be predicted from anthropometrics then the intracellular nitrogen estimate could replace potassium as the best index in the metabolic model of body composition.

1.2 Delayed Versus Prompt Neutron Activation Analysis

Two techniques for the in-vivo measurement of nitrogen by neutron activation analysis have been developed; each utilising a different neutron reaction. Since the delayed method was the first to be developed it is appropriate to discuss this technique first.

1.2.1 The Delayed Method

The DELAYED method depends upon the FAST neutron reaction:-

$$^{14}N(n,2n)^{13}N \qquad \sigma = 6 \text{ mb}$$

The product, ^{13}N, is radioactive and decays with a 10 minute half-life by positron emission to ^{13}C. The method relies upon the detection of the 511 keV annihilation quanta in a whole body counter after the irradiation period.

The greatest advantage of the delayed technique is the low background during the detection period. This is a direct consequence of the separate irradiation and counting periods. The disadvantages of the technique are many and include:-

a) The 11.3 MeV threshold energy necessitates a fast neutron generator or a cyclotron. Such apparatus, with the additional cost of a whole body counter, make the technique expensive.

b) Attenuation of the neutron beam by the body results in a poor fast neutron fluence uniformity through the body. This leads to poor uniformity of activation and makes the technique very dependent on patient size.

c) The annihilation radiation detected is not specific to the reaction of interest. The technique is subject to interference from reactions with other body elements which generate ^{13}N as a product, from other positron emitting reaction products and from pair production and Compton scatter from higher energy gamma emitters. The greatest interference is caused by the reaction:-

$$^{16}O(p,\alpha)^{13}N$$

which can contribute up to 19% of the total annihilation counts.

d) The separate irradiation and detection facilities introduce repositioning errors and the inconvenience of having to transfer ill patients quickly after activation to a whole body counter for the detection of the annihilation radiation.

e) There is a higher patient dose compared with the prompt method. This is a consequence of many factors: the higher incident neutron energy; the smaller cross-section for the reaction and the decay between irradiation and counting. Doses of between 0.5 mSv and 10 mSv have been adopted at different

centres. However the dose used may be higher than necessary for the measurement of nitrogen to enable simultaneous determination of additional elements.

The feasibility of using this reaction to measure total body nitrogen was first demonstrated by Palmer et al (80) in 1968. Cohn and Dombrowski (24) in 1971 at Brookhaven, USA, were the first to report absolute measurement of nitrogen in patients using this technique. This reaction has also been successfully used for clinical studies at Leeds, England (109,2,21), and also at East Kilbride, Scotland (58). The technique has also been used at Hammersmith, England (88), but no patient studies have been reported.

1.2.2 The Prompt Method

The PROMPT method depends upon the THERMAL neutron reaction:-

$$^{14}N(n,\gamma)^{15}N \qquad \sigma_T = 80 \text{ mb}$$

^{15}N is formed in the excited state ($^{15*}N$). $^{15*}N$ de-excites in 10^{-15} seconds, with approximately 15% of the de-excitations taking place directly to the ground state with the emission of a 10.83 MeV gamma ray. The method relies upon the detection of these gamma rays during the irradiation period.

The greatest problem of the prompt method is that the simultaneous irradiation and detection creates a high background at the detectors which can lead to pulse pile-up in the nitrogen region.

The prompt method has several advantages over the delayed method;-

a) Because the reaction is a thermal one, radioisotopic neutron sources can be used. Radioisotopic sources are cheaper and inherently more reliable than cyclotrons and fast neutron generators. Their neutron output is also constant and predictable from the half-life.

b) Although the reaction is a thermal one, fast neutrons are still used to irradiate the patient. Thermalisation of the fast neutrons within the body maintain the thermal neutron fluence at depth, and good thermal neutron fluence uniformity can be achieved. This leads to good uniformity of activation through the patient depth.

c) The 10.83 MeV gamma ray is specific to nitrogen. The method has been shown by Vartsky et al (95) to be essentially free from interfering reactions. This is because no other major body element has a neutron capture gamma ray of this energy. Those elements which do give capture gamma rays of sufficient energy to interfere with the nitrogen measurement are of such low isotopic abundance, or their low percentage of emission per neutron capture, mean that they make an insignificant contribution to the nitrogen region (< 0.03% of the nitrogen counts).

d) The simultaneous irradiation and detection means that the patient does not need to be transferred during the measurement procedure, and so avoids the associated practical difficulties as well as

removing repositioning errors. In addition, apparatus can be constructed which is suitable for the critically ill intensive care patient.

e) Prompt hydrogen gamma rays can be collected simultaneously for use as an internal standard . The hydrogen peak was first shown by Vartsky et al (96) in 1979 to be useful in solving the problem of converting the detected gamma ray counts to an absolute mass of nitrogen. These workers found that the ratio of nitrogen to hydrogen counts was much less dependent on body habitus than the nitrogen counts alone. This is because both the nitrogen and hydrogen signals depend on thermal neutron reactions, and the cross-sections for the capture vary in the same manner with neutron energy for the two elements. Assuming that nitrogen and hydrogen are distributed in proportion to each other throughout the body, then the absolute mass of nitrogen can be calculated if an independent estimate of the absolute mass of hydrogen is made. The use of hydrogen therefore places less importance on the need to obtain a uniform activation/detection profile through the body thickness. Sequential nitrogen measurements will also be rendered more reliable because changes in the patient's weight and shape will not influence the measurement.

f) The use of lower energy neutron sources results in a reduced patient dose compared with the delayed method of between 0.26 mSv and 0.5 mSv.

This technique was first used to measure total body nitrogen with a

pulsed neutron source from a cyclotron at Birmingham, England (10) in 1972. Apparatus using radioisotopic ^{237}Pu-Be neutron sources were then developed in Toronto, Canada (72) in 1977 and later at the Brookhaven National Laboratory, USA (95) in 1979. More recently (1984) apparatus using ^{237}Pu-Be sources has been developed at Auckland, New Zealand (4).

The points raised above indicate the clear advantages of the prompt method over that of the delayed, not only in terms of freedom from interfering reactions and reduction of body habitus dependence by the use of an internal standard, but also in terms of patient dose and affordability of the apparatus.

1.3 Irradiation/Detection Geometries for Prompt Neutron Activation Analysis

Two basic irradiation/detection geometries have been adopted by centres measuring nitrogen by prompt activation analysis. Apparatus in Toronto (72) and Auckland (4) have a bilateral irradiation achieved with the positioning of neutron sources above and below the patient. Detectors are positioned at either side of the patient where they are shielded from the direct neutron beam. This arrangement approximates to a 90° geometry (neutron source and detector axes perpendicular) and a schematic diagram of the arrangement can be seen in Fig. 1.1 a). The alternative geometry has been adopted at Brookhaven (95). Here, the patient is irradiated unilaterally from below; bilateral irradiation being achieved by turning the patient through 180° half-way through the measurement.

Fig.1·1 Irradiation Geometries

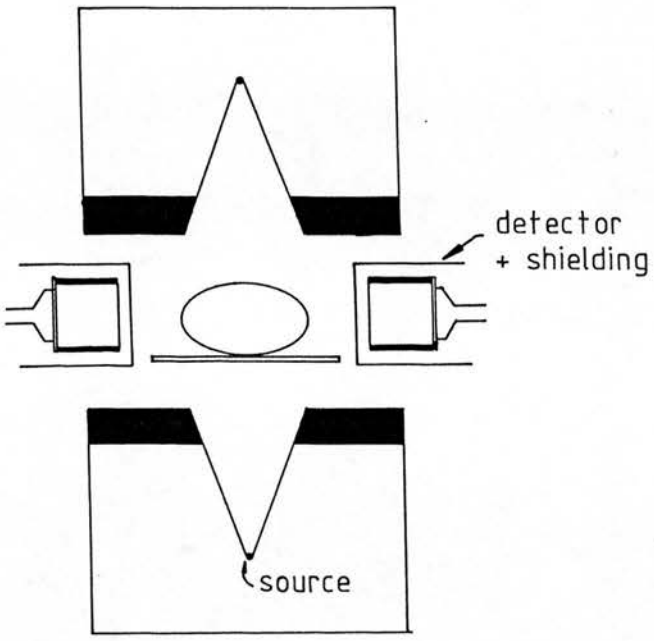

a). Bilateral geometry

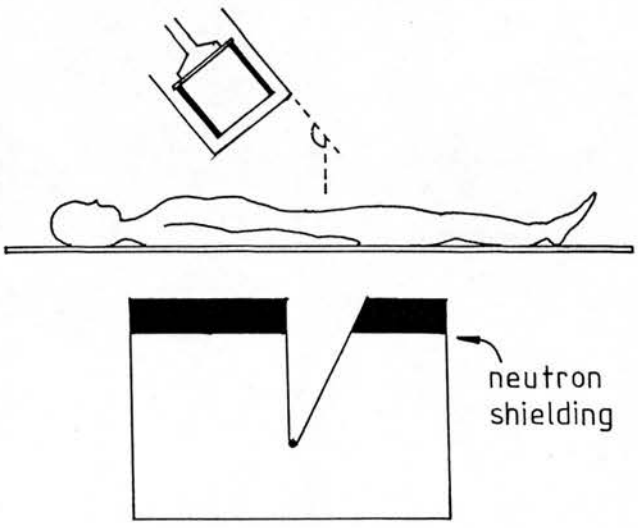

b). Unilateral geometry

Two detectors are positioned above the patient just outside the direct neutron beam, orientated towards the irradiated section of the body. This arrangement approximates to a 140° geometry - the angle between the neutron source and detector axes being indicated in b) of Fig. 1.1.

The "bilateral" irradiation geometry is preferred for measurements of the critically ill, since such patients cannot be turned to lie face down for half of the irradiation as would be required by the "unilateral" irradiation geometry. However, the construction time and cost of this bilateral geometry would be approximately twice that of the unilateral geometry. A further disadvantage of the bilateral geometry is that the fixed detector separation limits the maximum patient width which can be accommodated; the unilateral geometry having no such limitation.

1.4 Comparison of the Techniques Employed at Different Centres for the Measurement of Nitrogen

Given that total body nitrogen can be measured by either the "delayed" or the "prompt" technique of neutron activation analysis, the procedures for the techniques can be expected to differ substantially. Despite the utilization of a thermal neutron reaction in the prompt technique, both methods require fast neutron sources. A variety of neutron sources have been used including cyclotrons, neutron generators and radioisotopic neutron sources. The high count rates experienced during the irradiation in the prompt technique have been tackled variously by pulsing neutron beams, heavily shielding

TABLE 1.1

SYSTEMS FOR MEASURING NITROGEN TOGETHER WITH DOSE EQUIVALENTS, PRECISION AND ACCURACY

Centre (References)	Neutron Source	Mean Neutron Energy	Type of Analysis	Patient position Neutron beam direction Total analysis time	Dose Equivalent (mSv)	Precision (coefficent of variation (CV))	Accuracy
Auckland (4,5)	2x7.5 Ci Pu-Be (nominal)	5 MeV	Prompt total body	Supine Bilateral AP/PA 35 min	0.30	±4.2% [a] ±4.5% [b]	<5% [a] <2.5% [b]
Birmingham (96,93)	Cyclotron	2.5 MeV	Prompt total body	Prone and supine AP and PA 25 min	1.0	±2.5% [c]	±4%(CV)[d]
Brookhaven (95)	85 Ci Pu-Be	5 MeV	Prompt total body	Prone and supine AP and PA 35 min	0.26	±3% [e]	±3%(CV)[f]
East Kilbride (99,15)	Two Neutron Generators	14 MeV	Delayed total body	Supine Bilateral AP/PA 70 min	10.0 [g*]	±1.4 to 3.2% [h]	±4.3%(CV)[i]
Hammersmith (88)	Cyclotron	7.5 MeV	Delayed total body	Erect AP and PA 40 min	10.0 [*]	±4% [j]	
Leeds (78,69)	Neutron Generator	14 MeV	Delayed total body	Supine LR and RL 40 min	0.50 [g]	±3.6% [k]	<6% [l]
Toronto (72)	4x5 Ci Pu-Be	5 MeV	Prompt thorax only	Supine Bilateral AP/PA 10 min	0.50	±3%(4.8%)[m]	<10% [n]

KEY TO TABLE 1.1

a Precision is based on 25 scans of a Bush phantom over a 2 week period, and accuracy on scanning of box phantoms of varying sizes filled with known amounts of N.

b Precision based on 10 scans of human cadaver with 24% protein depletion; and accuracy on comparison with chemical analysis of same cadaver. (Knight GS, Beddoe AH, Streat SJ et al, 61).

c For the ratio N/H on phantoms of various shapes.

d Obtained from measurements on phantoms with gross nonuniformity of nitrogen distribution.

e Determination from 8 irradiations of an Alderson phantom filled with tissue equivalent liquid (2.6% due to counting statistics, 1.5% due to variations in the N/H ratio).

f Also based on Alderson phantom study; includes correction for different thicknesses and applies to the ratio N/H from shoulder to knee region.

g Dose equivalents quoted for entry body surface.

h Reproducibility on phantoms classified as small, medium and large.

i Obtained from a re-examination of absolute accuracy using a calibration method based on body weight.

j Obtained from 4 measurements of an anthropomorphic phantom.

k Based on 8 phantom measurements over a 24 week period.

l This figure includes the inaccuracy inherent in estimating the contribution of N annihilation quanta from the $^{16}O(p,\alpha)^{13}N$ reaction from estimates of TBW.

m For single thorax section, with precision for whole body estimate in parentheses.

n Based on absolute measurements of N in a pig by chemical analysis.

* Dictated by the requirements to simultaneously determine other elements.

the neutron sources and detectors and by simply reducing the neutron output of the source. The details of the apparatus and procedure at each of the centres is too detailed for discussion here. Instead a table has been shown (Table 1.1) to summarise some of the salient features together with reported values of precision, accuracy and radiation dose equivalent.

Centres adopting the prompt activation technique have different ways of making the independent estimate of the hydrogen compartment, required for the calculation of total body nitrogen from the nitrogen:hydrogen counts ratio obtained from the patient spectrum. Total body hydrogen (TBH) has been estimated in the following ways at different centres:-

a) $TBH = 0.1\ M$ Toronto (47)

where M is body mass.

b) $TBH = 0.097\ M + 0.0219\ TBF$ Birmingham (96)

The body fat (TBF) is calculated from skinfold thickness. The above equation was derived from tabulated concentrations of hydrogen in the fat free mass and fat (Diem et al, 38). Whilst the accuracy of estimating TBF from skinfolds was realised not to be high it was estimated that an error of $\pm 30\%$ in TBF would be required to introduce an uncertainty of $\pm 1\%$ in the hydrogen compartment.

c) $TBH = 0.11\ TBW + 0.12\ TBF + 0.052\ (M-TBW-TBF)$ Brookhaven (95)

where TBF was estimated from skinfold thickness and total body water (TBW) from tritium dilution.

d) $TBH = 0.11\ TBW + 0.12\ TBF + 0.07\ TBP$ Brookhaven (97)

The hydrogen compartment is estimated from the known fractional amounts of hydrogen in water, fat and protein (Reference Man, 55).

The mineral compartment has been ignored since its fractional hydrogen content is negligible. The carbohydrate compartment has also been ignored since it represents less than 1% of the fat free mass in normal subjects. The TBF and TBP compartments do not have to be calculated separately. Instead the TBF compartment is expressed as M - (TBW + TBP + BMA), where BMA is the bone mineral ash. BMA is estimated at Brookhaven by measuring or predicting the bone mineral ash since this represents the largest portion (82% by weight in normals) of the mineral compartment. An expression presented by Bigler and Woodard (11) for the calculation of BMA from total body calcium is measured by an activation analysis technique. Alternatively, TBCa is derived from algorithms based on sex, age, weight and height (Cohn et al, 25). This model superceded model c) at Brookhaven in 1983.

e) TBH = 0.11 TBW + 0.12 TBF + 0.07 TBP + 0.062 TBG Auckland (4)

There is only a very small difference between this model and that used at Brookhaven (d). Essentially, the carbohydrate compartment, total body glycogen (TBG), is included for completeness. However, as stated in d) the size of this compartment is small in normals and has to be estimated in patients since it cannot be directly measured. Its inclusion would therefore not be expected to make any significant difference to the magnitude of the hydrogen compartment. The estimation of fat by difference is also slightly different here compared with that at Brookhaven since the glycogen compartment is included in the fat free mass. Additionally, the mineral compartment is estimated as a percentage of the fat free mass (from water) in normals and is predicted in patients. The prediction equations used at Auckland are:-

$$TBG = 0.0091\ FFM = 0.0091\ \frac{TBW}{0.71}$$

$$TBM = 0.0622\ FFM \qquad \text{for normal subjects}$$

and

$$TBG = 0.15\ TBM$$

$$TBM = 0.116 + 2.67 \times 10^{-5}\ S \qquad \text{for patients}$$

where S = Height (cm^3) x Mediastinal Thickness (cm) x Biacromial Diameter (cm)

Essentially the inclusion of glycogen as a fifth compartment serves only to make the model more complicated without bringing benefits of accuracy. The accuracy is not improved because glycogen cannot be directly measured. For normals it is reasonable to assume that glycogen constitutes approximately 0.9% of the fat free mass. However, for patients it is being assumed that the glycogen compartment is in the same ratio with the mineral compartment as it is on average for normal subjects. This is likely to be in error in wasting illness, where prior to parenteral nutrition the glycogen compartment will almost certainly be depleted.

The methods a), b) and c) of estimating total body hydrogen depend either on anthropometric measurements or on the assumption that the mass of hydrogen is proportional to body mass. Anthropometric estimates of fat are based on regression equations relating skinfold thickness to body density. Such regression equations relate only to normal healthy subjects. Anthropometry cannot be expected to yield results with suitable accuracy in patients whose body composition is grossly different from that of the normal population from which the regression equations were derived. The methods d) and e) eliminate

anthropometric uncertainties from the estimate of hydrogen by expressing fat as the difference between body mass and the fat free mass compartment which is in part measured and in part estimated. The techniques introduce a circularity into the equations which result in fat never having to be directly estimated.

Beddoe et al (5) showed how the different techniques of estimating hydrogen in normal studies made little difference to the calculation of total body nitrogen. Substituting Reference Man values for the compartments (M = 70 kg, TBF = 13.3 kg, TBW = 42 kg, TBP = 10.6 kg, BMA = 3.7 kg (TBCa = 1 kg), extraskeletal minerals = 0.63 kg), and using the relationships assumed between TBCa and BMA at Brookhaven and that between TBG and TBM and TBW at Auckland yields:-

TBH (Toronto) = 7.00 kg (10.00% M)

TBH (Birmingham) = 7.09 kg (10.10% M)

TBH (Brookhaven (c)) = 6.88 kg (9.80% M)

TBH (Brookhaven (d)) = 7.10 kg (10.14% M)

TBH (Auckland) = 7.04 kg (10.05% M)

It can be seen that the percentage of hydrogen of the body mass varies over a relatively small range. Since total body nitrogen is proportional to the mass of hydrogen these percentage differences would yield systematic differences in the nitrogen calculated of -0.50% (Toronto), +0.50% (Birmingham), -2.49% (Brookhaven (c)) and +0.90% (Brookhaven (d)) with respect to the Auckland values. These small but significant systematic differences were reflected in the values of nitrogen calculated at Auckland using the different internal standardisation techniques (except for Brookhaven (d)), where the values ranged, on average, between +0.8% and -2.8% of the

corresponding values calculated by the Auckland calibration approach.

It is important to be aware of the systematic differences which arise when using different internal standardisation techniques when interpreting the results obtained with predictor equations generated from normal subjects by the various centres.

The good agreement between the calibration techniques of different establishments with that at Auckland has, so far, only been demonstrated in normal subjects.

The good agreement is a consequence of the validity of the assumptions inherent in the calculations during health. The question now arises as to the validity of these relationships during wasting disease when body composition is known to undergo significant changes. Beddoe et al (5) have presented data for total body nitrogen calculated using the different calibration equations for hydrogen for five patients with varying degrees of malnutrition and wasting. The average nitrogen values were -3.22% (Toronto), -1.46% (Birmingham) and -4.44% (Brookhaven (c)) (with a range of -10.2% to +3.6%) with respect to the values obtained with the Auckland calibration. The results reflect both the problems associated with the estimation of fat by anthropometry in overhydrated patients and also the effects of assuming hydrogen to be a constant fraction of body weight.

1.5 Summary of Clinical Trials Undertaken

Total body nitrogen has been measured by either the prompt or delayed method of neutron activation analysis at Leeds, Birmingham, Toronto, Brookhaven and Auckland. The following is a summary of the nature of the studies undertaken where total body nitrogen measurements have helped to elucidate the distortion of body composition or the possible benefits of a particular patient management regime. Total body potassium measurements have often been made in conjunction with the nitrogen measurement. Where this is the case both measurements are discussed.

a) Estimates of Total Body Fat

Total body fat (TBF) has been widely estimated from skinfold measurements. However, the four compartment nutrition model of body composition enables the estimation of fat by a difference technique, viz:-

$$TBF = M - (TBP + TBW + TBM)$$

where M is the body mass and TBP, TBW and TBM represent the total body compartments of protein, water and minerals respectively.

Many investigators have shown that skinfolds consistently underestimate the fat compartment compared with the difference method in many disease states as well as in normal subjects (5, 89, 31, 28, 66, 33, 34). A similar underestimation of the fat compartment by the densitometric technique of 7.8% compared with the difference technique was demonstrated on 36 volunteers by Streat et al (89).

The densitometry method in these normals also lead to values of TBW/FFM ratio which were biologically unreasonable. The range of values for the TBW/FFM ratio were smallest for the difference method, demonstrating that although skinfolds, densitometry and the difference method gave similar values for the mean TBF in groups that the TBF value in an individual will be least in error when the difference method of estimation is used. Another study (89) of 21 gastrointestinal surgical patients matched with normals demonstrated a significant systematic underestimation (19%) of TBF estimated from skinfolds relative to the difference method; indicating that such systematic differences do not derive from age and sex differences.

b) Cancer Patients

Long term body composition studies of cancer patients have shown that the degree of distortion of the body composition depends on the type of malignancy (patients with solid tumours undergoing the largest distortions of body composition) as well as changes in dietary intake (32, 26, 42, 29, 30).

A study of the benefits of total parenteral nutrition on patients with small-cell carcinoma of the lung, receiving combinations of chemotherapy and radiotherapy, showed that total body nitrogen did not increase with total parenteral nutrition (83).

c) Renal Patients

A study of 15 renal patients undergoing maintenance haemodialysis for

one year (33) showed no significant changes in body composition compared with normals except for an increased total body water; this was normally partitioned between the intra- and extracellular compartments.

Two studies (50, 101) have been reported on the long term effects of continuous ambulatory peritoneal dialysis (CAPD) on end-stage renal disease patients. Both studies reported significant increases in total body potassium and body weight over 18 months with continuing significant decrease in TBN (20%). A decreased dietary intake (owing to the absorption of glucose from the dialysate) was associated with the nitrogen loss.

d) Obese Patients

Compartmental analysis has been used to estimate the efficacy of two weight reducing diets, varying in quantity of carbohydrate applied, in 17 obese females (32).

e) Gastroenterological Patients

(i) Total Parenteral Nutrition (TPN) Versus Amino Acid Infusion

A study of body composition in 30 patients (35, 106, 51, 107), 15 days after proctocolectomy or rectal excision showed significant advantage of total parenteral nutrition over amino acid infusion in terms of clinical complications, despite the maintenance of TBN in both groups. Both types of nutritional support were shown to

maintain total body nitrogen compared with a control group, allowed an unrestricted oral intake, who lost an average of 9.1% of total body nitrogen.

(ii) Glucose or Fat as the Energy Source During Total Parenteral Nutrition

A significant clinical advantage of a glucose (60%) and fat (40%) diet has been demonstrated above that of a glucose only diet in gastroenterological patients (67). It has been suggested that the reason for this is that too much glucose may saturate the oxidative pathways of glucose. The addition of fat would enable more energy to be generated along alternative pathways, so making more energy available for protein synthesis. The addition of fat also prevented the increase in total body water which is seen when glucose alone is used during total parenteral nutrition (51, 57, 71, 104, 54, 105). The water retention is thought to be due to the fact that the antinaturesis (prevention of the excretion of sodium in the urine) that occurs on refeeding the starved subject is due exclusively to carbohydrate and is not induced by fat or protein fed in isocaloric amounts.

(iii) The Optimal Calorie/Nitrogen Ratio During Total Parenteral Nutrition

A study of 30 gastroenterological surgical patients (86) has shown that the optimal calorie/nitrogen ratio is ≤135 cal/gN and that gains in nitrogen require more than 0.3 gN/kg/day.

(iv) Should Insulin Be Added During Total Parenteral Nutrition?

The administration of insulin during total parenteral nutrition (TPN) therapy has been shown to have a protein sparing effect when given to highly stressed patients. A study has been performed to determine whether or not this is the case in less stressed patients over a short period.

A two week study of 32 gastroenterological patients showed that patients receiving insulin during total parenteral nutrition therapy gained significant amounts of total body potassium but not TBN (68), when receiving 44.7 kcal(glucose)/kg and 0.28 gN/kg. However, the group gained both water and fat; the latter indicating that the energy supply was adequate. The failure to gain nitrogen suggests that the nitrogen levels supplied were inadequate, as suggested by the previously mentioned "optimal" levels of nitrogen. It was concluded that there was no advantage in administering insulin during total parenteral nutrition in these patient groups. Additionally, the gain of potassium without a concomitant gain of nitrogen highlights the importance of not interpreting a gain of potassium as a gain of fat free mass.

f) Surgical Patients

(i) Total Parenteral Nutrition Versus Continuous Intragastric Infusion of an Elemental Diet

Two studies (104, 105) concluded that an elemental diet was as effective at maintaining TBN in surgical patients as was TPN. An elemental diet was considered advantageous since it is cheaper, safer and easier to manage.

(ii) Voluntary Food Intake After Major Surgery

A study of 12 surgical patients (46) over a 2 week period following elective colectomy, demonstrated that their voluntary food intake was related to habit and not requirement; that is that there was no relation to energy output or energy lost. This study helps explain how patients with high energy expenditures develop protein energy malnutrition while recovering from major surgical procedures.

(iii) Should Steroids Be Supplied During Total Parenteral Nutrition Therapy?

Anabolic steroids have been used to improve nitrogen balance in a variety of conditions. This is because they are thought to enhance amino acid and water uptake by tissues and increase the utilization of fat, so promoting protein synthesis.

A study of 24 surgical patients (108) receiving total parenteral

nutrition for 2 weeks showed that the addition of an anabolic steroid (Nandralone Decanoate) gave no greater increase in total body nitrogen. Anabolic steroids were concluded to be disadvantageous since they increase water retention and have possible virilising and toxic side effects.

g) The Clinical Value of the Hydration Index: TBW/FFM

It is well known that wasting patients, particularly those suffering from the septic shock syndrome, can and do undergo large changes in their fluid compartments. Moore and Boyden (75) produced a nomogram of TBW/FFM against the intracellular:total body water ratio (ICW/TBW) on which were drawn lines for the limiting circumstances in which exists either wasting of the body cell mass (BCM) alone or expansion of the extracellular water (ECW) alone. This nomogram predicts increased hydration of the body arising from a combination of BCM loss and from the frequently associated expansion of the ECW. It would therefore be expected that the ratio TBW/FFM would increase during the wasting process.

One study (86) of 41 normals and 56 surgical patients demonstrated that the mean hydration coefficient for patients could be as high as 82% of the FFM compared with 75% in normals, for patients and normals having a similar amount of total body protein (TBP). A further study (7) of 68 normals and 95 surgical ward patients (studied before total parenteral nutrition) showed a subpopulation of patients (48 out of 95) who, despite having lost a mean of 15.5% TBP, had a normal ratio of TBW/FFM. Errors due to estimation of the various compartments and

the possibility of these patients being dehydrated have been ruled out as a cause for this discrepancy. Beddoe et al (7) suggest that the cause of the discrepancy is due to the combined effects of protein depletion, intracellular water depletion and moderate extracellular water expansion. A modification of the nomogram proposed by Moore and Boyden (75) in accord with observed TBW:FFM ratios was proposed, so enabling mean changes in ECW and ICW to be followed. This nomogram can only be applied to studies of groups because of the large errors involved. For the subpopulation of patients discussed here the nomogram showed that the 15.5% depletion in TBP was accompanied by a 27% depletion of intracellular water and a 12% expansion of the extracellular water i.e. a mean net loss of TBW of 9%.

This data clearly demonstrates that the TBW/FFM ratio itself is not of much clinical value because it masks the underlying shifts in the extracellular and intracellular water volumes. These shifts and the absolute values of the entities themselves are of considerable clinical importance. The implication of this work is that the hydration ratio alone provides little information on the body composition of the ill because it masks the underlying shifts in body water compartments, thereby discounting the possibility of using the ratio as an accurate index of illness. However, knowledge of the changes in the hydration ratio in disease is essential if estimates of fat are to be accurately made from total body water measurements. Whilst a normal hydration ratio in disease indicates that the technique of estimating fat from the total body water method may be valid, it is clear that this value of the fat free mass need not

necessarily contain its normal compliment of protein; the state of health of the tissues therefore is not necessarily apparent using this technique.

h) Application of the Prompt Gamma Neutron Activation Analysis Technique to Critically Ill, Intensive Care Patients with Fluid Overload

Body composition studies of critically ill, intensive care patients are complicated for the following reasons:-

1). Large expansion of the ECW is common. Such expansion is frequently in ascites which increase the equilibrium time necessary for an accurate estimate of TBW using a tritiated water dilution technique.

2). Total parenteral nutrition cannot be stopped for the long equilibrium times necessary for the accurate measurement of TBW. This affects the fluid volume which the tritiated water is to equilibrate with, as also do fluid losses through surgical drainage of ascites, nasogastric losses, urine production, profuse sweating, etc.

TBW measurements of 11 critically ill, intensive care patients (90) produced the following findings:-

(i) TBW measurements increase by 6% at the third hour compared with the first hour and thereafter remain stable (up to 6 hours).

(ii) The extent of measured isotope losses (urine, etc.) at four hours after injection varied from 0.53% to 3.29% (mean of 1.24%), illustrating the importance of measuring such losses in individual patients.

(iii) The precision of the TBW measurement (averaged over the fourth, fifth and sixth hour measurements) varied from 0.4% to 3.0% (mean of 1.2%).

(iv) The prediction of TBW from analysis of the early (first hour) arterial kinetics is inappropriate in this patient group.

(v) The TBW was, on average, 31% above the predicted pre-illness value. The pre-illness value was estimated by measuring total body protein (TBP), assuming that this had not changed during the illness, and using a regression equation based on the data from 68 normals from two previous studies (5, 89), viz:-

TBW_{pi} = 2.56 TBP + 8.95 $\pm$ 7.1% (CoV) r = 0.925

This study has shown that the prompt gamma neutron activation analysis technique can be applied to the critically ill, intensive care patient. Thus making body composition studies possible in patient groups in which the delayed activation technique can only be used with difficulty.

This chapter has discussed the various techniques available for body composition analysis. The dependence of the simple two compartment

(fat free and fat masses) model on a reference body which differs only in the percentage of fat by weight leads to two problems: a large biological variation in normals leading to an uncertainty in fat estimation of approximately ±4% of body weight in individuals and an increasing error in wasting disease as departure from the assumed reference body occurs. The four compartment nutrition model was shown to be less subject to biological variation since no assumptions are made concerning the relationships between compartments. Estimation of three of the compartments enables the fourth, fat, to be determined by difference from the body mass. This model therefore enables the delineation of the body mass into its nutritionally important compartments. The "metabolic" model attempts to determine the size of the body mass associated with respiration, biosynthesis and replication. Total body potassium was advanced as a suitable index but intracellular nitrogen presented as a more suitable alternative. However, the techniques of neutron activation analysis can make no distinction between intracellular and extracellular nitrogen. Perhaps relationships derived from anthropometrics to predict extracellular nitrogen would enable intracellular nitrogen to be determined from a total body nitrogen measurement. In this way the element most closely associated with the life supporting functions could be followed with disease processes.

Two techniques of nitrogen measurement by neutron activation analysis (prompt and delayed) have been described. A brief summary of important parameters of the nitrogen measurement at different centres has been presented in Table 1.1. Different calibration procedures for the independent estimate of total body hydrogen, necessary for the

prompt technique, have been discussed. These differences generate small systematic differences in the nitrogen calculation for studies on normal subjects. However, it is important to be aware of such differences when comparing the prediction equations for nitrogen generated from different centres. Additionally, the assumptions inherent in the different calibration procedures may become invalid in disease states, such that results generated in patient populations may vary significantly dependent upon the calibration procedure used.

The summary of the clinical trials undertaken is by no means exhaustive, but illustrates the important role played by body composition analysis in the evaluation of patient management regimens.

CHAPTER 2

CHAPTER 2

DELAYED NEUTRON ACTIVATION ANALYSIS FOR THE MEASUREMENT OF TOTAL BODY NITROGEN

Until October of 1984 the Medical Research Council cyclotron at Edinburgh was available for experiments to compare the delayed method of measuring total body nitrogen with the prompt method. This chapter discusses the investigations which were performed before the cyclotron closure to determine the activation sensitivity profiles with phantom thickness and the extent of the oxygen interference in the nitrogen measurement. The detection sensitivity profiles for the whole body counter at the Western General Hospital, Edinburgh are also presented along with estimates of the necessary dose required to measure total body nitrogen with a coefficient of variation of $\pm$4%.

2.1 Potential Problems

The potential problems in measuring total body nitrogen by delayed neutron activation analysis were addressed in section 1.2, where a brief comparison was drawn between the prompt and delayed techniques.

Two centres (Scottish Universities Research Reactor Centre (SURRC) (99) and the Department of Medical Physics, University of Leeds (69)) have developed procedures for patient measurements adopting the delayed technique. However the method has not gained universal acceptance because of doubts concerning the accuracy of the measurement considering the enormity of the interferences, and also

TABLE 2.1

NITROGEN AND INTERFERING REACTIONS

Reaction	Abundance of Target Nuclide (%)	Mass of Target Element in Standard Man (g)	Half-Life of Product (min)	Reaction Threshold Energy (MeV)	Principal Emissions & Energy (MeV)
Principal Reaction					
1). $^{14}N(n,2n)^{13}N$	99.6	1800	10	11.3	β^+ only
Other Reactions for ^{13}N Production					
2). $^{16}O(p,\alpha)^{13}N$ ("knock-on" protons)	99.8	43000	10	5.5	β^+ only
3). $^{13}C(p,n)^{13}N$	1.1	16000	10	3.2	β^+ only
Other Positron Emitters					
4). $^{16}O(n,2n)^{15}O$	99.8	43000	2.05	16.6	β^+ only
5). $^{18}O(p,n)^{18}F$	0.2	43000	110	2.6	β^+ only
6). $^{14}N(p,\alpha)^{11}C$	99.6	1800	20.3	3.1	β^+ only
7). $^{31}P(n,2n)^{30}P$	100	780	2.3	12.7	β^+ γ : 2.23
8). $^{35}Cl(n,2n)^{34m}Cl$	75.8	95	32	12.9	β^+ γ : 1.17 2.12 3.30
9). $^{39}K(n,2n)^{38}K$	93.3	140	7.7	13.3	β^+ γ : 2.17
Nuclides Giving Rise to Compton Continuum and Pair Production					
10). $^{31}P(n,\alpha)^{28}Al$	100	780	2.3	2.0	γ : 1.78
11). $^{37}Cl(n,\gamma)^{38}Cl$	24.2	95	37.2	thermal	γ : 1.64 2.17
12). $^{23}Na(n,\gamma)^{24}Na$	100	100	900	thermal	γ : 1.37 2.75
13). $^{48}Ca(n,\gamma)^{49}Ca$	0.19	1000	8.9	thermal	γ : 3.08

doubts (63,87) about direct calibration using multicompartment anthropomorphic phantoms in which nitrogen is uniformly distributed (ie. not anthropomorphically).

Table 2.1 lists the possible interfering reactions to the nitrogen measurement. It is clear that the interfering reactions are of three kinds, viz:-

i) N-13 produced in reactions other than that involving N-14.
These interfering reactions are the most difficult to correct for since the products are indistinguishable from that for N-14. The interference from oxygen is estimated by determining the amount of oxygen in the body (either by direct determination using an activation reaction or by estimation dependent on the calculation of total body water using regression equations based on height and weight). The interference from carbon is assumed to be negligible for patients since it has been determined to be so from phantom experiments.

ii) Other positron emitters.
The interference caused by these reaction products can be estimated by decay curve analysis because of their differing half-lives.

iii) Nuclides giving rise to Compton continuum and pair production.
These interferences may be estimated by fitting standard spectra to their photopeaks to determine their Compton contribution to the annihilation peak. The interference from pair production

will be included in the estimate if the standard spectra are obtained by the irradiation and counting of anthropomorphic phantoms containing the nuclide of interest.

Additional background counts are contributed from natural room background and the body burden of potassium-40.

The N-13 counts produced from the fast neutron reaction with N-14 as a percentage of the total counts in the annihilation region, will vary with the delay period between irradiation and counting and the counting period. This is a consequence of the more rapid decay of the shorter lived isotopes. However, prolonged delay before counting to reduce the interferences will result in a proportionately larger natural background in the annihilation region. Spinks et al (88) estimated that the N-13 counts from N-14 would contribute approximately 15% of the total counts in the annihilation energy region (for a 3 minute irradiation, 6 minute delay and 30 minute counting period)!

Reaction 2) in Table 2.1 is the largest N-13 producing interference in the delayed method. Its percentage contribution to the net N-13 counts has been estimated at many centres for a standard man composition. Normalising to a 3 minute irradiation, 6 minute delay and 30 minute counting period the results are:-

	Birmingham (Ref.63)	Hammersmith (Ref.88)	Leeds (Ref.69)	SURRC (Ref.99)
$\frac{\text{N-13 counts from O}}{\text{Net N-13 counts}}$	16%	19%	18%	21%

These centres are all in reasonable agreement with one another regarding the magnitude of the oxygen interference.

The absolute calibration of the nitrogen measurement involves comparison of patient data with that from anthropomorphic phantoms (99, 69). In patients the greatest part of the variation of response with position in the body arises from the combined effects of reduced penetration of the thicker body regions by fast neutrons and reduced counting sensitivity for annihilation radiation in those regions. Profiles of fast neutron fluence versus depth measured in water phantoms for bilateral irradiations have been reported by several authors. Elliot et al (SURRC) reported an RMS variation of $\pm$19% (square root of the mean square deviation from the mean expressed as a percentage of the mean) for the fast neutron profile (88) with depth through a 25 cm thick phantom. Haywood et al reported an RMS variation $\pm$25.5% (49) for the detection profile for the 25 cm phantom under the same irradiation conditions (SSD of 70 cm with a 14 MeV neutron generator). The combined activation/detection profile has an RMS variation of approximately $\pm$44%. Vartsky et al (Birmingham) reported a range (difference of highest and lowest values from their mean) of $\pm$46% for the fast neutron profile through a 25 cm thick phantom at an SSD of 1.4 m using a 14 MeV neutron generator (92). Unfortunately no RMS variation from the mean was quoted. The range was stated to vary only slightly with increasing target to skin distances. These results were combined with a calculation to interpret the effects of self-absorption of 0.511 MeV photons in the phantom en route to the detectors, and the detector's

sensitivity (63). The combined activation/detection sensitivity was calculated to have an RMS variation of ±81%. Similarly, McCarthy et al (Leeds) (69) measured the activation (SSD = 2.1 m for a 14 MeV neutron generator) and the detection profiles for a 25 cm thick phantom to have ranges of ±17% and ±23% respectively about the mean. The range for the combined activation/detection sensitivity for a 23.5 cm thick phantom was calculated to be ±31%. However, the geometries used at Leeds for the measurements did not accurately reflect the procedure which was adopted for patient irradiation. The activation profiles with depth were measured across the phantom width since patients were irradiated laterally. Consequently the combination of the two profiles does not reflect the combined activation/detection uniformity which would be obtained in practice with patients. Variation in the activation profiles discussed here should, in theory, vary only with the SSD since all profiles were determined with 14 MeV neutron generators. At an SSD of 70 cm the RMS variation due to the inverse square law effect for a bilateral irradiation is approximately ±2.3% and that at an SSD of 2.1 m is ±0.5%. Therefore, if the results are modified to remove the inverse square law contribution to the RMS variation in the activation profile the variation is reduced to ±16.7% for the SURRC. The variation in the detection sensitivity profiles will vary with the detector separation and spatial distribution of detector volume. For the reasons already mentioned the three results for the combined activation/detection profiles presented here are not directly comparable. The RMS variation for the combined sensitivity determined at Birmingham is significantly worse than that reported by the group at the SURRC. The reason for this is uncertain since the

details of the calculation are not specified in the paper. The non-uniformity of the activation, detection and combined sensitivity profiles also varies with body thickness as would be expected; profiles becoming less uniform as the body thickness increases (49). The total response of the method to body nitrogen therefore depends not only on the quantity of nitrogen in the body, but also on how the nitrogen is distributed over body regions of different thickness and how it is distributed as a function of depth within those regions. In response to this problem Haywood et al (49) argued that less than 25% of the body's nitrogen is seriously under-represented. This conclusion was drawn after consulting Reference Man (ICRP 1974), in which 60% of the body nitrogen is shown to reside in regions with typical thicknesses of 160 mm or less. It was argued that of the remainder, a proportion is near enough to the body surface (within about 30 mm) to have a combined response within 25% of the mean value for the thinner regions.

Calibration of the method using phantoms will be valid only if the observed element responses are little affected by the difference between the element distribution in a phantom (mainly homogeneous) and the corresponding range of distributions in patients (inhomogeneous). For the nitrogen measurement this condition must hold not only for nitrogen but also for the interfering elements. If the condition does not hold then the changes will be most important for nitrogen and its larger interferences (only oxygen is distributed differently in the body compared to its distribution (uniform) in the phantom and contributes a significant interference to the nitrogen measurement to be of concern). Haywood et al (49) developed a

calculation which divided the body into small rectangular segments. At the centre of each segment the response was calculated allowing for the neutron and gamma ray attenuation and the tissue type. The sum of all these responses was the expected response from a human of similar composition. The calculation was tested against phantom irradiations and gave good predictions for the results obtained when:-

a) Mixing and no mixing of a homogeneous solution was allowed between irradiation and counting (showed that mixing made no difference to the result).
b) Inhomogeneous phantoms were counted before and after mixing (showed a big difference in the result depending on the distribution of the element).
c) Different sized homogeneous phantoms were counted (showed that larger phantoms give fewer counts per gram of element).

The calculation was then used to determine the response over a wide range of body weights (40 to 100 kg) and degree of adiposity (0 to 65% of body weight). The response was shown to be very dependent upon body weight but mostly independent of degree of adiposity. The calculation for homogeneous and inhomogeneous distributions of nitrogen and oxygen differed by no more than 2%. Therefore, the calculation supports the use of homogeneous phantoms for calibrating the delayed method of measuring total body nitrogen. McCarthy et al (69) built complex phantoms to investigate the effect of mixing the homogeneous phantoms, used in their calibration procedure, between irradiation and counting. The complex phantoms were built up of

tubes to a variety of heights and weights; mixing being limited to within individual tubes. The measured nitrogen, using the patient calibration procedure, was compared with the known content and a maximum departure of 4% was observed for the heaviest phantoms. In these experiments the interference from oxygen was measured directly by an activation technique and was found to contribute 23% of the annihilation counts. This is greater than the 18% which oxygen is calculated to contribute in patients. The difference is that in patients the oxygen is estimated from anthropomorphic relationships. This may lead to a large error in the nitrogen measurement in a minority of patients and highlights the advantage of measuring the oxygen interference directly. The authors of this paper point out that differences in the nitrogen and oxygen distributions between patient and phantom remain uncorrected and add that no method of applying the necessary corrections is available. However, combined sensitivities for the measurement of nitrogen have been measured with small nitrogen samples distributed at many positions throughout an anthropomorphic phantom. Calculations show that if, in an extreme case, a patient had nitrogen only in the left side of his body, then the TBN measurement would be 13% greater than the value for a uniform nitrogen distribution. Similarly, if the patient only had nitrogen in the right side of his body, the measured TBN would be 2% less than the value for a uniform nitrogen distribution. For a distribution in which nitrogen was situated only in the centre of the body, the measured TBN would be 16% below the value for a uniform distribution. These extreme examples illustrate the maximum errors which could arise owing to the non-uniform distribution of nitrogen in the body. For patients however the errors caused by

non-uniformity should be smaller than those for these extreme cases.

2.2 Experimental Investigations

The MRC cyclotron at Edinburgh generated fast neutrons by the bombardment of a beryllium target with deuterons. The neutron spectrum had a maximum energy of 18 MeV and a mean energy of 5.9 MeV. Experiments are presented which investigated the magnitude of the oxygen interference on the nitrogen measurement using delayed neutron activation analysis to enable comparison with values quoted in the literature from other establishments. Activation profile uniformities with phantom thickness are also presented to determine the improvement possible with the higher energy cyclotron neutron source compared with 14 MeV neutron generators. Additionally, the detection sensitivity profiles for the department's four detector whole body counter are presented. Combination of the activation and detection sensitivity profiles enables the variation in the sensitivity of the nitrogen measurement to be observed with position in the body. The uniformity of the profiles is expressed in terms of the RMS variation and the range. The RMS variation was calculated at 2.5 cm intervals and is the square root of the mean square deviation from the mean expressed as a percentage of the mean. The range is the maximum and minimum variation from the mean value. Finally the radiation dose for a $\pm$4% coefficient of variation on the nitrogen measurement is calculated. These measurements enable comparison with the equivalent values obtained for the measurement of nitrogen using prompt neutron activation analysis.

2.2.1 Oxygen Interference

The oxygen interference to the N-13 counts which would be expected for Reference Man was investigated using a Bush phantom thorax section (20 cm minor axis x 30 cm major axis x 40 cm long). The phantom was unilaterally irradiated with the nearside at a distance of 1.7 m from the target for a period of 13 minutes (dose to the front of the phantom = 159 cGy, dose to the back of the phantom = 29.4 cGy). After irradiation the phantom was transfered to a shadow-shield whole-body counter containing four 15 cm diameter by 10 cm thick sodium iodide detectors, two above and two below the bed, arranged in line across the phantom. The separation of the upper and lower detectors was 62 cm. The phantom was scanned six times across the field of view of the detectors for a period of 16 minutes. Three investigations were performed, viz:-

i) Irradiation and counting of a nitrogen phantom containing 16.42 litres of water and 500 g of ammonium nitrate (NH_4NO_3).

ii) Irradiation and counting of a water phantom containing 16.7 litres of deionized water.

iii) Irradiation of a water phantom (as in ii)) and counting of the empty phantom only.

The post-irradiated nitrogen phantom contained N-13 from the activation of both nitrogen and oxygen as well as O-15, F-18 and C-11 (positron emitters) from other possible activation reactions with these elements. Additionally, there were interfering reactions with carbon in the polyethylene phantom material. The water phantom

generated counts from all these sources except for those from N-14. The counting of an empty phantom after irradiation when containing water enabled a correction to be made for the interferences from the phantom material itself. These three irradiations enabled the counts/gram of element to be calculated for both nitrogen and oxygen. The calculation involved normalisation of the spectra for the same delay and counting times. The counts in both the annihilation and the annihilation sum peaks were determined from which the total counts per gram of oxygen or nitrogen were calculated. This enabled the expected counts for the Reference Man content of nitrogen (1.8 kg) and oxygen (43 kg) to be calculated, from which the N-13 counts from oxygen to the N-13 counts from both oxygen and nitrogen was calculated to be approximately 18%. This value compares favourably with the magnitude of this interference as reported from other centres (see section 2.1).

2.2.2 Fast Neutron Fluence, Detection Sensitivity and Combined Sensitivity Profiles

a) Activation Profile

The activation profile for the delayed technique of nitrogen measurement was determined using a water phantom of dimensions 30 cm x 30 cm x 30 cm. The phantom was centred in the neutron beam at a target to phantom front distance of 1.25 m. Universal containers (2.4 cm diameter) containing urea powder (NH_2CONH_2) were used to plot the fast neutron profile with depth through the phantom; the fast neutron fluence being directly proportional to the normalised N-13

counts from the activation of N-14. The column of urea powder was approximately 2.7 cm high to maximise the counts which could be detected in the well detector used for counting the containers. Each container was irradiated at a known depth in the phantom for 13 minutes, after which time they were withdrawn, dried and transferred to the well detector for counting. The oxygen interference was compensated for by activating water columns in the same positions as were the urea columns. Universal containers are composed of the elements C, H and O, and interferences from the activation products of C and O were expected. Because of the possibility of the $^{16}O(n,2n)^{15}O$ and $^{18}O(p,n)^{18}F$ reactions, whose product nuclides have half-lives of 2.05 and 110 minutes respectively, the half-life of an empty activated universal container was determined. This half-life was very close to 10 minutes, and it was concluded that only the product N-13 was being generated, which simplified the correction for activation of the containers. Since the majority of the counts from the container material were likely to be from activation of oxygen it was considered necessary only to determine the ratio of the counts from the container to the counts from the water at one position in the phantom, and to assume that this ratio was constant at all depths in the phantom. The possible interference from the carbon in the urea remains to be corrected for. To estimate the magnitude of this interference an equivalent volume of wax to that occupied by the urea samples was irradiated and counted under the same conditions. At a depth of 2 cm the counts from the carbon activation products was only 0.3% of the counts from N-14 activation products. Although at greater depths the interference from the carbon could be expected to increase, owing to the lower threshold energy for the carbon

reaction, it was expected to remain small and consequently no correction was made for the interference of carbon in the urea. All the counts were normalised to a delay and counting period of 100 and 700 seconds respectively, and the fast neutron fluence as a percentage of that at a 2 cm depth calculated from the activation of N-14 is displayed in Table 2.2 for a unilateral irradiation. Table 2.2 also lists the expected reduction in the fast neutron fluence due to the inverse square law effect. The fast neutron profile relative to that at a 2 cm depth has been calculated at an SSD of 5.4 m since this was the distance adopted for whole body irradiation for calcium measurements (59) and is therefore approximately the distance which would need to be adopted for whole body nitrogen studies. The fast neutron fluence profile for the unilateral irradiation enables the profiles for a bilateral irradiation to be calculated for any antero-posterior thickness up to 30 cm. Fig. 2.1 illustrates the calculated fast neutron profiles for a bilateral irradiation at four different thicknesses (SSD of 5.4m). The RMS variation from the mean is illustrated alongside the profiles. It can be seen that the uniformity of the fast neutron fluence through a patient will deteriorate with patient thickness. At 25 cm the RMS variation of the fluence was approximately $\pm$14.5%, which is an improvement on the values reported in Section 2.1 at this thickness when the inverse square law effect was removed. The improved uniformity is most probably a consequence of the higher maximum energy neutron source used at Edinburgh (up to 18 MeV) compared with the 14 MeV neutron generator used at the SURRC. The narrow energy spread of the neutrons from a 14 MeV generator means that the number of neutrons above the 11.3 MeV threshold energy of the nitrogen reaction will be

TABLE 2.2

FAST NEUTRON PROFILE FOR A UNILATERAL IRRADIATION OF A 30 cm THICK PHANTOM

Depth in Phantom	Fast Neutron Fluence at SSD = 1.25m	Inverse Square Law (ISQL) Fall-Off at		Fast Neutron Fluence at SSD = 5.4m (%)
		SSD = 1.25m	SSD = 5.4m	
2.0	100	100	100	100
5.2	75	95.1	98.8	78
8.5	56.3	90.5	97.6	60.7
11.7	41.1	86.3	96.5	45.9
15.0	30.3	82.3	95.4	35.1
18.3	21.5	78.5	94.2	25.8
21.5	15.7	75.2	93.2	19.5
24.8	11.4	71.9	92.1	14.6
28.0	8.7	68.9	91.1	11.5

All fast neutron fluence magnitudes are relative to that at a depth of 2 cm in the phantom

TABLE 2.3

UNILATERAL DETECTION SENSITIVITY PROFILE FOR THE EDINBURGH WHOLE BODY COUNTER TO ANNIHILATION RADIATION

Depth in Phantom (cm)	Relative Detection Sensitivity (%)
0	100
1.5	90.1
5.2	49.7
7.0	37.7
8.9	27.2
11.6	18.6
14.2	12.0
16.8	8.5
19.2	6.1
21.1	4.7
23.0	3.6
24.9	3.0
28.5	2.0
30.0	1.1

Fig. 2·1 Fast Neutron Flux Profiles with Depth in Four Phantoms of Different Thicknesses.

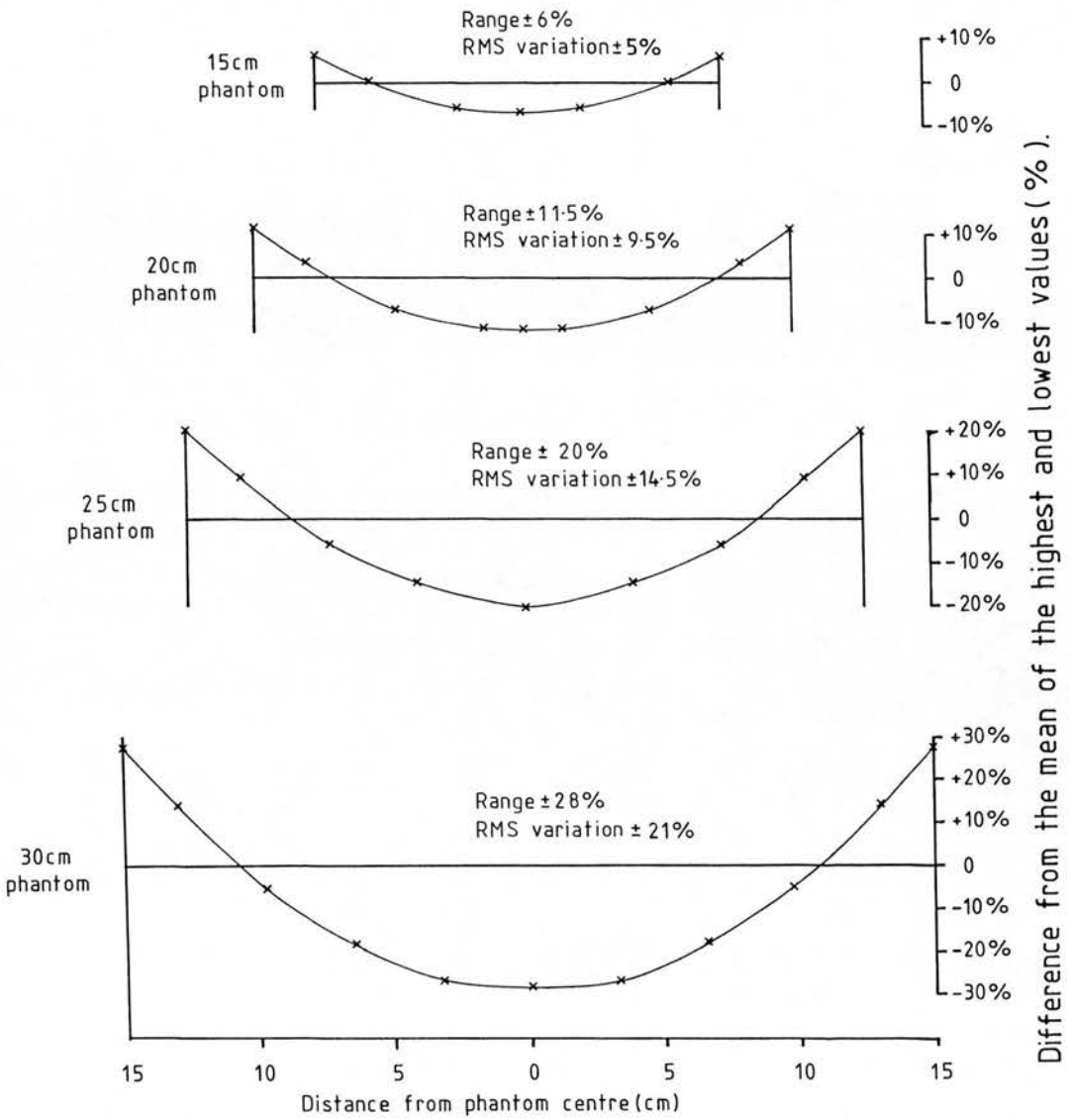

a strong function of depth i.e. rapid fall off of activation. However the greater energy spread of a cyclotron produced neutron source, coupled with the higher maximum energy, leads to a situation where the fall off of activation with depth is less steep.

b) Detection Sensitivity Profile

Counting of irradiated patients at Edinburgh would be performed in a shadow-shield whole body counter consisting of four 15 cm diameter by 10 cm thick sodium iodide detectors, two above and two below the patient. The detection sensitivity profile with depth for the whole body counter was determined by activating a hollow circular perspex phantom (external dimensions : 33 cm diameter x 3 cm deep, internal dimensions : 30 cm diameter x 1.8 cm deep) containing a concentrated solution of ammonium nitrate, in the cyclotron beam. The activated disc was quickly transferred to the whole body counter where it was placed at varying depths in a cylindrical perspex phantom (30 cm diameter x 30 cm deep - including the thickness of the activated disc). The detectors were in their shadow-shield position (62 cm apart), though only the bottom two detectors were used. This was because it was appreciated that for the majority of phantom thicknesses the top detectors would be further from the phantom than would the bottom detectors. This would normally lead to an asymmetrical detection sensitivity profile. However, it was considered more important to determine the profile for a unilateral detection geometry so that profiles could be generated for all phantom thicknesses on the assumption that the detectors would be placed equidistant from the phantom. The crystal separation of 62 cm

was chosen to reduce the inverse square law variation on the detection profile uniformity compared with shorter crystal separations. Although in practice the crystal separation may have to be reduced so as to increase the detected nitrogen counts despite the associated deterioration in the uniformity of the detection profile. The assumption was made that any interferences to the N-13 peak would be small and could be ignored, and consequently only normalisation of the detected annihilation counts to a common time was necessary.

The densities of perspex and water are 1.19 gcm^{-3} and 1 gcm^{-3} respectively. Perspex will therefore attenuate the annihilation radiation more severely than would water. This effect can be compensated for by considering the attenuation equation, viz:-

$$I = I_o \exp(-\mu_m p x)$$

where I = intensity of radiation at a point having traversed a thickness x of medium

I_o = intensity of radiation at the same point as I in air

μ_m = mass attenuation coefficient of the medium (cm^2g^{-1})

p = density of medium (gcm^{-3})

At 660 keV $\mu_m = 0.085\ cm^2g^{-1}$

Therefore $I_w = I_o \exp(-\mu_m x)$

and $I_p = I_o \exp(-1.19\mu_m x)$

where the suffixes $_w$ and $_p$ denote the media water and perspex respectively.

Therefore, dividing one equation by the other we obtain:-

$$I_w = I_p \exp(0.19\mu_m x)$$

This correction factor has been applied to the data obtained from the perspex phantom to determine the profile for unilateral detection for

a 30 cm thick water phantom. The data is displayed in Table 2.3 ; the detection sensitivities at 0 and 30 cm have been obtained from extrapolation of the profile depths and the data then normalised to the sensitivity at 0 cm. This data has enabled bilateral detection sensitivity profiles to be calculated for a range of phantom thicknesses (up to 30 cm) along with their RMS variation from the mean. These profiles are displayed in Fig. 2.2. It can be seen that the non-uniformity of the profiles, as expressed by the RMS variation, increased from ±18% at a thickness of 15 cm to ±55% at 30 cm. For a 25 cm thick phantom the RMS variation and the range of the detection sensitivity profile was ±43% and ±53% respectively. This profile displays a higher degree of non-uniformity than those measured at SURRC (RMS variation of ±25.5%) and Leeds (Range of ±23%). The reasons for these differences are presumably related to the detector distribution relative to the phantom in the whole body counters at the various centres. The source to skin distance (SSD) used for the detection sensitivity profile through a 25 cm thick phantom at SURRC was undisclosed. However, if it was performed with a 34 cm detector separation (Boddy et al, 17) then the SSD would have been approximately 4.5 cm. This SSD being shorter than the 15 cm used at Edinburgh, does not explain the improvement in the uniformity compared with the Edinburgh counter. The SSD used at Leeds varies for the different detectors because the whole body counter performs detection of a static phantom with 8 detectors distributed at various positions along the couch. The closest detectors, which therefore contribute the greater proportion of the counts, have a SSD of approximately 7 cm. The furthest detectors have an unknown SSD. The explanation for the improvement in uniformity at Leeds is unclear

Fig. 2·2 Detection Sensitivity Profiles with Depth in Four Phantoms of Different Thicknesses.

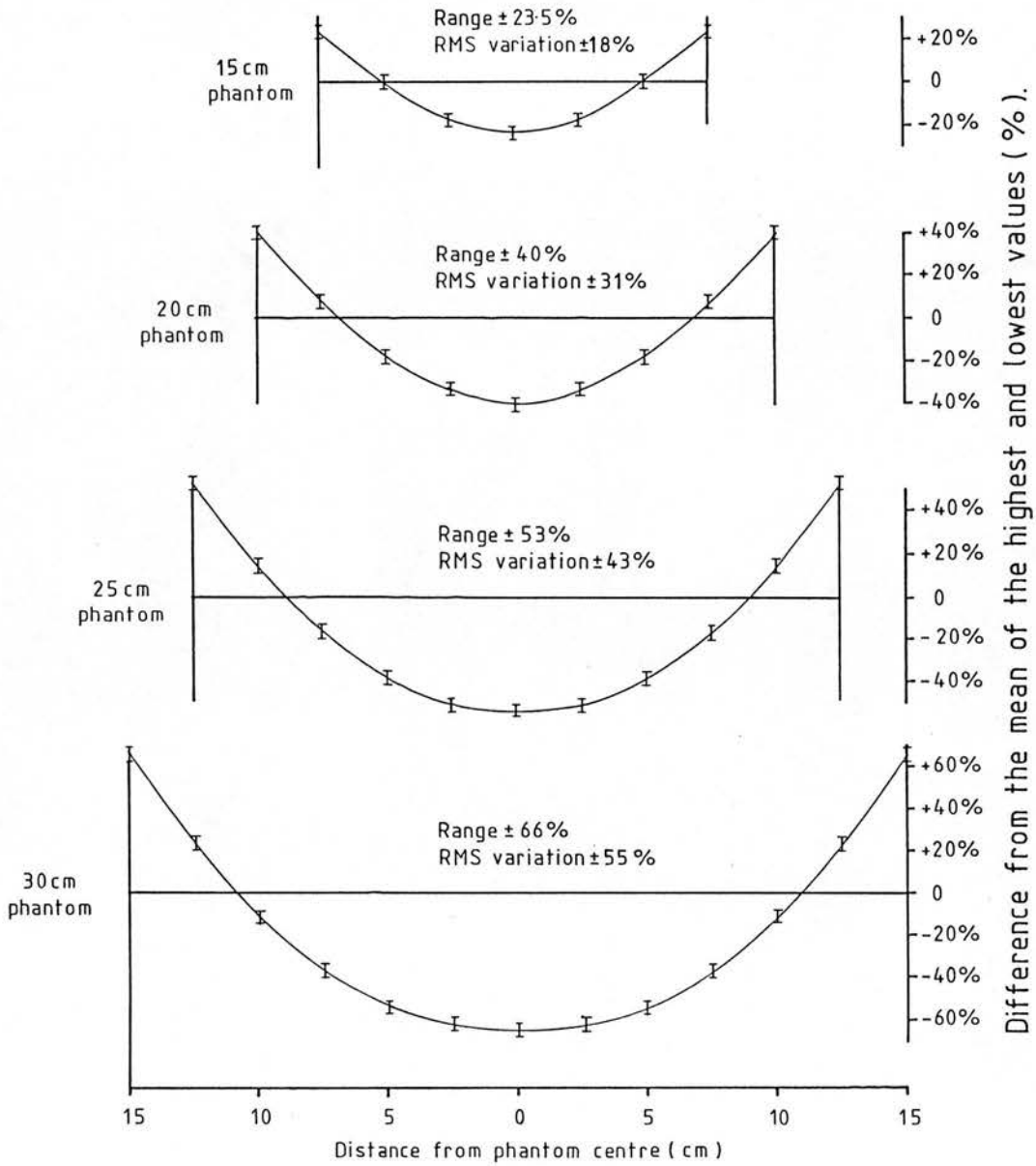

since it would be expected to be worse because of the shorter SSD.

c) Combined Activation/Detection Sensitivity Profile

The sensitivity with which nitrogen is measured at different positions within the body is dependent upon both the activation and detection sensitivity profiles. Combination of the experimentally determined profiles generated the combined sensitivity profiles for phantoms of different thicknesses shown in Fig. 2.3. The non-uniformity of the sensitivity of the measurement with depth increases with patient thickness. For a 25 cm thick patient the RMS non-uniformity of the measurement about the mean is ±58%. This value compares favourably with the ±81% calculated at Birmingham, though for reasons already discussed the difference cannot be explained since the details of the calculation for the detection sensitivity profile determination were not disclosed. The ±58% variation is higher than that determined at the SURRC of ±44%, the difference being mainly due to the difference in the detection sensitivity profiles.

These results indicate that 62% of the nitrogen counts arise from the outer 5 cm for a 25 cm thick patient. This compares with 55% calculated by McCarthy (69) and with Leach (63) who concluded that this region contributed all the measured counts.

Fig. 2·3
Combined Activation/Detection Sensitivity Profiles with Depth in Phantoms of Different Thicknesses.

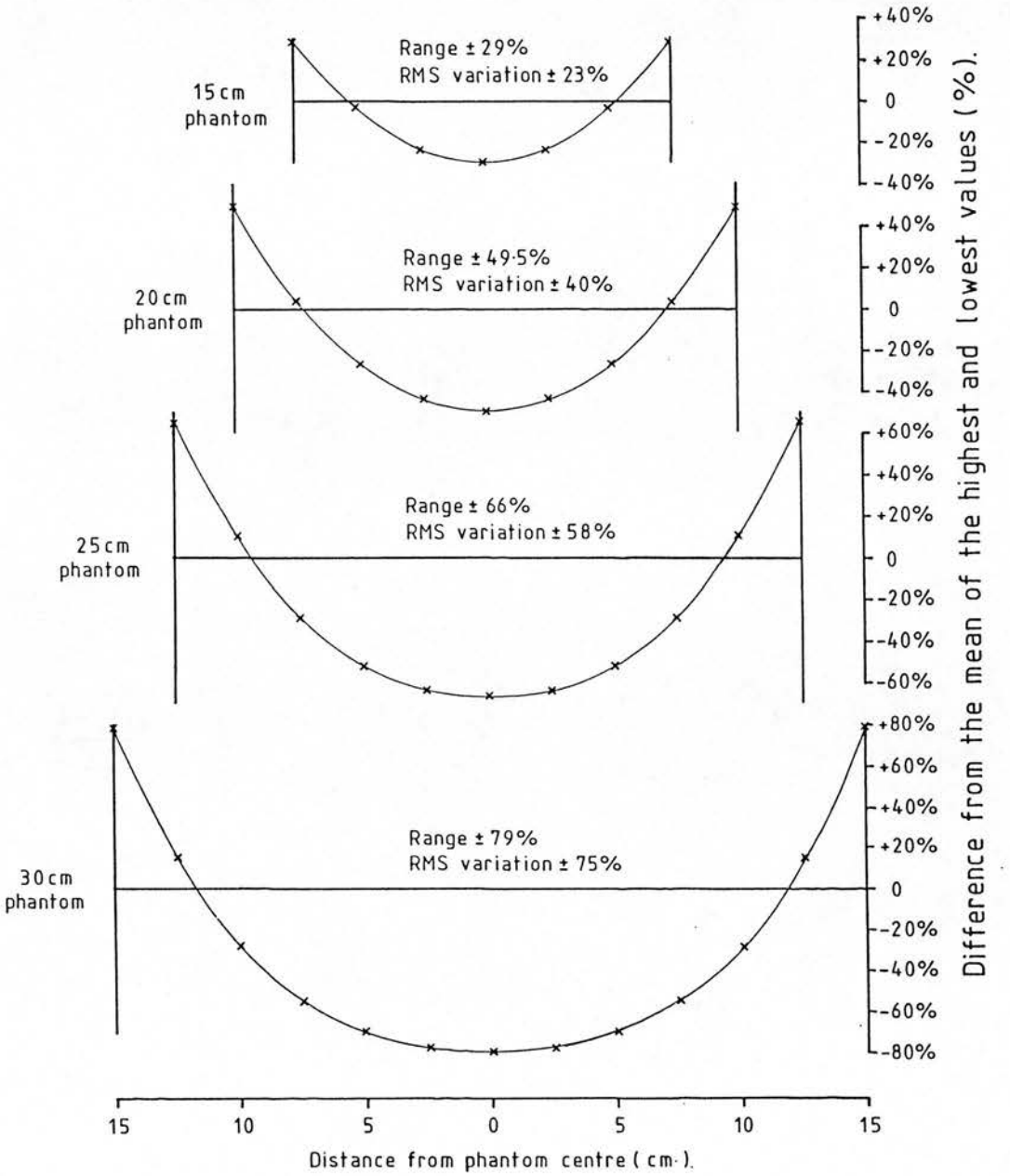

2.2.3 Estimated Coefficient of Variation and Body Dose of a Total Body Nitrogen Measurement Using the Delayed Technique

Calculation of the expected coefficient of variation (CoV) of a total body nitrogen measurement using the delayed technique would require detailed investigation of the level of interferences from all body elements. Such investigations would have been unjustified since the measurements were required only for comparative purposes with the prompt technique. Also, sufficient time may not have been available to complete the investigations given the rapid loss of staff from the cyclotron unit once closure had been announced.

An estimate of the CoV which could be expected to be obtained for a given dose imparted for a known irradiation period was calculated by comparison with the results presented by Spinks et al (88). These authors have estimated that a dose of 1 mGy delivered over a 30 second irradiation period would enable total body nitrogen to be measured with a CoV of $\pm$4%. The patient would be counted for 30 minutes in a ten crystal (15 cm x 10 cm NaI(Tl)) whole body counter following a 5 minute delay. The contribution to the overall CoV from counting statistics alone was $\pm$2.5%, leaving other variables responsible for $\pm$3.1% of the total CoV. This group used cyclotron produced neutrons having a maximum energy of 20 MeV and a mean energy of 7.5 MeV. The percentage interferences of the different product nuclides to the annihilation region were listed. The M.R.C. cyclotron at Edinburgh produced neutrons with a maximum energy of approximately 18 MeV having a mean energy of 5.9 MeV. The cyclotron neutron spectra can therefore be expected to alter the ratio of the

interfering reactions in the annihilation region compared with those ratios present when using 14 MeV neutron generators. For this reason it was assumed that the interfering reactions at Edinburgh would be in the same ratio to the counts from nitrogen as they were at Hammersmith (interfering nuclide counts = 3.35 x N-13 counts from nitrogen). Furthermore it was assumed that variables other than counting statistics would also be the same at Edinburgh as they were at Hammersmith ($\pm$3.1%). Only the natural background in the whole body counters was expected to differ as a consequence of their different designs.

The same data as was used in Section 2.2.1 to determine the level of the oxygen interference on the nitrogen counts was used to estimate the CoV which could be expected for a total body nitrogen measurement. The equations used are described in Appendix I.

Using equation (iii) of Appendix I the total N-13 counts from nitrogen normalised to the same irradiation and counting conditions as used at Hammersmith for a 2 m patient scan were 8908. These counts would be collected with the detection sensitivity profiles of Fig. 2.2. In order to determine the necessary nitrogen counts under these conditions to obtain a coefficient of variation due to counting statistics alone of $\pm$2.5% equation (ii) was used, where CV_c = $\pm$2.5% and C_B = 15260 (experimentally determined). This equation yielded C_N = 9520. The irradiation period required to produce this number of counts was calculated using equation (iii) where the delay and counting terms can be ignored. An irradiation period of approximately 32 seconds was calculated, which would yield a dose of

approximately 4 mGy at body entry surface. However, the dose varies little with depth and is therefore approximately equal to the whole body dose equivalent. Approximately 6% of this dose is from gamma radiation, the remainder being from neutron irradiation. Using quality factors of 10 and 1 for neutron and gamma radiation respectively, the whole body dose equivalent would be approximately 38 mSv. Therefore, it can be seen that with the Edinburgh set-up a dose of approximately 4 mGy would need to be given to determine total body nitrogen with a coefficient of variation of $\pm$4%. This compares unfavourably with an estimated dose of 1 mGy required in the Hammersmith set-up. The difference is expected to be caused by the difference in the counting conditions. At Hammersmith the whole body would be counted simultaneously by 10 crystals. However, at Edinburgh a scanning arrangement is necessary whereby only part of the body would be counted at any one time. For a 1 mGy dose at Edinburgh (necessary t_r = 8.2 s) total body nitrogen could be determined with a coefficient of variation of approximately $\pm$7%.

These coefficients of variation have been estimated for a crystal separation of 62 cm. However, increased sensitivity for the nitrogen counts could be achieved by decreasing the crystal separation and accepting the deterioration in the detection sensitivity profile uniformity. The minimum crystal separation possible with the whole body counter is 44 cm. With this separation the nitrogen counts determined for the Hammersmith irradiation and counting conditions increase to 23787. Repeating the calculations performed with the 62 cm crystal separation (C_n = 34330 for 44 cm crystal separation) it was calculated that a dose of approximately 1.8 mGy (corresponding to

a whole body dose equivalent of approximately 17 mSv) would be required to measure total body nitrogen with a coefficient of variation of $\pm$ 4%. Similarly a dose of 1 mGy would enable total body nitrogen to be measured with a coefficient of variation of approximately $\pm$ 5%. However, the required doses to measure total body nitrogen with a reasonable precision ($\leq$ 4%) are still significantly higher when using a cyclotron than those required with 14 MeV neutron generators (approximately 0.05 mGy). This difference is associated with the mean energy of the neutrons in the beam from the 14 MeV generator being above the threshold energy of the reaction, whereas the mean energy of the neutrons in both cyclotron beams is below this threshold energy. Additionally the counting geometry of the whole body counter will affect the dose required for a given precision.

This chapter has discussed the known problems of the delayed technique as regards the variation of response with position in the body and also the nature and extent of the interfering reactions. The oxygen interference to the nitrogen counts was determined experimentally to be approximately 18%, which is in close agreement to values quoted by other centres. The uniformities of the fast neutron fluence and detection sensitivity profiles with depth, as measured for the Edinburgh set-up have been compared with those reported by other groups. Whilst the uniformity of the activation profile has been better than that determined using 14 MeV neutron generators because of the higher neutron energies in the cyclotron spectrum, the detection sensitivity profile uniformity has been poor

compared with other centres. This latter difference cannot be explained. The combined activation/detection sensitivity profile indicates that 62% of the nitrogen counts would arise from the outer 5 cm for a 25 cm thick patient. Such large variations in the sensitivity of the measurement with distribution pose serious problems when nitrogen is to be measured for the total body. However, recognising these difficulties it was argued by Haywood et al (49) that in the combined response less than 25% of total body nitrogen is seriously under-represented. On the assumption then that it is possible to measure total body nitrogen with reasonable precision using the delayed technique the required dose to measure total body nitrogen with a coefficient of variation of $\pm$4% was calculated to be 1.8 mGy. This precision can only be achieved with additional loss of detection sensitivity uniformity with depth and the detectors of the whole body counter operated with minimum separation. In such circumstances an even larger proportion of the total nitrogen counts would have been generated from the outer 5 cm of a 25 cm thick patient. The composite sensitivity uniformity through a 22.5 cm thick phantom for the delayed technique compares unfavourably with that of the prompt technique using a bilateral irradiation geometry (RMS variation of $\pm$23.2%). The difference is caused by the poor tissue penetration of fast neutrons and the fact that the detection sensitivity varies in the same direction as the fast neutron flux. In consequence the prompt technique is better at measuring deep seated nitrogen than the delayed technique. In conclusion even when the problems of the interfering reactions and the variation of response with position in the patient are ignored, the delayed technique still appears a poor alternative to the prompt

technique in that the necessary dose required to measure total body nitrogen with reasonable precision is so much higher. Finally, the prompt technique is preferable for studies involving critically ill, intensive care patients.

CHAPTER 3

CHAPTER 3

PULSE PROCESSING SYSTEM

The detector shielding was to be designed to reduce the background in the nitrogen region as much as possible. In so doing the overall count rate at the detectors would be reduced. However, even after optimisation of the shielding materials the count rate at each detector was anticipated to be in excess of 50 kcps. Since the detectors were to be summed together at least some part of the nucleonics system must be able to handle count rates in excess of 100 kcps. In view of this fact due consideration was given to the pulse processing system. This chapter concerns itself with the design of dynode base divider networks for high count rates and with the choice of nucleonic systems. The principles behind alternative system designs are discussed and the results of experimental investigation reported. Finally, the nucleonic system determined to be most suited to the requirements of prompt neutron activation analysis is presented.

3.1 Detectors

The two 15.2 cm by 15.2 cm NaI(Tl) detectors were supplied by Nuclear Enterprises (Type 24AX16/DM1-5). Such large crystal volume is necessary to provide a high photopeak detection efficiency for the 10.8 MeV nitrogen gamma rays. Each detector had a full width at half maximum (FWHM) and full width at tenth maximum (FW10M) for ^{137}Cs of approximately 11.2% and 22.5% respectively. However, the resolution

Fig.3·1 Original Voltage Divider and Associated Preamp.

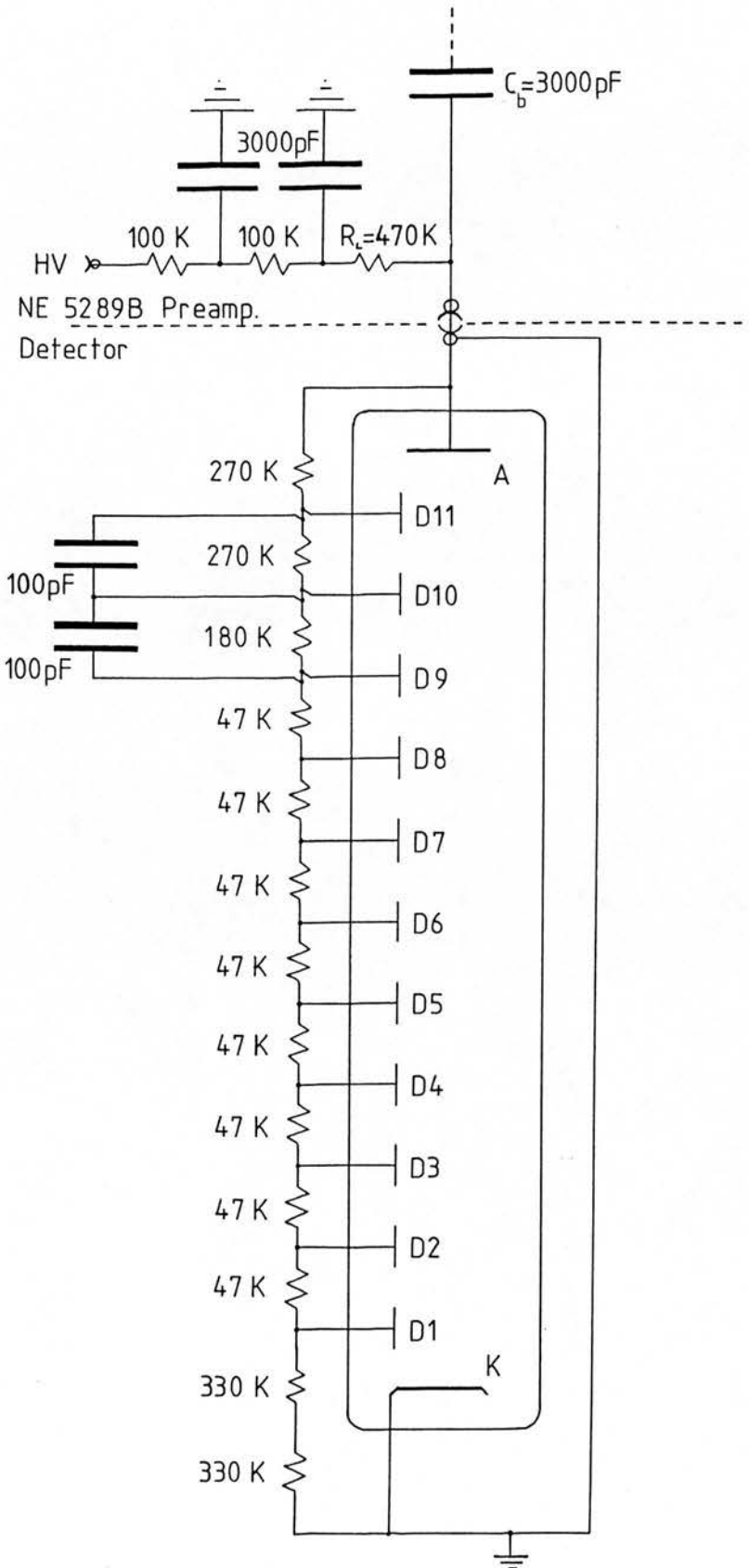

Fig. 3·2

Pulse Overshoot Associated with CR Networks

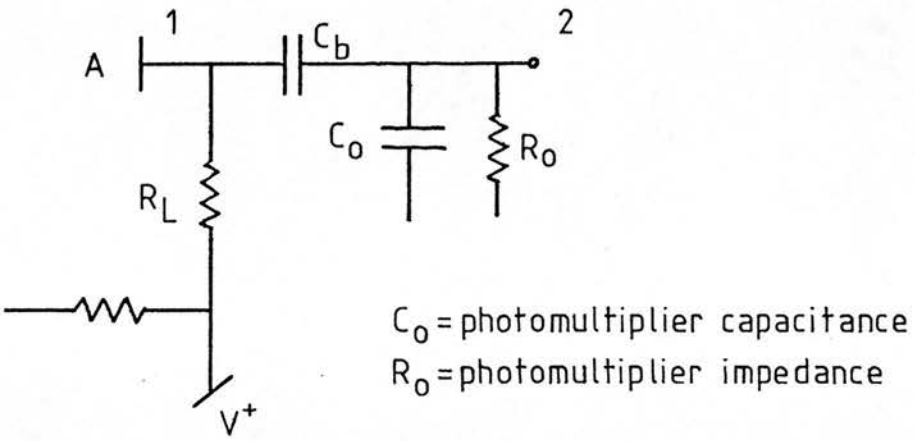

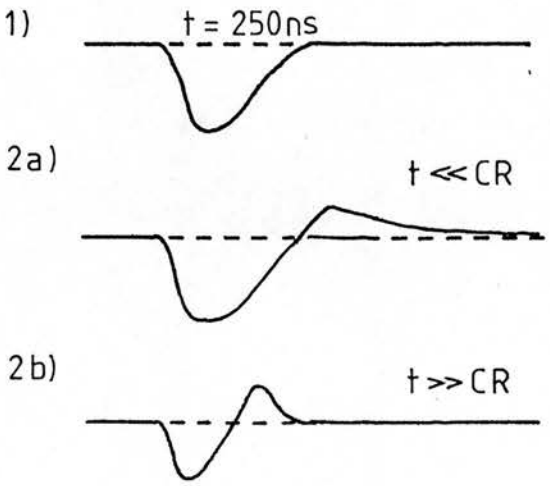

at higher energies was significantly poorer for one detector than for the other. The detectors have venetian blind photomultipliers, 13cm in diameter, EMI Type 9530A. The photomultiplier dynode base design and associated preamplifier, supplied with the detectors, is shown in Fig 3.1. The dynode base was designed to operate with the cathode earthed and the anode at a high positive potential; this mode of biasing a dynode chain is known as "anode high potential" (AHP). However, with this mode of operation it is necessary to isolate the anode signal output from the high voltage supply by use of a blocking capacitor, C_b. Capacitative coupling can affect the anode pulse shape depending on the resultant time constant of the circuit, CR. The effect of CR on the output pulse shape is depicted in Fig 3.2 where for simplicity only the effect of the blocking capacitor C_b, has been considered; 1) shows the signal pulse shape at the anode and 2a) and 2b) the resultant pulse shape after passage through the CR network for the cases where CR>>t (t being the decay time constant of the light source - 250 ns for NaI(Tl) and CR<<t respectively. When CR is much greater than t there is a long recovery to the baseline but a reduced overshoot compared with that when CR is much less than t and the rapid return to the baseline is accompanied by a large overshoot. The overshoots associated with capacitative coupling can cause the baseline of the output signal to shift with count rate. This form of distortion can be avoided by operating with the anode earthed (thus removing the need for the blocking capacitor) and running the cathode at a high negative potential; this mode of operation is known as "cathode high potential" (CHP). A dynode base was designed to be operated at CHP (see Appendix II) which would be stable at the count rates experienced during activation analysis (see Fig 3.3).

Fig. 3·3 Voltage Divider for Operation at Cathode High Potential

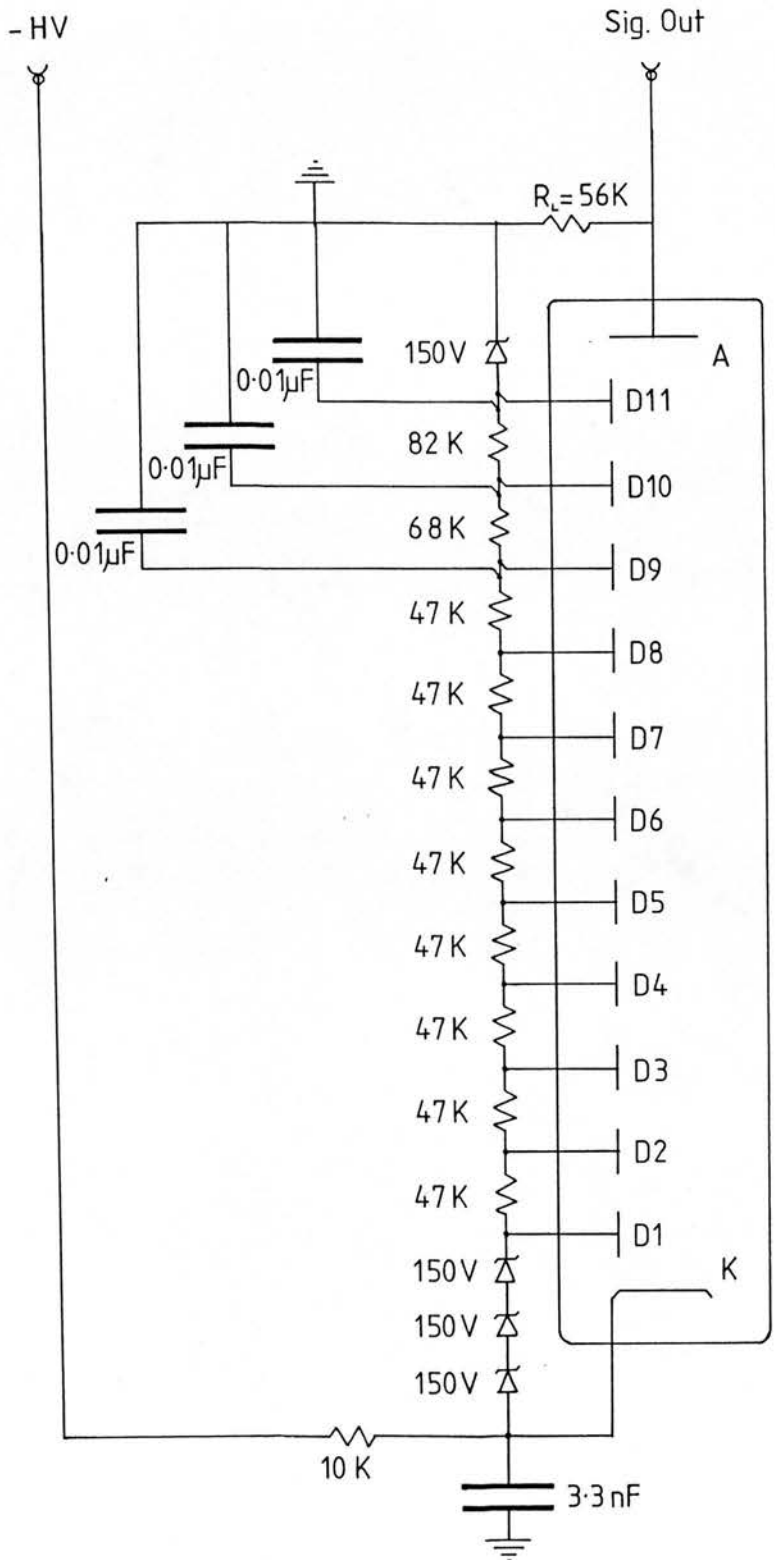

Since the two detectors would ultimately be coupled any differential drift in their gain would make measurement impossible. It was thought necessary therefore, to determine the gain stability under simulated operating conditions, especially over the initial forty minute period when counting was anticipated to occur. An experiment was conducted whereby the cathode and mu-metal shield of the detector were operated at -1250V. A 7μA mean anode current ($\bar{I}_a$) was generated from a source of ^{24}Na. ^{24}Na emits gamma rays at 1.37 MeV and 2.75 MeV in 100% of its disintegrations. The mean anode current was approximately 0.56% of the calculated current in the divider chain (I_D = 1.24mA). The gain change was observed from changes in the 1.37 MeV gamma ray peak position on an analyser. The percentage change in the gain was calculated from the difference in the peak position relative to that at the moment of introduction of the ^{24}Na source. Measurements were made at 10 minute intervals and the results plotted in Fig 3.4. It can be seen that the gain initially increased and then fell towards its initial value over the first 40 minutes. After this time the gain continued to fall and was still falling after 6.5 hours. This observation was in contrast with the manufacturers specification of a gain change of no more than 2% over a 24 hour period if a mean anode current of 10μA is maintained. Several possible causes of this phenomenon were investigated. Zener diodes are known to drift with temperature and whilst the small current flowing was not expected to cause significant heating effects this possibility was investigated by artificially increasing the temperature with a hot air gun. However, no temperature effect was noticed. To further exclude the zener diodes as the cause of the

Fig.3·4 Photomultiplier Gain Stability

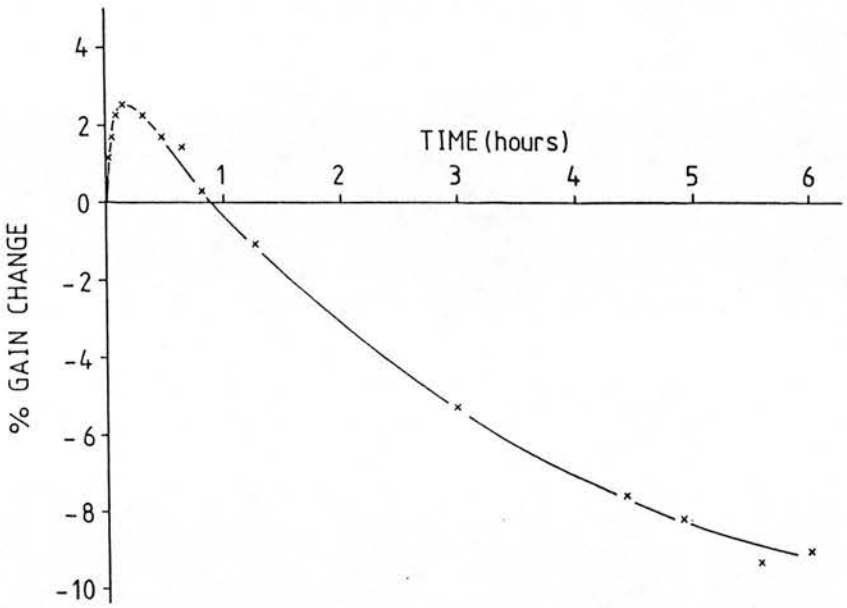

Fig.3·5

COUNT RATE THROUGHPUT CURVES FOR THE SPECTROSCOPY AMPLIFIER (UNI O/P) FOR DIFFERENT TIME CONSTANTS

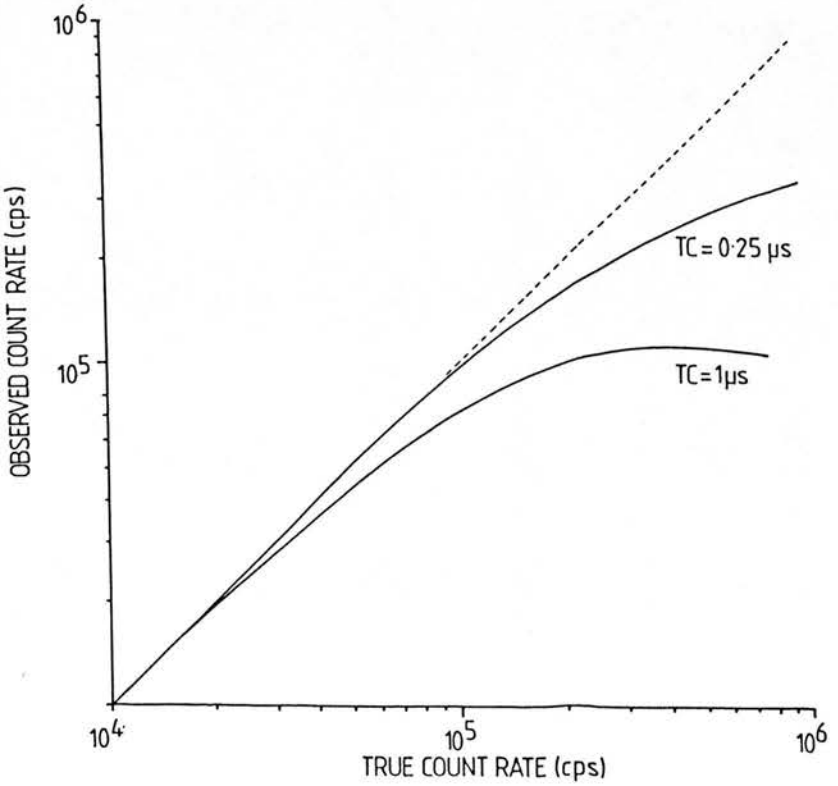

gain drift the diodes were replaced with resistors (150V zener ≡ 120kΩ and 450V zener ≡ 363kΩ at the operating voltage of -1250V). The same experiment was repeated on this now purely resistive chain but the same trend of gain changes was observed. To exclude the possiblity that a gradual redistribution of voltage along the divider network was occurring as a consequence of some temperature effect the voltages across the last two stage resistors (82kΩ and 120kΩ) were monitored under the above conditions. No measurable voltage change occurred throughout the 7 hour period, during which time the same gain change was observed as exhibited previously. Finally, to investigate the nucleonics as the possible cause of gain drift a ^{137}Cs source was observed at 2 kcps. No gain change was observed. This experiment also highlighted the problem as being current dependent. The problem was resolved by reducing the mean anode current to below 1μA by reducing the operating voltage. Indeed the problem was acknowledged in the following years EMI catalogue (PMC/86) where current dependent gain loss was attributed to a gradual change in the secondary electron emission coefficient of the dynodes caused by electron bombardment.

3.2 Pulse Processing System

3.2.1 Design Philosophy

In designing a pulse processing system there are two philosophies which may be adopted, viz:-

a) To allow pile-up to occur, detect and reject it.

b) To prevent pile-up throughout the system by keeping the pulses as short as possible.

With the first alternative the resolution can be optimised, though some pulses of interest (nitrogen) will be lost when they have piled-up with other pulses. With the second alternative all of the nitrogen pulses will be retained, but the resolution will deteriorate the shorter the time constant of the pulse. Whichever design philosophy is adopted will depend on the nature of the work to be undertaken. In the case of nitrogen determination by neutron activation analysis the nitrogen integral is large (9.75 MeV to 11.5 MeV). Consequently, the loss of a nitrogen pulse through pile-up with a low energy pulse which would have left the resultant pulse within the integration limits would be detrimental to the counting statistics. Furthermore, when using NaI small losses of resolution are unimportant and resolution may be sacrificed to improve the counting statistics.

3.2.2 Pile-Up Rejection Circuits

Pile-up rejection (PUR) circuits have evolved to reduce the spectral distortion caused by misplaced events. They are principally intended for use with semiconductor detectors where the long shaping time constants required to take advantage of the inherently good energy resolution lead to an increase in the degree of pulse pile-up. The most conventional design consists of a discriminator which triggers on each pulse and sets a reject state if two pulses are detected too close together, that is the second pulse arrives before the first one

has peaked and closed the linear gate. The limitation is the pulse pair resolution (PPR) of the pile-up rejection circuit. Pulses closer together than the PPR will cause an undetected event in the spectrum. Pulses further apart will lead to the first event being processed (no pile-up) and the second one either lost in the deadtime of the analogue-to-digital convertor (ADC) or processed (for much longer spacings than the ADC conversion time), as though the PUR was absent. Genuine coincident events (true sum peaks) cannot be detected by PUR circuits. The limitation of the pulse pair resolution ensures that as shorter amplifier time constants are used the period during which pile-up can be detected is reduced. Furthermore, for very short time constants only pulses which arrive close to the time to peak of the first pulse could be detected. Such timing relationships would have resulted in piled-up pulses which were only marginally misplaced in the energy spectrum. A major problem with PUR circuits is their ability to accurately extend the live time of the ADC to compensate for rejected pulses. Such limitations can make quantitative analysis of intensity inaccurate.

3.2.3 Pulse Shortening for Pile-Up Reduction

Pulse shortening can be achieved at the amplifier stage of a pulse processing system. As the time constant of an amplifier is shortened more rapid return to the baseline is achieved, which is a requirement for high count rate work. However, signal quality is degraded because too much noise is allowed through the amplifier. The optimum signal to noise ratio is provided by Gaussian shaping. This technique involves one pulse differentiation followed by several

stages of active integrator filtering, all set to the same cut off frequency (the shaping time constant). Such shaping is provided by "Spectroscopy Amplifiers", for which the Canberra model 2020 offers a time constant as low as 0.25μs. The probability of pile-up is also dependent on the baseline restoration of the amplifiers, whereby the unipolar output pulse is returned to its reference ground level. Bipolar output pulses return the pulse immediately to the baseline and are consequently the more usual choice in high count rate applications. A similarly quick return to the baseline is provided by "Double Delay Line Amplifiers". A delay line inverts the preamplifiers signal and delays it (delay determined by the length of the delay line) before adding it to the original signal. The output is therefore cancelled after the rising edge signal has been passed. A double delay line amplifier repeats the process, resulting in a bipolar output. Since the rising edge is passed without modification and the baseline is achieved rapidly, the delay line amplifier is useful in high count rate applications.

The effect of time constant on countrate throughput performance was demonstrated by a decay experiment involving ^{113m}In (a 392keV gamma ray emitter with a $T_{\frac{1}{2}}$ of 99.5 min). The observed countrate was plotted against the true countrate (determined by extrapolation of the linear portion of the decay curve) for time constants of 0.25μs and 1μs for a unipolar output of a "Canberra 2020 Spectroscopy Amplifier" (see Fig.3.5). It can be seen that for the shorter time constant counts begin to be lost at a higher countrate and that at any true countrate above this fewer counts are lost compared with the longer time constant. A similar experiment was performed to compare

the bipolar output (TC = 0.25μs) of the spectroscopy amplifier with the output of a "Canberra 1411 Double Delay Line Amplifier" (DDL). The spectroscopy amplifier gave slightly better performance, presumably as a result of its slightly shorter pulse width (approximately 2.5μs compared with 3μs). The spectroscopy amplifier was therefore chosen for use with the clinical apparatus.

3.2.4 Pulse Processing System Design

Initial System Design

The philosophy behind the system design was to minimise pile-up throughout the system by minimising the pulse width. An attempt at reducing the deadtime at the multichannel analyser (MCA) was also to be made. This would be achieved by dividing the entire spectrum by an optional 10 or 100 so that fewer pulses would be presented to the ADC (analogue to digital converter). The division process would reduce the MCA deadtime, so enabling shorter collection periods for the acquisition of a set count, whilst retaining the counting statistics of an undivided spectrum. The theory behind the system operation is as follows (see Fig 3.6):-

a) The two detector outputs would be integrated in charge sensitive preamplifiers and then summed at a signal junction box.

b) One output of the signal junction box would feed a single channel analyser/discriminator which would generate a logic pulse for every input pulse above its lower level discriminator (set just

Fig.3·6 Initial Pulse Processing System Design

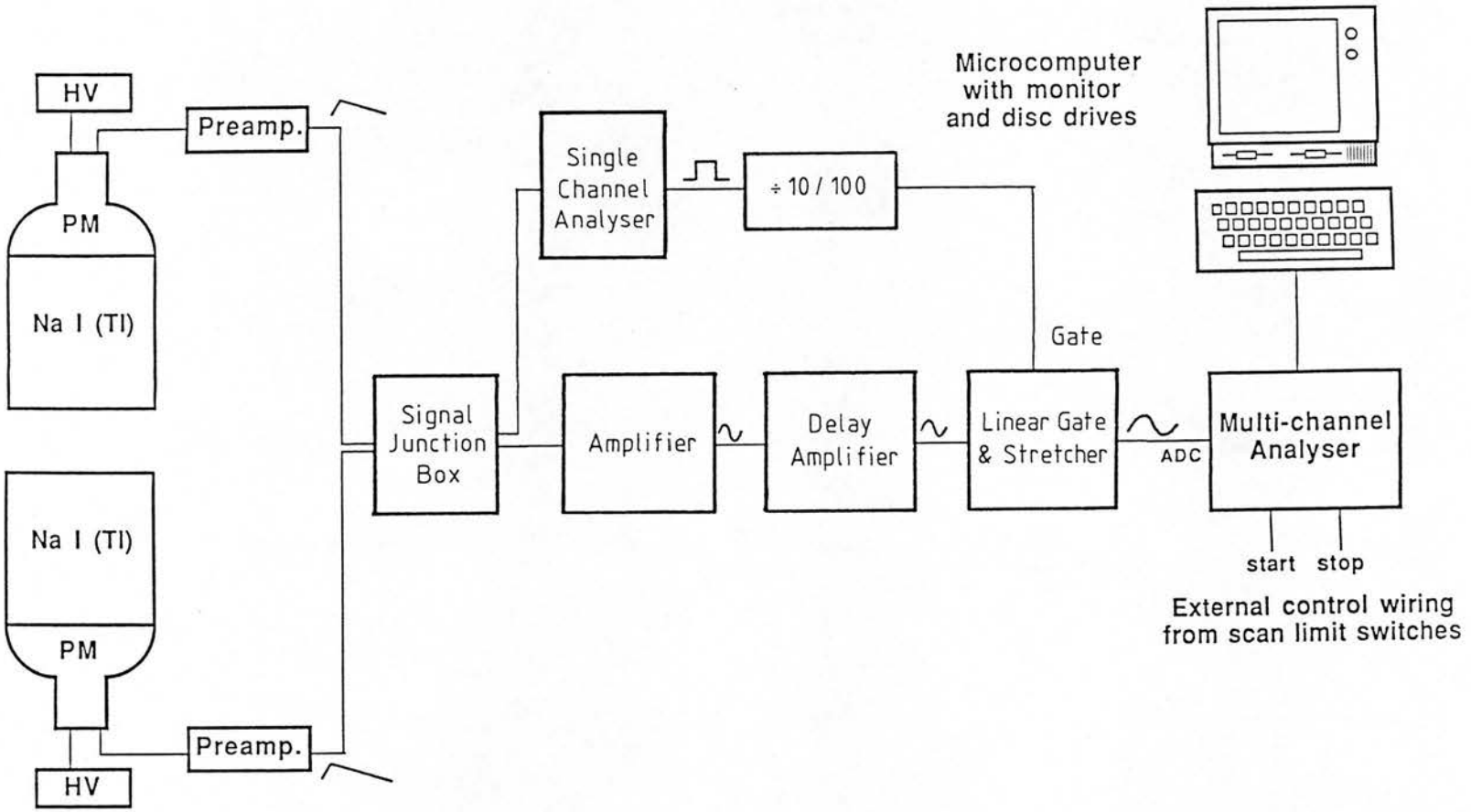

above noise level).

c) The number of logic pulses would be reduced to 1 in 10 or 100 dependent on the setting of a divider unit built by the electronics section of this department.

d) The second output of the junction box would provide the input to an amplifier chosen for its short time constants and good baseline restoration.

e) The analogue pulse will need to be delayed to maintain the timing coincidence of the analogue and logic pulses; this is achieved by a "Delay Amplifier".

f) The "Linear Gate and Stretcher" serves two functions. Firstly, it can stretch the analogue pulse width to allow proper operation of the ADC. Secondly, the unit can be gated with the logic pulses so that only one tenth or one hundredth of the total counts are presented to the MCA for digitization.

The countrate performance of the system was investigated using the "Canberra 2020 Spectroscopy Amplifier" with a bipolar output pulse and a 0.25μs time constant. A "Canberra 2037A Edge/Crossover Timing Single Channel Analyser" was used in crossover mode to generate logic pulses for division by the divider unit. The timing relationship between the analogue and logic pulses at a "Canberra 1454 Linear Gate and Stretcher" was maintained by a "Canberra 1457 Delay Amplifier". Countrate throughput measurements were again made with ^{113m}In. Both

the delay amplifier and the linear gate and stretcher were found to introduce deterioration in the countrate performance through the increase in the pulse width caused by both units, even when operated with minimum delay or "stretch" settings. Additionally, gating the stretcher unit with only one in 10 or 100 logic pulses produced no gain in the countrate performance. This was found to be due to the fact that the gate at this unit operates at the output rather than the input. Such serious count losses as imposed by those additional units considered necessary for gating, must be counterbalanced by the reduction in analyser deadtime to be gained by gating the spectrum. The "Linear Gate and Stretcher" proved superfluous to the system since the MCA could handle the amplifier pulses directly without loss of linearity. If the MCA was gated directly, then the count rate capability of the system would be significantly increased. An experiment was performed to determine the effect of gating the MCA input on the deadtime. The detector was exposed to a ^{226}Ra source. The counts were accumulated in 512 channels of the MCA memory. The system gain was modified to ensure that all counts were above the lower level discriminator. The resultant measured count rate and analyser deadtime for ungated and gated spectra are shown in Table 3.1 for two different detector count rates. It can be seen from Table 3.1 that no further reduction in the MCA deadtime was achieved when dividing the number of logic pulses by more than 10. This effect can be understood by an examintion of the operation of the analyser digitization process as depicted in Fig 3.7. All input pulses to the analyser are inspected to determine whether or not they lie within the lower and upper discriminator levels. The time allocated to examination of each input pulse (linear gate period) is

TABLE 3.1

EFFECT ON ANALYSER DEADTIME FROM GATING

Gated/Ungated	Count Rate (cps)	Deadtime (%)
Ungated	350,000	60
Gated/ ÷ 10	35,000	30
Gated/ ÷ 100	3,500	30
Ungated	160,000	30
Gated/ ÷ 10	16,000	10
Gated/ ÷ 100	1,600	10

TABLE 3.2

SIGNAL:NOISE RATIO FOR AMPLIFIER-TO-ANALYSER COMBINATIONS

	N	Bgd(B)	N:B	DT(%)
Both detectors via Mixer to Amplifier and single ADC				
Spec.Amp.(TC=0.25μs) Bipolar	10967	5796	1.89	9.6
DDL (1μs)	13681	11418	1.20	19.7
DDL (0.4μs)	11435	4741	2.41	4.0
Each detector to separate Amplifier and separate ADC				
Spec.Amp.(0.25μs)	5732	2026		3.4
DDL (0.4μs)	+5290	+1779		2.1
	=11022	=3805	2.90	

Fig.3·7

DIGITIZATION OF AN INPUT PULSE

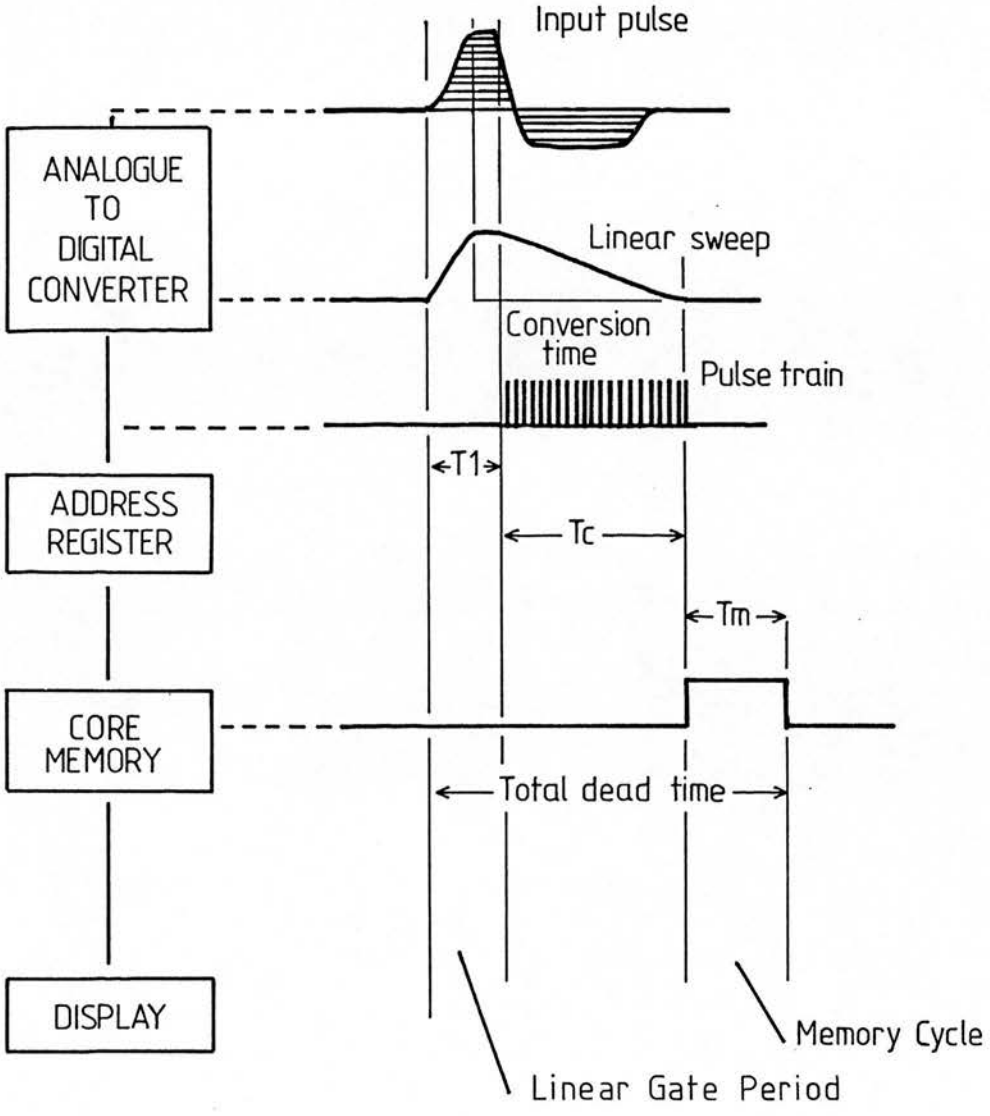

set at T1. Only after this point does the gate logic affect the analyser operation, in determining whether or not an analysed pulse should be digitized. Therefore, the deadtime contribution from T1 is fixed by the analyser input count rate. The deadtime contributions from Tc and Tm are variable for a given energy spectrum dependant on the gating logic. Considering the detector count rate of 350,000 cps the deadtime was reduced when the analyser was gated by 1 in 10 logic pulses. However, no further reduction in deadtime occurred when the analyser was gated by only 1 in 100 logic pulses. This infers that when gated by 1 in 10 logic pulses the majority of analyser deadtime was from T1 contributions from the 350,000 cps, with a much smaller deadtime contribution arising from the 35,000 cps which were being digitized. Consequently, a further reduction in the number of pulses being digitized made a negligible difference to the overall analyser deadtime. In the experimental situation during the accumulation of a prompt nitrogen spectrum the analyser deadtime will be reduced by raising the lower level disciminator (LLD) to just below the hydrogen peak. This practice reduces the deadtime by reducing the number of pulses being digitized. However, even pulses below the LLD will still be contributing to the deadtime through T1. In the case of a prompt nitrogen spectrum only approximately 12% of the total counts will be above the LLD. It is reasonable to assume, therefore, that the reduction in deadtime that could be achieved by gating would be negligible.

The initial nucleonic system design has been shown to be subject to many unforeseen problems. The design was therefore reconsidered, attempting to retain the philosophy of reducing pulse pile-up by

keeping pulses as short as possible whilst discarding attempts to reduce analyser deadtime by gating.

Adopted System Design

The nucleonic configuration adopted for the prompt nitrogen measurement system is shown in Fig 3.8. The system is now extremely simple in design. The dynode base divider network has already been described. The anode pulses are integrated by a "Canberra 2005 Charge-Sensitive Preamplifier", to yield a voltage pulse with an amplitude proportional to the integrated charge output of the detector. The two preamplifier outputs must be summed; achieved here by an "NE 4618 Mixer". The "Mixer" output feeds the "2020 Spectroscopy Amplifier" which has been shown to provide the maximum count rate capability of those amplifiers investigated. The bipolar output of this amplifier provides the analyser input. The external control wiring to the "Start Collect" and "Stop Collect" pins of the analyser are also shown in Fig 3.8. These signals are generated from microswitches marking the scan limits on the patient couch. The effect of the addition of the "Mixer" on the count rate capability of the system was investigated with both one and two detector/preamplifier combinations included in the system. The count rate capability was observed to be the same as that determined for the amplifier alone.

This nucleonic configuration is that which was employed for the shielding experiments as well as for the final patient apparatus.

Fig.3·8 Adopted Pulse Processing System

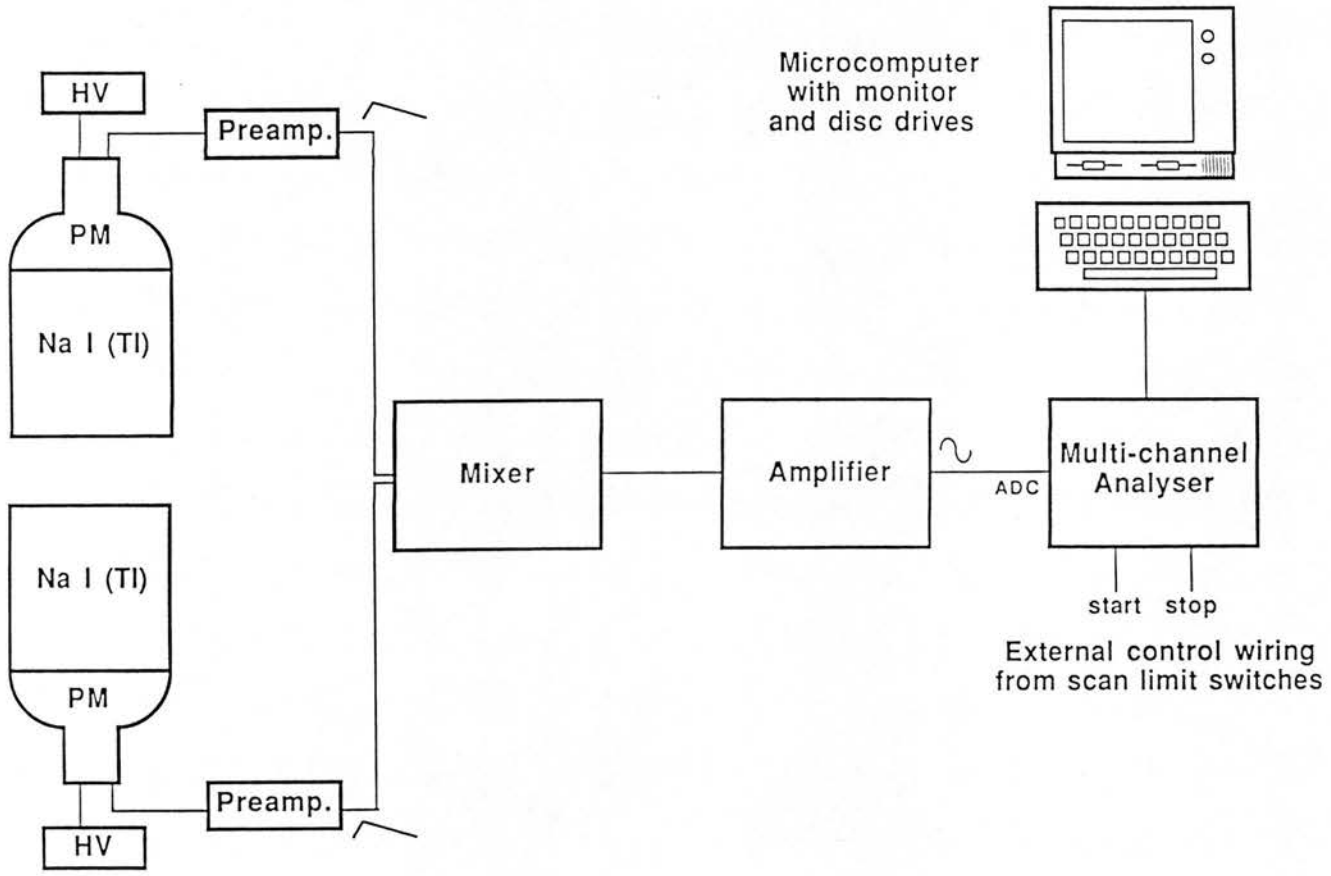

3.2.5 Pulse Processing System Improvements

Since the completion of the clinical apparatus and the normal study several alterations have been made to improve the performance of the pulse processing system. These improvements are best illustrated with reference to the signal:noise ratio obtained using 30 litre phantoms, containing either tissue equivalent or nitrogen-free tissue equivalent solution, with the clinical apparatus (see Table 3.2). A double delay line amplifier has been acquired with a shorter delay line than that used in the previous discussions (0.4μs compared with 1μs); the pulse width is therefore correspondingly shorter. Additionally since much experimental evidence had pointed to a large pile-up contribution in the nitrogen region separate 100MHz ADC's were acquired so that each detector could have a separate pulse processing system; only the 3μs memory cycle time of the analyser being shared. Table 3.2 illustrates the net nitrogen counts (N), background counts (B), signal:noise ratio (N:B) and analyser deadtime (DT) obtained for a live time acquisition of 2400 seconds. Significant improvements in the signal:noise ratio were obtained with the shorter pulses from the double delay line amplifier (0.4μs) (results for the previously discussed DDL amplifier (1μs) have also been included for comparison) compared with the bipolar pulse from the spectroscopy amplifier. Additional improvement, as expected, was obtained from separate pulse processing lines for each detector. The improvement in the deadtime of the analyser is in agreement with the trends for the signal:noise ratio. The improvements achieved with these modifications are additional evidence in support of a large proportion of the nitrogen background being due to piled-up pulses.

CHAPTER 4

CHAPTER 4

NEUTRON SOURCES, IRRADIATION AREA AND WHOLE BODY DOSE EQUIVALENT

This chapter describes the physical characteristics of Californium-252, the neutron source adopted for the construction of clinical apparatus for the measurement of total body protein, and compares these charactaristics with those of alternative radio-isotopic neutron sources. The activation room where the apparatus is housed is described. Finally the method of calculation of the whole body dose equivalent imparted for a 40 minute measurement in the apparatus is described.

4.1 Neutron Sources

4.1.1 Californium-252

Two Californium-252 sources, each having an activity of 252 MBq (equivalent to 2.9×10^7 neutrons per second) in May 1987, are used in the apparatus to measure total body nitrogen by prompt neutron activation analysis. The sources are doubly encapsulated in welded stainless steel capsules. Californium-252 produces a typical fission neutron spectrum which can be approximately represented by the Watt formula:-

$$N(E) = E^{\frac{1}{2}} \exp(-E/1.39)$$

where $N(E)$ = fraction of neutrons per unit energy range

E = neutron energy (MeV)

Fig.4·1 Neutron Energy Spectra for Radionuclide Sources

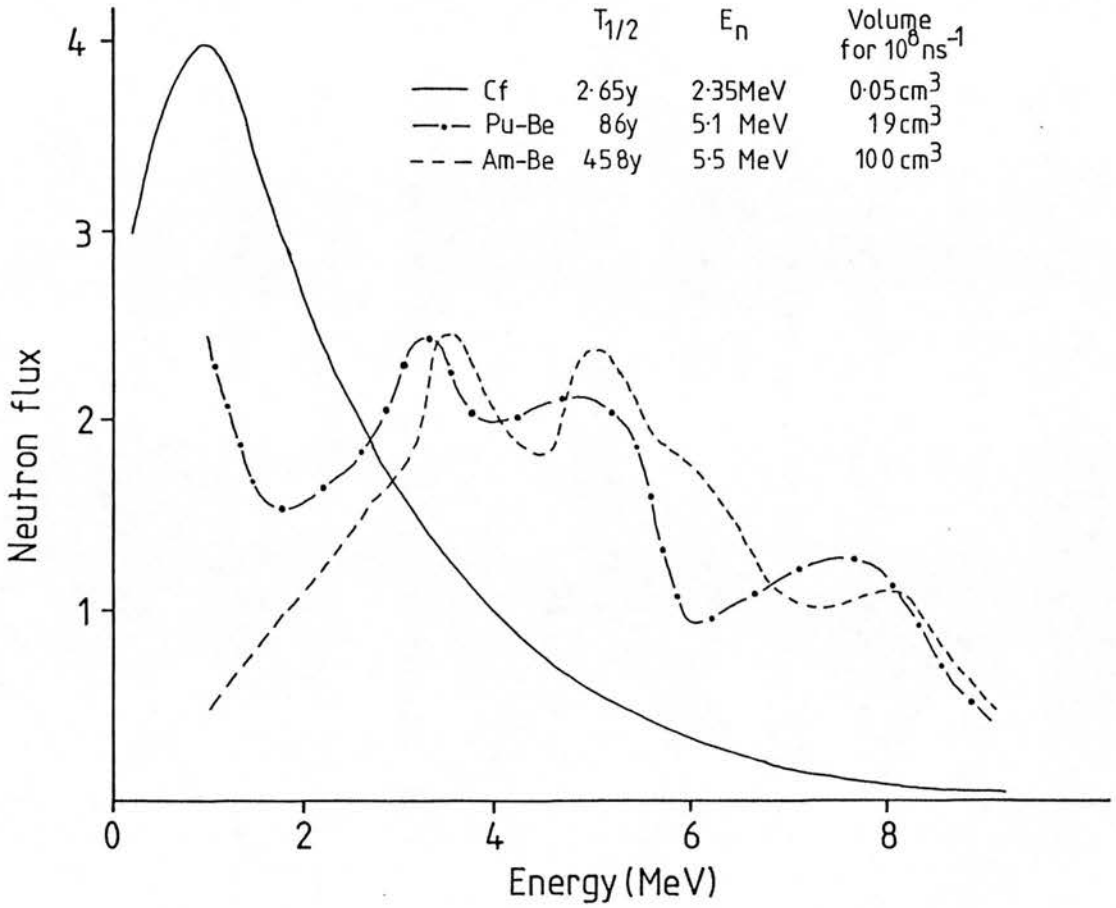

Reproduced with kind permission from Smith (85)

1.39 = Maxwellian "temperature". 1.39 ±0.03 is the weighted average of 8 values reported in the literature (Pauw,81)

The neutron spectrum is shown in Fig.4.1 along with the neutron spectra of Plutonium-Beryllium (Pu-Be) and Americium-Beryllium (Am-Be) sources. Californium-252 has a mean neutron energy of approximately 2.35 MeV and an effective half-life (combination of 96.9% alpha decay and 3.1% spontaneous fission) of 2.65 y (Amersham). 5.7 gamma rays are emitted per neutron between 0.6 and 5 MeV.

4.1.2 The Advantages and Disadvantages of Californium-252 over Alternative Neutron Sources for Prompt Gamma Neutron Activation Analysis

Advantages

The lower mean neutron energy of Californium-252 (^{252}Cf) source neutrons over alternative neutron sources (^{241}Am-Be, ^{238}Pu-Be) gives ^{252}Cf advantages for prompt gamma analysis. A comparison of ^{252}Cf and ^{238}Pu-Be neutron sources for partial body in vivo activation analysis has been carried out by Morgan et al (76). The study listed several advantages of ^{252}Cf over a ^{238}Pu-Be source. These advantages will also apply for ^{252}Cf over ^{241}Am-Be since ^{238}Pu-Be and ^{241}Am-Be neutron sources have similar neutron energy spectra and mean neutron energy. These advantages are as follows:-

a) ^{252}Cf generates nearly 40% more thermal neutron fluence in the patient per incident neutron dose. This is a consequence of the lower mean neutron energy of ^{252}Cf.

b) The fast neutron shielding is more effective in reducing the neutrons from ^{252}Cf which reach the patient and detector. Again, this is a consequence of the lower mean neutron energy of ^{252}Cf.

c) ^{252}Cf has a smaller physical size for the same neutron output, so enabling more effective collimation and easing the pneumatics of the source delivery system. A comparison of the volume per neutron output is given in Fig.4.1.

d) ^{252}Cf has less stringent transport regulations, which is important when considering mobile facilities.

Additionally the dose rate from the gamma ray emissions is significantly lower for ^{252}Cf compared with alternative sources.

Disadvantages

The lower mean neutron energy of ^{252}Cf neutrons which is responsible for two of its advantages for prompt gamma neutron activation analysis over alternative sources, is also responsible for its major disadvantage for whole body studies (see a) below). The disadvantages of ^{252}Cf over alternative radio-isotopic neutron sources are:-

a) The relative thermal neutron flux with depth in a phantom falls off more rapidly for ^{252}Cf. Consequently it is more difficult to achieve a uniform activation profile through body sections.

b) ^{252}Cf has a relatively short half-life of 2.65 years compared with 86 years and 458 years for ^{238}Pu-Be and ^{241}Am-Be respectively. This difference will necessitate increasing the irradiation period with time if the same counting statistics are to be maintained for the measurement.

4.2 Irradiation Area

The "Neutron Activation Room" is sited on the lower ground floor of the Western General Hospital. The room was enlarged to its present size to accommodate the patient apparatus (see Fig.4.2). The shielding wall consists of 11 cm of paraffin wax sandwiched between 3 inch breezeblock. This wall affords protection to the operator during subject measurements. Wax was also placed in the ceiling space above the apparatus to reduce the dose rate in the ward above. These precautions reduced the dose rate in the corridor and in the ward above to negligible levels when the sources were in their irradiation positions. The neutron sources are stored 3 m below ground in the concrete floor at the position marked by the neutron portal. The ^{252}Cf sources are taken to and from the shielding apparatus by a pneumatic delivery system, depicted in Fig.4.3. A control box for raising and lowering the sources is positioned on the shielding wall (see Fig.4.2). The sources are automatically withdrawn at the end of the irradiation period by the scanning bed control wiring.

Fig.4·2 Irradiation Area

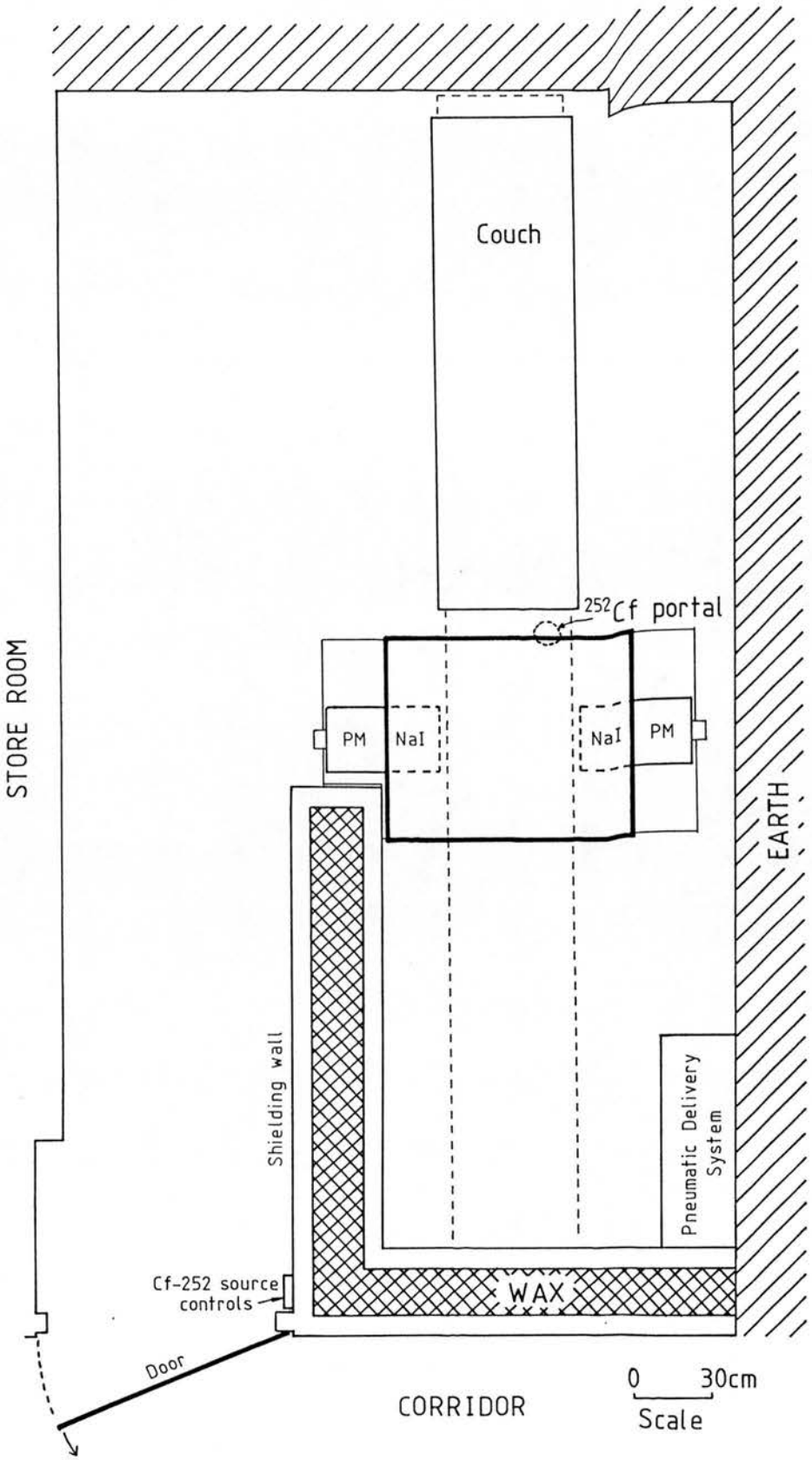

Fig.4·3 Pneumatic Delivery System

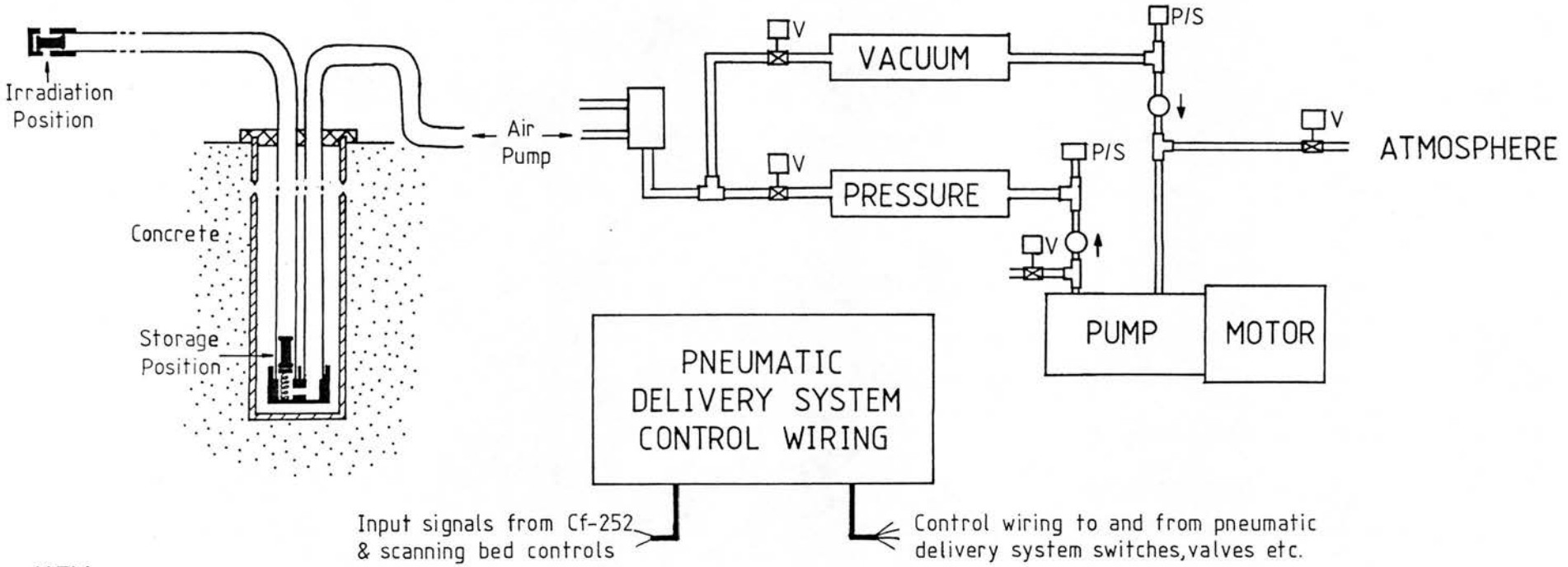

KEY

Non-return valve (arrow indicating direction of permitted flow)

V Electro-magnetic valve

Pressure switch

4.3 Whole Body Dose Equivalent

4.3.1 Neutron Activation

Neutron and gamma ray dose equivalents from the neutron activation of nitrogen were estimated with neutron and gamma ray badges positioned in their holders at five depths in a hardboard thorax phantom (minor axis = 19 cm, major axis = 30 cm, length = 49.5 cm). The phantom was scanned repeatedly for 19 hours and the dose was averaged over the whole body by scaling for mass. Values of 0.11 mSv for neutrons and 0.035 mSv for gamma radiation were estimated, using quality factors of 10 and 1 for neutron and gamma radiation respectively, for a 40 minute measurement. This radiation dose will decrease with the decay of the ^{252}Cf neutron source.

4.3.2 Tritiated Water

Calculation of the total body protein compartment requires an independent estimate of the hydrogen compartment. This requires the measurement of the total body water compartment which is estimated from an isotope dilution technique using tritiated water. 2 MBq are given by oral administration. The effective dose equivalent from the resultant beta particle irradiation was taken from dose tables prepared by the Administration of Radioactive Substances Advisory Committee (ARSAC) as being 0.03 mSv.

The resultant whole body dose equivalent from the protein measurement was calculated to be approximately 0.175 mSv in May, 1987.

In the study of total body nitrogen by prompt neutron activation analysis ^{252}Cf will impart a reduced neutron dose to the patient for the same thermal neutron fluence compared with alternative radio-isotopic neutron sources. However, the relatively short half-life of the source will require longer irradiation periods or a reducing source-to-skin distance with time if the same counting statistics are to be maintained. The importance of the poorer uniformity of the thermal neutron flux profile through the body compared with higher energy neutron sources is reduced by the use of hydrogen as an internal standard in the prompt measurement of nitrogen. Despite the apparent suitability of ^{252}Cf for total body nitrogen measurements this thesis describes the first purpose built apparatus, dedicated to this measurement, designed for use with this radio-isotopic neutron source. However, apparatus built at Swansea for multi-element analysis also uses ^{252}Cf and is currently being calibrated to measure total body nitrogen.

CHAPTER 5

CHAPTER 5

THE PROMPT NITROGEN SPECTRUM

A typical prompt nitrogen spectrum can be seen in Fig 5.1. This chapter discusses the reactions which create this spectrum. Particular attention is paid to the source of the nitrogen background. Possible reactions which could eventually generate a scintillation light pulse equivalent to that corresponding to a 9.5 MeV gamma ray in the crystal are investigated, and evidence is presented for the contribution of piled-up pulses to the nitrogen background.

5.1 Contributing Reactions to the Prompt Spectrum

a). Fast Neutron Inelastic Scattering - (n,n'γ)

Inelastic scattering with intermediate or heavy nuclei is important for neutrons with energies above 1 MeV, but becomes practically negligible below this energy. In this process the neutron and scattering nucleus form a temporary compound nucleus which then emits the neutron with reduced energy. The scattering is inelastic because the kinetic energy of the incident neutron has not simply been shared as kinetic energy between the scattered neutron and the recoiling target nucleus, but has also excited the target nucleus above its ground energy level. The excitation energy will be lost by the target nucleus in returning to its ground state by the emission of one or more gamma rays. It follows that gamma rays generated through

Fig. 5·1 A Typical Prompt Nitrogen Spectrum

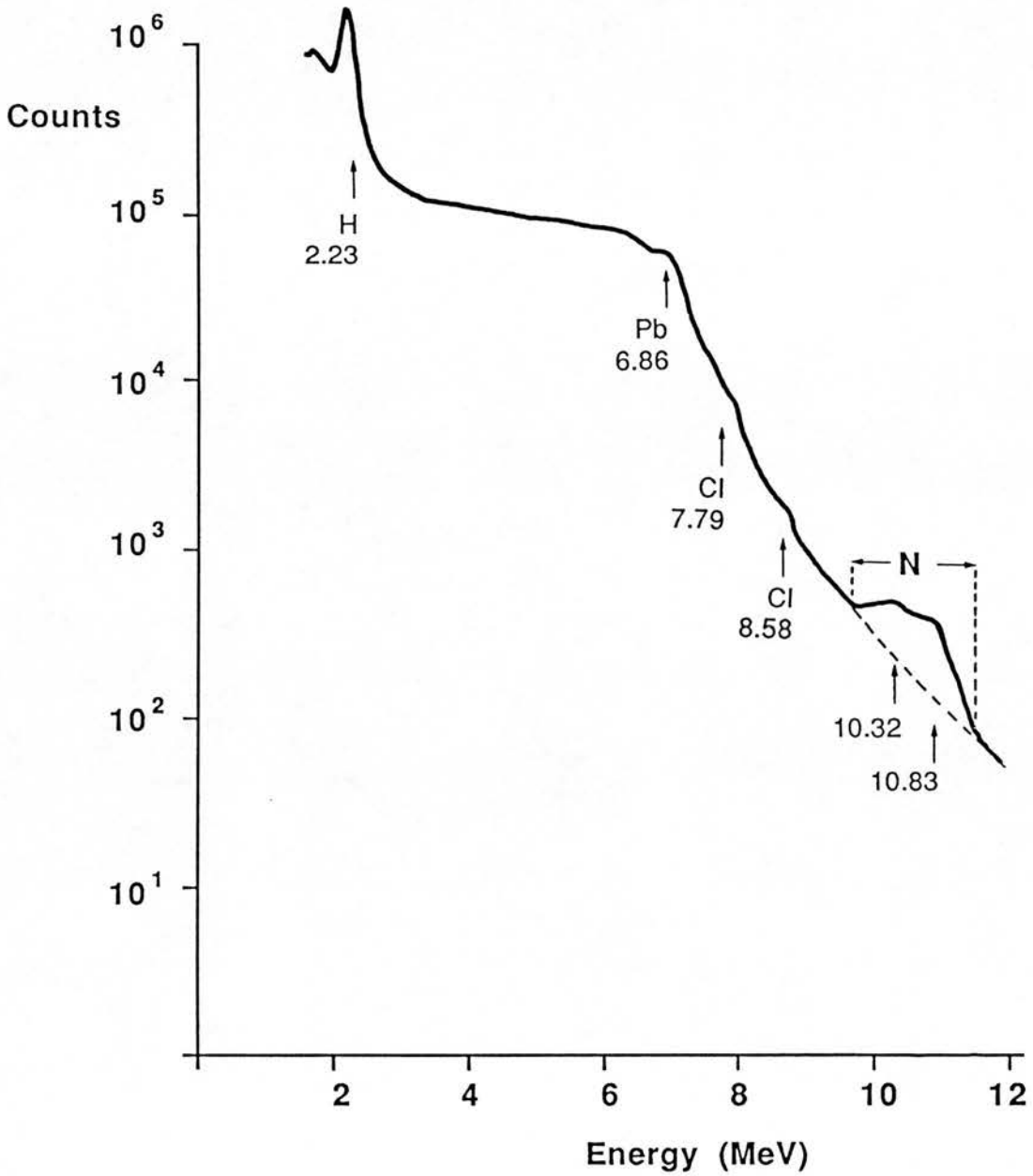

this reaction cannot have energies greater than that of the incident neutron which was scattered. For ^{252}Cf neutrons, therefore, such gamma rays will form a continuum with a maximum energy of approximately 8.5 MeV.

b). Prompt Capture Gamma Rays - (n,γ)

The capture of a neutron results in the formation of a compound nucleus with an excitation energy. Either neutron emission (scattering) or gamma emission (radiative capture) may occur. The radiative capture cross-section is much greater at slow and thermal neutron energies. The excitation energy lost by gamma ray emission depends upon the neutron binding energy and the kinetic energy of the captured neutron; negligible for thermal neutrons. The prompt capture gamma rays generated in shielding, structural and detector materials as well as those generated from the major body elements are listed in Table 5.1. It can be seen that a continuum will be formed with a maximum energy of approximately 7.7 MeV (except for Boron) for the shielding and detector materials; body elements whose abundance or cross-section leads to significant numbers of gamma rays could contribute to the spectrum up to 8.6 MeV (from Chlorine).

c). Activation Products

When a neutron is captured by a target nucleus without being later re-emitted (scattered) the product nucleus has an excess of neutrons and can be radioactive. Nuclei with an excess of neutrons are generally beta emitters. Table 5.2 lists activation data for thermal

TABLE 5.1

PROMPT GAMMA RAYS FROM THERMAL NEUTRON CAPTURE

Element	Cross-Section, (b)	Gamma Rays in designated (MeV) energy intervals per 100 neutron captures					Highest energy gamma ray (MeV)
		0-1	1-3	3-5	5-7	>7	
H*	0.33	-	100	-	-	-	2.23
B!	752	478	1.36	-	-	0.8	11.45
C+	0.0034	-	-	67	-	-	4.95
N	0.075	23.5	57.5	41	87.5	27.5	10.83
Na	0.534	105	111	73	31.5	-	6.40
Al	0.235	21	18	33	5	24.5	7.72
P	0.19	35	102.5	75	22.5	6	7.42
Cl	33.2	21.5	64	12	33.5	17.5	8.58
K	2.10	35	66	28	28	4.5	7.77
Ca	0.43	6	94	21	33	-	6.42
I	6.6	22.5	35.5	1.5	3	-	5.20
Tl	3.3	20.5	4.5	5	19.5	-	6.52
Pb$	0.17	-	-	-	-	94.5	7.37

Data taken from references 39 and 82
* Data taken from reference 95
! 98% of the B prompt gamma rays are at 0.48 MeV
\+ 100% of the C prompt gamma rays are at 4.95 MeV
$ 100% of the Pb prompt gamma rays are at 7.37 MeV

TABLE 5.2 SELECTED ACTIVATION DATA FOR THERMAL NEUTRON CAPTURE

Element	Target Nucleus	Percentage Abundance in Natural Element(%)	Thermal Capture Cross-Section (b)	Product Nucleus	Half-Life $T_{\frac{1}{2}}$	Beta Particles - Maximum Energy (MeV) & Number per Disintegration (%)	Gamma Rays - Energy(MeV) & Number per Disintegration(%)
B	^{11}B	80.2	0.003*	^{12}B	20.3ms	13.4 (98.7%)	4.43 (1.3%)
Na	^{23}Na	100	0.10	^{24}Na	15h	4.17 (0.003%)	2.75 (100%)
Al	^{27}Al	100	0.23	^{28}Al	2.24m	2.85 (100%)	1.78 (100%)
P	^{31}P	100	0.18	^{32}P	14.3d	1.71 (100%)	None
Cl	^{35}Cl	75.77	43	^{36}Cl	$3x10^5y$	0.71 (98.1%)	None
	^{37}Cl	24.23	0.43	^{38}Cl	37.3m	4.91 (57.6%)	2.17 (42%)
						2.77 (11.1%)	1.64 (30%)
K	^{39}K	93.26	2.1	^{40}K	$1.43x10^9y$	1.33 (89.3%)	1.46 (10.7%)
	^{41}K	6.73	1.46	^{42}K	12.3h	3.56 (81.2%)	1.52 (18.8%)
						1.97 (18.3%)	
I	^{127}I	100	6.4	^{128}I	25m	2.12 (93.6%)	0.97 (0.3%)
							0.74 (0.2%)
							0.53 (1.4%)
							0.44 (14%)
Tl	^{205}Tl	70.5	0.11	^{206}Tl	4.2m	1.52 (100%)	None
	^{203}Tl	29.5	11	^{204}Tl	3.8y	0.77 (97.9%)	None

Data taken from reference 64

* Cross-section obtained from OECD, Nuclear Energy Agency, France

neutron capture for those elements listed in Table 5.1 where applicable. It can be seen that activation of the detector will yield radioactive products emitting a range of beta particles and gamma rays up to a maximum of 4.17 MeV and 2.75 MeV respectively. The build up of activity during a neutron irradiation is determined by many factors including the cross-section (σ) for the reaction and the half-life ($T_{\frac{1}{2}}$) of the product nucleus; the greater is σ and the smaller is $T_{\frac{1}{2}}$ then the greater is the contribution of the reaction to the prompt spectrum. Iodine (I) has by far the greatest cross-section and the activation spectrum immediately following a neutron irradiation is dominated by its beta spectrum. Of the beta particles generated from abundant elements within the phantom, those from Cl-38 have the highest maximum energy (4.91 MeV).

The range of beta particles depends primarily on the electron density of the absorber, and is generally expressed in terms of the "density thickness".

$$\underset{(\text{mg cm}^{-2})}{\text{Density thickness}} = \underset{(\text{mg cm}^{-3})}{\text{Absorber density}} \times \underset{(\text{cm})}{\text{thickness}}$$

The relationship between the beta particle range (R) and the maximum beta energy (E) is approximated by:-

$$R = 530E - 106 \qquad \text{for } E > 2.5 \text{ MeV}$$

where R is in mg cm^{-2} and E in MeV (Reference 22, p 100).

The range of the 4.91 MeV beta particles from ^{38}Cl in tissue, air and boric acid powder is therefore 2.21 cm, 2.12 m and 2.83 cm respectively. Since each detector face is shielded with 3 cm of boric acid powder, beta particles of this and lower energy will not reach the detector from the phantom. The activation of ^{11}B generates

beta particles of maximum energy 13.4 MeV. 13.4 MeV beta particles have a range of approximately 6996 mg cm^{-2}. Most boric acid would be separated from the crystal by 2 cm of lead (density = 11.34 g cm^{-3}). The minimum thickness of lead required to completely stop all 13.4 MeV beta particles is approximately 0.62 cm; showing that all beta particles which must pass through the lead to reach the crystal will be stopped. However, those beta particles generated in the boric acid on the crystal face will be capable of reaching the crystal,since their range in boric acid powder and aluminium is 7.77 cm and 2.59 cm respectively. For those beta particles interacting with the lead the possibility of generating Bremsstrahlung radiation must be considered. The Bremsstrahlung continuum ranges downward from a theoretical maximum (E) equal to the kinetic energy of the beta particle. The fraction of the incident beta energy converted into photons (f) increases with atomic number (Z) and so is high for lead, viz:

$$f = 3.5 \times 10^{-4} ZE$$ (from Reference 22, p 106)

Therefore for a 13.4 MeV beta particle in lead f = 0.38.

It is possible, therefore that Bremsstrahlung radiation from these beta particles may contribute to the nitrogen background. With air or light elements as an absorber, as is the case for beta particles generated in the boric acid on the detector face, very little Bremsstrahlung will be generated.

Activation products can also be generated through (n,p) and (n,α) reactions. Table 5.3 lists the activation products generated through these fast neutron reactions in sodium (Na), iodine (I) and aluminium

TABLE 5.3

ACTIVATION PRODUCTS FOR (n,p) AND (n,α) REACTIONS IN NaI AND APPARATUS MATERIALS

Reaction	Half-Life $T_{1/2}$	Beta Particles - Maximum Energy (MeV) & Number per Disintegration	Gamma Ray Energy(MeV) and Numbers per Disintegration
$^{23}_{11}Na(n,p)^{23}_{10}Ne$	38s	4.38 (100%)	1.64 (0.9%), 0.439 (33%)
$^{23}_{11}Na(n,\alpha)^{20}_{9}F$	11s	5.41 (100%)	1.63 (100%)
$^{127}_{53}I(n,p)^{127}_{52}Te$	9.4h	0.7 (100%)	0.417(0.3%), 0.36 (0.05%) 0.21 (0.03%), 0.058 (0.01%)
$^{127}_{53}I(n,\alpha)^{124}_{51}Sb$	60d	2.31(100%)	2.09 (7%), 1.69 (50%), 1.45 (2%), 1.37 (5%), 1.31 (3%), 1.05 (2.4%), 0.97 (2.4%), 0.72 (14%), 0.64 (7%), 0.60 (97%)
$^{27}_{13}Al(n,p)^{27}_{12}Mg$	9.46m	2.65 (0.34%) 1.75 (58%) 1.59 (41%)	0.84 (73%), 1.01 (29%)
$^{27}_{13}Al(n,\alpha)^{24}_{11}Na$	15h	4.17 (0.003%) 1.39 (100%)	2.75 (100%), 1.37 (100%)

Data taken from reference 64

(Al). The cross-sections for these reactions will vary with neutron energy.

d). Californium-252 Source Gamma Rays

The gamma rays generated from ^{252}Cf have been discussed in section 4.1. There are 5.7 gamma rays emitted per neutron over the energy range 0.6 to 5 MeV. However, 95% of all gamma rays have energies below 0.6 MeV. Although, many of these gamma rays will be attenuated by the lead shielding some will contribute to the prompt spectrum.

e). Background Radiation

Background radiation may be considered in two parts:-

(i) Natural Radioactivity

Most naturally occurring radioactive elements are members of one of three radioactive decay series; the series are named the uranium, actinium and thorium series.

Shielding alone cannot necessarily eliminate part of this background contribution. For example, gaseous radionuclides such as ^{220}Rn and ^{222}Rn will be present and their daughter products may be deposited upon the detector face. Similarly, naturally occurring ^{40}K will form part of the photomultiplier glass envelope.

(ii) Cosmic Radiation

Cosmic rays are highly penetrating radiations which originate outside the earth and consist of protons, electrons, neutrons, photons and other particles. The nature of the radiation is affected by the earth's atmosphere. The counts observed in detectors are principally due to secondary particles generated by the interactions of these high energy particles with matter.

f). Fast Neutron Reactions - (n,p), (n,α)

A compound nucleus can de-excite in an increasing number of ways as its excitation energy increases. If the Q-value of a reaction (the energy released during a reaction) involving charged particle emission is high enough then the charged particle will overcome the Coulomb barrier and escape from the nucleus if its kinetic energy is great enough. The kinetic energy of the reaction products is equal to the Q-value of the reaction plus the kinetic energy of the incident neutron. This explains why charged particle reactions of large Q-values are more probable than those of low or negative Q-value and why the probability of the reactions increases with neutron energy. For reactions with negative Q-values there is a threshold energy for the incident neutron below which the reaction can not occur. (n,p) and (n,α) reactions may contribute to the nitrogen spectrum throughout the energy range, however such reactions have been considered in greater detail as a possible source of nitrogen background in section 5.2.

These sources of radiation can be seen to contribute to the prompt spectrum up to a maximum of the neutron energy, with the exception of the Boron 11.45 MeV prompt gamma ray, beta particles of maximum energy 13.4 MeV from the production of ^{12}B, possible fast neutron (n,p) and (n,α) reactions and cosmic radiation which may contribute to the spectrum beyond 8.5 MeV. It remains to identify specific neutron induced reactions which could contribute to the nitrogen background. This will be attempted in the following section.

5.2 Contributing Reactions to the Prompt Nitrogen Background

5.2.1 Theoretical Contributions to the Nitrogen Background

The possible sources of the nitrogen background can be considered in three parts, namely:-

a). Natural Background Radiation

Cosmic radiation is the source of such high energy background radiation. It has been measured with and without a phantom present for the clinical apparatus and found to be independent of the phantom size. The percentage contribution to the net nitrogen background will be greater the larger the patient size. For an average patient size (34 cm wide by 22 cm thick) the natural background would contribute 4.2% of the counts (Feb. 1987).

b). Neutron Induced Reactions

Section 5.1 has shown that (n,γ) and (n,n'γ) reactions and activation products generate few radiations of sufficient energy to contribute to the nitrogen background. ^{252}Cf produces few neutrons with energy greater than 8.5MeV. There is however a possibility of generating a scintillation pulse equal in magnitude to that of a 9.5 MeV gamma ray in the crystal from charged particle reactions of large Q-values in elements of the detector and housing, where the emitted charged particles may reach the crystal. It must be emphasised that it is the equivalent light pulse to that generated from a 9.5 MeV gamma ray which is of interest, since for charged particles this may correspond to an energy of less than 9.5 MeV. Birks (12) illustrates the change in scintillation efficiency (light pulse height per unit energy) in NaI(Tl) for charged particles with specific energy loss. It can be shown from this graph that the scintillation efficiency for charged particles is greater than that for gamma rays over a range of specific energy losses from 2 to 200 keV cm^2 mg^{-1}. This range of specific energy losses corresponds to electrons and protons only. The difference in scintillation efficiency over the range of specific energy losses peaks at a value of 1.43 compared with that for gamma rays. Since it is difficult to calculate the specific energy loss for a charged particle of a particular energy, given that the average excitation potential required in the appropriate equation is difficult to calculate theoretically, it is assumed that all electrons and protons have a scintillation efficiency of 1.43 compared with that for gamma rays. In consequence, it is assumed that an electron or proton of 6.6 MeV energy could initiate a

scintillation event equivalent to that for a gamma ray of 9.5 MeV energy and so particles of this or higher energy could contribute to the nitrogen background. Equations for calculating the Q-value of a reaction and the threshold energies for reactions of negative Q-values (endothermic reactions) are given in Appendix III. For (n,p) and (n,α) reactions in the crystal elements themselves only the total kinetic energy of the emitted particle and the recoiling nucleus is of interest since all this energy will be deposited within the crystal. The total kinetic energy is the sum of the kinetic energy of the incoming neutron and the Q-value of the reaction. For (n,p) and (n,α) reactions within the aluminium crystal housing and the boron on the crystal face only the charged particle may reach the crystal to deposit its energy. For these events the special case whereby all the kinetic energy is given to the charged particle is considered. This will occur only for that proportion of reactions whereby the charged particle is emitted in the same direction as the incident neutron. This special case will determine the minimum energy of the incident neutron which will generate alpha particles of 9.5 MeV and protons of 6.6 MeV energy, and will therefore indicate whether such reactions are theoretically possible for ^{252}Cf neutrons. Table 5.4 lists the reactions considered along with their Q-values, threshold energies (E_{th}) and the minimum neutron energy which is required to produce events which could contribute to the nitrogen background (E_n(min)). The results indicate that with a ^{252}Cf neutron source (n,α) and (n,p) reactions in many elements are theoretically capable of contributing to the nitrogen background. The reaction rate for each of these reactions is given by:-

TABLE 5.4

SELECTED DATA FOR (n,p) AND (n,α) REACTIONS IN DETECTOR MATERIALS

Reaction	Abundance of Target Nuclide in Natural Element (%)	Q (MeV)	E_{th} (MeV)	E_n(min) (MeV)
$^{23}_{11}Na(n,p)^{23}_{10}Ne$	100	-3.087	3.22	9.69
$^{23}_{11}Na(n,\alpha)^{20}_{9}F$	100	-3.869	4.04	13.37
$^{127}_{53}I(n,p)^{127}_{52}Te$	100	0.604	0	6.00
$^{127}_{53}I(n,\alpha)^{124}_{51}Sb$	100	4.249	0	5.25
$^{203}_{81}Tl(n,p)^{203}_{80}Hg$	29.5	0.80	0	5.80
$^{205}_{81}Tl(n,p)^{205}_{80}Hg$	70.5	-0.356	0.36	6.96
$^{203}_{81}Tl(n,\alpha)^{200}_{79}Au$	29.5	7.18	0	2.32
$^{205}_{81}Tl(n,\alpha)^{202}_{79}Au$	70.5	5.945	0	3.56
$^{27}_{13}Al(n,p)^{27}_{12}Mg$	100	-1.321	1.37	7.92
$^{27}_{13}Al(n,\alpha)^{24}_{11}Na$	100	-3.13	3.25	12.63
$^{10}_{5}B(n,p)^{10}_{4}Be$	19.8	0.74	0	5.86
$^{11}_{5}B(n,p)^{11}_{4}Be$	80.2	-10.22	11.16	16.82
$^{10}_{5}B(n,\alpha)^{7}_{3}Li$	19.8	2.79	0	6.71
$^{11}_{5}B(n,\alpha)^{8}_{3}Li$	80.2	-6.63	7.24	16.13

$$\text{Reaction Rate, } R = \int_{E_{th}}^{\infty} N\,\sigma(E)\,\phi(E)\,dE$$

where N = number density of the target nuclide

$\phi(E)\,dE$ = neutron flux of energy E to (E + dE)

Since the neutron flux will be approximately constant for each of the reactions with crystal elements then the relative reaction rates will depend on the variation of cross-section with energy. Unfortunately, cross-section data for (n,α) reactions in Tl is limited to 14 MeV energies; being 0.75 mb at 14.8 MeV for ^{205}Tl and somewhere around 0.37 and 2.2 mb at 14.5 MeV for ^{203}Tl. Cross-section data is available for the (n,α) reaction in ^{127}I being a maximum of 0.1 mb at 8 MeV. The low cross-sections and the low percentage abundance of the element Tl will make these reaction rates small. The (n,α) reaction cross-section at 6.7 MeV for ^{10}B is approximately 50 mb. This is by far the largest cross-section for any of the (n,α) reactions. However, the range of alpha particles in a medium is given by:-

$$R_m\ (\text{mg cm}^{-2}) = 0.56A^{1/3}\ R\ (\text{cm}) \qquad \text{(Reference 22, p 108)}$$

where A = atomic number of the medium, and

R = range of alpha particle in air (R = 1.24E(MeV) - 2.62 for $4 < E < 8$ MeV)

The range of a 9.5 MeV alpha particle in lead and aluminium is therefore 0.02 mm and 0.045 mm respectively. Therefore, only those alpha particles generated in boric acid powder directly adjacent to the crystal face will have any probability of reaching the crystal in order to contribute to the nitrogen background. The absolute values for E_n(min) required for (n,p) reactions are less certain given that the maximum scintillation efficiency in NaI(Tl) relative to that for

gamma rays was assumed for all particles. However, cross-section data for these reactions is also limited, being available only for specific energies if available at all. The cross-section for the (n,p) reaction in ^{27}Al is 25 mb at 5.1 MeV. In ^{127}I the cross-section is 25 mb at 14.1 MeV and for ^{203}Tl it is 30 mb at 14.8 MeV. No cross-section data is available for the (n,p) reaction in ^{205}Tl.

This data shows that the reaction rates for (n,α) and (n,p) reactions in detector elements or in boron can be expected to be low. However, such reactions as those discussed above must be considered possible when detailing sources of nitrogen background counts.

c). Pulse Pile-Up

Pulse pile-up occurs when a second pulse arrives before the first pulse has returned to its baseline. For bipolar pulses if the second pulse arrived on the negative lobe of the first pulse, then the first pulse would be unaffected whilst the second pulse would appear lower down the energy scale than its true position. If, however the second pulse arrived on the falling edge of the positive lobe of the first pulse, then the second pulse would appear higher up the energy scale than its true position. The third case would be if the second pulse arrived on the leading edge of the first pulse. Then both events would be lost from their normal position in the energy distribution. The piled-up event would appear higher up the energy scale the closer the pulse peaks overlap. As the count rate increases the probability of pile-up increases. Multiple pile-up events, involving three or

more pulses, become more probable at higher count rates. Consequently, it is possible at high count rates to generate pile-up as far up the energy scale as nitrogen for a prompt spectrum. The count rate throughput experiments of section 3.2.4 showed that counts were lost as the count rate increased for the nucleonics arrangement adopted for the clinical apparatus. The clinical apparatus had a total count rate ranging from 85 kcps to 120 kcps dependent upon the phantom dimensions (Feb. 1987). The lowest count rate corresponded to the smallest phantom (20 cm wide by 10 cm thick), though the nitrogen background for this phantom was greater than that for any other phantom used! This fact illustrates the change in spectrum shape with phantom dimensions. At such high count rates pulses will pile-up. Whilst most events will have piled-up below the nitrogen region (because the probability of pile-up will depend upon the count rate in the energy region under observation), there remains the possibility of pile-up in the nitrogen region. This section will present some inferential evidence in support of the phenomenon of pile-up in the nitrogen region.

5.2.2 Experimental Evidence of the Contributing Reactions to the Nitrogen Background

a). Evidence Against Fast Neutron Reactions Being the Sole Contributors to the Nitrogen Background

Fast neutron reactions could theoretically generate nitrogen background through (n,α) and (n,p) reactions where a ^{252}Cf neutron could generate particles of sufficient energy to generate a

scintillation pulse equivalent to that for a 9.5 MeV gamma ray.

Fig 7.5 in Chapter 7 shows the spectra for two of the three irradiation geometries which differ in their ratios of thickness of lead to wax (see section 7.2.3 for details of the experiment). Table 7.9 shows the variation in the nitrogen background count rate. It can be seen that as the fast neutron shielding is increased, with the concomitant loss of gamma ray shielding, the count rate in the nitrogen background is increased. This is evidence in support of such fast neutron reactions not being the principal cause of the nitrogen background.

Other reactions which could contribute to the nitrogen background such as 11.45 MeV prompt gamma rays from boron and 13.4 MeV beta particles from the production of ^{12}B in boron surrounding the detector will probably decrease as the thickness of wax is increased, since fewer thermal neutrons will reach the boric acid (thermal neutrons generated within borated wax will be captured by the boron within the wax, whereas thermal neutrons generated within lead are more likely to reach the boric acid powder). These results would infer that the background in the nitrogen region of the spectrum increases as the fast neutron shielding increases as a consequence of increased pile-up. The total count rate at the detectors increases as lead is replaced with borated wax (as indicated by the analyser deadtime in Table 7.9) because of the reduced shielding of ^{252}Cf source gamma rays, prompt gamma rays and gamma rays from activation products and fast neutron inelastic scattering reactions. This increase in the total count rate would increase the probability of

pile-up in the nitrogen region and may explain the increase in the nitrogen background observed during this experiment.

b). Evidence Against Reactions Concerning Boron Being The Sole Contributor To The Nitrogen Background

Neutron reactions in boron can contribute to the nitrogen background in the following ways:-

(i) (n,α) and (n,p) reactions in ^{10}B can generate alpha particles and protons respectively with sufficient energy to initiate a scintillation response equivalent to that from a 9.5 MeV gamma ray with ^{252}Cf neutrons.

(ii) (n,ϑ) reactions in boron can generate 11.45 MeV prompt gamma rays in 0.8% of captures.

(iii) The activation product of an (n,ϑ) reaction in ^{11}B emits beta particles with a maximum energy of 13.4 MeV in 98.7% of its disintegrations.

The experiment described in section 7.1.6, which investigated different thermal neutron shielding materials (H_3BO_3 or LiF) for the detector face, has its results in Table 7.6. The results show that the nitrogen background decreased with an increase in the thickness of shielding material and that H_3BO_3 was more effective than LiF at any given thickness. Since H_3BO_3 is more effective than LiF at reducing the nitrogen background it can be concluded that the

reactions with boron which can theoretically contribute to the nitrogen background are not the principal cause of the nitrogen background. Since other fast neutron reactions which could contribute to the nitrogen background would remain unchanged under these experimental circumstances, it is further concluded that the nitrogen background is being reduced because of the reduced probability of pulse pile-up. The minimum nitrogen background was obtained when the relative thermal neutron fluence at the crystal was a minimum. This reduced thermal neutron fluence reduces prompt gamma rays from detector elements (up to 7.7 MeV from Al, 6.4 MeV from Na, 6.5 MeV from Tl and 5.2 MeV from I). The reduced count rate in the 5 to 8 MeV energy region reduces the probability of pile-up in the nitrogen region. Consequently, pile-up would appear to be a greater contributor to the nitrogen background than reactions in boron.

c). Direct Evidence in Support of the Contribution of Pulse Pile-Up to the Nitrogen Background

Direct evidence to support the idea of pile-up being responsible, at least in part, for the nitrogen background comes from three experimental sources, viz:-

(i) Iron Versus Lead Collimator

Section 6.2 describes the effect on the nitrogen background of an iron collimator compared with a lead collimator. Whilst the two elements would have had slightly different effects on the direct

neutron beam to the crystals, the overwhelming difference as seen in the water phantom spectra was the presence of high energy prompt gamma rays from iron; particularly at 7.6 MeV and 9.3 MeV. The nitrogen background for the iron collimator was 14% greater (see Table 6.7) than that for the lead collimator. It is suggested that pile-up of these high energy prompt gamma rays with lower energy gamma rays has been the cause of the increase in the nitrogen background for the iron collimator.

(ii) Nitrogen-Free Tissue Equivalent Solution Versus Water Phantom Spectra

A nitrogen-free tissue equivalent solution (TES) was made which contained the major body elements in physiological concentrations. The prompt spectrum with this solution was compared with that from water using a box phantom 38 cm wide by 22 cm deep. The TES spectrum showed peaks for prompt gamma rays from the major body elements; particularly from chlorine up to 8.58 MeV. The nitrogen background for the TES was 32% greater than that obtained for the water. Since the only difference between these two experimental situations is the number of prompt gamma rays generated from the phantom, it is concluded that the increase in the nitrogen background when using the TES was solely due to pile-up of the increased number of high energy prompt gamma rays.

(iii) One and Two Californium-252 Sources with One and Two Detectors

The ^{252}Cf neutron sources were positioned centrally in the apparatus

TABLE 5.5

EVIDENCE FOR PILE-UP CONTRIBUTING TO THE NITROGEN BACKGROUND

	F	B	F + B
U	0.472 cps	0.484 cps	
L	0.517 cps	0.482 cps	
U + L (E)	0.989 cps	0.966 cps	1.955 cps
U + L (O)	1.349 cps	1.118 cps	3.574 cps
O/E	1.364	1.157	1.828

Key

F	Front i.e. most accessible detector
B	Back detector
U	Upper ^{252}Cf source
L	Lower ^{252}Cf source
E	Expected value
O	Observed value

by equalising the counts in the nitrogen background for the two detectors with a water filled Bush phantom thorax section. Having achieved this the various combinations of ^{252}Cf source and detector were investigated to observe the changes in the nitrogen background. The results are shown in Table 5.5. For each detector the observed counts in the nitrogen background for two sources was greater than that expected from the sum of the counts obtained when using each source separately. Similarly, when the two detector outputs were summed the observed nitrogen counts were greater than the expected sum of the two detectors used separately. In this case the observed counts were approximately 45% greater than the expected counts. This is conclusive evidence that a large proportion of the nitrogen background counts are generated by pulse pile-up in the nucleonics.

This chapter has detailed the many reactions which contribute to the prompt nitrogen spectrum and has elucidated the energy regions in which different reactions are important. Most importantly the discussion has shown that few reactions could initiate a scintillation response in NaI(Tl) equivalent to or greater than that from a 9.5 MeV gamma ray, and so contribute to the nitrogen background directly. Moreover, those reactions which could achieve this have such low cross-sections and the isotopes are in such low abundance that the probability of the reactions is extremely low. Direct evidence to suggest that these reactions are not the sole contributors to the nitrogen background has been presented. The evidence when summing outputs for 1 and 2 neutron sources and 1 and 2 detectors clearly implicates pile-up of lower energy pulses as being responsible for at least 83% of the nitrogen background counts with a Bush phantom thorax section (December 1986).

CHAPTER 6

CHAPTER 6

SHIELDING AND COLLIMATOR MATERIALS

Ultimately the choice of shielding and collimator materials is made in order to minimise the coefficient of variation (CoV) of a total body nitrogen measurement. Throughout the investigations to optimise the detector apparatus the CoV calculated was that based on the counting statistics alone. The reproducibility of the net nitrogen counts, as determined from eight repeat measurements for one irradiation geometry, was found to be in good agreement with the CoV determined from counting statistics. All spectra were obtained using one Californium-252 source and one detector in order to simplify shielding construction. An 8 litre phantom (23 cm x 18 cm x 19.3 cm) was employed. The nitrogen phantom contained urea in deionised water to give a nitrogen concentration four times that of standard man, thus increasing the net nitrogen counts to that which would be obtained in practice. The nitrogen background was determined by irradiation of a deionised water phantom; in practice the nitrogen background could be expected to be four times that obtained (ignoring the possibility of pile-up) since both detectors and neutron sources would be used. The net nitrogen and background counts were modified to produce a CoV for two ^{252}Cf sources and two detectors for a "REAL" time irradiation of 40 minutes (live time spectra corrected for analyser deadtime).

This chapter discusses the effect of shielding materials on the prompt spectrum and reports the changes in the relative thermal

neutron fluence at the detector, as estimated from the crystal activation (see Appendix IV). These studies assist in understanding the importance of the different shielding materials in minimising the background in the nitrogen region of the spectrum. The changes in the thermal neutron profile across the patient width and the effect on the CoV of a total body nitrogen measurement with choice of collimator material is also discussed.

6.1 Shielding Material

As has already been stated the shielding materials are chosen to minimise the coefficient of variation of a total body nitrogen measurement. The materials can achieve this aim by either reducing the nitrogen background or increasing the net nitrogen counts. Only the former effect will be discussed in this section. The latter effect has been demonstrated with lead in Section 7.1.5 of Chapter 7. As discussed in Chapter 5 the nitrogen background is thought to be principally pile-up of lower energy gamma rays. The shielding materials could therefore be expected to reduce the nitrogen background simply by reducing the overall count rate; particularly the higher energy counts.

6.1.1 Fast Neutron Shielding

Fast neutrons (energy $\geq$ 0.1 MeV) lose most energy through elastic scattering with light elements, particularly hydrogen. A good shield for fast neutrons therefore is one which has a high density of hydrogen atoms, such as water and wax. Water presents problems of

containment and therefore has not been considered here.

The effect of additional fast neutron shielding on the prompt nitrogen spectrum was investigated with the geometry shown in Fig 6.1, where the effect of inserting the additional wax block (X) was investigated. The spectra with and without the additional wax block are shown in Fig 6.2. Regions A and B, as shown in Fig. 6.2, identify the energy range 2.5 to 7 MeV and 7 to 9.75 MeV respectively. The nitrogen integral was taken over the region 9.75 to 11.5 MeV as this had been determined to be optimum from consideration of the counting statistics. Table 6.1 details the results of the experiment. With the additional wax block present there was a 21% reduction of the counts in region A of the spectrum, this represents a combination of the reduction of $(n,n'\gamma)$ and (n,γ) reactions. The 22% reduction in the relative thermal neutron fluence at the crystal is evidence of the reduction of these reactions. The 39% reduction in the nitrogen background with the additional shielding is thought to be associated with reduced pile-up.

This experiment highlights the importance of maximising the amount of fast neutron shielding in reducing the background in the nitrogen region.

6.1.2 Thermal Neutron Shielding

Once a neutron has been thermalised (energy = 0.025 eV) it can be captured by any element with the subsequent emission of prompt gamma rays and the generation of activation products. The cross-section

Fig. 6·1

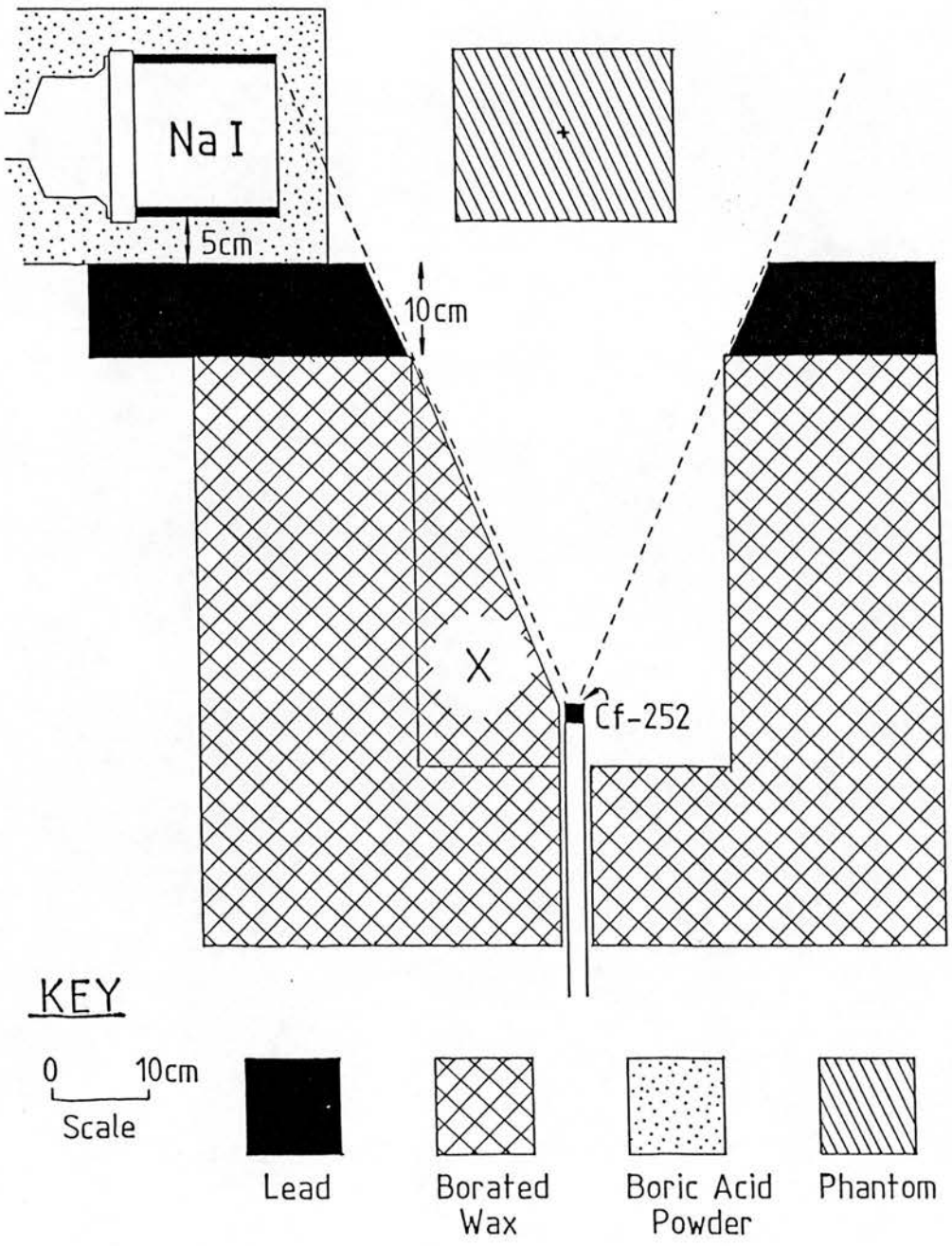

d=Crystal distance from phantom centre (cm)=30cm
w=Geometric beam width at the phantom centre (cm)=53cm
l=Geometric beam length at the phantom centre (cm)=26cm

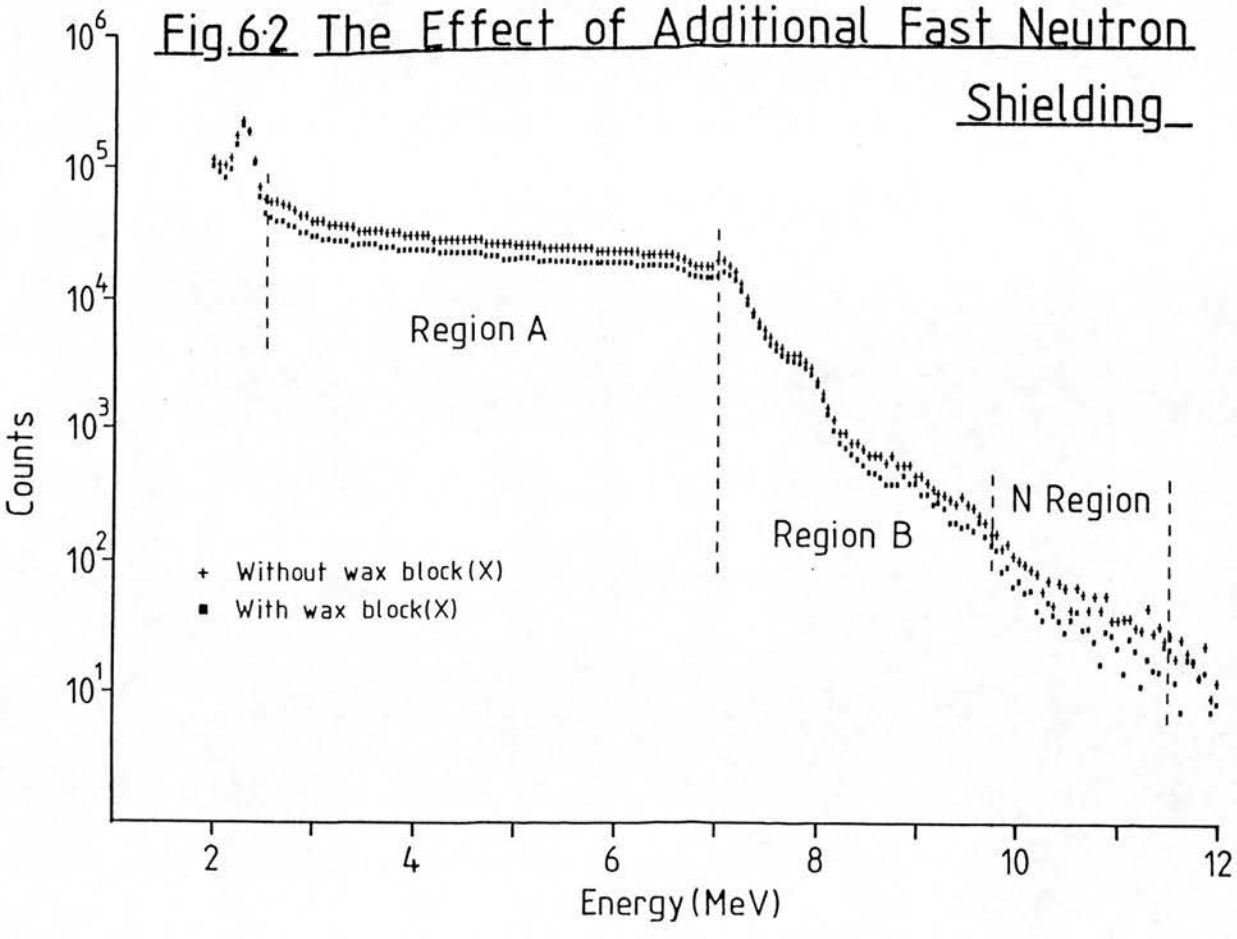
Fig.6·2 The Effect of Additional Fast Neutron Shielding
Counts
10^6
10^5
10^4
10^3
10^2
10^1
Region A
Region B
N Region
+ Without wax block(X)
■ With wax block(X)
2
4
6
8
10
12
Energy (MeV)

TABLE 6.1

THE EFFECT OF ADDITIONAL FAST NEUTRON SHIELDING ON THE PROMPT GAMMA SPECTRUM

	Without Added Wax Block X	With Added Wax Block X
Total Count Rate (cps)	56,145	52,478
Analyser Deadtime (%)	13.3	12.2
Net H Counts (cps)	0.777	0.772
Count Rate in Region A (cps)	4,301	3,362
Count Rate in Region B (cps)	239	205
N Background Count Rate (cps)	3.31	2.01
Relative Thermal Neutron Fluence (arbitrary units)	513	400

TABLE 6.2

EFFICIENT THERMAL NEUTRON ABSORBERS

Element	^{10}B	^{6}Li
Percentage Abundance of Natural Element (%)	20	7.4
Thermal Neutron Cross-Section (b)	3840	950
Reaction	$^{10}B(n,\alpha)^{7}Li$	$^{6}Li(n,\alpha)^{3}H$
Prompt Gamma Ray (MeV)	0.48	-
Number of Prompt Gamma Rays per 100 Neutron Captures	94	-

for the capture and the energy and number of prompt gamma rays per neutron capture for different elements are of concern since they will affect the prompt nitrogen spectrum. Suitable elements for the capture of thermal neutrons are listed in Table 6.2.

Boron-10 compares favourably with lithium-6 since it has a four times greater cross-section, is a higher percentage abundance of the natural element and is approximately one third the price per atom. The disadvantage of boron-10 is the high percentage of emission per neutron capture of it's 0.48 MeV prompt gamma rays. However, since the prompt gamma rays are of relatively low energy they will be effectively shielded by lead (HVL of 0.4 cm). Because of these factors boron was chosen as the thermal neutron absorber for the clinical apparatus; boron was used in the form of boric acid powder.

A comparison of paraffin wax and borated paraffin wax (containing 20% H_3BO_3 by weight) was performed. The addition of boron was intended to reduce the number of prompt hydrogen gamma rays generated since the thermal neutron capture cross-section of boron-10 is 3840 b compared with that of hydrogen of 0.33 b. The shielding and irradiation/detection geometry used is shown in Fig 6.3 and the spectra in Fig 6.4. Table 6.3 gives the count rates in the different regions of the spectrum. The relative thermal neutron fluence was approximately 6% lower for the borated wax; although an unknown experimental error due to rebuilding was associated with this, some of this reduction may have been due to the capture of thermal neutrons close to their point of origin by the boron in the wax. Since there should have been no difference in the fast neutron

Fig. 6·3

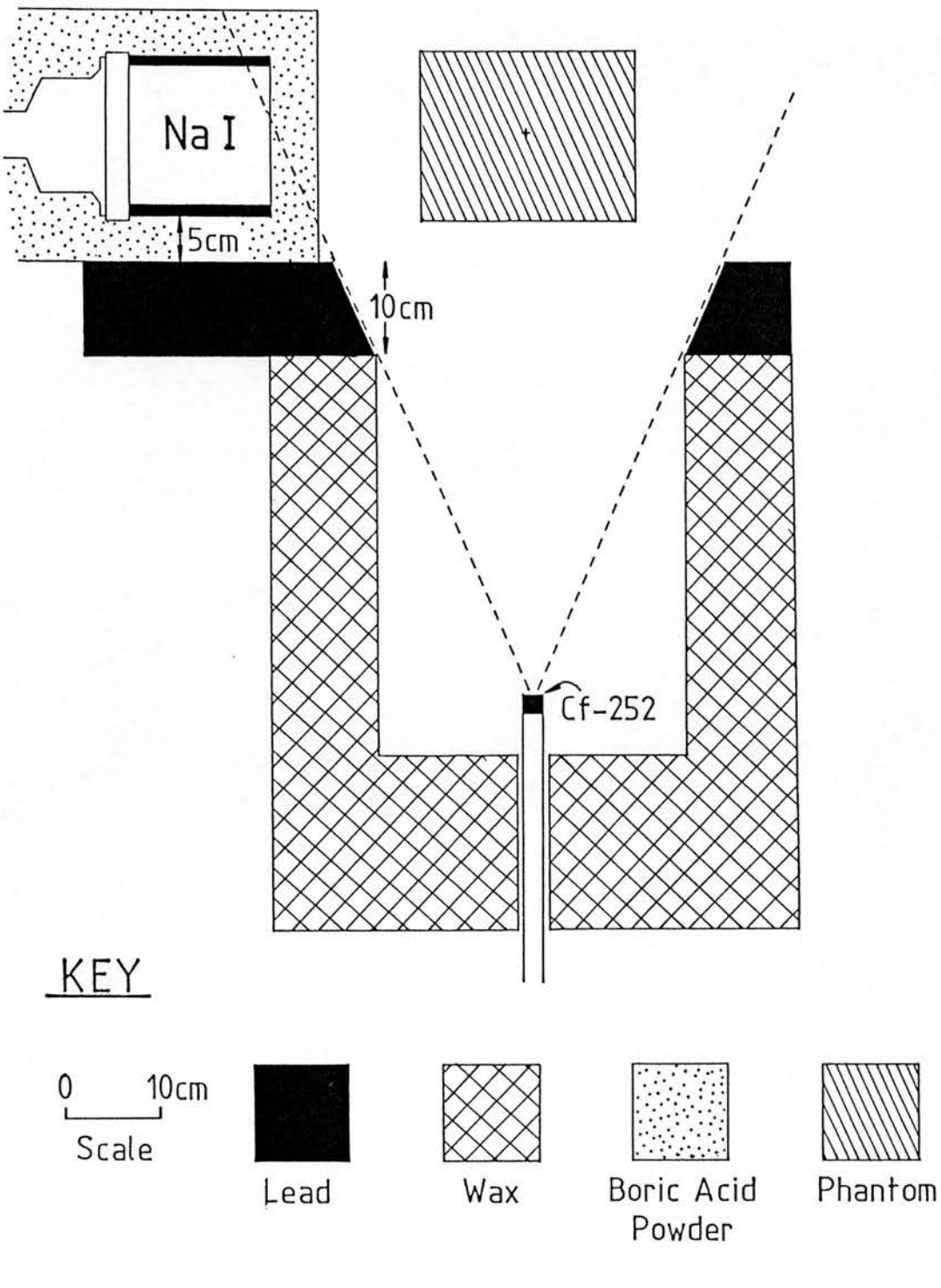
Na I
5cm
10cm
Cf-252
KEY
0 10cm
Scale
Lead
Wax
Boric Acid Powder
Phantom
d = 27cm
w = 53cm
l = 26cm

Fig.6·4 The Effect of Borating the Wax

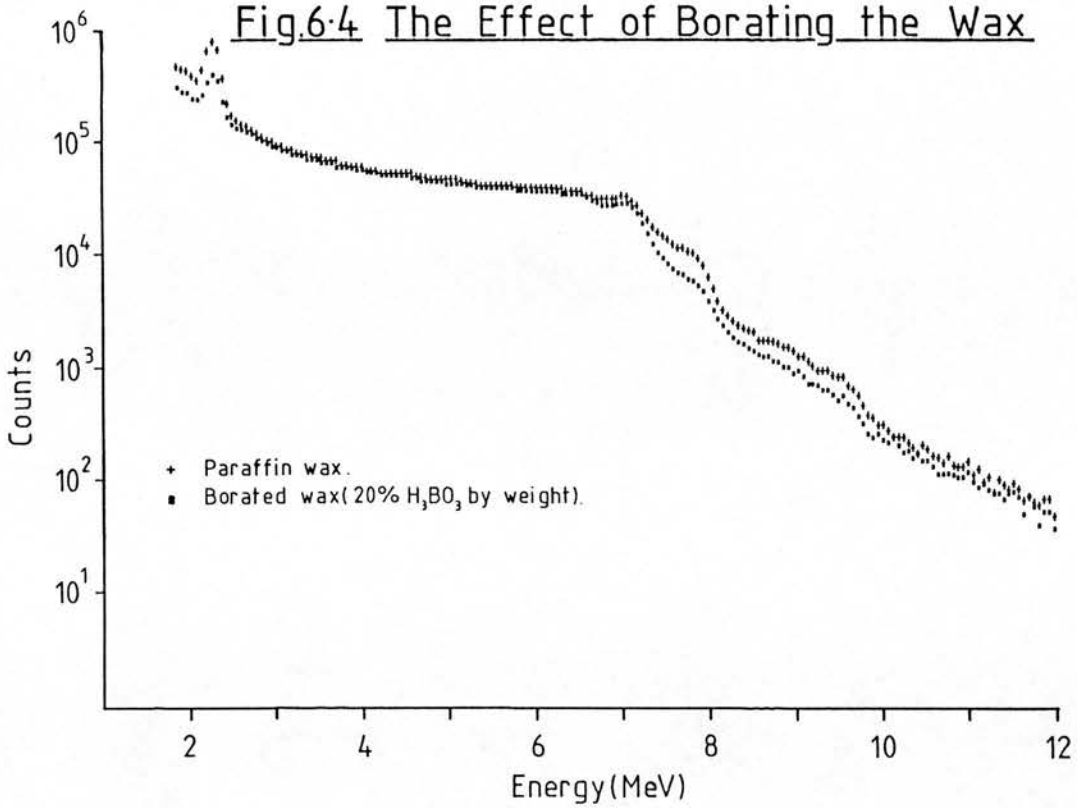

Fig.6·5 The Effect of Boron for Shielding the Detector

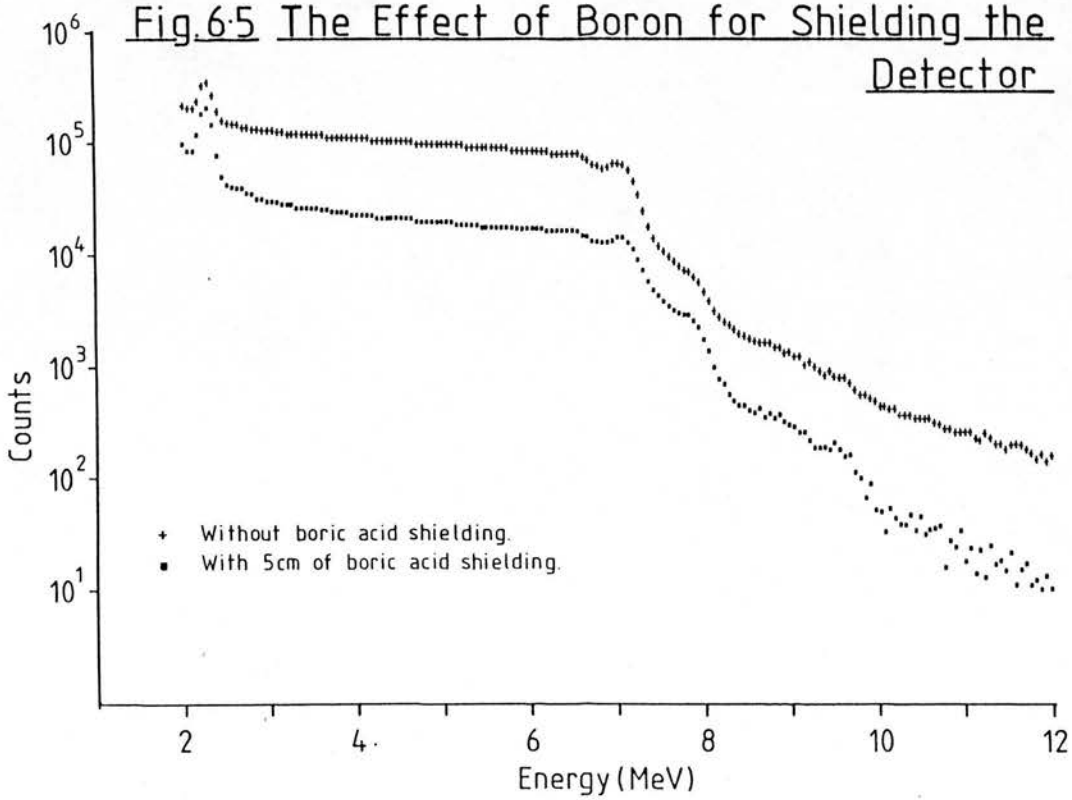

TABLE 6.3

THE EFFECT OF USING BORATED WAX ON THE PROMPT GAMMA RAY SPECTRUM

	Paraffin Wax	Borated Wax
Total Count Rate (cps)	123,587	108,453
Analyser Deadtime (%)	32.1	27.0
Net H Counts (cps)	3.109	1.126
Count Rate in Region A (cps)	9,364	8,095
Count Rate in Region B (cps)	611	405
N Background Count Rate (cps)	10.42	8.107
Relative Thermal Neutron Fluence (arbitrary units)	880	829

TABLE 6.4

THE EFFECT OF BORIC ACID ON THE PROMPT GAMMA RAY SPECTRUM

	With 5 cm Boric Acid Powder	Without Boric Acid Powder
Total Count Rate (cps)	52,478	76,322
Analyser Deadtime (%)	12.2	21.9
Count Rate in Region A (cps)	3,362	15,633
Count Rate in Region B (cps)	205	736
N Background Count Rate (cps)	2.01	19.80
Relative Thermal Neutron Fluence (arbitrary units)	400	2,187

spectrum throughout the shielding materials for both waxes the 13.6% reduction in the counts in region A of the spectrum was probably associated with a reduction in the prompt gamma rays generated in shielding and detector materials. A subsidiary experiment for the borated wax without the water phantom indicated that the water phantom contributed 50% of the net hydrogen counts. This indicates that borating the paraffin wax reduced the number of hydrogen gamma rays being generated within the wax by 78%. This reduction in the number of extra-corporeal hydrogen gamma rays is important when hydrogen is being used as an internal standard. The borated wax gave a 12% reduction in the analyser deadtime. The nitrogen background decreased by 22% when borated wax was used. This reduction was assumed to be due to decreased pile-up at the lower count rate since no reaction directly associated with the nitrogen background should have been changed by the addition of Boron to the wax.

In conclusion the advantages of using borated wax include:-

(i) the reduction of the total count rate and analyser deadtime,

(ii) a reduction in the nitrogen background, and

(iii) a reduction in the number of extra-corporeal hydrogen gamma rays.

Investigation of the effect of packing boric acid powder around the detector was performed using the geometry shown in Fig 6.1. The spectra are illustrated in Fig 6.5 and the results in Table 6.4. Clearly boric acid had a significant effect on the prompt spectrum. The total count rate at the detector decreased by 31%, producing a 44% reduction in the analyser deadtime. The counts in region A of the spectrum decreased by 78% in the presence of boric acid; that this reduction was due to reduced prompt gamma rays from (n,γ) reactions within the detector materials is indicated by the 81%

TABLE 6.5

GAMMA RAY SHIELDING DATA FOR PRINCIPAL PROMPT GAMMA RAYS

Element	Prompt Gamma Ray Energy (MeV)	μ_1 (cm^{-1})	HVL (cm)
^{10}B	0.48	1.70	0.41
^{2}H	2.23	0.50	1.39

TABLE 6.6

THE EFFECT OF LEAD ON THE PROMPT GAMMA RAY SPECTRUM

	With 10 cm of Lead	Without 10 cm of Lead
Total Count Rate (cps)	52,478	127,026
Analyser Deadtime (%)	12.2	32.5
Net H Counts (cps)	0.772	1.785
Count Rate in Region A (cps)	3,362	7,483
Count Rate in Region B (cps)	205	268
N Background Count Rate (cps)	2.01	4.37
Relative Thermal Neutron Fluence (arbitrary units)	400	357

Fig. 6.6 The Effect of Gamma Ray Shielding.

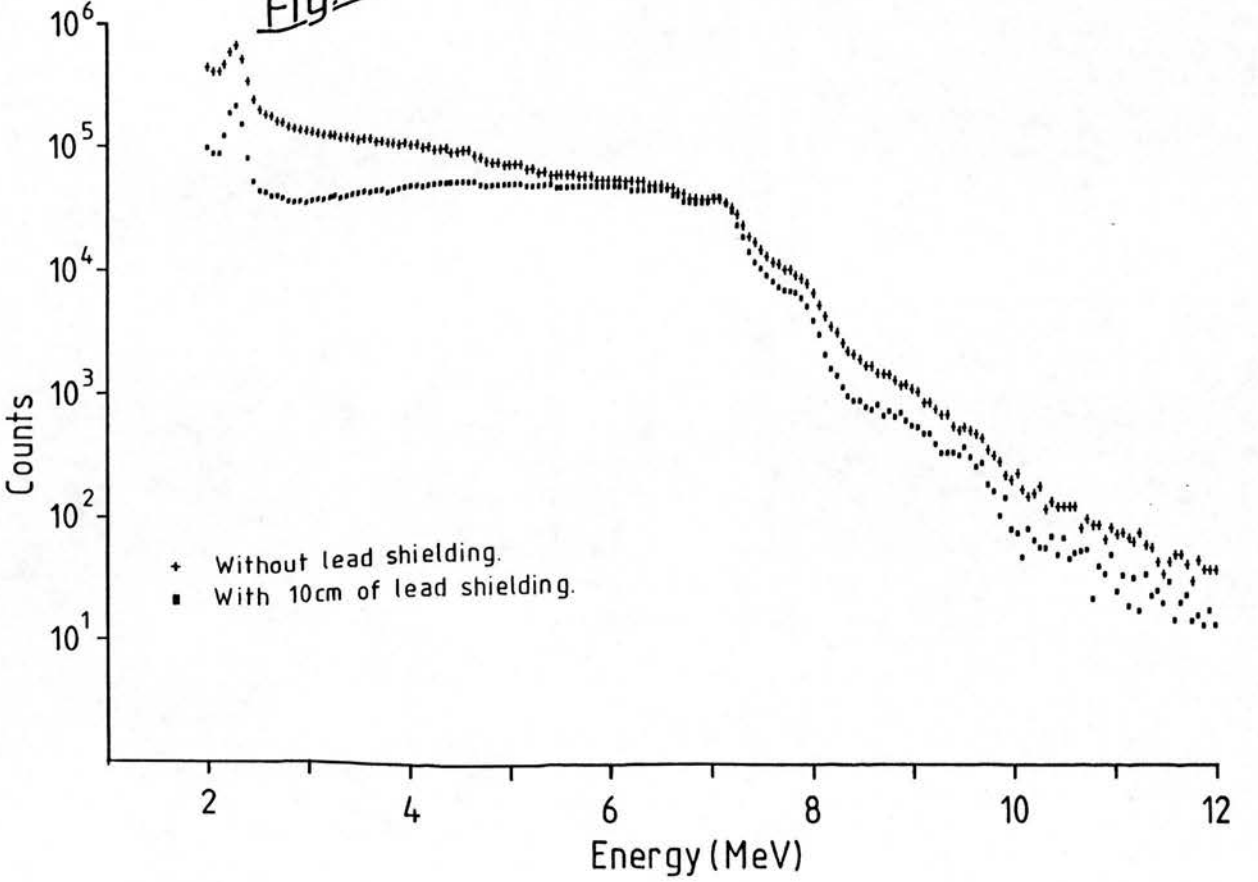

the hydrogen counts of 99% and reflects the area of wax collimator which is not shielded from the detector by lead. The counts in region A of the spectrum decreased by 55%, thereby emphasising the importance of shielding the detector from ^{252}Cf source gamma rays and prompt gamma rays generated within the shielding materials. The reduction of the overall count rate has resulted in a 54% reduction in the nitrogen background.

This experiment has demonstrated the importance of shielding the detector from gamma radiation.

6.2 Collimator Materials

Collimation of the neutron beam reduces the amount of background radiation generated which will reach the detectors. The choice of collimator materials can affect the neutron energy spectrum at the patient by scattering neutrons back into the main beam. In this way the signal:background ratio in the nitrogen region may be improved.

High atomic number elements are the most efficient at backscattering fast neutrons; conveniently available elements include lead and iron.

Experiments were performed to measure the relative thermal neutron fluence profile at the centre of a perspex water tank of width 32.5 cm and thickness 22.5 cm; this phantom width was increased with perspex slabs so as to approximate to an "infinite" scattering medium both sides of the point of interest. The relative thermal neutron

fluence was measured by activating indium foils (approximately 2 cm x 2 cm) for 500 seconds by irradiating with two ^{252}Cf neutron sources and counting in a standard geometry for 400 seconds (see Appendix V). Three collimator materials were investigated, namely lead, iron and borated wax. A ^{252}Cf to phantom centre distance of 60 cm was maintained. A collimator length of 34 cm surrounded by borated wax gave a geometric field size at the phantom centre of 37 cm by 37 cm. The collimator material was 3 cm thick and lined all four sides in the case of borated wax but only three sides in the case of lead and iron (owing to construction difficulties). The thermal neutron fluence profiles relative to the maximum for the borated wax collimator are shown in Fig 6.7 for the three collimators. It can be clearly seen that the use of an iron collimator increased the thermal neutron fluence for a 22.5 cm thick phantom by a minimum of 20% at the centre up to 55% at 23 cm from the centre; the corresponding increases for a lead collimator were 19% and 49% respectively. Thus the use of a high atomic number collimator material could be expected to significantly increase the nitrogen signal from a patient. However, the effect of the collimator material on the nitrogen background remains to be investigated. To do this the collimator and wax shielding remained unchanged and one detector was introduced and shielded with lead; the geometry is shown in Fig 6.8. Irradiations were performed with both nitrogen and water phantoms for each of the collimators and the background spectra are shown in Fig 6.9 with the results in Table 6.7. Both lead and iron collimators increased the net nitrogen counts by approximately 14.4% compared with the borated wax collimator. However, the percentage increase in the nitrogen background was markedly different for the two collimators, being 55%

Fig.6·7 Thermal Neutron Fluence for Different Collimators -relative to the maximum for a borated wax collimator

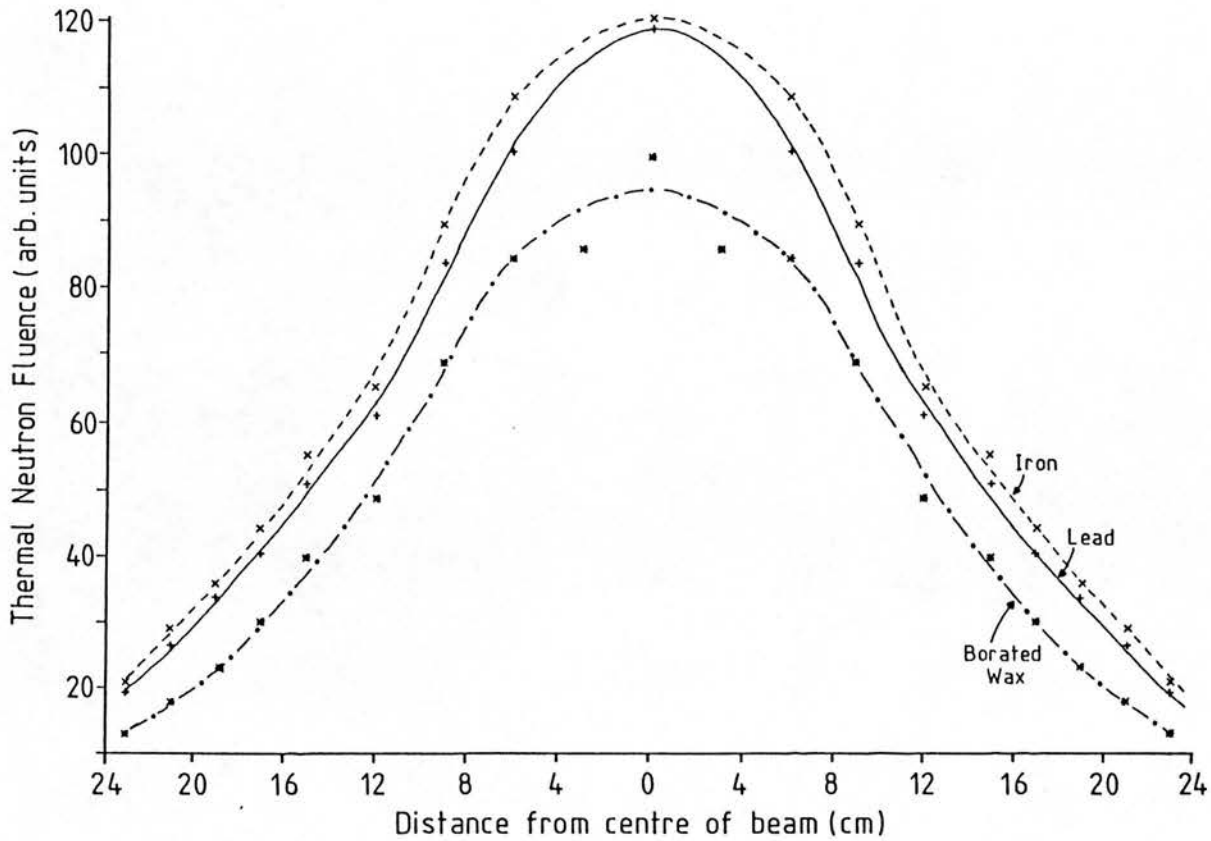

Fig.6·8

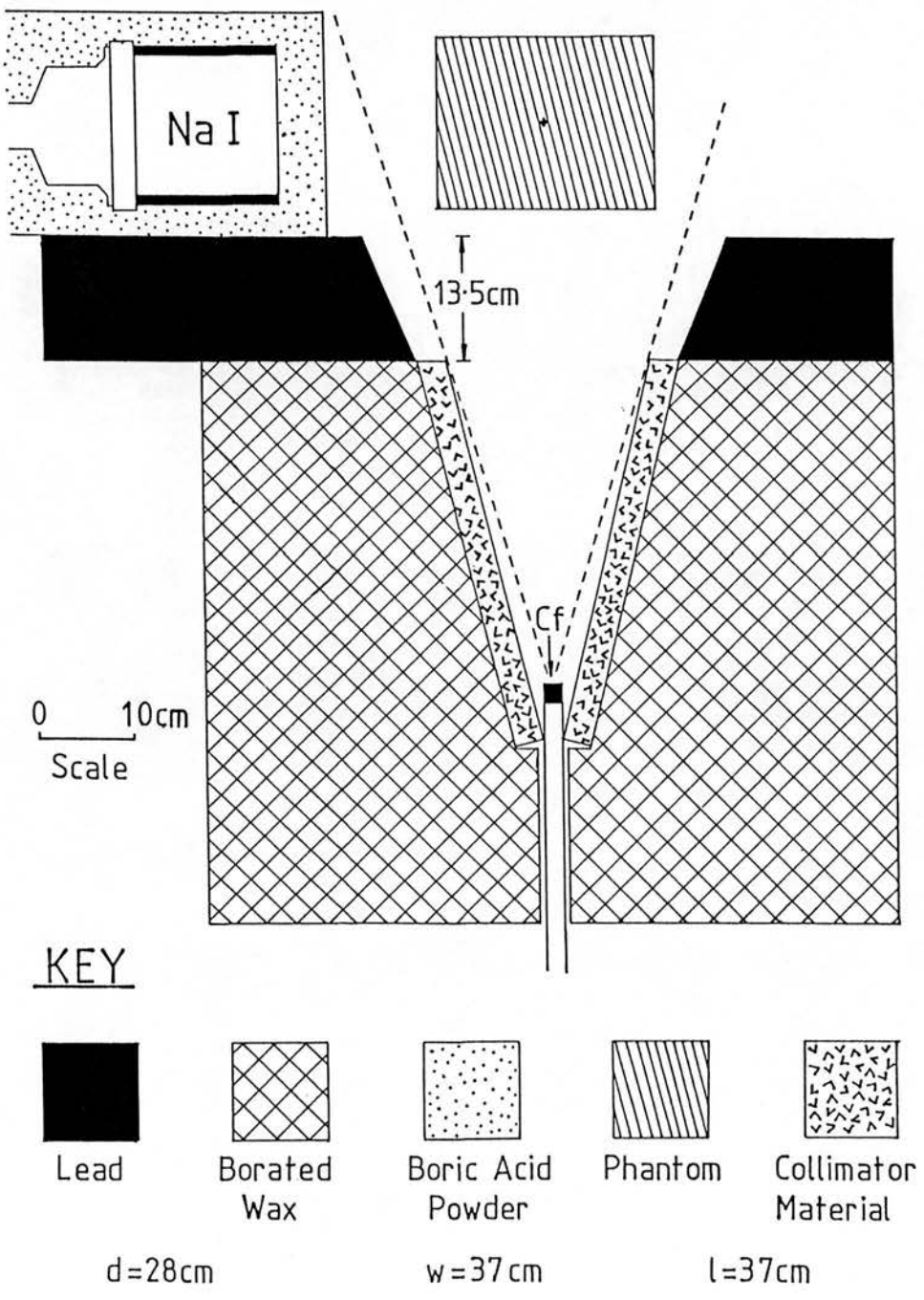
Na I
13·5cm
Cf
0 10cm
Scale
KEY
Lead
Borated Wax
Boric Acid Powder
Phantom
Collimator Material
d=28cm
w=37cm
l=37cm

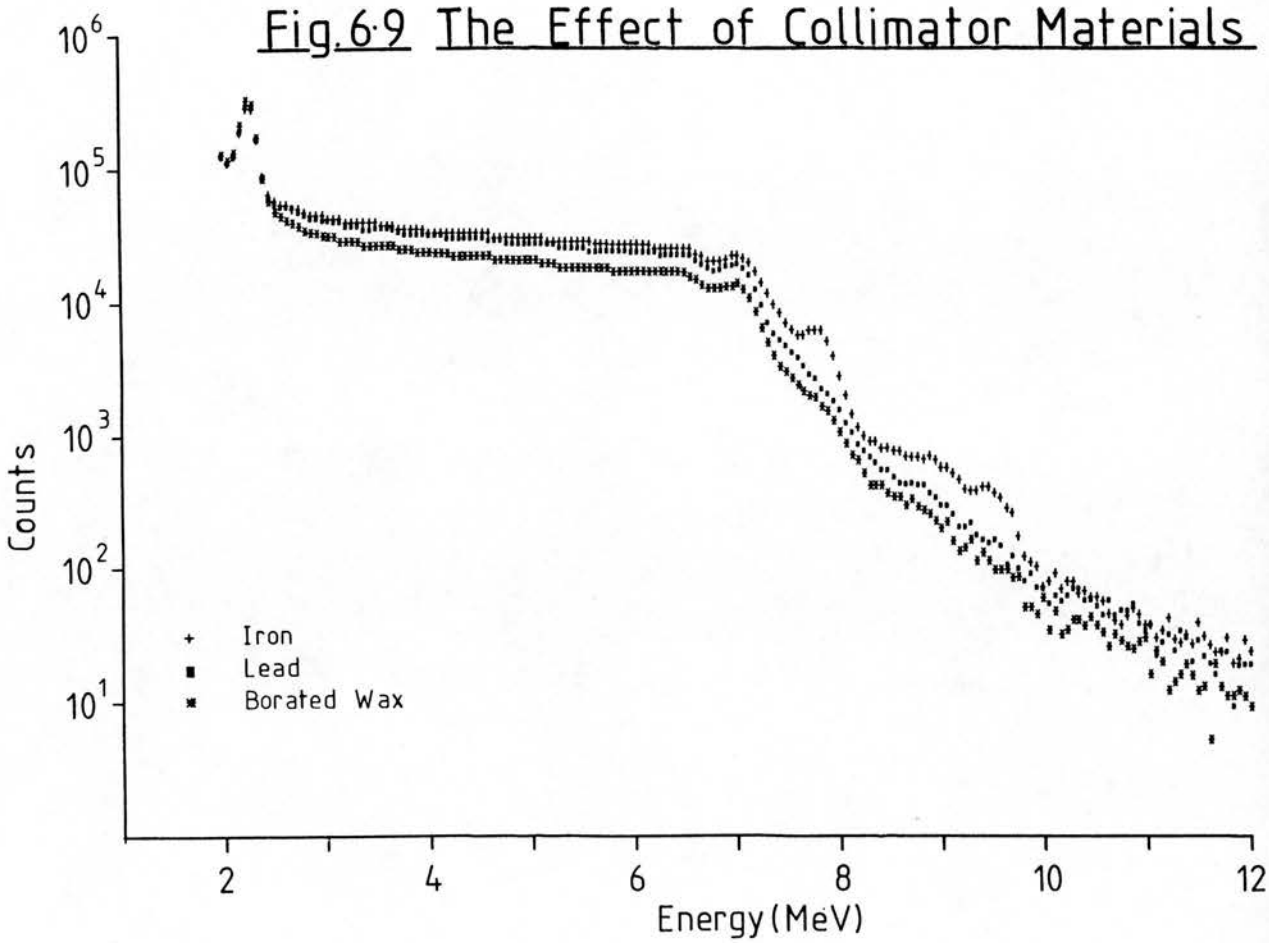
Fig.6·9 The Effect of Collimator Materials
Counts
10^6
10^5
10^4
10^3
10^2
10^1
Iron
Lead
Borated Wax
2
4
6
8
10
12
Energy (MeV)

TABLE 6.7

THE EFFECT OF COLLIMATOR MATERIAL ON THE PROMPT GAMMA RAY SPECTRUM

	Collimator Material			
	Borated Wax	Lead	Iron	Lead/ Borated Wax
Analyser Deadtime (%)	6.1	5.6	6.5	6.1
Count Rate in Region A (cps)	3,429	4,613	5,046	4,096
Count Rate in Region B (cps)	147	218	340	178
N Background Count Rate (cps)	1.83	2.84	3.24	2.17
Net N Count Rate (cps)	3.88	4.44	4.46	4.02
Coefficient of Variation of a Total Body Nitrogen Measurement (%)	2.33	2.46	2.60	2.42
Relative Thermal Neutron Fluence (arbitrary units)	410	588	615	-

for the lead collimator and 77% for the iron collimator. Observation of the water phantom spectra indicates significant peaks at 7.6 MeV and 9.3 MeV from thermal neutron capture in iron. Iron produces a range of other less prominent prompt gamma rays, and it is thought to be the pile-up of these high energy gamma rays which result in the greater increase in the nitrogen background for the iron collimator over that for the lead collimator. The increase in the relative thermal neutron fluence at the crystal for both metallic collimators is a consequence of the reduction in the degree of fast neutron shielding when heavy metals replace wax in the direct path between the ^{252}Cf and the crystal. The result of the increase in the nitrogen background was to increase the coefficient of variation of a total body nitrogen measurement despite the increase in the net nitrogen counts. In view of these results a composite collimator of lead and borated wax was constructed; the lead was placed at the start of the collimator, behind the ^{252}Cf source. In this way it was hoped to increase the net nitrogen counts without increasing the nitrogen background. However, no improvement over the results for the borated wax collimator was observed.

These investigations have shown that all three shielding materials, borated wax, lead and boric acid powder, significantly reduce the background in the nitrogen region of the spectrum. However, for a given irradiation/detector geometry the distance between the neutron source and detector is fixed. It is therefore important to optimise the relative proportions of these shielding materials in order to minimise the nitrogen background. The investigations of the collimator materials have shown how the thermal neutron fluence at

the patient can be increased with the consequent improvement in the nitrogen signal. However, a detrimental increase in the nitrogen background has also been demonstrated and has been shown to lead to a deterioration in the coefficient of variation of a total body nitrogen measurement.

CHAPTER 7

CHAPTER 7

COMPARISON OF BILATERAL AND UNILATERAL IRRADIATION/DETECTION GEOMETRIES AND CONSTRUCTION OF THE CLINICAL APPARATUS

The relative merits of the alternative "bilateral" and "unilateral" geometries have previously been discussed in section 1.3. Before building clinical apparatus these two geometries were investigated in order to determine the best precision obtainable for a total body nitrogen measurement. Estimates of precision were obtained using the coefficient of variation (CoV) based on counting statistics for a 40 minute irradiation of total body nitrogen (TBN). Only after such a study could a decision be made concerning the patient apparatus to be constructed, based on the optimum geometry with due consideration given to the patient groups to be studied.

All studies were performed using one detector, two ^{252}Cf neutron sources and Bush phantom thorax sections (major axis = 30 cm, minor axis = 20 cm, length = 40 cm); the nitrogen phantom contained 16.2 litres at twice body nitrogen concentration.

This chapter will first address itself to the optimisation of the bilateral geometry. The unilateral geometry will then, similarly, be optimised. Finally, a comparison of the two geometries will lead to the adoption of the design for the clinical apparatus.

7.1 Optimisation of the Bilateral Geometry

A 50 cm source to skin distance (for a 20 cm thick patient) was

Fig. 7·1

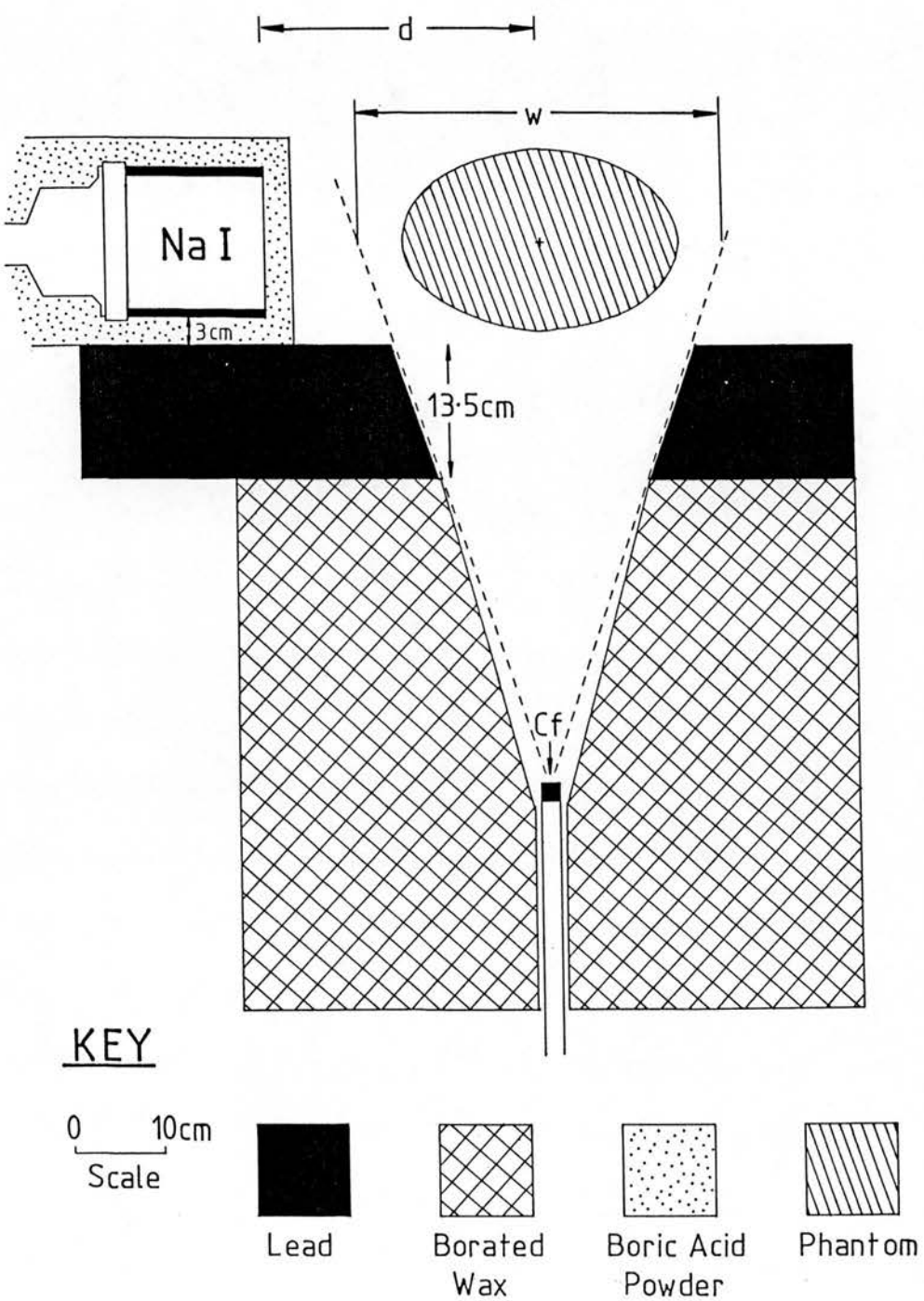

d = Crystal distance from phantom centre (cm)
w = Geometric beam width at the phantom centre (cm)
l = Geometric beam length at the phantom centre (cm)

chosen for the initial investigations since this distance has been adopted by centres elsewhere. The combination of lead, borated wax and boric acid was changed in an effort to minimise the nitrogen background. The shielding material combination determined is shown in Fig 7.1.

7.1.1 Detector Separation

The shielding arrangement of Fig 7.1 was adopted where the geometric beam width at the centre of the phantom was 40cm and the beam length 26 cm. The detector distance from the phantom centre (d) was varied between 23 cm and 30 cm. The results of the experiments differ from the rest of those in this chapter in that they were obtained using only one ^{252}Cf source and the phantom used in Chapter 5 (four times standard man nitrogen concentration); the results are shown in Table 7.1. It can be seen that as the detector separation increased the nitrogen background decreased owing to the improved detector shielding. However, the net nitrogen counts also decreased. The overall effect of increasing the detector separation was to increase the coefficient of variation of a total body nitrogen measurement. Although it is appreciated that a more uniform combined activation/detection profile across the patient width would be achieved with a greater detector separation, because of the reduced inverse square law variation in the detection profile, it was not considered to be the major concern since it was intended to normalise with total body hydrogen. It was therefore considered more appropriate to consider the coefficient of variation of the nitrogen measurement as the parameter to be reduced. In conclusion,

TABLE 7.1

THE EFFECT OF DETECTOR SEPARATION ON THE COEFFICIENT OF VARIATION OF A TOTAL BODY NITROGEN MEASUREMENT FOR THE BILATERAL GEOMETRY

	Detector-Phantom Centre Distance (d)		
	23 cm	25 cm	30 cm
Analyser Deadtime (%)	9.8	8.9	5.5
N Background Count Rate (cps)	1.36	1.32	0.83
Net N Count Rate (cps)	4.04	3.70	2.49
CoV of TBN Measurement (%)	1.95	2.08	2.48
Relative Thermal Neutron Fluence (Arbitrary Units)	323	318	228

TABLE 7.2

THE EFFECT OF GEOMETRIC BEAM WIDTH ON THE COEFFICIENT OF VARIATION OF A TOTAL BODY NITROGEN MEASUREMENT FOR THE BILATERAL GEOMETRY

	Geometric Beam Width (w)		
	40 cm	30 cm	20 cm
Analyser Deadtime (%)	9.3	7.7	5.5
N Background Count Rate (cps)	3.32	2.26	1.19
Net N Count Rate (cps)	6.49	5.91	4.28
CoV of TBN Measurement (%)	1.46	1.39	1.46
Relative Thermal Neutron Fluence (Arbitrary Units)	686	485	298

therefore, it appears appropriate to minimise the detector separation for the maximum patient width required to be accommodated. In order to accommodate a 50 cm wide patient and to allow for 3 cm of thermal neutron shielding material on the detector faces the detector separation was set at 56 cm (d = 28 cm). All further investigations were therefore performed with d = 28 cm.

7.1.2 Geometric Beam Width at the Patient Centre

The geometry of Fig 7.1 was adopted with d = 28 cm and the geometric beam width at the patient centre (w) varied between 20 cm and 40 cm (geometric beam length remaining constant at 26 cm).Water and nitrogen thorax phantoms were irradiated alternately and the results for the various beam widths are shown in Table 7.2. As the beam width was reduced the nitrogen background decreased owing to the improved detector shielding. However, the net nitrogen counts also decreased with the beam width as a consequence of the activation of a decreasing proportion of the phantom. There is little difference in the coefficient of variation (CoV) for a total body nitrogen measurement with geometric beam width. However, in order to ensure a "total body" nitrogen measurement it is important to activate as much of the body as possible. For this reason, a 40 cm geometric beam width was adopted for the patient studies, although it is appreciated that the patient's arms may lie outwith this field. For patients there may also be some improvement in the CoV for the 40 cm beam width by virtue of the activation and detection of nitrogen beyond the limits of the phantom used in this study.

7.1.3 Geometric Beam Length at the Patient Centre

The shielding combination and irradiation/detection geometry of Fig 7.1 was adopted with d = 28 cm and w = 40 cm. The geometric beam length is the length of beam which would be defined by the extension of the collimator, in any line parallel to the patient longitudinal axis. In this experiment the geometric beam length at the patient centre was varied from 13 cm to 39.5 cm (phantom length = 40 cm) and the results for the water and nitrogen phantom spectra are shown in Table 7.3. It can be seen that the nitrogen background increased with geometric beam length. A separate experiment performed without a phantom showed that the background in the nitrogen region increased with increasing geometric beam length. Therefore the increasing background in the nitrogen region with the phantom present for increasing beam lengths was shown to be due to increased counts from room activation as well as from the phantom. The net nitrogen counts detected also increased because of the increased proportion of the phantom coming to lie within the limits of the geometric beam length and being activated. The resulting changes in the signal:background ratio produced a minimum for the coefficient of variation of a total body nitrogen measurement at a geometric beam length of 26cm. It is important to remember that increases in the geometric beam length produce greater patient doses, and that increased patient dose must be balanced against the improvement in the CoV. If the geometric beam area is equated to dose then for an equivalent dose geometric beam lengths of 13cm and 26cm would give approximately equivalent CoV values for a total body nitrogen measurement. However, with a beam length of 26cm this precision could be achieved in half the time

TABLE 7.3

THE EFFECT OF BEAM LENGTH ON THE COEFFICIENT OF VARIATION OF A TOTAL BODY NITROGEN MEASUREMENT FOR THE BILATERAL GEOMETRY

	Geometric Beam Length				
	13 cm	20 cm	26 cm	33 cm	40 cm
Analyser Deadtime (%)	5.3	8.1	9.3	11.7	12.8
N Background Count Rate (cps)	1.43	3.07	3.32	5.58	6.67
Net N Count Rate (cps)	3.30	4.78	6.49	7.36	7.96
CoV of TBN Measurement (%)	1.91	1.83	1.46	1.60	1.60
Relative Thermal Neutron Fluence (Arbitrary Units)	467	682	686	962	1071

TABLE 7.4

THE EFFECT OF SOURCE TO SKIN DISTANCE ON THE COEFFICIENT OF VARIATION OF A TOTAL BODY NITROGEN MEASUREMENT FOR THE BILATERAL GEOMETRY

	SSD (for 20 cm thick patient)		
	45 cm	50 cm	55 cm
Analyser Deadtime (%)	11.5	9.3	8.2
N Background Count Rate (cps)	5.50	3.32	2.98
Net N Count Rate (cps)	7.03	6.49	5.09
CoV of TBN Measurement (%)	1.65	1.46	1.72
Relative Thermal Neutron Fluence (Arbitrary Units)	964	686	651

required for a 13cm beam length. It was therefore decided that the optimum geometric beam length is 26cm.

7.1.4 Californium-252 Source to Skin Distance

The 50 cm source to skin distance (SSD) used in the optimisation of the shielding combination geometry to date was chosen as a compromise between increased activation of the patient and the uniformity of activation across the patient width and through the patient depth. It remains to be seen whether or not an alternative SSD may improve the CoV for the nitrogen measurement. In order to investigate this the shielding material combination of Fig 7.1 was adopted, but the collimator dimensions altered to maintain a geometric beam width and length at the patient centre of 40 cm and 26 cm respectively when the SSD was changed. Source to skin distances (for a 20 cm thick patient) of 45 cm and 55 cm were investigated and the results are presented in Table 7.4. It can be seen that both the net nitrogen and the nitrogen background counts increased with a reduction in the SSD. However, the resultant effect on the CoV has been to minimise it for a SSD of 50 cm. This may well be a consequence of having optimised the shielding material combination and geometric beam width and length for this SSD! A SSD of 50 cm was therefore adopted as being optimum for the bilateral geometry.

7.1.5 Shielding Material Combination

If the shielding of Fig 7.1 was to be adopted for the construction of clinical apparatus, then in order to accommodate a scanning bed with

wheels and tracking, its shielding would have to be modified. The clinical apparatus was intended to accommodate patients of up to 50 cm width and 30 cm thickness. For the centre of a 30 cm thick patient to be aligned with the detector longitudinal axis and to allow 4.5 cm for the bed wheels and tracking then the shielding materials must finish 19.5 cm below the detector axis over a 50 cm wide region. This would require the reduction by 7 cm of the shielding materials. Such a loss may change the optimum shielding material combination. To investigate this the geometry shown in Fig 7.2 was adopted. The amount of lead composing "Z" was varied from 1.5 cm to 11 cm. The results for the different shielding arrangements are shown in Table 7.5. It can be seen that the nitrogen background and the relative thermal neutron fluence at the detector were greatest for the greatest thickness of lead, as also was the net nitrogen count. Presumably the net nitrogen counts increased with the thickness of lead used because of the backscatter of neutrons into the main beam, as discussed in section 6.4 on collimator materials. The resultant effect on the coefficient of variation of a 40 minute total body nitrogen measurement was to minimise it with 13.5 cm of lead shielding.

7.1.6 Thermal Neutron Shielding of Detector Face

The advantages and disadvantages of using ^{10}B or ^{6}Li as thermal neutron absorbers have already been discussed in section 6.3. It has been noted that ^{10}B produces a prompt 0.48 MeV gamma ray in 94% of its thermal neutron captures. Whilst lead can be used to shield these gamma rays around the detector sides, large thicknesses of

Fig. 7·2

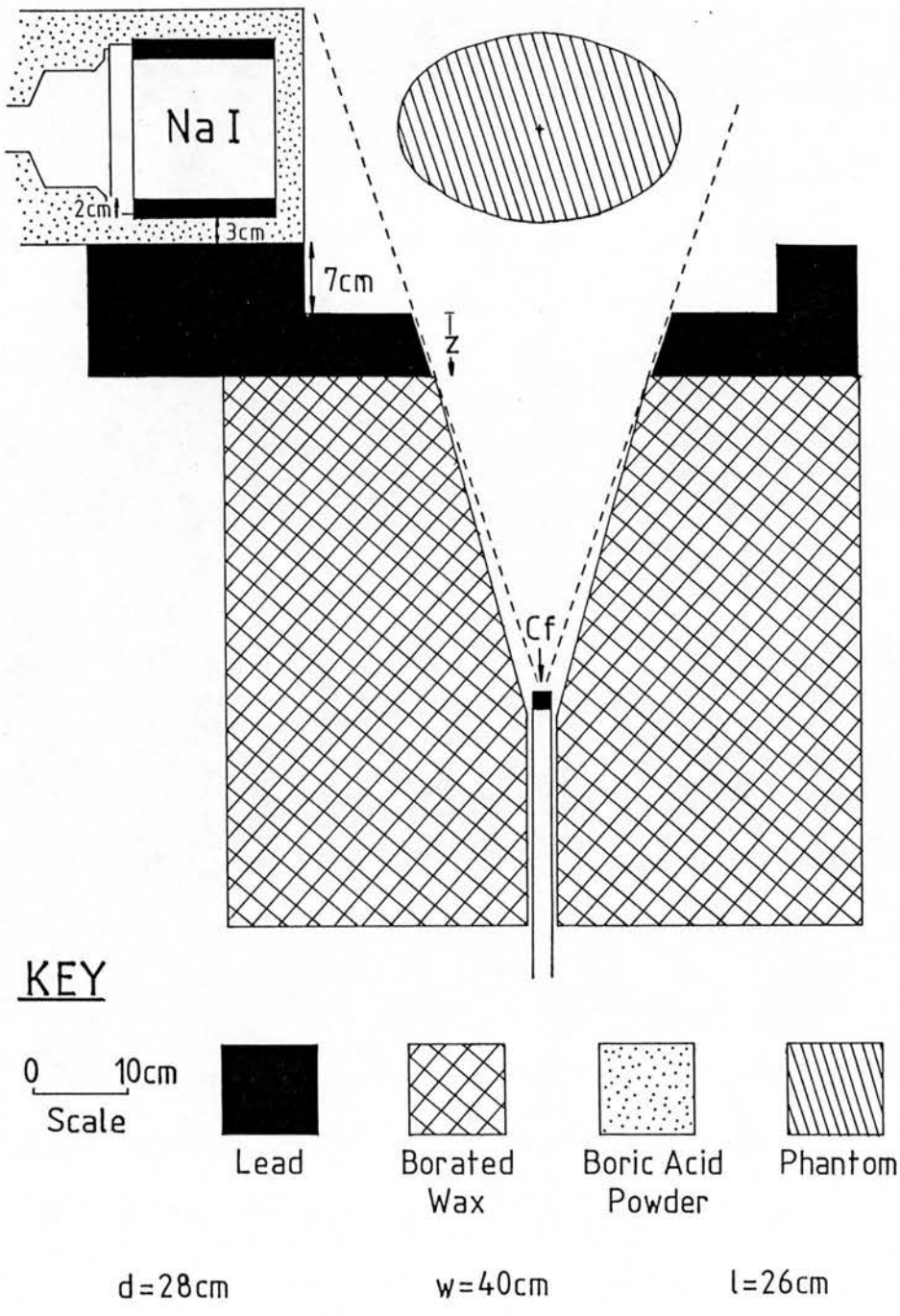
Na I
2cm
3cm
7cm
IZ
Cf
KEY
0 10cm
Scale
Lead
Borated Wax
Boric Acid Powder
Phantom
d=28cm
w=40cm
l=26cm

TABLE 7.5

OPTIMISATION OF THE BILATERAL GEOMETRY SHIELDING MATERIAL COMBINATION

	Thickness of Lead Shielding		
	8.5 cm	13.5 cm	18.0 cm
Analyser Deadtime (%)	11.1	9.0	11.0
N Background Count Rate (cps)	3.66	3.08	5.00
Net N Count Rate (cps)	5.42	5.63	6.05
CoV of TBN Measurement (%)	1.78	1.60	1.81
Relative Thermal Neutron Fluence (Arbitrary Units)	682	660	870

TABLE 7.6

EFFECT OF THE DETECTOR FACE THERMAL NEUTRON SHIELDING ON THE BACKGROUND IN THE NITROGEN REGION FOR THE BILATERAL GEOMETRY

	Thermal Neutron Shielding Thickness					
	H_3BO_3			LiF		
	1 cm	2 cm	3 cm	1 cm	2 cm	3 cm
Total Count Rate (kcps)	76.0	73.8	69.7	71.8	66.6	63.0
Analyser Deadtime (%)	20	19	18	20	18	17
0.48 MeV Gamma Ray Count Rate (kcps)	7.57	7.73	7.55	1.79	1.57	1.37
N Background Count Rate (cps)	4.10	3.22	3.01	6.99	4.88	4.34
Relative Thermal Neutron Fluence (Arbitrary Units)	867	780	659	1353	1129	983

lead on the detector face would reduce the net nitrogen counts. It was therefore considered worthwhile investigating the possible advantages of shielding the crystal face with lithium fluoride (LiF). The geometry of Fig 7.2 was used where Z = 6.5 (a total of 13.5 cm of lead), and the thermal neutron shielding of the detector face was varied for 1,2 and 3 cm of both LiF and H_3BO_3. The results are presented in Table 7.6. With increasing thermal neutron absorber thickness the total count rate, 0.48 MeV gamma ray count rate, analyser deadtime, nitrogen background count rate and thermal neutron fluence at the crystal all decreased. The reduction of the thermal neutron fluence at the crystal was due to the greater number of thermal neutrons removed from the scatter into the detector face, and the consequent reduction of the crystal prompt gamma rays has reduced the pile-up in the nitrogen background. Comparison of the prompt gamma ray spectra for a given thickness of LiF and H_3BO_3 shows that the greater cross-section of ^{10}B has reduced the relative thermal neutron fluence at the crystal and so reduced the nitrogen background significantly below that for LiF. This has occurred despite the reduction of the 0.48 MeV gamma rays when using LiF. As a consequence of this investigation it was decided to shield the detector face with 3 cm of boric acid powder.

7.1.7 Composite Sensitivity Uniformity

The uniformity of the combined activation and detection sensitivity through a 22.5 cm thick phantom was measured for the clinical apparatus. The measurement was not considered necessary to reach a decision about which irradiation/detection geometry to use for the

Fig.7·3 Uniformity of Combined Activation/Detection Sensitivity Through a 22·5cm Thick Phantom for a Bilateral Geometry

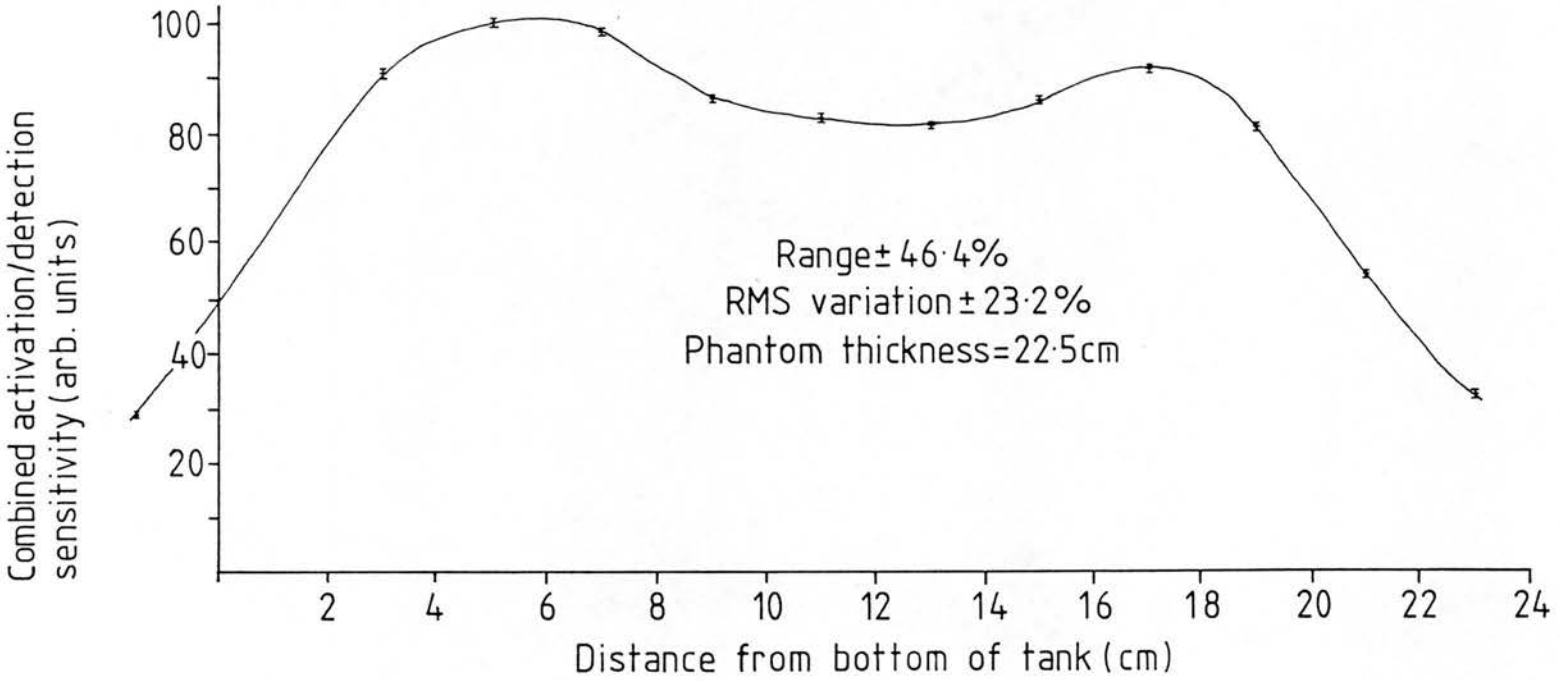

clinical apparatus since the uniformity is much less important when hydrogen is used as an internal standard. However, it remains worthwhile to compare the composite sensitivity uniformities for the two geometries. Nickel (Ni) was used as an alternative element to nitrogen for the reasons outlined in Appendix VI. The activation/detection sensitivity profile with depth through the 22.5 cm deep phantom can be seen in Fig 7.3. The profile is asymmetrical because only 30 cm deep phantoms would be aligned with the centre of the apparatus. The maximum counts are generated at the peak corresponding to the bottom of the phantom as expected, since this side was closest to a neutron source. The profile has an RMS variation of ± 23.2% about the mean. If calculated over the central (2-20 cm), region the RMS variation reduces to ± 9.35%; giving an indication of the uniformity which could be achieved if premoderation was adopted.

7.2 Optimisation of the Unilateral Geometry

Investigation of the unilateral geometry was performed with certain limitations placed on the source to skin distance and shielding dimensions, viz:-

(i) The same SSD of 50 cm was used. This SSD ensured the same uniformity of activation with depth through a phantom for the unilateral geometry as that for the bilateral geometry. However it is appreciated that although both the net nitrogen counts and the counts in the nitrogen background could be expected to decrease with increasing source to skin distance,

Fig.7·4

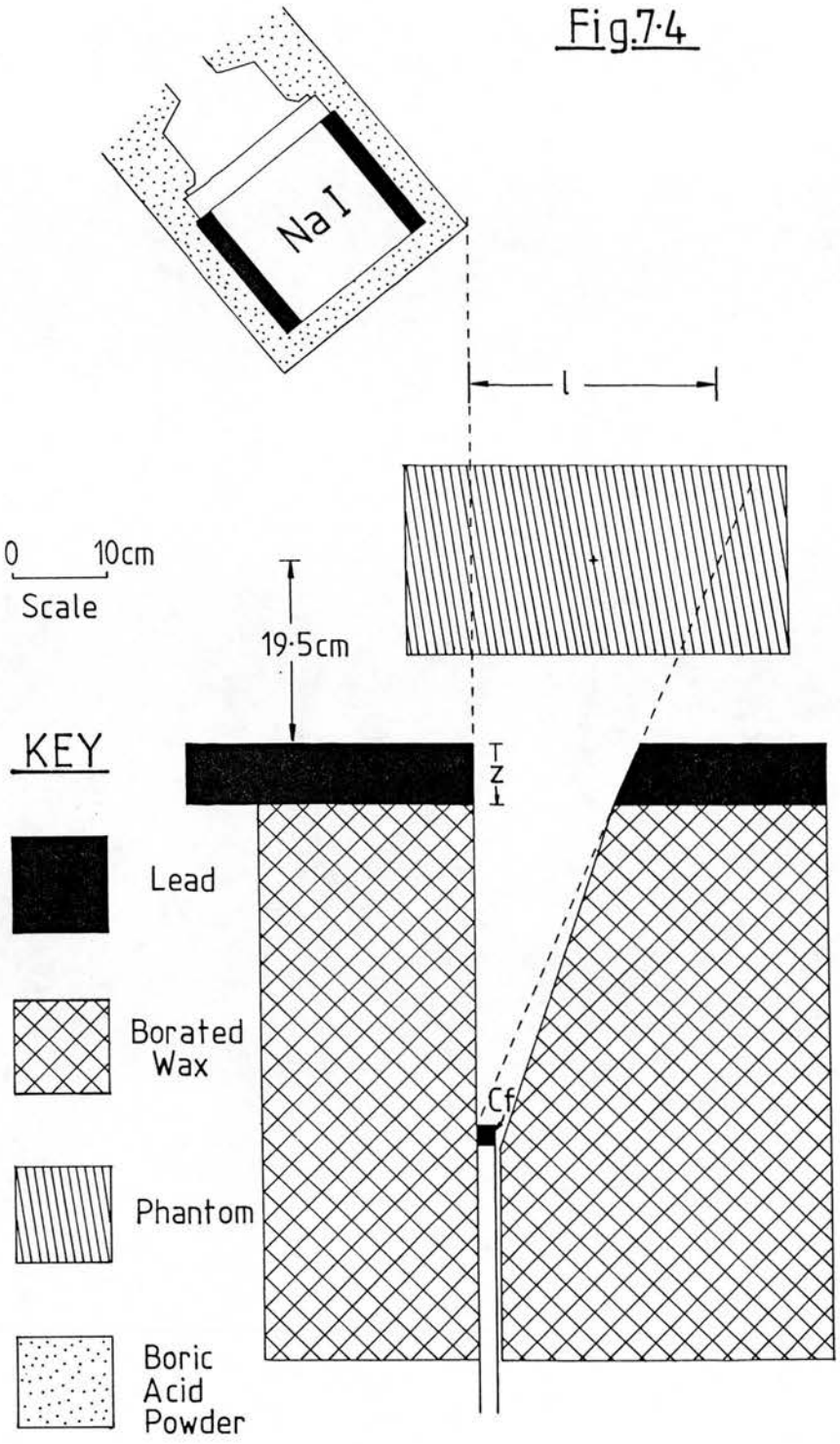

l=Geometric beam length at the phantom centre (cm)
w=Geometric beam width at the phantom centre (cm)

that their resultant effect on the CoV for a total body nitrogen measurement would remain unknown for different SSDs.

(ii) The detector housing was to be the same.

(iii) The distance between the patient centre and the source shielding materials was to be 19.5 cm since this distance would be required in practice to accommodate the scanning bed.

(iv) The detector housing distance from the patient centre was fixed at 20 cm so as to accommodate a 30 cm thick patient with 5 cm clearance.

The geometry used for the investigations is shown in Fig 7.4. The thorax phantom remained in the position shown throughout and the detector was orientated such that its longitudinal axis passed through the beam centre on the phantom longitudinal axis.

7.2.1 Geometric Beam Width at the Patient Centre

The geometry of Fig 7.4 was adopted where Z = 6.5 cm and 1 = 26 cm. The geometric beam width (w) was altered between 30 cm and 50 cm and the results are presented in Table 7.7. As the beam width was increased both the nitrogen background and the net nitrogen counts increased. The resultant change of the coefficient of variation of a total body nitrogen measurement was minimal. It should be noted that with patients the coefficient of variation may be improved with larger beam widths because of activation of nitrogen beyond the

TABLE 7.7

THE EFFECT OF GEOMETRIC BEAM WIDTH ON THE COEFFICIENT OF VARIATION OF A TOTAL BODY NITROGEN MEASUREMENT FOR THE UNILATERAL GEOMETRY

	Geometric Beam Width (w)		
	30 cm	40 cm	50 cm
Analyser Deadtime (%)	5.2	5.7	6.2
N Background Count Rate (cps)	1.19	1.46	1.60
Net N Count Rate (cps)	2.60	2.80	3.03
CoV of TBN Measurement (%)	2.18	2.20	2.13
Relative Thermal Neutron Fluence (Arbitrary Units)	138	198	239

TABLE 7.8

THE EFFECT OF GEOMETRIC BEAM LENGTH ON THE COEFFICIENT OF VARIATION OF A TOTAL BODY NITROGEN MEASUREMENT FOR THE UNILATERAL GEOMETRY

	Geometric Beam Length (l)			
	13 cm	20 cm	26 cm	33 cm
Analyser Deadtime (%)	3.8	4.5	5.8	6.3
N Background Count Rate (cps)	0.89	1.10	1.39	1.78
Net N Count Rate (cps)	1.35	2.05	2.89	3.29
CoV of TBN Measurement (%)	3.41	2.59	2.11	2.06
Relative Thermal Neutron Fluence (Arbitrary Units)	125	143	189	215

extent of the 30 cm wide phantom used here. It was therefore concluded that a 50 cm geometric beam width should be adopted for the unilateral geometry. This beam width should ensure that the total width of the patient lies within the beam area.

7.2.2 Geometric Beam Length at the Patient Centre

The geometry of Fig 7.4 was adopted where Z = 6.5 cm and w = 40 cm. The geometric beam length (l) was varied between 13 cm and 32 cm. The results of the irradiations are presented in Table 7.8. As the geometric beam length was increased both the net nitrogen and nitrogen background counts increased. The combination of these two changes was to reduce the coefficient of variation for increasing geometric beam lengths. However, any improvement in the CoV must be considered in conjunction with the increasing patient dose with beam length. A doubling in beam length is equated to an approximate doubling in patient dose. The CoV can be seen to decrease little in changing from a 26 cm to a 32.5 cm beam length. Therefore, there is no advantage in using beam lengths greater than 26 cm. There is indeed only an 18.5% decrease in the CoV when changing from a 19.5 cm to a 26 cm beam length for an approximate 33% increase in patient dose. Therefore for a beam length of 26cm the same patient dose would be imparted in 30 minutes as that which would be imparted in 40 minutes for a 19.5cm beam length. This shorter, 30 minute counting period would generate 2,168 net nitrogen counts and 1,043 nitrogen background counts, resulting in a CoV of 2.44%. This compares favourably with a CoV of 2.59% for a 40 minute scan with a 19.5 cm beam length and has been attained in 30 minutes instead of 40

Fig.7.5 Shielding Material Combination

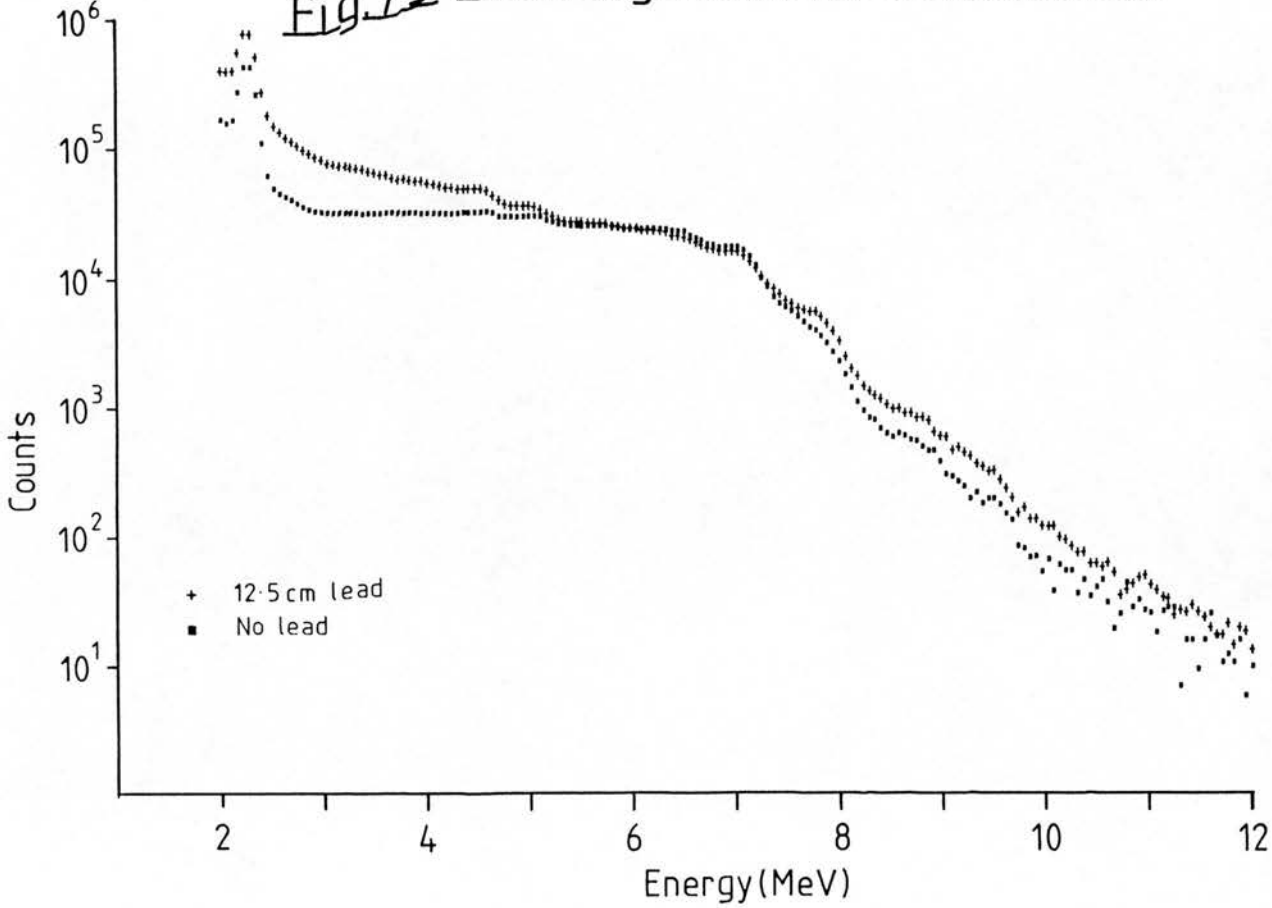

TABLE 7.9

OPTIMISATION OF SHIELDING MATERIALS FOR THE UNILATERAL GEOMETRY

	Thickness of Lead Shielding		
	0 cm	6.5 cm	12.5 cm
Analyser Deadtime (%)	11.6	6.2	5.8
Net H Count Rate (cps)	2,908	1,999	1,950
N Background Count Rate (cps)	2.88	1.58	1.73
Net N Count Rate (cps)	2.51	2.56	2.88
CoV of TBN Measurement (%)	3.22	2.45	2.28
Relative Thermal Neutron Fluence (Arbitrary Units)	218	220	276

minutes, whilst administering the same radiation dose. This study concludes that the optimum geometric beam length for the unilateral geometry is 26 cm.

7.2.3 Shielding Material Combination

The geometry of Fig 7.4 with a fixed geometric beam width (w) at the phantom centre of 50 cm and a geometric beam length (l) of 26 cm was utilised. The thickness of lead (Z) used in the source shielding was varied from 0 cm to 12.5 cm with concomitant changes in the thickness of borated wax. The spectra are shown in Fig 7.5 and the results presented in Table 7.9. It can be seen that as the fast neutron shielding was maximised the thermal neutron flux at the crystal was reduced but the nitrogen background was increased. As has previously been observed the net nitrogen counts increase as lead becomes an increasing component of the collimator. The resultant effect on the coefficient of variation of a total body nitrogen measurement was to reduce it for increasing thicknesses of lead. The conclusion of these investigations was that a minimum of 12.5 cm of lead should be used as shielding.

7.2.4 The Effect of Phantom Position on the Prompt Gamma Spectrum

The position of the phantom in the unilateral geometry could reasonably be expected to affect the prompt nitrogen spectrum more severely than it would in the bilateral geometry. This is because the phantom can intervene in the direct path between the ^{252}Cf and the detector and may:

Fig.7·6

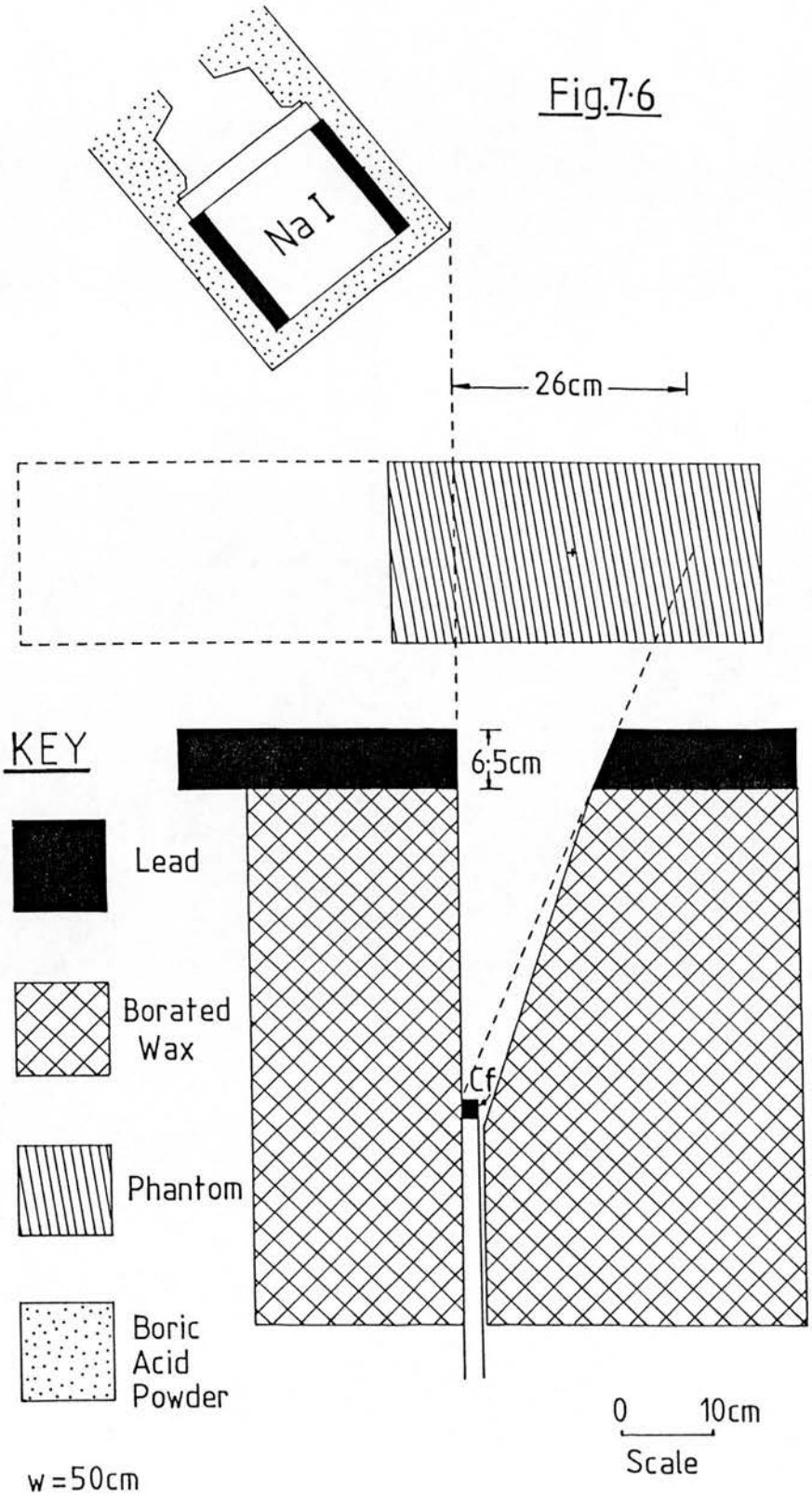
NaI
26cm
KEY
Lead
Borated Wax
Phantom
Boric Acid Powder
6·5cm
Cf
0 10cm
Scale
w=50cm

TABLE 7.10

THE EFFECT OF PHANTOM POSITION ON THE COEFFICIENT OF VARIATION OF A TOTAL BODY NITROGEN MEASUREMENT FOR THE UNILATERAL GEOMETRY

	N Phantom Alone	N Phantom + Extension
Analyser Deadtime (%)	6.2	5.4
Net H Count Rate (cps)	1,999	2,080
N Background Count Rate (cps)	1.58	1.43 *
Net N Count Rate (cps)	2.56	2.56 +
CoV of TBN Measurement (%)	2.45	2.36
Relative Thermal Neutron Fluence (arbitrary Units)	220	202

\+ The net nitrogen counts are assumed to remain unchanged when the water phantom is used to extend the limits of the nitrogen phantom. This is a reasonable assumption. In practice the water phantom may increase the thermal neutron scatter into the nitrogen phantom so increasing the net nitrogen counts and further improving the coefficient of variation.

* This value has been calculated by subtracting the assumed net nitrogen counts from the measured counts in the nitrogen region when the water phantom was used to extend the nitrogen phantom. For reasons explained in + this value may be overestimated in which case the coefficient of variation would also be overestimated.

(i) attenuate the fast neutron beam, so reducing the activation of the crystal;

(ii) attenuate the hydrogen prompt gamma rays generated in the source shielding (linear attenuation coefficient of 2.23 MeV gamma rays in soft tissue = 0.045 cm^{-1});

(iii) generate hydrogen and nitrogen gamma rays from thermal neutron capture in the phantom; and

(iv) increase the thermal neutron scatter into adjacent phantom sections so increasing the nitrogen signal from those regions.

The geometry of Fig 7.6 was adopted where the water phantom extension is shown by the dashed line. Water and nitrogen phantoms were irradiated without the phantom extension in place, and then the nitrogen phantom was irradiated with the water phantom used to extend the phantom limits. The results are shown in Table 7.10. In order to derive a coefficient of variation for the situation with the "extended" phantom it was necessary to assume that the net nitrogen counts would remain unchanged (see Table notes for explanation) when the phantom was extended. This experiment demonstrated the dependence of the CoV on the position and extent of the phantom. It should be noted that in a patient nitrogen gamma rays would also be generated from the "extension" and that this would further improve the CoV. In conclusion then the CoV for a total body nitrogen measurement in vivo for the unilateral geometry cannot be accurately

Fig.7·7

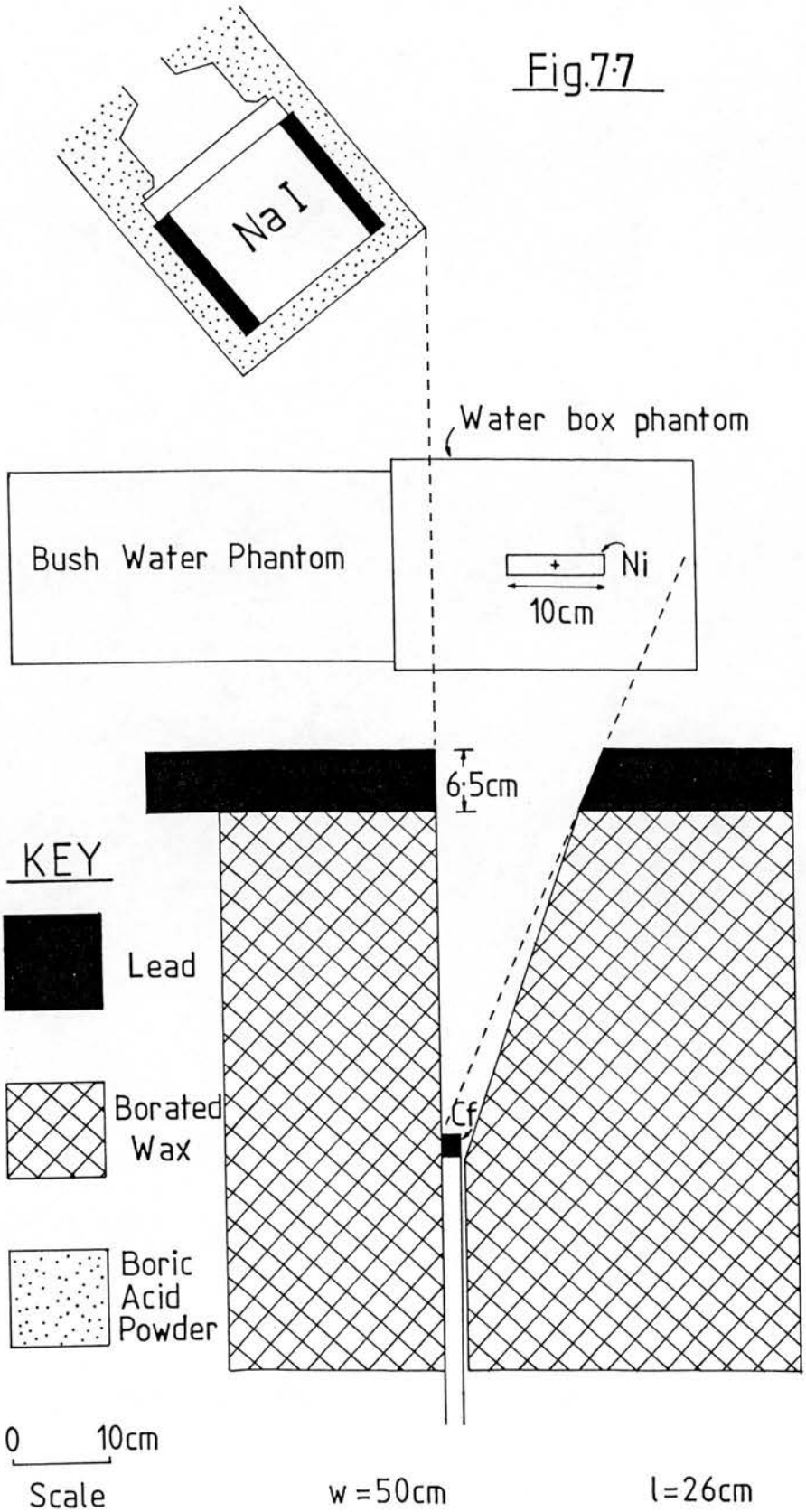
NaI
Water box phantom
Bush Water Phantom
Ni
10cm
6·5cm
KEY
Lead
Borated Wax
Cf
Boric Acid Powder
0 10cm
Scale
w = 50cm
l = 26cm

Fig.7·8 Uniformity of Combined Activation/Detection Sensitivity Through a 22·5cm Thick Phantom for a Unilateral Geometry

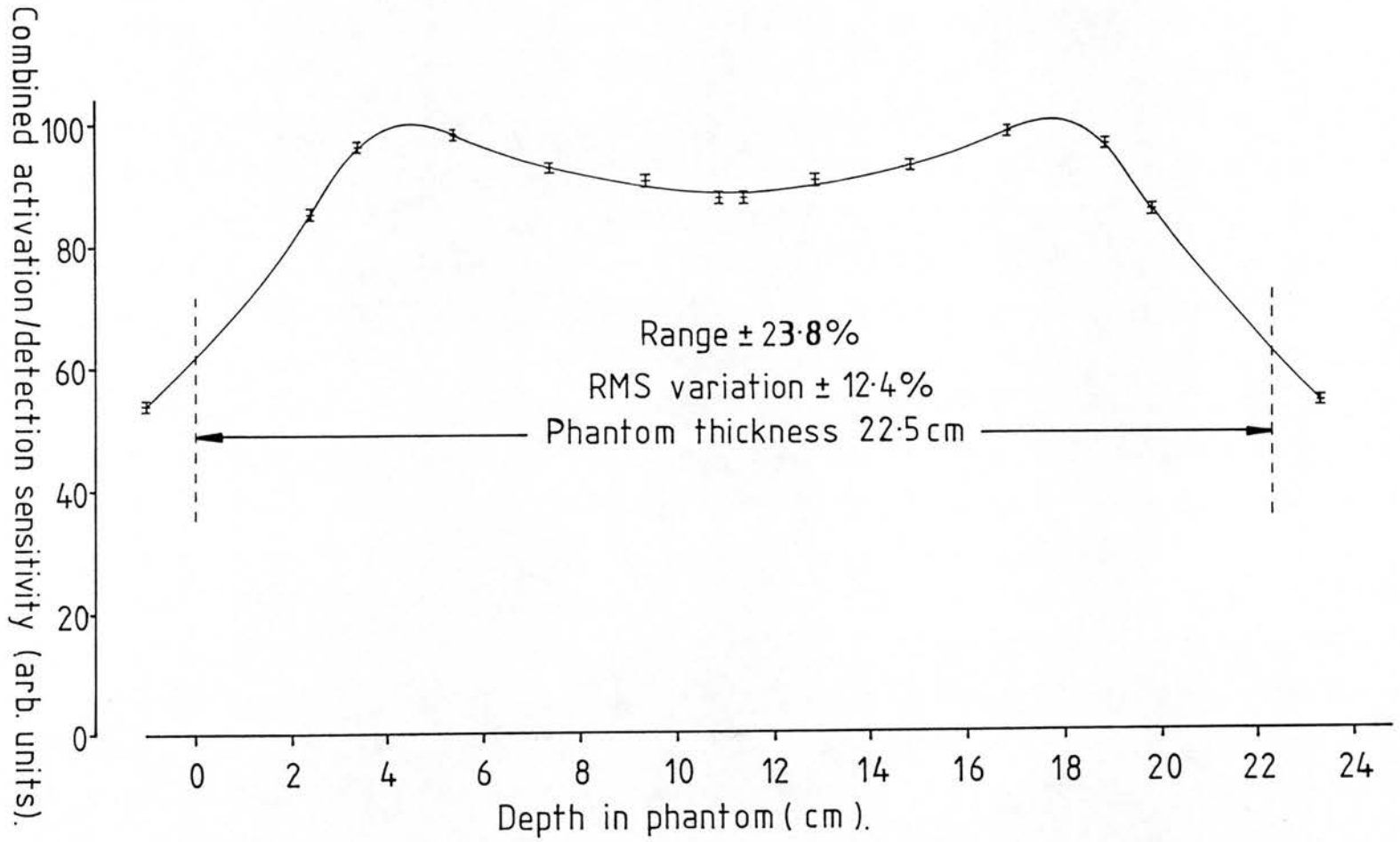

determined without scanning an entire anthropomorphic phantom. This, unfortunately, was not possible with this experimental set-up.

7.2.5 Composite Sensitivity Uniformity

The uniformity of the composite sensitivity through a phantom depth was determined with the arrangement shown in Fig 7.7. However, the crystal axis was displaced 13 cm from the ^{252}Cf to phantom centre line to measure the composite sensitivity which would be achieved in practice when two detectors are mounted side by side above the patient. The water phantom shown was 30 cm wide by 32.5 cm long by 22.5 cm thick. Fig 7.8 shows that the composite sensitivity peaks at a depth of approximately 4 cm into the body. The RMS variation through the full thickness of 22.5 cm was ± 12.4%. However, the RMS variation between 2 and 20 cm was ± 5.5%; this value could realistically be achieved with suitable premoderation. This uniformity of ± 5.5% is in good agreement with results obtained at Brookhaven (95) where 5 cm of premoderation and scanning yielded ± 4% to ± 6.5% for phantom thicknesses ranging from 10 cm to 25 cm respectively.

7.3 Comparison of the Bilateral and Unilateral Geometries

The optimum shielding combination for each of the geometries has been determined empirically. This was essential since neutron and gamma ray transport calculations, whilst detailing numbers in different energy groups, do not predict the effect of the incident neutron and gamma ray spectra on the prompt nitrogen spectrum from a sodium

iodide detector.

Optimisation of the shielding materials to minimise the coefficient of variation of a total body nitrogen measurement for each of the irradiation/detection geometries has yielded values of approximately $\pm$1.60% and $\pm$2.28% for the bilateral and unilateral geometries respectively. This improvement in the coefficient of variation for the bilateral geometry was achieved through the increase in detection sensitivity when the detectors are closer to the site of activation. The increase in the nitrogen counts was accompanied by an increase in the background counts; a consequence of the proximity of the detectors to the neutron sources. In view of these facts the bilateral geometry would appear to be superior in respect of achieving the minimum CoV per unit dose. However, in practical terms the bilateral geometry has limited the maximum patient width which can be accommodated to 50 cm, whereas there is no such limit for the unilateral geometry. The construction time and weight of the bilateral geometry apparatus would be almost twice that for the unilateral geometry apparatus because of the doubling in shielding materials. Despite these practical disadvantages the bilateral geometry has a significant practical advantage in that bilateral irradiation of the patient makes the apparatus most suitable for the critically ill intensive care patient. This is because such patients cannot be laid in a prone position throughout half of the irradiation period, as required with unilateral irradiation geometries. For these reasons the bilateral geometry was chosen for construction of the clinical apparatus.

Measurement of the composite sensitivity profiles with depth in a 22.5 cm deep phantom showed the RMS variation to be ± 23.2% and ± 12.4% for the bilateral and unilateral geometries respectively. The profile for the bilateral geometry was asymmetrical for reasons explained in section 7.1.7. The unilateral geometry can be seen to have a response which is more uniform with depth. The improved uniformity is a consequence of both the detection sensitivity and the self-absorption of the escaping photons acting in opposite directions to the thermal neutron flux depression. The gain in the composite sensitivity profile uniformity achieved with the unilateral geometry would not justify the adoption of this geometry since the factors responsible for its improved uniformity are also those which were responsible for the reduction of the net nitrogen counts, which contribute to the increase in the coefficient of variation of the measurement compared with the bilateral geometry.

7.4 Construction of Clinical Apparatus

Apparatus for the measurement of total body nitrogen, adopting the bilateral geometry, have been constructed at Auckland (4), New Zealand. It has been found that the detector separation of 48 cm is inadequate to accommodate larger patients (private communication). It was therefore decided to increase the detector separation in the clinical apparatus from 56 cm to 60 cm in order to accommodate patients up to 54 cm in width. The dimensions of the "Neutron Activation Room" (see Section 4.2) impose serious limitations on the dimensions of the clinical apparatus to be installed in the room.

7.4.1 Shielding Construction

The external dimensions of the wax shielding will affect the room background and the weight of the apparatus. Perpendicular to the line of scan the wax is limited by the room dimensions and therefore cannot exceed 95 cm; this is sufficient width to maximise the fast neutron shielding in the direct path between the ^{252}Cf and the crystals. Parallel to the line of scan the wax dimension was chosen to be 80 cm. This length should limit the dose to the patient outwith the beam area whilst limiting the weight of the apparatus. The external dimensions of the lead shielding were limited to those of the wax. This arrangement would weigh approximately 2.3 tonne excluding the detectors and housing. Such a mass requires support, which for the reasons outlined in Appendix VII is provided by aluminium (Al). The two main Al plates (3/4 inch thick HE30 Al) were supported by 3 inch, 0.5 inch thick angle Al at the four corners of the apparatus. The thickness of lead was reduced to accommodate the Al plates, since the experimental spectra discussed in Section 7.1.5 showed a smaller increase in the CoV when decreasing the 13.5 cm of lead than when increasing it. Also, this helped to reduce the mass of the apparatus. A cross-section of the central section of the apparatus perpendicular to the line of scan is shown in Fig 7.9. The Al plates can be seen; the lead suspended below the top Al plate is fixed by 6 bolts either side (not shown). A 10° slope of the ^{252}Cf delivery tubes ensures that the neutron sources fall under gravity into their correct irradiation position.

Each detector was shielded by a series of lead annuli of

Fig.7·9

Cross-Section of the Clinical Apparatus

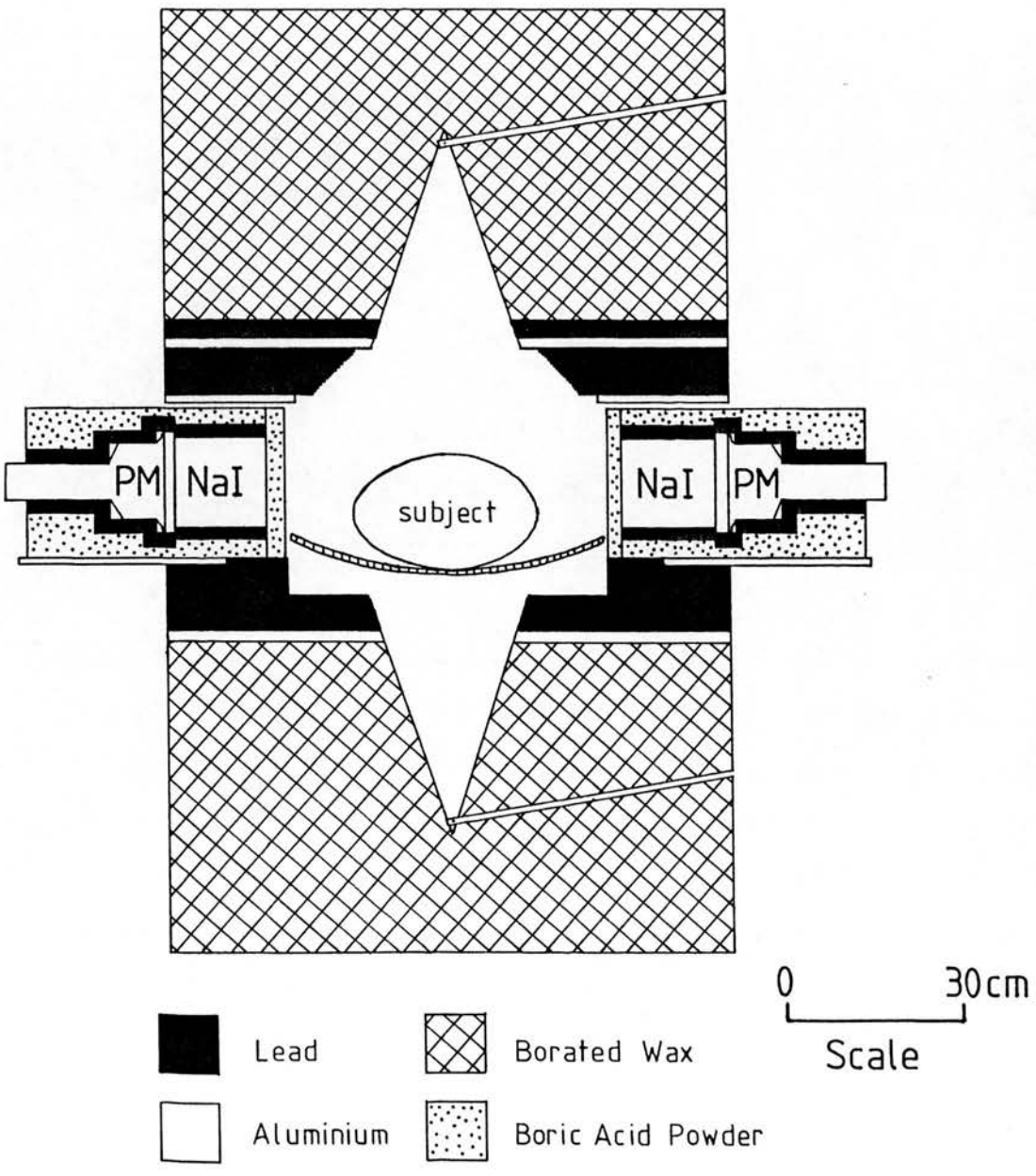

approximately 2 cm thickness. Each detector, with lead shielding, was then surrounded with boric acid powder, contained by an aluminium can, at least 3 cm thick at all places. Each detector face was then shielded with 3 cm of boric acid powder, held in position with sheets of bakelite. Bakelite was used in preference to other construction materials in order to reduce the number of high energy prompt gamma rays which would be generated in close proximity to the crystal volume. Each detector plus shielding arrangement weighs approximately 80 kg. In designing the detector shielding consideration was given to the ease with which the detector could be removed should the need arise. Unfortunately, it was not considered possible to do this without first removing the boric acid powder. However, once this is done removal of the lead annulus from around the crystal volume, enables the detector to be withdrawn with relative ease. Access to the dynode chain is readily available since this end of the detector was left to protrude beyond the shielding. A photograph of the part-completed detector shielding can be seen in Fig 7.10.

7.4.2 Scanning Bed

The bed was curved (see Fig 7.9) to raise the subject's arms nearer to the beam centre for improved activation and detection. The centre of the couch was 15 cm below the beam centre to enable a 30 cm thick patient to be positioned in the centre of the detector's field of view. The couch controls included:-

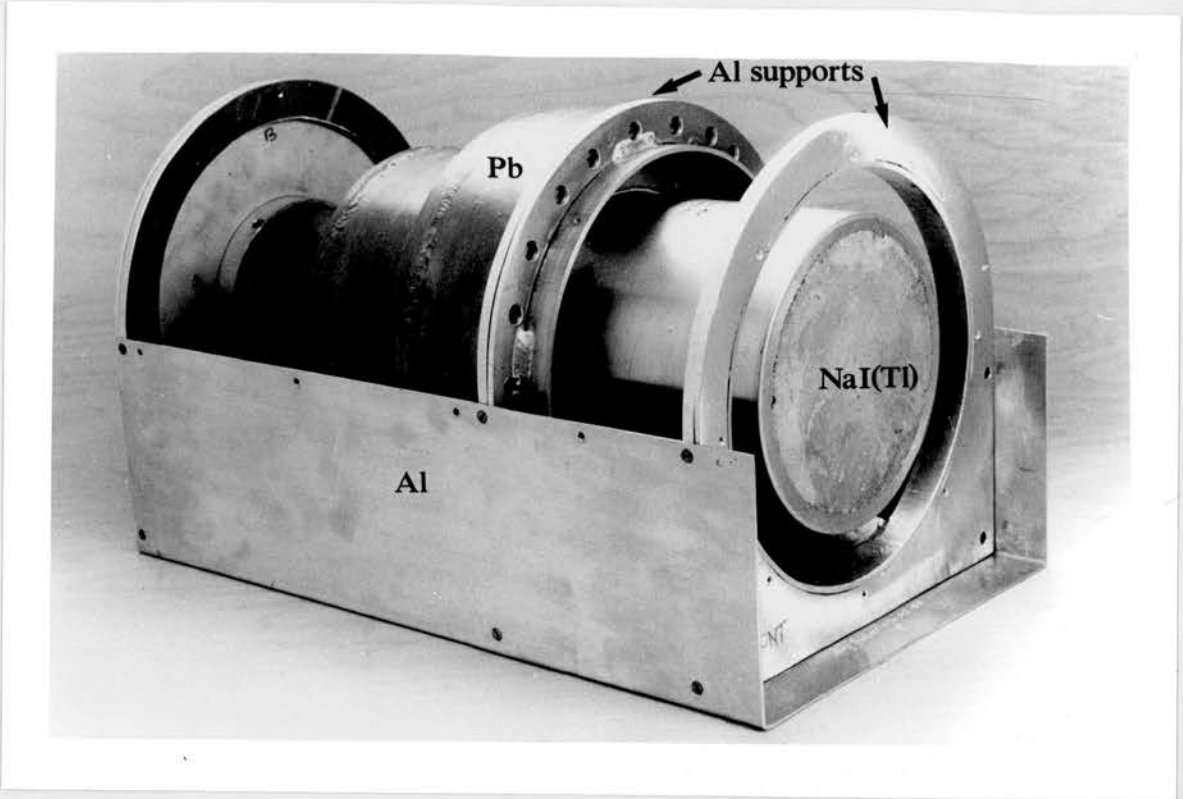

Fig 7.10 Part completed detector shielding indicating the position of the crystal volume.

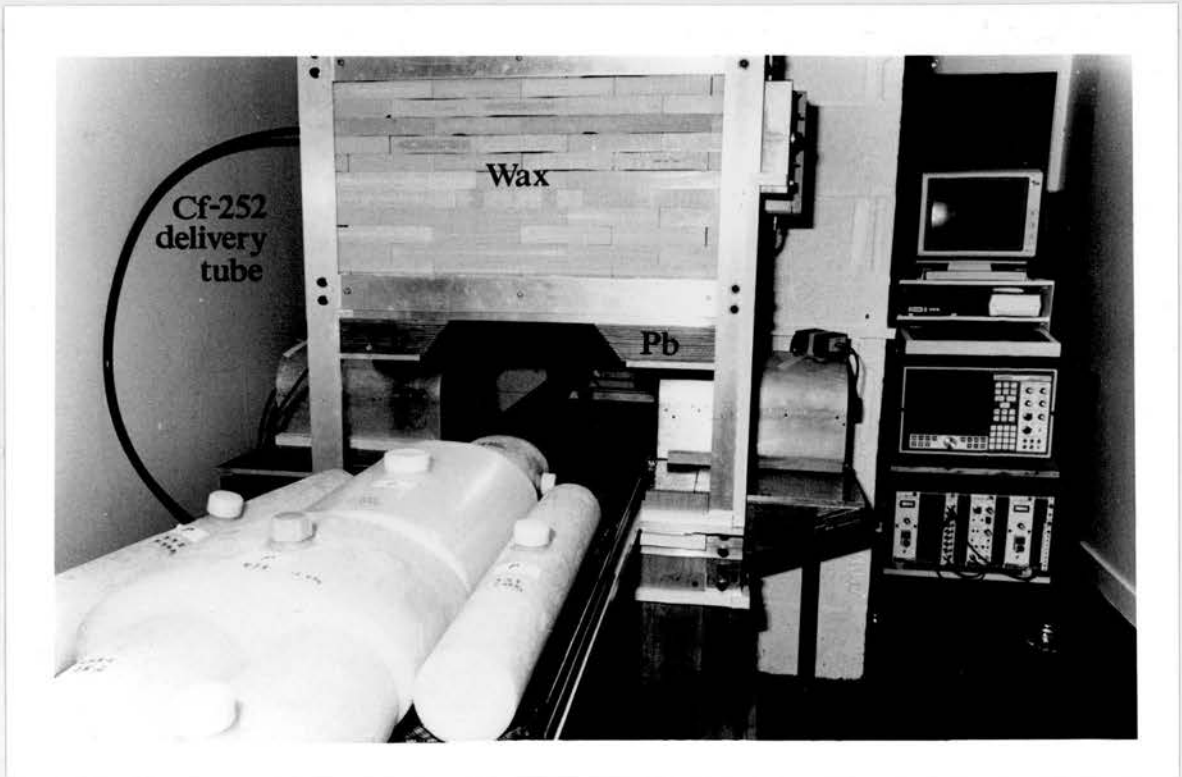

Fig 7.11 Clinical apparatus ' in situ'.

a) Forward/reverse.

b) Clutch release for manual positioning of the couch.

c) Variable speed control.

d) Scan limit switches for external control of the analyser collection time.

e) Electronic wiring for the automatic withdrawal of the ^{252}Cf sources as the second scan limit switch is triggered.

Fig. 7.11 is a photograph of the clinical apparatus as erected in the Activation Room.

This chapter has discussed how each of the two geometries was optimised to minimise the coefficient of variation of a nitrogen measurement. The bilateral geometry was shown to have a less uniform composite sensitivity profile with depth, though this is relatively unimportant when hydrogen is being used as an internal standard. This geometry also approximately doubles the time and cost of construction of the apparatus. However, despite these disadvantages the geometry was chosen for the construction of clinical apparatus since it was intended to study the critically ill, and such a geometry would not require the subject to be turned to lie face down mid-irradiation. Construction details of the clinical apparatus which will accommodate subjects up to 54 cm wide have been presented.

CHAPTER 8

CHAPTER 8

CALIBRATION OF CLINICAL APPARATUS

Calculation of the absolute mass of total body nitrogen from a subject spectrum requires a technique for estimatng the nitrogen background and a calibration factor for relating the nitrogen:hydrogen counts ratio to the mass ratio, which may be a function of body habitus. This chapter presents evidence of the effect of body habitus on both nitrogen background and the calibration factor "q". Various techniques for predicting the nitrogen background for a subject spectrum are presented and their limitations discussed. Finally a protocol for the necessary re-calibration of the apparatus as the ^{252}Cf decays is presented.

The optimum nitrogen energy integral had been determined from examination of a Bush phantom spectrum to give the minimum coefficient of variation for a nitrogen measurement. The limits of integration were fixed between 9.75 MeV and 11.5 Mev. The optimum hydrogen energy integral was fixed between 2.0 MeV and 2.52 MeV from reproducibility measurements on 10 Bush phantom spectra.

8.1 Methods for the Determination of the Nitrogen Background for a Subject Spectrum

The nitrogen background was determined from 40 minute (true time) irradiations of box phantoms, using nitrogen-free tissue equivalent solution (see Appendix VIII). It was important to use a tissue

Fig.8·1 Nitrogen Background as a Function of Size

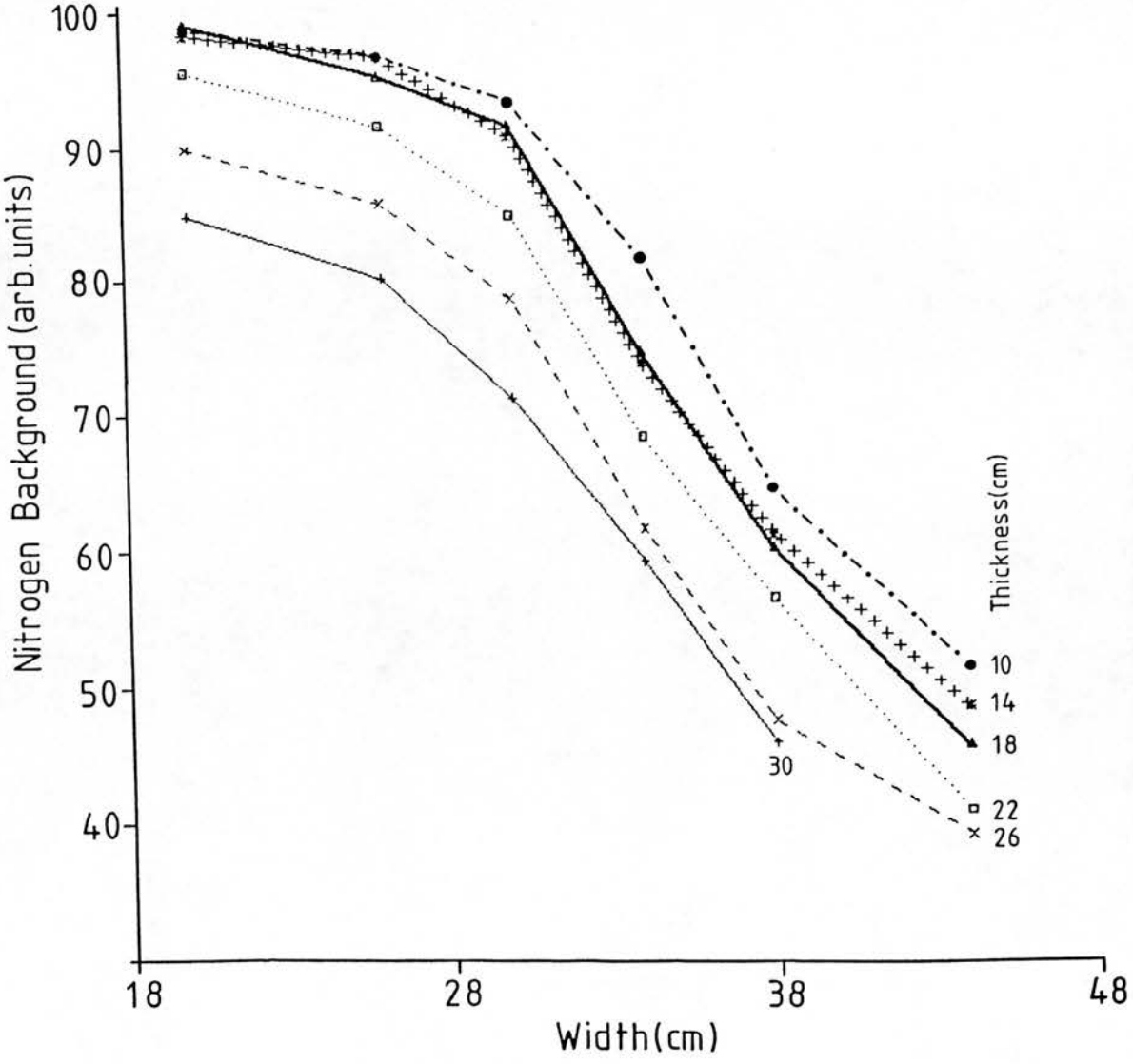

equivalent solution since elements generating high energy prompt gamma rays (particularly chlorine) affect the magnitude of the nitrogen background. Six perspex tanks covered a 20 cm to 44 cm width range in approximately 4 cm intervals (20,26,30,34,38,44 cm). The thicknesses used ranged from 10 cm to 30 cm in 4 cm intervals. All tanks were 60 cm long. 35 spectra in all were collected over a 25 day period and their counts in the nitrogen energy region (natural radiation subtracted) were normalised to a fixed date. The nitrogen background counts as a function of width and thickness can be seen in Fig 8.1. The nitrogen background can be seen to decrease as the phantom size increases, having a greater variation with width than with thickness.

A method needed to be determined which would enable the prediction of the nitrogen background for a given subject spectrum. Several methods were investigated and are discussed below.

8.1.1 Weighting Width and Thickness

It is possible that a computer look-up table could be generated from the data shown in Fig 8.1. However, there are many problems involved in relating a subject to such a table:-

a) A subject's width and thickness varies with position along the body. Since only one spectrum is generated, corresponding to the section between shoulders and knees, the subject's width and thickness would need to be measured at intervals and weighted to account for the variation with length.

b) In cross section body sections are approximately elliptical or circular and not rectangular, as were the phantoms from which the data points were generated. An ellipse with major and minor axes equal to a rectangular phantom could be expected to have a greater background in the nitrogen region given its smaller overall volume. Some method of weighting would need to be applied to allow for this effect.

Multiple measurements of width and thickness and the application of weighting factors could prove time-consuming and complicated. Additionally, since the nitrogen background is known to be principally pile-up its magnitude as a function of time cannot be predicted from decay alone. Percentage changes in magnitude would therefore need to be followed in only a few phantoms to make recalibration possible in a relatively short period of time.

Attempts at weighting the Bush phantom dimensions for different combinations of the sections, to predict the nitrogen background, proved unsuccessful and the idea was abandoned for use with subject spectra.

8.1.2 Curve Fitting

Background spectra (generated from nitrogen-free tissue equivalent solution with the natural radiation contribution subtracted) were found to have shapes which could be fitted by two second order polynomials over the energy regions 8.63 MeV to 10.72 MeV and 10.72

MeV to 13.04 MeV using the logged data. It was proposed that the curves could be fitted to a subject spectrum over the region beyond the nitrogen peak corresponding to 11.6 MeV to 13.0 MeV. The curve which gave the minimun sum of squares of the deviations of the data points about the fit would be chosen. The integral corresponding to the nitrogen region would then be used as the background for the subject spectrum.

However, when the same spectra from which the curves were generated were used to fit the curves, the curve generated from a given spectrum was not always the curve chosen as giving the best fit! This happened for 8 spectra out of the 35 and produced estimates of the nitrogen background which were up to 9% from the true, measured value. Allowing the curves to be moved vertically up and down and smoothing the background spectra before choosing a fitted curve produced no improvement in the prediction of the nitrogen background from a spectrum. Additionally, using such a technique it would not be possible to follow changes in a few background curves with time and simply apply a percentage change to the remaining curves. This is because percentage changes would differ with the energy region, so changing the entire curve shape and not just its height. Consequently to make the technique practical fewer curves would need to be used, and each of these curves followed with time. The use of fewer curves would generally mean greater error in the estimated nitrogen background for a subject spectrum. The greatest drawback of this technique is that the addition of nitrogen to the phantom solution increases the counts in the energy region over which the curves are fitted. This occurs as a consequence of pile-up of

nitrogen counts in the region. Whilst few nitrogen counts are lost through pile-up, as evidenced by the linearity of the net nitrogen counts with nitrogen mass (see section 8.4), the counts in the 11.6 MeV to 13 MeV region are so low that this effect makes a significant difference to the choice of fitted curve.

8.1.3 Fits by Eye

Two techniques of fitting a nitrogen background by eye were investigated. The first technique involved using a computer programme to move a cursor in small increments to draw an estimated background for a nitrogen spectrum displayed on a logarithmic scale (manual technique). The use of a logarithmic scale was preferred since background spectra show a more curved appearance on this scale, which it was felt would be easier to follow. It was appreciated that small differences on a logarithmic scale could make larger differences to the integral, but a similar investigation using a linear scale was not performed. Two different operators used this programme to fit backgrounds to 30 nitrogen spectra generated from phantoms up to 44 cm wide by 26 cm thick. The range of predicted nitrogen backgrounds varied from 80% to 165% of the true, measured values. However, excluding phantoms considered to be outside the normal range (see later discussion of q-value) the range of predicted backgrounds reduced to 80% to 132% of the true, measured values. The second technique involved the use of a "standard" background spectrum ("mean bgd" technique). This was derived as the mean of three measurements of a nitrogen-free Bush phantom. A logarithmic scale was again used for displaying the nitrogen spectra. The

programme enabled the "standard" background spectrum to be moved vertically up and down until the operator judged it to best represent the anticipated background. Two different operators used this programme to fit backgrounds to 30 nitrogen spectra. The range of predicted nitrogen backgrounds varied between 88% and 175% of the true, measured background. However, excluding phantoms considered to generate spectra outside the normal range the range of predicted backgrounds was reduced to between 88% and 134% of the true, measured background.

The error of the predicted background generally increased with the size of the phantom, using both techniques. This effect is a consequence of the decreasing counts in the nitrogen background with increasing phantom size. However, the improving signal:noise ratio with phantom size would make the increasing error in the predicted background less important.

8.1.4. Prediction Equations

It was proposed to relate the counts in part of the nitrogen spectrum to the nitrogen background counts from a nitrogen-free spectrum, so that the latter could be predicted from the former for a subject spectrum. Energy integrals either side of the nitrogen region were investigated.

The 8.5 MeV to 8.7 MeV region was shown to bear no relationship with the nitrogen background. Presumably this is because this energy region contains counts from genuine events, particularly from

Fig.8·2 Regression of Nitrogen Background on Higher Energy Integral

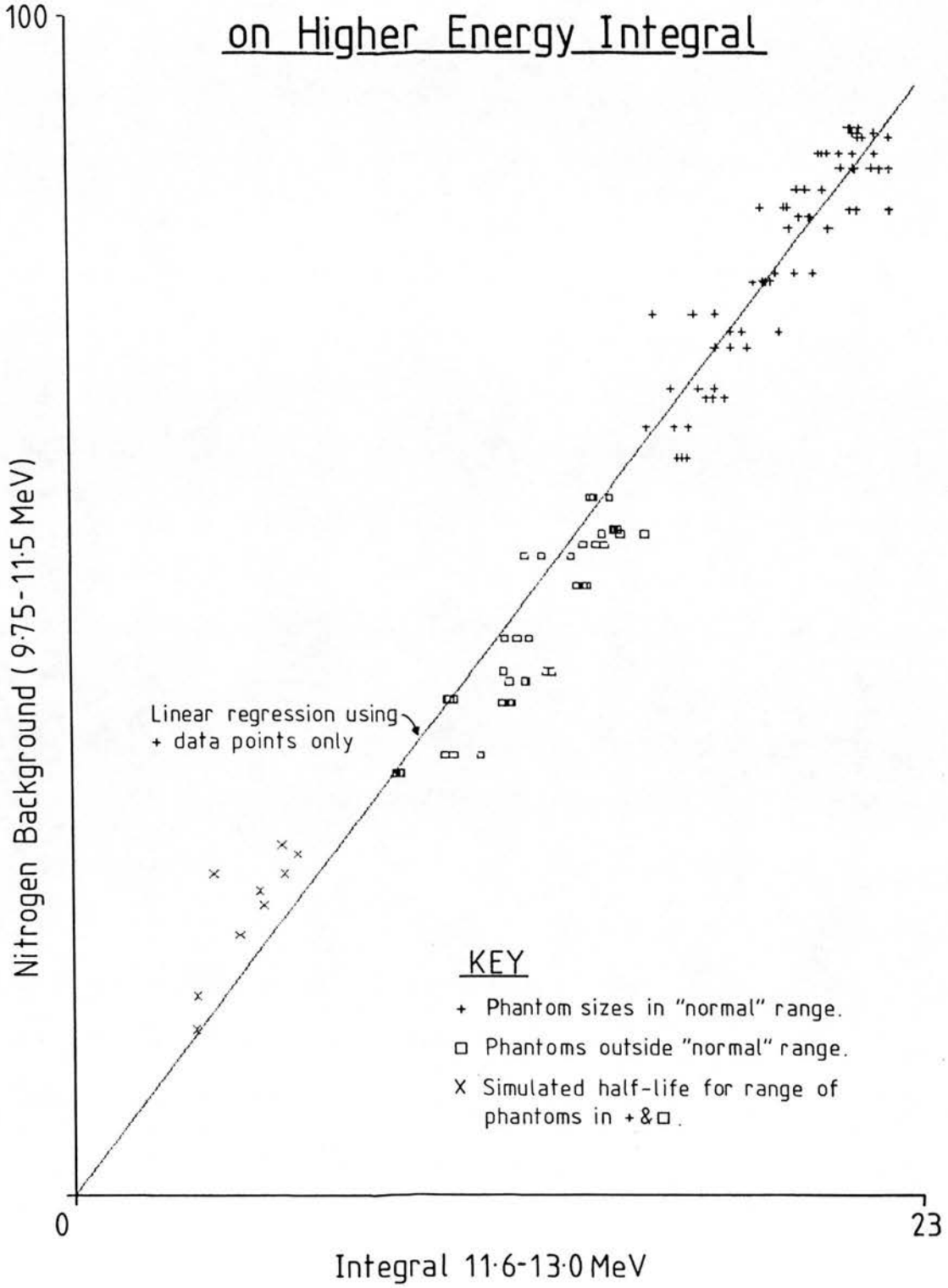

chlorine, as well as pile-up from lower energy events. However the nitrogen background has been associated principally with pile-up.

The 11.6 MeV to 13.0 MeV region from nitrogen-containing phantoms was shown to have a good relationship with the nitrogen background counts for the equivalent background spectrum (both integrals having the natural radiation contribution subtracted). The relationship is shown in Fig 8.2. The general trend of the data points is towards increasing values of the counts with decreasing phantom size. Presumably the good relationship is a consequence of the counts in both energy integrals being principally due to piled-up events (since the natural background radiation contribution is subtracted from the integrals). As the phantom size increases the data points move away from the regression through the origin. This effect is a consequence of the improving signal:noise ratio for large phantoms causing the piled up nitrogen counts in the higher energy integral to constitute an increasing proportion of the counts in this energy region i.e. there is an increasing extra contribution from piled-up nitrogen counts in the higher energy integral which does not make a contribution to the nitrogen background counts. The large degree of scatter of the data points is in part a consequence of the time interval over which the measurements were made i.e. 25 days for the background spectra, a 45 day delay and then 26 days for the nitrogen-containing spectra. The time involved in making the measurements was inevitable, though the delay between the nitrogen-free and the nitrogen-containing spectra measurements is seen in hindsight as an error of forethought. The spectra were corrected for decay to a date around the middle of the measurements.

The scatter is increased due to the time period over which the measurements were made since the degree of pile-up is dependent upon the count rate which in turn is related to the ^{252}Cf decay with time. This explanation is supported by a reduction in the standard error of the estimate (from ±4.3% to ±2.0%), when expressed as a percentage of the mean value, when a recalibration was performed some months later over a shorter period of time. An advantage of the technique is that it is independent of the physiological concentration of chlorine, since chlorine increases the counts in both energy integrals through pile-up. In the event of variations in chlorine concentration this technique will remain reliable whilst others would be subject to error.

For the purposes of recalibration it would be convenient if the linear regression line could be forced through the origin. This would enable the prediction equation to be generated from measurements on just two phantoms, corresponding to points at either side of the anticipated range of body sizes. Examination of the data from the normal study indicated a "normal" range of body sizes. Data points up to the largest size and a safety margin beyond were therefore included as the range of body sizes of interest. These data points included all very small phantoms (corresponding to wasting patients) and a few phantoms larger than the maximum of the normal range. This data set was considered to cover the range of values in which the prediction equation would be required to operate. Two linear regressions were performed using this data set, one of which was forced through the origin. A comparison of slopes was performed and indicated that there was no difference between the

slopes at the 5% confidence level. It was therefore concluded that future prediction equations could be generated using only two phantom sizes and forcing the regression through the origin.

The requirement for recalibration with time is indicated by the subset of data points, shown in Fig 8.2, generated from the box phantoms using only one detector i.e. simulated half-life. The increased scatter is a consequence of the poorer counting statistics. The range of phantom sizes used corresponds to that for the full set of data points shown in the original regression. The result indicates an increasing slope of the prediction equation with time and points to an intercept on the nitrogen background axis if the relationship between the two integrals is followed with time for any given phantom size. This second observation suggests either a small contribution to the nitrogen background from genuine events, or points to the fact that as the count rate decreases the multiple events required to produce pile-up in the 11.6 MeV to 13.0 MeV region become less probable than pile-up events which result in energies between 9.75 MeV and 11.5 MeV.

8.1.5 Comparison of Proposed Techniques for Estimating the Nitrogen Background for a Subject Spectrum

The idea of weighting subject dimensions and using a computer look-up table was abandoned since success could not be achieved for different combinations of Bush phantom sections. The remaining three techniques were tested by observation of the accuracy and reproducibility of the net nitrogen counts determined from the

TABLE 8.1

ACCURACY AND REPRODUCIBILITY OF TECHNIQUES FOR PREDICTING THE NET NITROGEN COUNTS FROM TEN BUSH PHANTOM SPECTRA

	"True" Bgd.	Curve Fitting	Eye Fit "Manual"	Eye Fit "Mean Bgd."	Prediction Eqn.
Mean N counts	8397	7021	8602	8597	8346
N count range	8137-8658	6686-7413	8189-9059	8264-8891	8013-8658
Accuracy	-	-16%	+2.4%	+2.4%	-0.5%
Reproducibility	±2.0%	±3.2%	±3.4%	±1.9%	±2.2%

analysis of ten forty minute Bush phantom spectra. The results of the analysis are shown in Table 8.1. The "true" background technique was that using an independently measured background spectrum, from a Bush phantom containing a nitrogen-free tissue equivalent solution. The mean net nitrogen counts from the ten spectra is taken to be the true value of the nitrogen count. The accuracy of the different techniques is calculated as the difference between the mean nitrogen counts using the technique and that obtained using the "true" background. The reproducibility is calculated as the standard deviation of the ten estimates from their mean value.

There is little difference between the reproducibility of the different techniques. It is not surprising that the "mean bgd", eye-fit technique is so good since the background spectrum used was a mean background from three bush phantom spectra. The accuracy of this technique should not therefore be taken to be that which could be achieved for non-Bush phantom spectra. The accuracy of the curve-fitting technique was poorest for reasons which are apparent when it is recalled that the nitrogen counts in a nitrogen-containing spectrum tend to pile-up, so increasing the counts in the 11.6 MeV to 13.0 MeV region compared to the nitrogen-free background spectrum. Picking a curve by minimising the sum of the squares of the deviations over this energy region, will therefore tend to generate a background greater than the true value. Consequently, the net nitrogen counts will be underestimated. The accuracy and reproducibility of the "manual" eye-fit technique is surprisingly good, but will be subject to intra-operator errors which have not been evaluated here. The technique involving a prediction equation

relating the 11.6 MeV to 13.0 MeV energy region to the nitrogen background has both the best reproducibility and the best accuracy of the three techniques. This technique is operator independent and requires less work for recalibration than the curve fitting technique. Additionally, once the prediction equations have been established for any spectroscopy system the rate of change of slope of the prediction equations can be utilised in the same analysis i.e. some allowance can be made for daily changes, which cannot be done for the curve fitting technique. The prediction equation technique has therefore been adopted for the analysis of subject spectra.

8.2 The Calibration Factor (q)

A subject spectrum generates a nitrogen:hydrogen counts ratio (N_c/H_c), from which the mass ratio (M_N/M_H) of the elements in the body must be calculated. This calculation is performed using the calibration factor "q" in the relationship:-

$$\frac{M_N}{M_H} = \frac{N_c}{H_c} \cdot q$$

The calculation of the mass ratio from the counts ratio enables total body nitrogen to be calculated if an independent estimate of total body hydrogen can be made.

"q" is expected to vary as a function of width and thickness for two reasons. The main reason is the difference in the linear attenuation coefficients in soft tissue for nitrogen (0.022 cm^{-1}) and hydrogen (0.045 cm^{-1}) gamma rays. The greater attenuation of hydrogen gamma rays causing the counts ratio to increase for a given

mass ratio, as the subject size increases. A second, less important effect is that the net hydrogen counts will contain a contribution from activated hydrogen in the apparatus shielding materials. This percentage contribution will also vary as a function of subject size. Both of these effects act to increase the counts ratio with increasing phantom size. Since the hydrogen count (H_c) consists of counts from both the subject and the apparatus, the calibration factor "q" could be expected to vary for different mass ratios in the subject. The mass ratio will vary most from that of reference man in extremes of obesity and over- or underhydration. However, the effect on the "q" value in such extremes of body composition has been shown in Appendix IX to be only a few percent.

8.2.1. Determination of the Calibration Factor (q) as a Function of Width and Thickness

The box phantom spectra for nitrogen-free and nitrogen-containing tissue equivalent solutions were used to generate q-values as a function of width and thickness. Counts were normalised for decay to a reference date corresponding to the mid-point of the time period over which the measurements were made.

A problem arose because the box phantoms were constructed from 1 cm thick perspex. Consequently, as the level of solution in the phantoms was reduced, the mass of hydrogen in the perspex which should be included in the phantom mass became uncertain i.e. the walls of the phantom above the level of solution would have a different activation and detection sensitivity from hydrogen within

the solution, and these differing sensitivities would not be matched by nitrogen. This latter point is crucial since it is the ratio of the nitrogen and hydrogen counts which is important and not the combined activation and detection sensitivity with distribution in the phantom. To overcome this problem an adjustable aluminium tank was constructed. This tank adopted the internal dimensions of the perspex tanks and was used to determine the net hydrogen counts for a given phantom size. The nitrogen counts from three measurements of each perspex tank were used by subtracting the measured background. An additional three estimates of the net nitrogen counts were determined by using the background prediction equation. These six estimates of the net nitrogen counts were used to calculate the mean value for each phantom size. Decay corrections were made to a common date and attenuation corrections applied for the attenuation of nitrogen and hydrogen gamma rays in perspex and for hydrogen attenuation in aluminium. In this way nitrogen:hydrogen counts ratios were determined as a function of phantom size for tissue equivalent solutions in "air" i.e. container-less. Subtracting the hydrogen counts from the equivalent aluminium tank enabled the contribution from the perspex to be calculated for each perspex phantom size. This contribution varied between 6% for the largest phantom to 28% for the smallest phantom.

The mean of the six values of the nitrogen counts together with one standard deviation of the estimate are plotted in Fig 8.3 as a function of width and thickness. A similar plot of the net hydrogen counts is shown in Fig 8.4. It can be seen that both the nitrogen and hydrogen counts increase, as expected, as a function of width and

Fig.8·3 Nitrogen Counts as a Function of Size

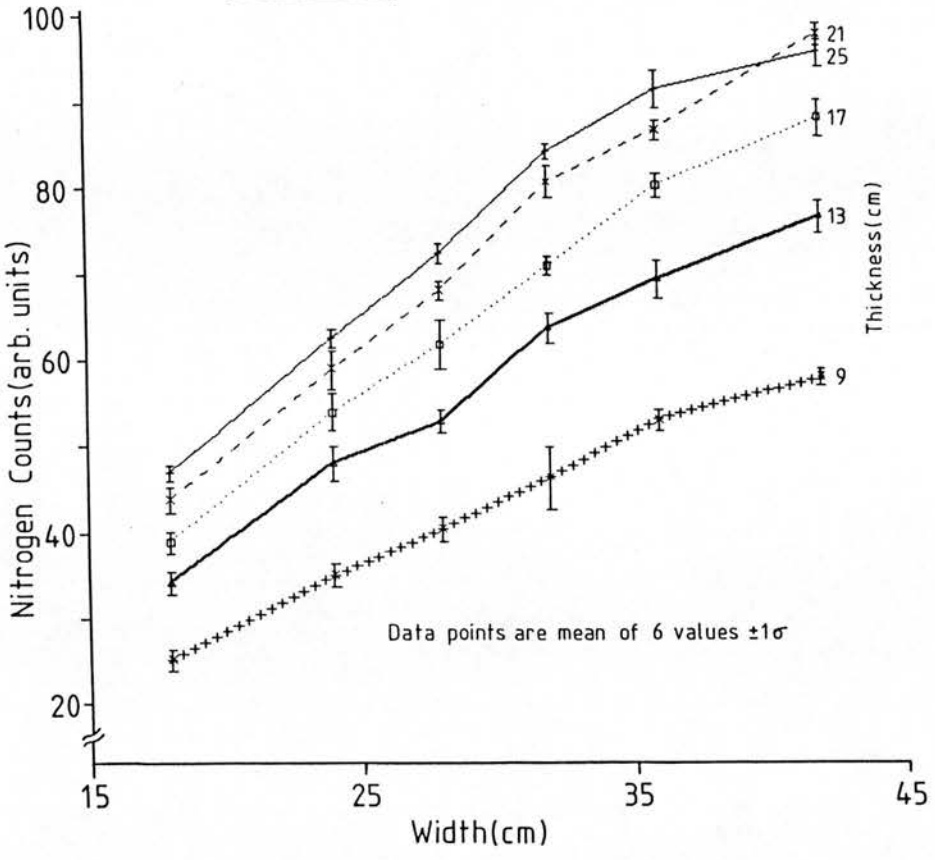

Fig.8·4 Hydrogen Counts as a Function of Size

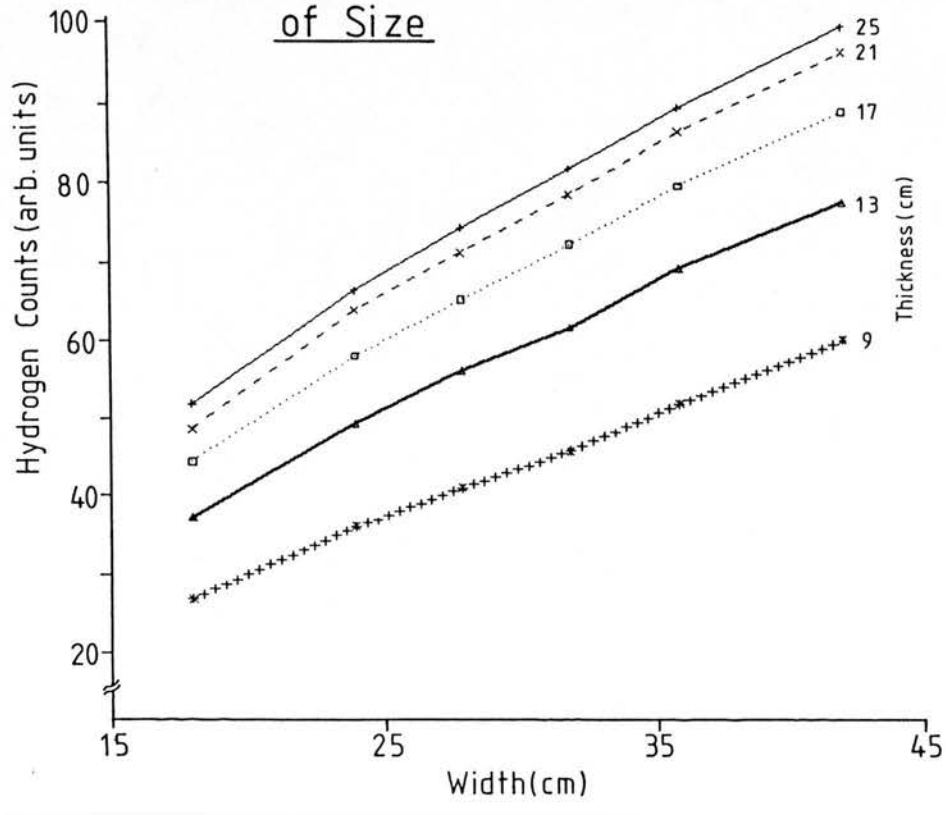

Fig. 8·5 Nitrogen:Hydrogen Counts Ratio as a Function of Phantom Size

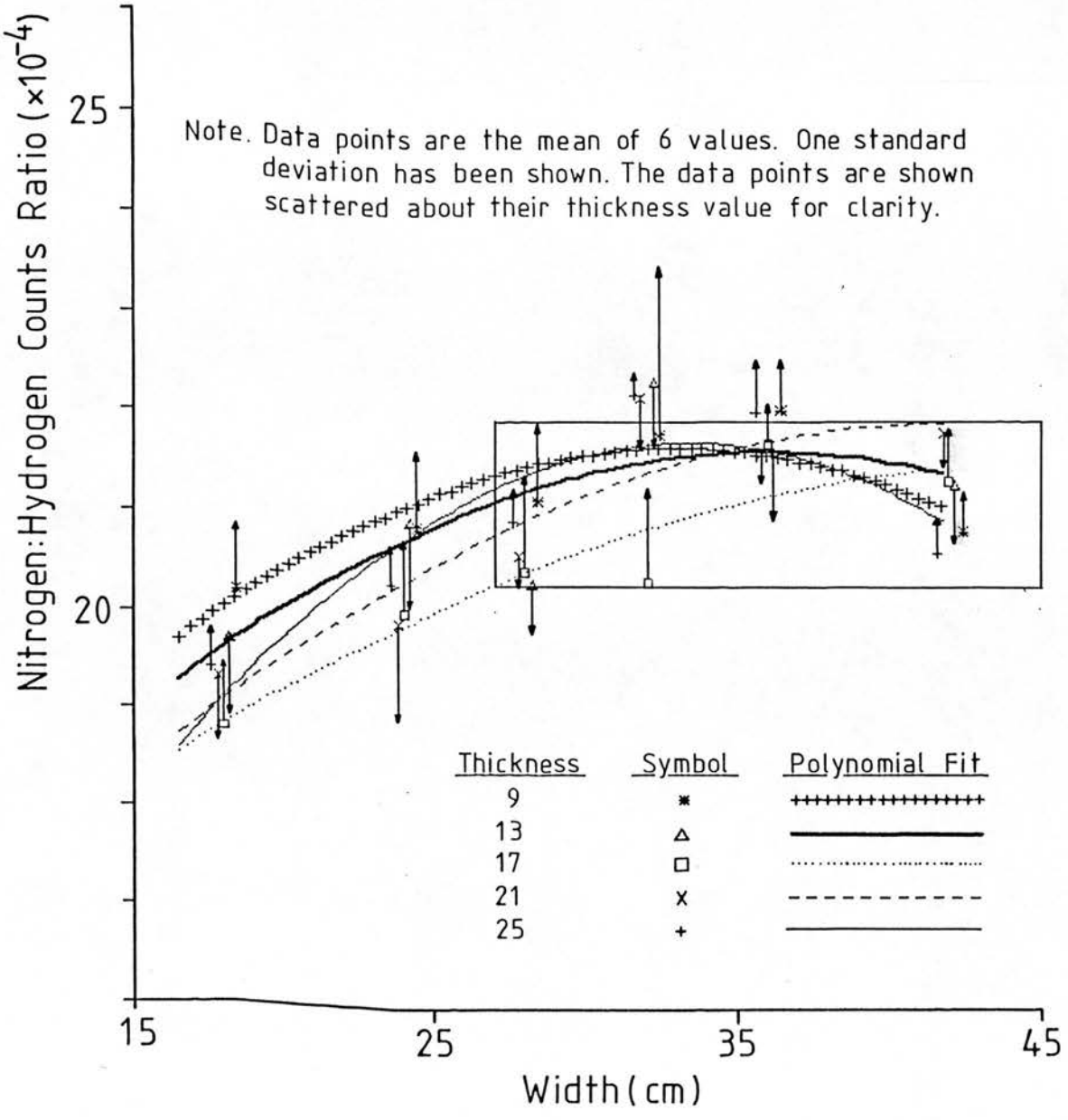

thickness. However, the hydrogen counts increase almost at the same rate as the nitrogen counts, in contradiction to that expected from the difference in attenuation coefficients at the two energies. The result is a nitrogen:hydrogen counts ratio which is relatively constant over a wide range of widths and thicknesses, as shown in Fig 8.5. Each point represents the mean of six values and one standard deviation of the estimate is indicated. First order polynomial curves have been generated from the data points and plotted to indicate the general trend. The box indicates the range of widths and thicknesses which could be met in individuals, and should include the extremes of body composition represented by obesity and anorexia nervosa. Within this box the central point represents a nitrogen:hydrogen counts ratio whose value varied by only ±3.7% within the limits of the box. The variation of the q-value with width and thickness is simply the inverse of the nitrogen:hydrogen counts ratio plot of Fig 8.5, since the nitrogen:hydrogen mass ratio for all phantom sizes was identical. This data supports the use of a single q-value for all subjects, since all subjects' body sizes will fall within the box and so the q-value will be within ±3.7% of the appropriate value. In addition, in following changes in total body protein the change in body dimensions between measurements will not be substantial, and so the use of a single q-value will bear an approximately fixed relationship to the appropriate q-value. The error introduced in repeat measurements by the use of a single q-value will therefore be substantially less than ±3.7%. The single q-value generated from the data was 128.

8.2.2 The Absolute Value of the Calibration Factor (q)

The single q-value of 128 was generated for tissue equivalent solutions in which nitrogen and hydrogen were equally distributed in "air". Indeed the most general assumption necessary in the prompt neutron activation analysis of protein is that nitrogen and hydrogen are equally distributed. This is known not to be true even in normal subjects, where the subcutaneous fat represents a superficial band of hydrogen rich, nitrogen poor tissue. In such circumstances the uniformity of the combined activation and detection sensitivity profile through the subject becomes more important. This situation of a superficial hydrogen rich band is akin to that realised in the perspex box phantoms. If the q-value generated for 26 cm thick phantoms (when all of the perspex in the phantom walls can be considered to be part of the phantom mass) is compared with that calculated to exclude the effect of the perspex walls, then the effect of a 1 cm thick fat layer can be seen. For 26 cm thick phantoms the effect on the q-value of 1 cm thick perspex walls was to increase it with decreasing width; being unchanged at 44 cm wide and increasing by up to 6.5% at 20 cm wide.

The density of the solution used to determine the q-value will also have an effect on the absolute value of q, because of the difference in the mass attenuation coefficients of nitrogen and hydrogen gamma rays. Generating q-values from urea in water, containing nitrogen at Reference Man percentage by weight (density of solution = 1.014 g cm^{-3}), would generate nitrogen:hydrogen count ratios lower than the equivalent ratios generated from a tissue equivalent solution

(density = 1.147 g cm^{-3}); approximately 6% lower for 44 cm wide subjects and 5% lower for 20 cm wide subjects. The consequence of performing calibration procedures with non-tissue equivalent solutions would therefore be to overestimate the q-value for use with subjects. Similarly, variation in body density in disease states would cause the q-value generated from a tissue equivalent solution to be in error. However density variations would not be as great as that between the urea and tissue equivalent solutions discussed above.

8.2.3 The Variation of the Calibration Factor (q) with Time

Examination of the single detector spectra used to simulate the effect of one half-life, showed a reduction in the nitrogen counts to 50%, as expected, but a concomitant reduction in the hydrogen counts to 60%. These changes would result in a 17% decrease in the counts ratio with a consequent increase in the q-value. This effect is associated with the high count rate in the hydrogen peak, its narrow energy integral and the very high count rate below 2 MeV. These factors combine to produce a high probability of a hydrogen gamma ray summing with a lower energy event and falling outside the integration limits. The nitrogen count rate, however, is lower and the energy integral wider. The probability of a nitrogen gamma ray summing with a lower energy event and falling outside the integration limits is therefore less than that for hydrogen gamma rays. As the ^{252}Cf decays and the count rate reduces, fewer hydrogen counts will be lost from their integration region and the counts ratio will decrease.

8.3 Recalibration Procedures

The regression equation, chosen as the best method of predicting the nitrogen background for a subject spectrum, can be seen in Fig. 8.2 to vary as a function of time. Similarly, the q-value calibration factor has been shown to increase as a function of time. Both of these variations are caused by changes in the pattern of pile-up as the ^{252}Cf decays.

8.3.1 Regeneration of Prediction Equations

Since the relationship between the nitrogen background counts and the counts in the 11.6 MeV to 13.0 MeV energy region was shown to be adequately described by a linear regression forced through the origin, changes with time could be followed by measurements on one phantom size. However, to ensure that a fit forced through the origin will apply with time it was decided to follow measurements on two phantom sizes, corresponding roughly to the extremes of anticipated body sizes of interest. Enclosed phantoms were chosen, i.e. a Bush phantom thorax section and a phantom consisting of six 5 litre containers. Two of each phantom type were required; one containing a nitrogen-free, tissue equivalent solution and the other containing a tissue equivalent solution. Integration of the appropriate energy limits and subtraction of the natural background contribution enables a new regression equation to be generated.

Once two such regression equations have been generated it is possible to modify the nitrogen spectrum analysis programme so that the rate

of change of the slope of the prediction equation is taken into account. In this way daily changes can be calculated and subject spectra analysed more appropriately than would be possible if the last prediction equation was used unmodified. The rate of change of slope is taken into account as follows:-

$$y = ax \qquad \text{on Date 1}$$

$$\text{and} \qquad y = bx \qquad \text{on Date 2}$$

Therefore on any day after date 1:-

$$y = \left[a + \frac{d}{D} (b-a) \right] x$$

where D = number of days between Date 1 and Date 2

d = number of days elapsed since Date 1.

This procedure should be performed every 2 or 3 months, whichever appears necessary once the rate of change of the slope of the equation has been determined.

8.3.2 Following Changes in the Calibration Factor

Changes in the q-value can most easily be followed using the results obtained with the six 5 litre containers phantom. Being the largest phantom of the two used for recalibration procedures it has the greatest signal:noise ratio in the nitrogen region. Both the nitrogen and hydrogen counts are determined from the nitrogen spectrum. The counting period should be long enough to generate a count ratio known to 1% or better. The q-value can then be calculated using the known mass ratio for this phantom. Percentage changes of this value can then be applied during the analysis of a subject spectrum, viz:-

$$q = \left[1 + \frac{d}{D}(q_2 - q_1)\right] q_1$$

where q_1 = q on Date 1

q_2 = q on Date 2

D = number of days between Date 1 and Date 2

d = number of days elapsed since Date 1.

This procedure should be performed every 3 months or whatever appears appropriate once the rate of change of the q-value has been established.

8.4 Linearity of Nitrogen Counts

The linearity of the nitrogen counts per unit mass was checked by determining the net nitrogen counts from a perspex tank phantom containing varying amounts of urea, ranging from a 1% to a 6% nitrogen solution (by volume). The linearity of the nitrogen counts versus nitrogen concentration showed a correlation coefficient of 0.9994 with a coefficient of variation about the regression line of <1%. The linearity of the response was considered satisfactory.

This chapter has illustrated the variation of nitrogen background with body habitus. Different approaches to the determination of this background for a subject spectrum have been discussed. The use of Californium-252 brings problems in the need for recalibration as the source decays, so changing the spectrum shape through count rate dependent pile up variations. Such variation influences the suitability of certain background determination techniques. The method of choice proved to be the use of a prediction equation generated from the regression of the measured nitrogen background on a higher energy integral. This technique was shown to have the best

accuracy of all the techniques investigated and a reproducibility very close to that obtained when using measured background spectra. This technique also has the advantage of utilising a relationship which can be easily re-established with time as the Californium-252 decays, and which enables daily corrections to be made for the rate of change of the relationship. Additionally, the technique is operator independent and does not involve laborious measurements of width and thickness. The calibration factor, "q", relating the nitrogen:hydrogen counts ratio was shown to be relatively independent of subject size; enabling the use of a single value which would not be greater than ± 4% in error at any given subject size over the range of body dimensions anticipated. Furthermore, since subject size is not expected to vary drastically between measurements, the error on repeat measurements introduced by the use of a single q-value would be substantially less than the ± 4%. However, the absolute value of q has been shown to be dependent upon the density of the solution used and the presence of a superficial hydrogen rich layer. The use of a urea in water solution was shown to generate q-values 6% higher than those which would be obtained when using a tissue equivalent solution, and the inclusion of a 1 cm thick layer of fat on 26 cm thick subjects was shown to generate q-values 6% higher for 20 cm wide subjects. The value of q was also shown to vary with time as a consequence of changing pile-up losses from the hydrogen integral, in particular, with time. It was shown that changes in q with time could be followed using the same measurements necessary for the re-establishment of the nitrogen background prediction equation. Finally, the linearity of the nitrogen counts with mass was shown to be satisfactory.

CHAPTER 9

CHAPTER 9

SUBJECT MEASUREMENT PROTOCOL AND COMPARTMENTAL ANALYSIS

The prompt neutron activation analysis technique of measuring total body nitrogen uses hydrogen as an internal standard; the use of hydrogen was first reported by Vartsky et al (96) in 1979 as a means of reducing the dependence of the absolute mass of nitrogen on body habitus corrections (see Section 1.2.2). The nitrogen measurement therefore involves the simultaneous acquisition of nitrogen and hydrogen gamma rays from the subject. This chapter discusses the derivation of the equation for calculating the absolute mass of total body nitrogen and the consequent assumptions and measurements which have to be made. The data analysis performed with a microcomputer is described. Finally, an analysis of the errors is performed.

9.1 Experimental Protocol

The subject fasts for one hour before the start of the study until its completion some three hours after the oral administration of 2 MBq tritiated water; a low energy beta emitter (18.5 keV) with an effective half-life of approximately 11 days in human subjects. This enables the calculation of the total body water compartment by an isotope dilution technique. The subject is given two 40 minute scans wearing a light-weight gown, one in a four detector shadow-shield whole body counter for the measurement of the naturally radioactive ^{40}K to determine total body potassium and one in the neutron activation analysis apparatus for the measurement of total body

nitrogen. In the latter measurement, a 100 cm section of the subject starting at the shoulders is scanned. The measurement starts with the subject's shoulders positioned at the far end of the geometric beam limit (13 cm from the beam centre), and finishes with that portion of the body 100 cm below the shoulders (approximately the knee region) at the nearside of the geometric beam limit. In consequence the scanning couch has moved 74 cm in 40 minutes, corresponding to a couch speed of 1.85 cm min^{-1}. Anthropometric measurements are then made i.e. height, weight, arm span, shoulder width and antero-posterior thickness. These measurements are necessary for the calculation of total body potassium from the ^{40}K counts (Boddy, K., et al, 13), as well as for the prediction of total body minerals (TBM_p) and total body nitrogen (TBN) from regression equations based on normal data relating these compartments to parameters which do not change in wasting illness. The subject must collect all urine for the three hour period following the administration of the tritiated water, at which time a 15 ml venous blood sample is taken.

9.2 Calculation of the Total Body Protein Compartment

Using body hydrogen as an internal standard the mass of nitrogen (M_N) in a subject is given by:-

$$M_N = \frac{N_c}{H_c} \cdot q \cdot M_H \qquad - (1)$$

where M_H = total body mass of hydrogen

N_c/H_c = the nitrogen:hydrogen counts ratio corrected for background

q = conversion factor to relate the counts ratio to the mass ratio. This conversion factor was determined from phantom measurements containing known masses of nitrogen and hydrogen (see Section 8.2).

The calculation of the absolute mass of nitrogen in the body therefore requires an independent estimate of the total mass of hydrogen in the body. Other centres which measure nitrogen by prompt gamma activation analysis have made assumptions: that M_H is a fixed percentage (10%) of body mass (McNeill et al, 71); that M_H could be determined from fat (as estimated by skinfold anthropometry) and body mass (Vartsky et al, 96); or that M_H could be estimated from a combination of total body water, fat and body mass (Vartsky et al, 95). However, when the technique is to be employed with critically ill patients whose body composition may depart radically from normal it is essential that no a priori assumptions are made about the ratios of the major body compartments. Additionally, the hydrogen estimate should not depend on direct measurement of the large variable fat compartment by techniques known to be subject to large errors such as skinfold anthropometry (Cohn et al, 31). Beddoe et al (4), in 1984, used a technique which made no a priori assumptions about the relationships between the major body compartments. To do this the hydrogen compartment must be expressed in terms of the other compartments, viz:-

$$M_H = a\,TBW + b\,TBF + c\,TBP + d\,TBM + e\,TBG \qquad - (2)$$

where TBW, TBF, TBP, TBM and TBG are the total body masses of water, fat, protein, minerals and glycogen respectively. a (0.111), b (0.12), c (0.07), d (negligible) and e (0.062) are the

fractional amounts of hydrogen in each of the compartments (taken from a "Reference Man" body composition, ICRP 1974).

However, d is so small that the mineral compartment can be ignored. The energy stores compartment has been represented as two compartments, TBF and TBG. This is necessary because of the differing fractions of hydrogen in the two compartments. Additionally, fat and glycogen have different calorific values thereby necessitating their separation for energy balance studies. The glycogen compartment has been retained at the facility in Auckland, where it is necessary to predict it from regression equations generated from normal data on skeletal size (Beddoe et al, 5). Use of such predictor equations would generate a "normal" value for the glycogen compartment, whereas in wasted patients prior to parenteral nutrition it would almost certainly be negligible. Since the glycogen compartment is not measurable and its exclusion would have little effect on the nitrogen calculation (glycogen is less than 1% of the fat free mass in normals) the glycogen compartment has been excluded from the analysis. Equation 2 then becomes:-

$$M_H = a\ TBW + b\ TBF + c\ TBP \qquad - (3)$$

Total body fat is not directly measurable, but can be indirectly estimated as body mass (M) minus the sum of the other compartments:-

$$TBF = M - (TBW + TBP + TBM) \qquad - (4)$$

Substitution of equation (4) into equation (3) generates:-

$$M_H = (a - b)\ TBW + bM + (c - b)\ TBP - bTBM \qquad - (5)$$

Now total body protein (TBP) is related to total body nitrogen (M_N) by the relationship:-

$$TBP = 6.25\ M_N \qquad - (6)$$

Using equations (1) and (5) in (6) we generate:-

$$TBP = 6.25 \left[\frac{b\,(M - TBM) + (a - b)\,TBW}{\left(\frac{N_c}{H_c} \cdot q\right)^{-1} - 6.25\,(c - b)} \right] \quad - (7)$$

Substitution of the coefficients gives:-

$$TBP = 6.25 \left[\frac{0.12\,(M - TBM) - 0.01\,TBW}{\left(\frac{N_c}{H_c} \cdot q\right)^{-1} + 0.3125} \right] \quad - (8)$$

It can be seen that the relationship requires certain parameters to be established. The value of q used was discussed in Chapter 8, N_c/H_c is determined from the subject spectrum, body mass (M) and total body water (TBW) can be measured and the total body minerals compartment estimated.

9.3 Calculation of the Total Body Water Compartment

The activity of the urine and plasma samples are measured in a beta scintillation counter and the total body water calculated from the relationship:-

$$TBW\ (cm^3) = \left(\frac{A - A_u\,V_u}{A_p} \right) + Vu \quad - (9)$$

where

A = activity administered

A_u = radioactive concentration of 3 hour urine collection (Bq cm^{-3})

V_u = volume of 3 hour urine collection (cm^3)

A_p = radioactive concentration of 3 hour plasma sample (Bq cm^{-3})

The relationship assumes that the subject was normally hydrated at the begining of the study, after voiding the bladder, and became increasingly dehydrated throughout.

For subjects who require a repeat measurement, and for whom the time between measurements is not considered long enough for the levels of tritiated water in the body to have been reduced to negligible levels, a baseline plasma sample before the start of the study is required. The total body water compartment is then calculated from:-

$$TBW\ (cm^3) = \frac{A - A_u V_u + A_p V_u}{A_p - A_{po}} \quad - (10)$$

where A_{po} = radioactive concentration of baseline plasma sample before the start of the study (Bq cm^{-3}).

9.4 Estimation of Total Body Mineral Compartment

Beddoe et al (5) demonstrated how the total mineral compartment represents 6.22% by weight of the fat free mass in normal individuals. This conclusion was drawn from a revision of the literature relating mineral compartments to the fat free mass. Assuming Reference Man mineral contents listed by ICRP ((55), p327), then the largest mineral compartment is the bone ash; being 2790 g in a 70 kg "Reference Man" with 5 kg of bone (4 kg cortical and 1 kg trabecular bone). The extra-skeletal minerals amount to 630 g comprising 245 g extra-skeletal phosphorous, 140 g potassium, 100 g sodium, 95 g chlorine and 50 g other elements. The element sulphur was not included in the mineral compartment since it is largely included in the protein compartment. The total mineral compartment was therefore shown to be 3240 g in 55 kg fat free mass i.e. 6.22% by weight of the fat free mass. This figure compares well with 6.8% calculated by Brozek et al (19) from the results of an analysis of three male cadavers and to 6.4% by Lukaski et al (66) using results derived by in-vivo neutron activation analysis.

9.4.1 Normal Studies

Studies on normal subjects can therefore estimate the total body mineral (TBM) compartment from the fat free mass. The fat free mass (FFM) is calculated from the total body water measurement assuming a normal hydration coefficient of 0.73 (Pace et al, 79), viz:-

$$\text{FFM (kg)} = \frac{\text{TBW (l)}}{0.73} \qquad - (11)$$

Therefore

$$\text{TBM (kg)} = 0.0622 \cdot \frac{\text{TBW (l)}}{0.73} \cdot k \qquad - (12)$$

k is 1 for males and for females less than 55 years of age. However, for females older than 55 years:-

$$k = 1 - 6.7114 \times 10^{-3} \ (\text{AGE} - 55) \qquad - (13)$$

This age correction is that made by Cohn et al (25) for the age dependence in females of their bone mineral ash content, which in normals is 82% of the total mineral compartment. This age correction for women is not applied by Beddoe et al (89). However, it is considered necessary since the composition of bone ash used in the derivation of equation (12) was generated from four males under 45 years of age (Woodard, 103). Furthermore, Woodard had noted the age dependence of the composition of bone ash.

9.4.2 Patient Studies

In patients a normal hydration coefficient for the fat free mass cannot be assumed. Furthermore, in the extremes of body composition the mineral compartment will cease to show the relationship with the fat free mass assumed to exist in normal subjects. In consequence

the mineral compartment is estimated from a regression equation generated from a group of 50 normal subjects (Beddoe et al, 5), relating minerals to parameters which do not change in wasting disease. This is important since 82% of the mineral compartment in normals is in the skeleton, leaving only 18% to fluctuate with body composition in wasting disease. The regression equation is:-

$$TBM\ (kg) = k\ \{0.116 + 2.67 \times 10^{-5}\ S(cm^3)\} \qquad - (14)$$

$$r = 0.91,\ CV = 8.5\%$$

where $S\ (cm^3)$ = Height (cm) x Antero-posterior thickness (cm) x shoulder width (cm)

and k is as detailed in equation (13) (k = 1 in the equation of Beddoe et al).

The antero-posterior (AP) thickness was measured at Auckland as the mean of measurements 12 and 24 cm below the suprasternal notch with the patient lying supine, with arms at sides and hands resting on lower abdomen (personal communication). However, at Edinburgh this has simply been taken as the maximum reading obtained along the full length of the sternum. This may be a problem in patients with chest disorders where the AP thickness may increase with distance from the suprasternal notch.

Measurements of the antero-posterior thickness and the shoulder width are made with the patient "squashed" to remove the effect of overlying tissue, so that the measurements are indicators of skeletal size.

9.5 Total Body Fat Compartment by Difference

Measurement of total body protein (TBP) and total body water (TBW) and the estimation of total body minerals (TBM) enables the calculation of total body fat (TBF) from the relationship:-

$$TBF = M - (TBP + TBW + TBM)$$

This difference technique has been shown to be more accurate in patients presenting with wasting disease than direct measurements which rely upon methods such as skinfold thickness determination (Streat et al, 89). The subject's body composition can now be expressed in terms of the four compartments discussed in Section 1.1

9.6 Total Body Potassium Measurements

As discussed in Section 1.1 a measurement of total body potassium can either be used to estimate the fat free mass through the assumption that it is at a fixed concentration in the fat free mass, or it can be used to calculate an estimate of the body cell mass. The measurement has been included in the experimental protocol to ascertain those patient groups in which an estimate of the body cell mass from total body potassium is as good a clinical indicator of patient health as the more complex four compartment body composition model involving nitrogen measurement.

9.7 Data Analysis

Two programs have been written for data analysis by microcomputer. The first program takes the data from the whole body potassium study

and calculates total body potassium (TBK) by relating the background corrected ^{40}K counts from the subject with that from a phantom containing a known mass of potassium. Corrections are applied to account for differences in self-absorption losses between the patient and the phantom and for the crossover of ^{134}Cs contamination into the ^{40}K energy region. The fat free mass (FFM) is then calculated using the equations described in section 1.1.1.

$$FFM(Kg) = \frac{TBK(g)}{2.533} \qquad \text{-for men}$$

$$FFM(Kg) = \frac{TBK(g)}{2.253} \qquad \text{-for women}$$

The total body fat is then calculated as the difference between the body mass and the fat free mass. The program also calculates the body cell mass (BCM) using the equation of Moore et.al. (74):-

$$BCM\ (Kg) = 0.213\ TBK\ (g)$$

The second program analyses the prompt nitrogen spectrum by using the nitrogen background prediction equation, modified for its rate of change of slope. The net nitrogen and hydrogen counts are determined. The program prompts the operator for the subject's age, sex and anthropomorphic measurements, along with the total body water (TBW) and total body potassium (TBK) compartments. The total body mineral (TBM) compartment is calculated from the TBW compartment for normal subjects and the predicted compartment (TBM_p) is calculated for both normals and patients. The total body nitrogen and total body protein (TBP) are then calculated using TBM for normal subjects or TBM_p for patients. The fat free mass (FFM) is calculated as the sum of TBW, TBP and TBM, and total body fat (TBF) as the difference between body weight and the FFM. The TBN:FFM and TBW:FFM ratios are then calculated. To enable comparison of the different calibration

techniques for the independent estimate of hydrogen the program continues to calculate values for TBN using the relationships adopted at other centres for the calculation of TBH. Where the eatimate of hydrogen differs the substitution for fat often also differs, viz:-

(a) $$TBNc\ (Auckland) = \frac{0.12\ M - 0.02125\ TBW}{\left(\frac{N_c}{H_c} \cdot q\right)^{-1} + 0.3125}$$

for normals except for females over 55 years of age where:-

$$TBNc\ (Auckland) = \frac{0.12\ M - 0.02125\ TBW - 7.0537 \times 10^{-5}\ TBW\ (AGE-55)}{\left(\frac{N_c}{H_c} \cdot q\right)^{-1} + 0.3125}$$

This age correction is not used at Auckland. It will have a negligible effect on the result but has been included for consistency.

For patients the equation reduces to:-

$$TBNc\ (Auckland) = \frac{0.12\ M - 0.01\ TBW - 0.1287\ TBMp}{\left(\frac{N_c}{H_c} \cdot q\right)^{-1} + 0.3125}$$

These equations derive from the relationships:-

$$TBH = a\ TBW + b\ TBF + c\ TBP + d\ TBG$$

where TBG = total body glycogen compartment.

In normals $TBG = 0.0091\ FFM = 0.0091 \cdot \frac{TBW}{0.71}$

where 0.71 is the normal hydration coefficient assumed at Auckland.

In patients an effective normal TBG complement is assumed and calculated from $TBG = 0.51\ TBM_p$, though TBM_p has no age correction.

b) $$TBN_c\ (Toronto) = \frac{N_c}{H_c} \cdot q \cdot 0.1 \cdot M$$

This relationship derives from the assumption that TBH = 0.1 M.

c) $$TBN_c\ (Brookhaven) = \frac{0.12\ M - 0.12\ BMA - 0.01\ TBW}{\left(\frac{N_c}{H_c} \cdot q\right)^{-1} + 0.3125}$$

This equation derives from the relationships :-

$$TBH = a\ TBW + b\ TBF + c\ TBP$$

and $$TBF = M - (TBW + TBP + BMA)$$

where BMA = Bone mineral ash

BMA replaces the total mineral compartment used at other centres. BMA is 82% of TBM in normal subjects.

$$BMA(Kg) = \frac{w\ (Ht/100)\ TBK^{0.5}}{0.34}$$

where w = 56.62 for females ≤ 55 years

= 56.62 - 0.38 (AGE - 55) for females > 55 years

= 54.5 for males

TBK = Total body potassium (g)

To enable comparison of the absolute value of total body nitrogen calculated using the Edinburgh technique, with that predicted using regression equations generated from normal data at other centres, the program goes on to generate predicted values. Where possible the program uses equations incorporating body mass as well as those without. For normal subjects the two equations should generate approximately equal values. However, in wasted subjects the regression incorporating body mass should not be used since this parameter will change in wasting disease.

i) TBN_p (Toronto) $= 0.50\left(\frac{Ht + AS}{200}\right)^{2.6}$ CV = ±11% for males

$= 0.42\left(\frac{Ht + AS}{200}\right)^{2.6}$ CV = ±11% for females

where AS = Arm span (cm)

These equations were generated from 121 normal studies (83 female, 38 male) on subjects up to 59 years of age (Harrison et al., 47).

ii) TBN_p (Brookhaven 1) $= \frac{1}{1000}$ (13.41Ht - 6.46AGE - 251.8) ±0.178

r = 0.69 for males

$= \frac{1}{1000}$ (14.16Ht - 5.11AGE - 756.6) ±0.145

r = 0.73 for females

These equations were generated from 136 normal studies (76 males, 60 females) with subjects between 20 and 80 years of age (Ellis et al., 42). The nitrogen values calculated in these studies used a different calibration for the independent estimate of hydrogen than that discussed in TBN_c (Brookhaven) which was used only from 1984 onwards. The equation involved in estimating hydrogen prior to 1984 was (Vartsky et al., 95) :-

$$TBH = 0.11\ TBW + 0.12\ TBF + 0.052\ (M - TBW - TBF)$$

where TBF was estimated from skinfold anthropometry.

TBN_p (Brookhaven 2) $= \frac{1}{1000}$ (- 7.11AGE + 7.3Ht + 5.41M + 423.3)

±0.169 r = 0.73 for males

$= \frac{1}{1000}$ (- 5.3AGE + 14.94Ht - 1.6M - 785.3)

±0.145 r = 0.73 for females

These equations were generated from the same study as TBN_p (Brookhaven 1).

iii) TBN_p (Leeds 1) $= \frac{1}{1000}$ (-0.14AGE + 20.38Ht - 1608) ±0.217 for males

$= \frac{1}{1000}$ (-0.14AGE + 20.38Ht - 2000) ±0.217 for females

These equations were generated using delayed neutron activation analysis techniques on 91 normal subjects (62 males, 29 females) (Burkinshaw et al., 20).

TBN_p (Leeds 2) $= \frac{1}{1000}$ (-4.1AGE + 6.63Ht + 18.65M - 397) ±0.165 for males

$= \frac{1}{1000}$ (-4.1AGE + 6.63Ht + 18.65M - 733) ±0.165 for females

These equations were generated from the same data as those in TBN_p (Leeds 1).

iv) TBN_p (East Kilbride) = $0.322(Ht/100)^3 + 0.081$

No information concerning the size of the normal group studied using delayed neutron activation analysis was given (Williams et al., 100).

9.8 Error Analysis

The precision of the protein measurement ultimately depends upon the random errors involved in the determination of the nitrogen:hydrogen counts ratio, body weight and total body water. Systematic errors will become increasingly important when comparing the results obtained at different centres or results obtained using different internal standardisation techniques.

9.8.1 Total Body Water

Random errors arise in dilution of the stock solution for use as a standard, pipetting errors of standard, urine and plasma samples, counting statistics and in the collection of urine samples. The overall precision of the measurement is estimated at ±1.5%.

Total body water was assumed to be the space into which the tritium was distributed and no correction has been made for non-aqueous exchangeable hydrogen (Culebras et al., 36) or losses through breathing and perspiration. Three hours was considered sufficient for equilibration of the tracer. This assumption was validated by

comparison of the total body water volume calculated from three and four hour plasma samples in 25 normal volunteers; TBW(3 hr.): TBW(4 hr.) showed a mean value of 1.0036 ±0.00129.

9.8.2 Nitrogen:Hydrogen Counts Ratio

The precision of the nitrogen and hydrogen counts were determined from ten measurements of a Bush phantom to be ±2.5% and ±0.3% respectively. The counting statistics alone accounted for ±1.85% for the nitrogen counts and ±0.04% for the hydrogen counts. The additional error on the nitrogen counts arises through the uncertainty in the background prediction equation, since when the counts were determined using a single measured background the error reduced to ±2.0%. The major error in the determination of the hydrogen counts is considered to be in the energy calibration. The precision of the nitrogen:hydrogen counts ratio was calculated to be ±2.7% from the ten Bush phantom measurements.

9.8.3 Body Mass

The body mass is considered to be measured with an error of ±0.1 kg. The percentage error is therefore a function of weight and considered to be $\leq$ ±0.2%.

9.8.4 Total Body Protein

The precision of the protein measurement is derived from equation (8) by propagation of component errors with the mineral compartment

expressed in terms of water, as given in equation (12), as ±2.7%.

Systematic errors in the estimates of other compartments would have an effect on the accuracy of the protein compartment. Beddoe et al.(5) have estimated the systematic errors in each of the compartments which would be needed to generate a 1% error in the protein compartment. Given the similarity of the Auckland calibration technique with that adopted at Edinburgh the errors would be approximately the same; 10% in the TBW compartment and 17% in the TBM compartment.

The equation used for the calculation of the total body protein compartment has been derived. The relationships used for the calculation or estimation of other body compartments have been described. The data analysis programs have been described. The precision of the protein compartment has been estimated at ±2.7% and systematic errors in the TBW and TBM compartments necessary for a 1% error in the protein compartment shown to be large. Ultimately, the accuracy of the protein compartment measurement will depend on the inherent assumptions of the technique: namely the effects of unmatched nitrogen and hydrogen distributions and the accuracy of the assumed relationships between different body compartments.

CHAPTER 10

CHAPTER 10

RESULTS FROM 53 NORMAL STUDIES

10.1 Normal Volunteers

This thesis has discussed the merits of prompt neutron activation analysis in deriving a four compartment model of body composition. The assumptions of the technique have been enumerated and it remains for the technique to be compared with alternative techniques adopted at other centres. This chapter attempts to evaluate the technique by comparison with results obtained when adopting alternative internal standardisation techniques and by comparison with results obtained from prediction equations based on anthropometrics generated from normal studies at other centres. Multiple regression analysis is performed to generate prediction equations for the protein compartment based on anthropometrics which do not change in wasting disease. The precision of the measurements of the protein and water compartments are determined by repeat measurements of ten normal subjects. Finally, the fat compartment as determined by the activation analysis difference method is compared with techniques utilising total body water or potassium.

Table 10.1 displays the mean ages, weight and height of the 26 male and 13 female volunteers, together with the standard deviations and ranges of these parameters. The distribution when the 14 repeat studies (11 males, 3 females) are included in the data set is illustrated by the values in parentheses. All normal volunteers were

TABLE 10.1

AGES, WEIGHTS AND HEIGHTS OF THE 39 NORMAL VOLUNTEERS

	Males			Females		
	Mean	σ	Range	Mean	σ	Range
Age (y)	37.1 (36.4)	10.7 (10.9)	24-65	36.8 (37.1)	10.5 (10.2)	22-64
Weight (kg)	71.0 (69.6)	9.3 (8.4)	55-101	64.2 (64.9)	11.1 (10.6)	49-89
Height (cm)	176.4 (175.7)	5.4 (5.2)	167-193	164.5 (164.7)	6.9 (6.6)	156-175

Values in parentheses show the distribution when the 14 repeat studies are included in the data set.

TABLE 10.2

NORMAL TBN VALUES BASED ON FOUR DIFFERENT INTERNAL STANDARDISATION TECHNIQUES

Calibration Technique	Edinburgh	Auckland	Toronto	Brookhaven
Mean TBN(kg) Value	1.411	1.403	1.434	1.414
Difference in Mean TBN Compared With Edinburgh Technique		-0.008 (0.6%)	+0.023 (1.6%)	+0.003 (0.2%)
Correlation Coefficient (r)		1.000	0.996	1.000
Coefficient of Variation (%) *		0.080	1.480	0.280

* The coefficient of variation is the standard deviation of the estimate of y upon x divided by the mean value of y and expressed as a percentage.

over 18 years of age. Women who were pregnant or intending pregnancy were excluded from the study. The normal volunteers followed the protocol outlined in section 9.1 with the exception that lightweight indoor clothing was worn. For clothing to have a significant effect on the nitrogen measurement the quantities of nitrogen and hydrogen present in the clothing would have had to be such as to alter the nitrogen:hydrogen ratio perceived in the whole body. Additionally, since superficial layers are less efficiently activated than deeper layers the effect of clothing on the nitrogen:hydrogen counts ratio will be less than their overall effect on the mass ratio might suggest. Chettle et al. (23) have shown for their geometry that unless very heavy clothing is involved, the subject's clothing should not affect the nitrogen measurement very significantly. Since only lightweight clothing was permitted and given the poorer activation of superficial layers it was concluded that clothing would have a negligible effect on the nitrogen measurement. An estimate of the mass of clothing was made, to enable a correction to be applied to the body mass, of 700g for women and 800g for men.

10.2 TBN Using Differnt Internal Standardisation Calibration Techniques

Regressions of total body nitrogen, as calculated by the Edinburgh technique, against total body nitrogen as calculated by applying the internal standardisation techniques used at Auckland, Toronto and Brookhaven (as detailed in section 9.7) to the same experimental data are illustrated in Table 10.2. The results are highly correlated with minimal spread about the regression lines. However, since total

body nitrogen is a function of the same measured quantities for each calibration technique the values are not totally independent, with some of the variation being systematic. The good correlation and small spread about the regression line is therefore to some extent expected and only to be taken as illustrative of good agreement between the different calibration techniques.

10.3 TBN/FFM and TBW/FFM Ratios

Total body nitrogen, as calculated using the Edinburgh calibration technique, was regressed against the fat free mass (FFM), calculated as the sum of total body protein, water and minerals. The regression equations for males and females treated separately and together are:-

TBN(g) = - 0.193 + 0.031FFM(kg) CV = ± 3.8% r = 0.958 for males

TBN(g) = 0.026 + 0.026FFM(kg) CV = ± 2.6% r = 0.983 for females

TBN(g) = - 0.117 + 0.030FFM(kg) CV = ± 3.7% r = 0.976 for males and females

The mean values for the TBN/FFM ratio are shown in Table 10.3 together with the TBW/FFM ratio generated from the data set. Values quoted for groups of normals in other centres are also shown, as well as results from chemical analyses of whole cadavers. Only the results from Auckland (5) use a value for the FFM from a difference technique (total body protein plus water, minerals and glycogen). The first study from Brookhaven (19) and that by Loeppky et al. (65) calculate the FFM from densitometry, whilst the second study from Brookhaven (27) assumes a constant hydration coefficient to calculate the FFM (FFM = TBW/0.73). The studies from Leeds (20,52) calculate

TABLE 10.3

MEAN VALUES OF THE RATIOS TBN/FFM AND TBW/FFM

Centre or Study	Subjects:- Number & Sex	TBN/FFM ± σ (g/kg)	TBW/FFM ± σ (kg/kg)
Auckland*	21 males 20 females 41 subjects	35.1 ± 2.1 33.0 ± 2.0 34.0 ± 2.3	0.710 ± 0.012 0.723 ± 0.011 0.716 ± 0.013
Brookhaven‡	14 males	32.74 ± 1.1	0.731 ± 0.020
Brookhaven†	73 males 62 females 135 subjects	32.8 31.2 32.1	0.73 (assumed 0.73 (assumed) 0.73 (assumed)
Edinburgh§	37 males (incl. 11 repeats) 16 females (incl. 3 repeats) 53 subjects (incl. 14 repeats)	27.3 ± 1.1 26.6 ± 0.7 27.1 ± 1.0	0.765 ± 0.006 0.768 ± 0.004 0.766 ± 0.006
Leeds‡†	33 subjects	33.8	----------
Leeds‖	44 males 29 females 18 policemen	32.5 ± 2.7 31.3 ± 2.9 33.5 ± 2.7	---------- ---------- ----------
Loeppky et al‖	35 males	---------	0.717 ± 0.051
Widdowson et al¶	1 female	31.0	0.732
Forbes et al**	1 male	37.5	0.694
Forbes et al‖‖	1 male	38.1	0.701

* 41 healthy subjects in the age range from 19 to 59 years. TBN obtained from prompt gamma IVNAA, TBW from tritium dilution and FFM from the sum of protein, water, minerals and glycogen. Mineral and glycogen compartments are estimated[5].

‡ Healthy males in the age range from 20 to 30 years. TBN obtained from prompt gamma IVNAA, TBW from tritium dilution and FFM from densitometry. [66]

† 135 healthy subjects in the age range of 20 to 79 years. TBN was obtained by prompt gamma IVNAA, TBW from tritium dilution and FFM from the relation FFM - TBW/0.73. The values quoted have been calculated from data previously presented. [27]

§ See section 10.3 for details.

‡† TBN was obtained from delayed gamma IVNAA and FFM from skinfold anthropometry.[52]

The 33 subjects included 9 normals (8 males, 1 female), 12 surgical patients with minimal weight loss (10 males, 2 females), and 12 surgical patients in whom there had been an average loss of 22.3% of body weight over the previous year (7 males, 5 females). All subjects were in a normal state of hydration.

| TBN was obtained from delayed-gamma IVNAA and FFM from skinfold anthropometry.[20]

| TBW and FFM were obtained from ethanol dilution and densitometry, respectively.[65]

† Chemical analysis of a 42 year-old female cadaver in good physical condition; death by drowning (lungs not edematous).[98]

†† Chemical analysis of 46 year-old male cadaver in good phyisical condition; death as a result of "fracture of skull due to fall".[43]

‡ Chemical analysis of 60 year-old male cadaver in good physical condition; death as a result of "heart attack".[44]

the FFM from skinfold anthropometry. All studies on living subjects measured TBN by prompt neutron activation analysis, except for those studies from Leeds where the delayed technique was used. Total body water was generally measured by tritium dilution in living subjects, except for the study by Loeppky et al. where ethanol dilution was used. All subjects were normal except for 24 surgical patients included in the 33 subjects of the first Leeds study, said to be "in a normal state of hydration". The three cadaver studies included were chosen because the cause of death in each case was unlikely to have influenced the individual's body composition.

Values of TBN/FFM (g/kg) of 27.3 and 26.6 for males and females respectively are lower than the corresponding values from any of the studies listed in Table 10.3. However, the values of TBW/FFM (1/kg) of 0.765 and 0.768 for males and females respectively are higher than the corresponding values from any of the studies detailed.

10.4 Comparison of the Absolute Mass of Nitrogen with that Predicted from Regression Equations Generated from Normal Data at Other Centres

Table 10.4 compares the TBN value calculated using the Edinburgh calibration technique with values predicted using regression equations generated from normal data at other centres. Only those regression equations discussed in section 9.7 which do not incorporate anthropometrics which change in wasting disease are used. As expected for a normal study regressions which include or exclude body mass give roughly comparable results, and so only the results

TABLE 10.4 TBN:PREDICTED TBN

Prediction Equation	Subjects (Sex)	TBN:Predicted TBN Mean (%) ± σ (%)	Correlation Coefficient (r)	CoV * (%)
Toronto	M	71.1 ± 6.8	0.5664	9.74
	F	74.6 ± 7.7	0.6269	11.27
	M+F	72.2 ± 7.3	0.8069	10.01
Brookhaven	M	81.2 ± 8.2	0.4488	10.56
	F	84.1 ± 10.4	0.4566	12.86
	M+F	82.1 ± 9.1	0.7638	10.94
Leeds	M	77.1 ± 7.3	0.5660	9.74
	F	86.2 ± 9.3	0.6108	11.45
	M+F	79.8 ± 9.1	0.7968	10.24
E. Kilbride	M	83.0 ± 8.0	0.5690	9.72
	F	76.5 ± 8.5	0.5986	11.58
	M+F	81.0 ± 8.8	0.7639	10.94

* The coefficient of variation (CoV) is the standard deviation of the estimate of y upon x divided by the mean value of y and expressed as a percentage.

derived using equations excluding body mass are shown. The regressions derived at Toronto and Brookhaven used prompt neutron activation analysis whilst those derived at Leeds and East Kilbride used delayed neutron activation analysis. The measured nitrogen value appears to be between 18% and 28% below the values predicted using the regression equations generated at the other centres. Despite the apparent systematic underestimation of the Edinburgh nitrogen value the coefficients of variation of the regressions of TBN on the predicted value are of the same magnitude as the coefficients of variation calculated for the prediction equations themselves. The observed variance is therefore largely biological as expressed in the original multiple regression.

10.5 Generation of Prediction Equations

The systematic underestimation of total body nitrogen using the Edinburgh calibration procedure compared with that predicted using regression equations generated from normal studies at other centres, is unfortunate and reflects on the accuracy of the technique. However, the precision of the technique is the more important factor. To enable measured nitrogen values calculated for patients to be compared with a predicted "normal" value, regression equations have been generated using the normal data set. The parameters age (A), body mass (M), height (H), shoulder-width (SW) and anteroposterior thickness (APT) were included in a multiple regression analysis of the data, treated separately for sex. The best subset of parameters was chosen using Mallow's CP and the regression equations generated were:-

$$TBN\ (kg) = \frac{1}{1000}\ (7.73M + 12.84H + 22.95SW + 31.3APT - 3.21A - 267.3)$$

S.E.E. = ± 0.079 (5.2%) r = 0.91 for males

$$TBN\ (kg) = \frac{1}{1000}\ (8.43M + 38.13SW - 4.18A - 614)$$

S.E.E. = ± 0.059 (5.0%) r = 0.95 for females

where lengths are in cm, mass in kg and age in years.

However, when predicting body nitrogen in patients suffering gross distortion of body composition the body mass should not be included in the regression, but rather only those parameters which do not change in disease states. Consequently multiple regression analysis was repeated, excluding body mass, and the best subsets generated gave the equations:-

$$TBN(kg) = \frac{1}{1000}\ (15.67H + 38.02SW + 58.55APT - 4.58A - 3709)$$

S.E.E. = ± 0.08(5.4%) r = 0.90 for males

$$TBN(kg) = \frac{1}{1000}\ (65.56SW + 25.07APT - 5.58A - 1467)$$

S.E.E. = ± 0.07(5.8%) r = 0.93 for females

As expected the error associated with the prediction of total body nitrogen increases when body mass is removed from the equations. However, only moderate increases in the error are experienced. The number of data points involved in the generation of the regression equations is small, particularly for the female group where three of the sixteen points are from repeat measurements. With such a small dataset it is not surprising that the best subset of parameters changes when body mass is removed from the equation.

10.6 Comparison of Different Techniques of Estimating Total Body Fat

Chapter 1 discussed the limitations of different models of body composition. The estimation of the fat free mass from a single parameter was shown to be a poor technique, due to the normal biological variation incorporated into the model. Table 10.5 summarises the results of total body fat determined by estimation of the fat free mass from three different techniques and the variation of the hydration coefficient in the groups studied. The "difference", "TBW" and "TBK" techniques use the relationships:-

$$\text{FFM("difference")} = \text{TBP} + \text{TBW} + \text{TBM}$$

$$\text{FFM("TBW")} = \frac{\text{TBW}}{0.73}$$

$$\text{FFM("TBK")} = \frac{\text{TBK(g)}}{2.533} \qquad \text{for men}$$

$$\text{and FFM("TBK")} = \frac{\text{TBK(g)}}{2.253} \qquad \text{for women}$$

respectively. It can be seen that there are significant systematic differences in the total body fat values for both males and females for the different techniques (except for "TBW" and "TBK" techniques for males only); the "difference" technique producing the largest value for fat and "TBK" the smallest value. The hydration coefficients (TBW/FFM) have also been determined, except for the "TBW" technique where the hydration coefficient is necessarily 0.73. Again the mean hydration coefficients for the two techniques compared are significantly different, with the "difference" technique generating the largest ratio. However, observation of the standard

TABLE 10.5

COMPARISON OF DIFFERENT TECHNIQUES FOR ESTIMATING FAT AND THE HYDRATION COEFFICIENT

a) Males

		Measurement Technique			Paired t Test			
		Difference (1)	TBW (2)	TBK (3)	Comparison	$\bar{x}$	t	P
TBF(kg)	$\bar{x}$	13.9	11.3	10.5	1 v 2	2.6	34.3	0.0000
	σ	4.9	5.0	3.9	1 v 3	3.4	5.3	0.0000
					2 v 3	0.8	1.2	0.1131
TBW/FFM	$\bar{x}$	0.765	-	0.722	1 v 3	0.043	6.0	0.0000
	σ	0.006	-	0.044				
Range		0.749 - 0.775	-	0.612 - 0.827				

b) Females

		Measurement Technique			Paired t Test			
		Difference (1)	TBW (2)	TBK (3)	Comparison	$\bar{x}$	t	P
TBF(kg)	$\bar{x}$	21.2	18.9	15.0	1 v 2	2.3	21.7	0.0000
	σ	5.7	5.5	6.5	1 v 3	6.2	9.8	0.0000
					2 v 3	3.9	5.8	0.0001
TBW/FFM	$\bar{x}$	0.768	-	0.674	1 v 3	0.094	10.4	0.0000
	σ	0.004	-	0.037				
Range		0.760 - 0.777	-	0.618-0.736				

deviation and the range of the values of the hydration coefficients for the "difference" technique show a much narrower distribution than that using the "TBK" technique.

10.7 Precision of Total Body Protein and Water Measurements

The precision of the total body protein measurement depends upon the component errors associated with the measurement or estimation of the body mass, mineral and water compartments and the nitrogen:hydrogen counts ratio. In section 9.8.4 the precision was estimated at ± 2.7%. Reproducibility measurements involving phantoms cannot imitate all of the errors associated with the measurement in subjects. Since multiple measurements in an individual would be unethical it was decided to measure the reproducibility of the activation analysis technique of measuring total body protein by repeat measurements on multiple volunteers. Fourteen individuals in all underwent the measurement protocol a second time. The time interval between measurements was kept as short as possible, to reduce genuine changes in body composition influencing the precision, though holidays occasionally intervened. Table 10.6 lists the time interval between measurements (δt), and the percentage changes in the parameters body mass ($\delta mass$), total body protein (δTBP) and total body water (δTBW). The mean period between measurements was 14.1 days. If individuals undergoing a weight change of more than 2% are excluded from the analysis, since such changes may represent a genuine change in body composition, then ten repeat measurements generate a mean change in the total body protein compartment of ± 3.2% (Range : - 9.5% to + 7.0%). This is close to the calculated precision. Similarly, for the

TABLE 10.6

PRECISION OF TOTAL BODY PROTEIN AND WATER MEASUREMENTS

Subject	δt (days)	δMass (%)	δTBP (%)	δTBW (%)
1	20	2.7	-3.1	-1.1
2	23	2.8	-5.4	2.4
3	17	-0.8	0.2	-4.7
4	6	-2.9	-4.2	-0.4
5	7	-0.9	-1.1	1.6
6	13	-0.3	-3.1	-4.8
7	12	-0.1	-3.6	0.2
8	19	-1.7	0.0	1.8
9	7	-0.7	-7.0	5.2
10	13	-0.7	0.3	-0.8
11	18	0.0	7.0	-0.9
12	13	-2.5	-2.8	-3.8
13	14	-0.7	-0.7	-5.8
14	21	0.9	-9.5	0.4

Key

δt Time elapsed between measurements

δMass Difference in body mass between measurements

δTBP Difference in total body protein values for the two measurements

δTBW Difference in total body water volume for the two measurements

same ten individuals the precision of the total body water compartment is ± 2.6%. This is greater than the estimated precision of ± 1.5%, the difference presumably being due to genuine fluctuations in the compartment within the normal population.

10.8 The Mineral Compartment Prediction Equation

The prediction equation for estimating the mineral compartment in patients is that derived at Auckland (see section 9.4.2). Since the equation uses the value of fat free mass (FFM) which includes the total body protein compartment, which has been shown to be approximately 20% below values predicted using regression equations generated at other centres, it was considered necessary to compare the estimated mineral compartment with the predicted compartment in the normal population studied. The mean TBM:TBMp ratio for the 53 normal subjects was 0.9693 ± 0.068, with a coefficient of variation of the regression of TBM on TBMp of ± 6.4%. The biological variation in the original regression was ± 8.5%. The prediction equation was therefore considered appropriate for patient studies.

10.9 Discussion

The results of this study have shown that the application of different internal standardisation calibration techniques yields small systematic differences in the estimated nitrogen compartment in normal subjects. The good agreement between the Edinburgh technique and those of Auckland and Brookhaven arises as a consequence of the similarity of the assumptions made. The techniques differ only in

the inclusion of glycogen as a fifth compartment at Auckland and in the use of total body calcium to represent the total mineral compartment at Brookhaven. Both the glycogen and mineral compartments are small and so these variations make only a small impression on the nitrogen compartment. The Toronto calibration assumes that body hydrogen is one tenth of the body mass. This generalisation makes a 1.6% systematic difference to the nitrogen compartment on average, but significantly increases the coefficient of variation of the regression of the Edinburgh measurement on that calculated using the Toronto calibration. Such systematic differences are small but may become increasingly important in wasting disease, particularly if the hydration coefficient is fluctuating.

Systematic underestimation of the nitrogen compartment compared with that predicted from equations generated at Toronto, Brookhaven, Leeds and East Kilbride of 28%, 18%, 20% and 19% respectively have been shown. These results auger badly for the accuracy of the Edinburgh technique. However, the coefficient of variation of measured against predicted total body nitrogen are of the same magnitude as the coefficients of variation calculated for the original multiple regressions used as prediction equations. This suggests that the observed variance is largely biological as expressed in the original regression. Many factors either singly or working in conjunction might account for some of the discrepancy in the absolute nitrogen values. The internal standardisation technique at Brookhaven would have underestimated the nitrogen compartment by approximately 2.5% compared with the Auckland calibration (see section 1.4), so

confounding the systematic difference! System calibration procedures could overestimate the nitrogen compartment if non-tissue equivalent solutions are used (calibrating with a urea in water solution overestimating the calibration factor by 6% compared with calibrating with a tissue equivalent solution) or by using calibration phantoms having a superficial "fat" layer. However, Knight et al (61) have verified the accuracy of the Auckland technique by comparison with chemical analysis of two human cadavers. No significant difference between the protein compartment as determined from neutron activation and chemical analysis was found. The determination of protein assumed total body water to be that found by freeze drying, since measurement by tritium dilution was impossible. However, a 10% error in the value of total body water would be required to produce a 1% error in the protein compartment. Furthermore their results on 41 normals showed very close agreement with the prediction equations of Leeds and Brookhaven. The independent verification of the Auckland technique by chemical analysis coupled with the good agreement demonstrated between the measured nitrogen in the normal groups with predicted values suggests that the Edinburgh calibration factor is underestimated by approximately 20%. The reasons for this discrepancy are unknown (see footnote on p.192).

Table 10.3 displays values of TBN/FFM and TBW/FFM derived from neutron activation and chemical analysis techniques. The Edinburgh TBN/FFM ratio is significantly below values from other centres. If the nitrogen compartment is indeed 20% too low then this discrepancy is largely resolved, bringing the ratio for all subjects up to approximately 32. The hydration coefficient (TBW/FFM) for all

subjects at 0.766 is significantly greater than that found at other centres. Again this ratio has been influenced by the magnitude of the nitrogen compartment, which is contributing to the fat free mass. If the protein is assumed to have constituted approximately 24% of the fat free mass then a 20% increase in the protein mass would reduce the hydration coefficient to approximately 0.723. This modified ratio is in much closer agreement with the values of the hydration coefficient calculated at other centres.

Prediction equations have been generated by multiple regression analysis of the measured nitrogen masses on anthropometrics. These equations can be used in clinical studies to express the measured nitrogen as a percentage of the predicted value for a normal subject of the same age, sex, height etc. The ratio obtained can be used as an index of nutrition. In such circumstances a systematic underestimation of nitrogen would be insignificant.

Significant systematic differences between the estimates of total body fat using the "difference" technique and those determined using "TBK" or "TBW" techniques have been found by paired t-test for both males and females. Significant differences were also found between the "TBW" and "TBK" techniques for females but not for males. Total body fat was greatest when determined from the "difference" technique and least when determined from the "TBK" technique. The fat compartment by the difference technique is affected by the systematic errors in all of the compartments constituting the fat free mass. Consequently an underestimation of the protein compartment by 2.2kg (the mean underestimation of the protein compartment assuming an

underestimation of 20%) would lead to an equivalent overestimation of the fat compartment. This would bring the TBF values calculated by the difference technique closer to those calculated by the total body water and total body potassium techniques, as might be expected for a normal population where the assumptions inherent in the water and potassium techniques are most likely to hold. Similarly any possible overestimation of the water compartment, as might be expected with the tritium dilution technique due to exchange with non-aqueous hydrogen, would lead to an equivalent underestimation of the fat compartment. Whilst the correction for an assumed underestimation in the protein compartment reduces the discrepancy in the mean values of fat derived by the three techniques Table 10.5 also shows that the range of the hydration coefficients calculated using the different techniques is much narrower for the "difference" technique. This fact suggests that whilst for larger groups the mean fat values may be in rough agreement for the three techniques, that for individuals the error on the measurement is likely to be least for the "difference" technique.

Precisions of ±3.2% and ±2.6% for the total body protein and water compartments respectively were estimated from repeat measurements on ten normal subjects, each showing weight changes of less than 2% between measurements. These values compare favourably with calculated precisions of ±2.7% and ±1.5% respectively; the differences presumably being due to genuine fluctuations in the compartments. Whilst the accuracy of the nitrogen measurement is in some doubt the precision is good and is the more important of the two factors when changes in body compartments are being followed.

However, as already discussed the accuracy will affect the fat compartment and therefore has an influence on the four compartment model of body composition.

Footnote

The apparent underestimation of the apparatus calibration factor warrants further investigation to identify the source of the discrepancy. The nitrogen:hydrogen mass ratio in the tissue equivalent solution is crucial in the calculation of the calibration factor. Whilst the mass per unit volume of nitrogen in the solution could be independently verified by chemical analysis it is not possible to obtain an independent estimate of the hydrogen mass. However, verification of some of the trace elements by mass spectrometry would increase the confidence with which the composition of the tissue equivalent solution is assumed to be known. A second investigation would be to compare the nitrogen:hydrogen counts ratio from a newly made-up solution with that from the existing solution for a small phantom. Good agreement between these counts ratios would confirm that the existing solution has been correctly made-up. In addition recalibration with aluminium tanks would avoid the complications introduced by the use of perspex tanks. Nitrogen:hydrogen counts ratios determined from aluminium tank irradiations would remove possible errors associated with determining hydrogen counts from aluminium tanks and nitrogen counts from perspex tanks, as was the case in the original calibration. System recalibration is presently underway with aluminium tanks and hopefully will resolve the problem.

CONCLUSION

CONCLUSION

A comparison between the various techniques available for delineating the body mass into its various components has shown the superiority of multiple compartment nutrition models over the simpler two compartment (fat free and fat masses) model. The dependence of the simple two compartment model on a reference body which differs only in the proportion of fat by weight leads to a large biological variation in normal subjects, leading to an uncertainty in fat estimation of approximately ±4% of body weight in individuals and an increasing error in wasting disease as departure from the assumed reference body occurs. The four compartment (water,protein,minerals and fat) model adopted for this thesis has been shown to be less subject to biological variation since no assumptions concerning the relationships between compartments are made.

Two techniques (delayed and prompt neutron activation analysis) for the direct measurement of the protein compartment have been compared. The major interference (from oxygen) of the delayed technique (using a cyclotron) was determined experimentally to be approximately 18% of the net nitrogen counts, which is in close agreement to values quoted by other centres. The combined activation/detection sensitivity profile had an RMS variation of ±58% and indicated that 62% of the nitrogen counts would arise from the outer 5 cm for a 25 cm thick subject. This confirmed a major disadvantage of the delayed technique, namely the poor ability to measure deep seated nitrogen. An estimate of the dose required to generate a precision for the nitrogen measurement of ±4% was calculated to be 1.8 mGy. However,

this precision could only be acheived through additional loss of detection sensitivity uniformity with depth by operating the whole body counter detectors at minimal separation. In such circumstances the RMS variation of the composite sensitivity profile uniformity would deteriorate still further and yet a greater proportion of the total nitrogen counts would be generated from the outer 5 cm of a subject. In contrast the prompt technique was shown to have negligible interference. For a bilateral irradiation geometry the RMS variation of the composite sensitivity uniformity with depth was measured at ±23% for a 22.5 cm thick subject. The improvement over the delayed technique arises through the use of a thermal rather than a fast neutron reaction (fast neutrons having poor tissue penetration) and because the detection sensitivity varies in the opposite direction from that of the activation profile. In consequence the prompt technique is better at measuring nitrogen deep within tissue. Additionally, the lower energy of the incident neutron beam generated from the radioisotopic neutron sources used for prompt neutron activation analysis enables a lower radiation dose to be imparted for a required precision. In conclusion the prompt technique has been shown to be superior in respect of uniformity of composite sensitivity, interfering reactions and radiation dose for a given precision. Additionally the requirements for the neutron source and detection apparatus are less expensive than those for the delayed technique.

Comparison has been made between alternative unilateral and bilateral irradiation geometries for prompt neutron activation analysis. Both geometries were independently optimised, by minimising the

coefficient of variation of a nitrogen measurement, through adjustments in the shielding material combination, source-to-skin distance, detector separation and geometric beam dimensions. The bilateral geometry was shown to have a less uniform composite sensitivity profile with depth, though this is relatively unimportant when hydrogen is to be used as an internal standard. However, the coefficient of variation of the nitrogen measurement is better for the bilateral geometry. This is because for the unilateral geometry the detection sensitivity and the self-absorption of the escaping photons act in opposite direction to the neutron flux, thus reducing the net nitrogen counts. The bilateral irradiation geometry was chosen for construction of the clinical apparatus primarily to avoid having to turn critically ill patients mid-irradiation. However, despite the coefficient of variation the geometry has several practical disadvantages compared with the unilateral geometry: namely a constraint on the maximum subject width and a doubling in the construction time and weight of the apparatus.

Experimental and theoretical investigations have helped to elucidate the nature of the prompt nitrogen background. Pulse pile-up, a consequence of the high background count rate at the detectors generated by the requirement for simultaneous irradiation and detection, has been shown to be responsible for a large proportion of the nitrogen background counts. The design philosophy adopted in the selection of units for the pulse processing system, being to minimise the pulse width, aided in minimising the background counts. Since this work was completed additional improvements in the pulse processing system have helped to reduce the nitrogen background and

so improve the signal:noise ratio further.

Calculation of the absolute mass of total body nitrogen from a subject spectrum requires a technique for estimating the nitrogen background and a calibration factor for relating the nitrogen:hydrogen counts ratio to the mass ratio for the clinical apparatus. The nitrogen background has been shown to vary with body habitus, being greatest for small subjects. Such variations influence the suitability of certain background estimation techniques. The best method investigated proved to be the use of a prediction equation generated from the linear regression of the measured nitrogen background (using a nitrogen free tissue equivalent solution) on a higher energy integral (using a nitrogen containing tissue equivalent solution). The good relationship arises as a consequence of piled-up events contributing a large proportion (if not all) of the background counts in both energy regions. Since the relationship is not significantly different from that arising when the line is forced through the origin, the relationship can be easily re-established with time from measurements on just two phantom sizes. The need to re-establish the relationship with time is a consequence of the changing pattern of pulse pile-up as the neutron sources decay and the overall count rate at the detectors decreases. The calibration factor has been shown to be relatively independent of body habitus; enabling the use of a single value which would not be greater than ±4% in error for any given subject size over the range of body dimensions anticipated. Furthermore, since subject size is not expected to vary markedly between measurements, the error on repeat studies introduced by the use of a single calibration factor

would be substantially less than ±4%. However the absolute value of the calibration factor has been shown to be dependent upon the density of the solution used (the lower energy hydrogen gamma rays being more readily attenuated) and the presence of a superficial hydrogen rich layer (generating hydrogen gamma rays in a region which contains no nitrogen thereby compromising the assumption inherent in the technique that nitrogen and hydrogen are equally distributed). Unfortunately the calibration factor has been shown to vary with time by simulating the effect of one half-life of the Californium-252 neutron source. The variation is a consequence of the changing pile-up losses from the hydrogen integral, in particular, with time. The magnitude of the calibration factor with time can be followed using the same measurements necessary for the re-establishment of the nitrogen background prediction equation. The linearity of the nitrogen counts per unit mass has been shown to be satisfactory for solutions containing up to twice the concentration of reference man.

The experimental protocol for subjects has been described. The measurement of total body water by tritium dilution coupled with the nitrogen measurement and several anthropometric parameters enables the delineation of the body mass into the four compartments described. The mineral compartment is estimated and the glycogen compartment is ignored since it is a very small compartment and cannot be measured or easily estimated. The fat compartment can be determined from the difference between body mass and the sum of the other compartments (water,protein and minerals). Since the fat compartment is small and it is determined by difference then small errors in the measurement or estimation of other compartments can

lead to much larger percentage errors in the estimation of total body fat. Data analysis of subject spectra included the calculation of the nitrogen mass using different calibration techniques for the independent estimate of the hydrogen mass. These different techniques have been shown to produce small systematic errors in the nitrogen mass as calculated for a normal subject, but results may vary significantly in disease states where the assumptions in the different calibration procedures become increasingly invalid. The data analysis program also calculates values of total body nitrogen from prediction equations, using anthropometrics, generated at other centres.

The results from 53 studies on 39 normal healthy volunteers have confirmed the small systematic differences in the estimated nitrogen compartment in normal subjects when different internal standardisation calibration techniques are adopted. Significant (approximately 20%) systematic underestimation of the absolute nitrogen compartment compared with that predicted from equations generated at four other centres was demonstrated. Given that the Auckland team have validated their technique by comparison with chemical analysis, and that the group finds very good agreement between their measured values and those predicted using regression equations generated at other centres, then this underestimation of the Edinburgh values appears to be genuine though remains to be explained. Calculated nitrogen:fat free mass and water:fat free mass ratios at Edinburgh are also in disagreement with values quoted from other centres. An underestimation of the protein compartment by 20% would explain these discrepancies and bring the ratios into close

agreement with those quoted from other centres. The normal nitrogen values have been used to generate regression equations from anthropometrics. In patient groups the prediction equations will enable a nutrition index (ratio of measured to predicted nitrogen) to be generated. Significant systematic differences between the estimates of total body fat using the "difference" technique and those determined using "total body potassium" or "total body water" techniques have been found by paired t-test for both males and females. Significant differences were also found between the "water" and "potassium" techniques for females but not for males. Total body fat was greatest when determined from the "difference" technique. However, this could have been because of the systematic underestimation of the protein compartment causing a systematic overestimation of the fat compartment. Indeed if a 20% overestimation of the protein compartment is assumed then the mean fat value by "difference" is much more in keeping with those by the alternative techniques. However, the range of the hydration coefficients calculated using the "difference" technique is much narrower than that obtained when using the "potassium" technique. This fact suggests that whilst for larger groups the mean fat values may be in rough agreement for the three techniques, that for individuals the error on the measurement is likely to be least for the "difference" technique.

Repeat measurements on ten healthy volunteers generated precision values of ±3.2% and ±2.6% for total body protein and water compartments respectively. These values compare favourably with calculated precisions of ±2.7% and ±1.5% respectively; the

differences presumably being due to genuine fluctuations in the compartments over the mean period of fourteen days between measurements. Whilst the accuracy of the protein measurement is in some doubt the precision is comparable with that reported at other centres and is the more important of the two factors when changes in body composition are being followed. However, since the fat compartment is determined by difference the accuracy of the protein compartment will influence the four compartment model of body composition adopted for this thesis.

In conclusion it has been demonstrated that clinical apparatus can be constructed for the prompt measurement of whole body nitrogen by neutron activation analysis, using Californium-252 neutron sources, with a precision of ±3.2% for a whole body dose equivalent of 0.18 mSv.

APPENDICES

APPENDIX I

EQUATIONS REQUIRED FOR THE CALCULATION OF THE ANTICIPATED COEFFICIENT OF VARIATION OF A NITROGEN MEASUREMENT FOR A GIVEN RADIATION DOSE USING THE DELAYED ACTIVATION TECHNIQUE

a) Calculation of Counting Statistics

The coefficient of variation due to counting statistics alone (CV_c) is calculated from the equation:-

$$CV_c = \frac{(C_N + C_I + C_B)^{1/2}}{C_N} \times 100\% \qquad - (i)$$

where C_N = counts from ^{14}N only.

C_I = counts from interfering reactions.

= $3.35C_N$ (calculated from Reference 88).

C_B = counts from natural background = constant

This equation reduces to:-

$$\left(\frac{CV_c}{100}\right)^2 C_N^2 - 4.35\ C_N - C_B = 0 \qquad - (ii)$$

which can be solved as for simple quadratic equations.

(b) Normalisation of Counts

The net ^{13}N counts from ^{14}N activation must be normalised to a given irradiation, delay and counting period. This is achieved by using the following formula:-

$$C_o = C_t \cdot \frac{\{1 - \exp(-\lambda t_{ip})\}}{\{1 - \exp(-\lambda t_{it})\}} \cdot \frac{\exp(-\lambda t_{do})}{\exp(-\lambda t_{dt})} \cdot \frac{\{1 - \exp(-\lambda t_{co})\}}{\{1 - \exp(-\lambda t_{ct})\}} \qquad - (iii)$$

where

C_o = counts to be determined for conditions "o".

C_t = counts measured under conditions "t".

t_{io}, t_{do}, t_{co} = irradiation, delay and counting periods respectively forming conditions "o".

t_{it}, t_{dt}, t_{ct} = irradiation, delay and counting periods respectively forming the conditions "t".

λ = decay constant = $\ln 2/T_{\frac{1}{2}}$

(c) Calculation of the Total Coefficient of Variation

The total coefficient of variation for a total body nitrogen measurement (CoV) is calculated from the formula:-

$$CoV^2 = CV_c^2 + CV_o^2 \qquad - (iv)$$

where

CV_c = coefficient of variation due to counting statistics alone.

CV_o = coefficient of variation due to variables other than the counting statistics.

APPENDIX II

VOLTAGE DIVIDER DESIGN FOR OPERATION AT CATHODE HIGH POTENTIAL

The prompt nitrogen spectrum has a wide energy range up to a maximum of approximately 11 MeV (nitrogen photopeak). It was anticipated that once the shielding and irradiation/detection geometry had been optimised, that the total count rate at each detector would be between 50 and 100 kcps.

The voltage divider chain has been designed following the recommendations of reference 91. In order to calculate the mean anode current flowing ($\overline{I}_a$) a count rate of 75 kcps of mean energy 5 MeV was assumed. The photomultiplier gain (G) was chosen so as to maintain the mean anode current below 10μA for stability.

The mean anode current, $\overline{I}_a$, is given by:-

$$\overline{I}_a = N\ e\ n\ G$$

where

N = number of photoelectrons produced by the photon

= photon energy (keV) x 5 (photoelectrons/keV incident energy)

e = electron charge = 1.6×10^{-19} C

n = count rate (cps)

Assuming a mean anode current of 5 μA then:-

$$5 \times 10^{-6} = 5 \times 10^{3} \times 5 \times 1.6 \times 10^{-19} \times 75 \times 10^{3}\ G$$

Therefore $G = 1.7 \times 10^{4}$

For the 9530A photomultiplier the standard graph of gain versus the cathode to anode voltage indicates that an overall voltage of approximately 900 V is required to maintain a gain of 1.7×10^4. However, this voltage can only be an estimate since the relationship between gain and voltage from which it was taken was that for the divider network shown in Fig.3.1.

Normally, to prevent voltage redistribution along the dynode chain the mean anode current should be much smaller than the voltage divider current (I_D) ie $I_D = 100\ \bar{I}_a$.

Therefore $I_D \geq 0.5$ mA for $\bar{I}_a = 5\mu A$

However, when the voltage across later stages of the divider are held constant this requirement for the divider current becomes less important. This is the situation for the divider design adopted here (see diagram) since the recommended operating voltages across the cathode to first dynode stage and that across the last dynode to anode stage are held constant with zener diodes at 450 V and 150 V respectively. The divider network is tapered so that increasing voltages are applied across the later stages to help minimise voltage redistribution at high count rates. The tapered divider has the form:-

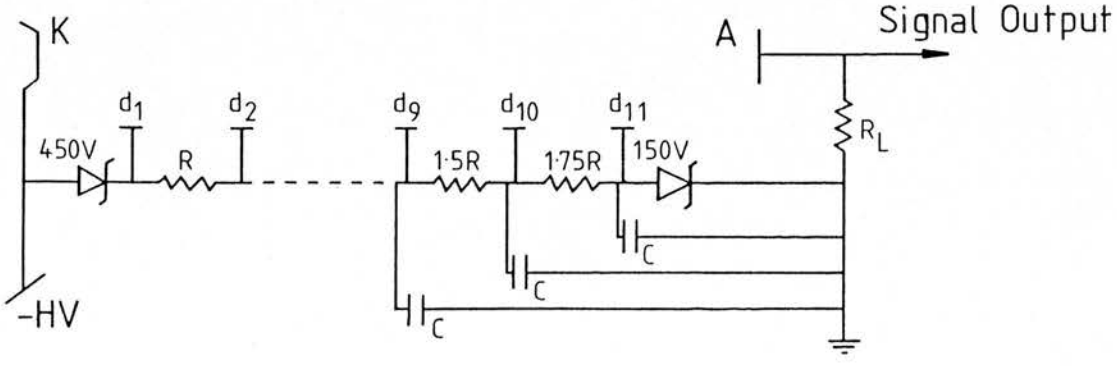

Only 300V of the 900V applied voltage will be distributed along the resistor chain. The value of the resistors, R, can therefore be calculated from:-

$$I_D = \frac{900 - 600}{11R} = 0.5 \times 10^{-3} \text{ A}$$

Therefore R = 54 kΩ

For convenience standard resistor values have been used such that:-

$$R = 47 \text{ k}\Omega$$

$$1.5\ R = 68 \text{ k}\Omega$$

$$1.75\ R = 82 \text{ k}\Omega$$

It is quite acceptable to operate with a peak pulse current ($\hat{i}_a$) as great as I_D provided the signal repetition rate is not excessive (as is the case for nitrogen signals). Decoupling capacitors are incorporated at the final three stages to supply the current for the duration of the peak pulse. The required capacitance (C) can be estimated from the basic equation relating voltage V, charge Q and capacitance C : Q = CV. From differentiation it follows that the relative voltage drop caused by a peak pulse is:-

$$\frac{\delta V}{V} = \frac{1}{C} \times \frac{\delta Q}{V}$$

Therefore $$C > \left(\frac{\delta Q}{V}\right) \Big/ \left(\frac{\delta V}{V}\right)$$

The most critical damping capacitor is that across the last dynode to anode stage since this will supply the maximum pulse current. The maximum peak current will be generated by a nitrogen pulse and will be:-

$$\hat{i}_a = \frac{10.83 \times 10^3 \times 5 \times 1.6 \times 10^{-19} \times 1.7 \times 10^4}{250 \times 10^{-9}} = 0.59 \text{ mA}$$

where 250 ns is the time over which the current has had to be supplied for a NaI detector pulse.

Therefore the charge which must be supplied by the capacitor during the generation of a nitrogen peak pulse is:-

$$\delta Q = 0.59 \times 10^{-3} \times 250 \times 10^{-9} = 1.48 \times 10^{-10} \text{ C}$$

Also, for stable voltage distribution $\delta V/V$ should remain less than 0.1%.

Therefore for a nitrogen pulse:-

$$C > \left(\frac{1.48 \times 10^{-10}}{150}\right) \Big/ 10^{-3}$$

$$C > 0.001 \ \mu F$$

Normally C is taken to be 10 times the calculated value to allow for pile-up events when the capacitor may not have had sufficient time to recharge completely; 0.01 μF capacitors were therefore used in the voltage divider chain whose construction can be seen in Fig 3.3.

It should be noted that whilst the assumed prompt nitrogen spectrum count rate and mean energy and operating voltages have been approximated, that the general concepts underlying the divider design still apply. This fact ensures that even if the final operating conditions vary from those assumed (within reasonable limits) that the divider design should still be adequate in practice.

APPENDIX III

THE Q-VALUE AND THRESHOLD ENERGY CALCULATIONS FOR NEUTRON REACTIONS

Consider the reaction:-

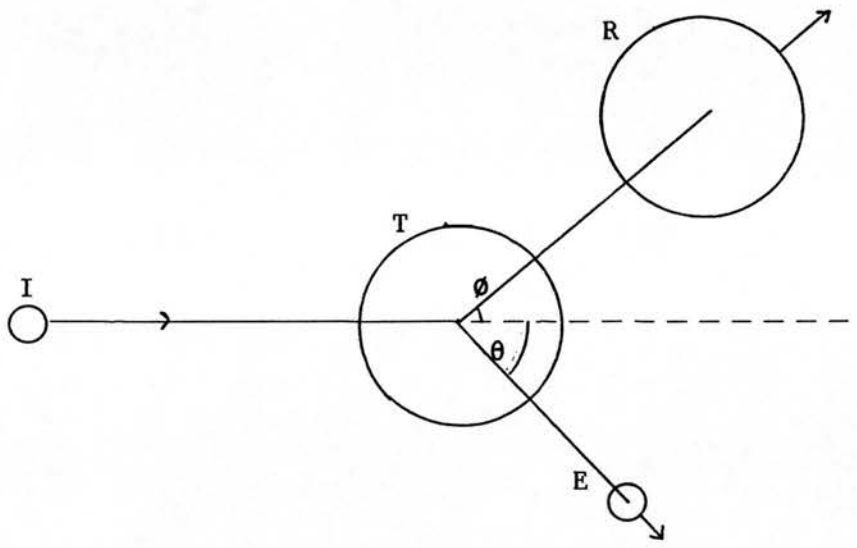

where T is the target nucleus, I the bombarding particle, R the residual nucleus and E the emitted particle. θ and ø denote the angles at which the emitted particle and residual nucleus respectively move off with respect to the direction of the incident particle.

The energy released during the reaction - (the Q-value) is given by:-

$$Q = E_R + E_E - E_T - E_I \qquad - (1)$$

$$\text{or} \quad Q = (M_T + m_I - M_R - m_E)\, c^2 \qquad - (2)$$

where E's represent kinetic energies and M_T, m_I, M_R, m_E represent the masses of the target nucleus, incident particle, residual nucleus and emitted particle respectively - i.e., the Q-value can be determined either from the energy difference or from the mass difference.

Here, the target nucleus is assumed to be at rest i.e. $E_T = 0$.

Equation 2 can be used to calculate the Q-value for any reaction if the masses of the particles involved are known. If nuclear masses are expressed in atomic mass units (μ) then the conversion factor 931.48 is necessary to express Q in MeV.

$$Q = (M_T + m_I - M_R - m_E)\ 931.48 \quad \text{MeV} \qquad - (3)$$

The distribution of the available energy between the emitted particle and the residual nucleus will depend on θ and ∅. For the special case where all of the energy is imparted to the emitted particle as kinetic energy, then $\theta = 0^{\circ}$

When Q is negative the reaction is said to be endothermic. The energy -Q is needed to excite the compound nucleus sufficiently so that it will break up. This energy must be supplied in the form of kinetic energy of the incident particle. However, not all of the kinetic energy is available for excitation because some is used to impart momentum to the compound nucleus. Consequently, E_I must exceed $|-Q|$ in order for the reaction to proceed. This threshold energy for an endothermic reaction is calculated, viz:-

Let M_C and V_C denote the mass and velocity of the compound nucleus.

For the conservation of momentum

$$m_I\ v_I = M_C\ V_C \qquad \text{i.e.} \quad V_C = \frac{m_I}{M_C} \cdot v_I$$

The part of the kinetic energy of the incident particle needed for excitation of the compound nucleus is:-

$$-Q = 0.5m_I v_I^2 - 0.5M_C V_C^2 = 0.5m_I v_I^2 \left(1 - \frac{m_I}{M_C}\right)$$

Substituting $M_C = M_T + m_I$

then $$-Q = 0.5m_I v_I^2 \left(\frac{M_T}{M_T + m_I}\right)$$

the threshold energy is then

$$E_{th} = 0.5m_I v_I^2 = (-Q)\left(1 + \frac{m_I}{M_T}\right) \qquad - (4)$$

Equation (3) has been used to calculate the Q-values for the endothermic reactions listed in Table 5.4, and equation (4) used to calculate the reaction threshold energies (E_{th}). The values of E_n(min) have been calculated as the sum of the Q-value and the minimum energy the reaction products require to contribute to the nitrogen background (9.5 MeV for alpha particles and 6.6 MeV for protons).

Considerations of Relativistic Effects

The maximum energy of a neutron from ^{252}Cf is in the region of 8.5 MeV. Theoretically, therefore, the maximum energy of a neutron reaching the detector is 8.5 MeV.

The kinetic energy (E) of the neutron is related to it's mass and velocity by the equation:-

$$E = 0.5mv^2 \qquad \text{(ignoring relativistic effects)}$$

For an 8.5 MeV neutron:-

$$E = 8.5 \text{ MeV} = 8.5 \times 10^6 \times 1.6 \times 10^{-19} \text{ J}$$

and $m = 1.008665u = 1.008665 \times 1.66043 \times 10^{-27}$ kg

Therefore $v = 2.85 \times 10^{7}$ m.s^{-1}

$= 0.1c$

where c = the velocity of light = 3×10^{8} m.s^{-1}

Since the maximum velocity of a neutron incident at the detector is approximately only 10% of the speed of light relativistic effects can be ignored.

APPENDIX IV

CALCULATION OF THE RELATIVE THERMAL NEUTRON FLUENCE AT THE CRYSTAL

Thermal neutrons reaching the crystal can be captured by the crystal elements sodium (Na) and iodine (I). Both of the activation products are radioactive and detection of the radiation from either could be used as a measure of the relative thermal neutron fluence at the crystal. However, in practice the cross-section for thermal neutron capture in I (σ_T = 6.6 b) is so much greater than that in Na (σ_T = 0.534 b) and the half-life of the I product so much shorter than the Na product that the radiation from I dominates the activation spectrum at the end of an irradiation. Consequently, the reaction utilised in the calculation of the relative thermal neutron fluence at the crystal is:-

$$^{127}I\ (n,\gamma)\ ^{128}I$$

The activation product (^{128}I) decays by β^- emission with a half-life of 24.99 minutes. Measurement of the beta spectrum (maximum energy 2.12 MeV) for 100 seconds after the end of an irradiation therefore serves as a measure of the relative thermal neutron fluence at the crystal.

Since most spectra are accumulated for a preset "LIVE" time of 1,000 seconds the ^{128}I counts must be corrected for the analyser deadtime to determine the true irradiation time. This is performed by the equation:-

$$\text{Relative Thermal Neutron Fluence} = \frac{^{128}I \text{ counts}}{\{1 - \exp(-\lambda t_I)\}}$$

where t_x = Irradiation time (s) = 1000 + 10D

D = Analyser deadtime (%)

λ = Decay constant (s^{-1}) = ln2/(24.99 x 60)

APPENDIX V

CALCULATION OF RELATIVE THERMAL NEUTRON FLUENCE USING INDIUM FOILS

The relative thermal neutron fluence as measured from the activation of an element is directly proportional to:-

$$C \times \frac{1}{M} \times \frac{1}{\{1-\exp(-\lambda t_I)\}} \times \frac{1}{\exp(-\lambda t_D)} \times \frac{1}{\{1-\exp(-\lambda t_C)\}}$$

where

C = Counts detected from a fixed counting geometry

M = Mass of foil (g)

λ = Decay constant (s^{-1}) = $\ln 2/T_{1/2}$

t_I = Irradiation period (s)

t_D = Delay between the end of irradiation and start of counting(s)

t_C = Counting period (s)

Indium (In) can be used as an activation foil by utilising the reaction in ^{115}In (96% abundant):-

$$^{115}In\ (n,\gamma)\ ^{116m}In \qquad \sigma_T = 170\ b$$

^{116m}In has a half-life of 54 minutes and emits a range of gamma rays from 0.417MeV to 2.111 MeV.

There is a fast neutron reaction in ^{115}In, viz:-

$$^{115}In\ (n,n'\gamma)\ ^{115m}In \qquad \sigma = 170\ mb$$

^{115m}In has a half-life of 4.5 hours and emits 0.336 MeV gamma rays. The reaction has a threshold energy of 1.2 MeV and therefore can occur with ^{252}Cf.

Indium foils, approximately 2cm x 2cm (2.5g), were irradiated for a fixed time of 400 seconds and counted for a fixed time of 200 seconds in a fixed geometry. By keeping the irradiation period short the build-up of ^{115m}In was minimised and the need to correct for the fast neutron reaction removed. Because of the constant irradiation and counting times the only variables which must be corrected for are the delay period (t_D) and the foil mass (M). The relative thermal neutron fluence for each of the foils is therefore calculated from:-

$$C \times \frac{1}{M} \times \frac{1}{\exp(-\lambda t_D)}$$

APPENDIX VI

MEASUREMENT OF COMPOSITE SENSITIVITY UNIFORMITY

Determination of the composite sensitivity uniformity (product of the uniformity of activation and detection) requires measurement of the prompt gamma rays from a point source stepped across the region of interest. Unfortunately, nitrogen is not available in a concentrated form. However, alternative elements can be used if they satisfy the following criteria:-

(i) The element's cross-section must vary with energy in the same way as does that of nitrogen.

(ii) The element must be available in a concentrated form.

(iii) The element should produce prompt gamma rays of the same energy as does nitrogen, so ensuring an equivalent degree of attenuation by the human body.

(iv) The sensitivity for the reaction should be as high as possible.

Nickel (Ni) satisfies the requirements (i) and (ii). The extent to which Ni satisfies (iii) and (iv) is illustrated in the following table:-

Element	Atomic Mass A	Thermal Neutron Cross-Section σ_T (b)	Prompt Gamma Rays (MeV)	Intensity, I (gamma rays/ 100 neutron captures)	Sensitivity (Iσ/A)
N	14.01	0.08	10.83	15	0.08
Ni	58.71	4.60	8.999	41.65	3.20
			8.533	18.74	1.50
			8.121	3.47	0.27
			7.819	9.04	0.70

All Ni prompt gamma rays of 7.7 MeV and above can be counted since the absorption coefficient in water does not differ markedly from that for 10.83 MeV gamma rays (2.5×10^{-2} cm^2 g^{-1} at 7.7 MeV and 2.1×10^{-2} cm^2 g^{-1} at 10.83 MeV).

Composite sensitivity measurements were made with a 10 cm long Ni rod, 2 cm in diameter (mass 179 g). Measurements of uniformity through the phantom depth were made by irradiating a static water phantom with the axis of the rod aligned with what would be the patient longitudinal axis. This orientation of the rod compensates to some extent for the static irradiation (an infinitely long rod irradiated in a static position is the equivalent of scanning a point source). 1,000 second irradiations were performed with the rod moved at 2 cm intervals. Reflection of the composite senstivity curve for a unilateral irradiation generates the uniformity curve for a bilateral irradiation. The uniformity of this composite sensitivity curve is expressed as a range and also as an RMS percentage variation from the mean where:

Range = highest and lowest values from their mean; and

$$\text{RMS variation from the mean} = \left(\frac{\Sigma | x_i - \bar{x} |^2}{n} \right)^{\frac{1}{2}} \cdot \frac{100\%}{\bar{x}}$$

where x_i = net Ni prompt gamma ray counts at a point

$\bar{x}$ = mean net Ni prompt gamma ray counts

n = number of measurements

The number of points (n) in the calculation varies with the thickness, since values are taken at 1 cm intervals.

APPENDIX VII

SUPPORTING FRAME FOR THE CLINICAL APPARATUS

The most frequently employed structural material is steel. Avoiding specific types of steel, such as stainless steel (contains up to 20% Chromium which produces prompt gamma rays up to 9.72 MeV), then except for minor impurities the only major component is iron (Fe).

The table below lists the energies (E) along with the intensities (I) of the prompt gamma rays and the sensitivites on a mass basis, for both iron (Fe) and aluminium (Al).

Element	σ (b)	Atomic Mass A	E (MeV)	I (gamma rays/100 neutron captures)	Sensitivity (Iσ/A)
Fe	2.62	55.847	9.298	3.85	0.181
			7.646	22.14	1.04
			7.632	27.19	1.27
			7.279	4.60	0.216
			6.018	8.08	0.379
			5.921	8.29	0.389
			+ others		
Al	0.235	26.9815	7.72	20.1	0.175
			7.694	4.17	0.0363
			6.316	1.47	0.0128
			+ others		0.0156

It is clear from the table that Fe produces many more gamma rays above 6 MeV than does Al during thermal neutron capture. This fact coupled with the higher maximum energy of emission (9.298 MeV) of Fe increases the probability of pile-up in the nitroge region (9.75 MeV to 11.5 MeV) above that of Al. Aluminium is therefore a much more suitable structural material for the clinical apparatus as regards minimisation of the nitrogen background.

APPENDIX VIII

TISSUE EQUIVALENT SOLUTIONS

The following solutions have been designed to contain the major body elements in their approximate percentages by weight as they appear in Reference Man. Only phosphorous has been omitted because of its incompatibility with calcium salts when in solution.

a) Nitrogen-Free Tissue Equivalent Solutions

Substance	Molecular Weight	Density (g cm^{-3})	Volume (cm^3)	Weight (g)	O 16.0	C 12.01	H 1.008	N 14.01	Ca 40.08	K 39.1	Na 22.99	Cl 35.45
Water H_2O	18.02	1	37229	37229	33055		4174					
Potassium Chloride KCl	74.55	1.984	101	200						105		95
Potassium Acetate KCH_3COO	98.14	1.8	48	87	28	21	3			35		
Sodium Acetate $NaCH_3COO$	82.04	1.528	234	357	139	104	13				100	
Glycerol $CH_2OHCHOHCH_2OH$	92.09	1.26	22006	27727	14452	10848	2428					
Calcium Acetate $Ca(CH_3COO)_2\ H_2O$	176.18	2.16	2037	4400	1998	1200	201		1001			
TOTAL			61655	70,000	49673	12173	6819		1001	140	100	95
% by weight					71	17.4	9.74		1.43	0.20	0.143	0.136
Reference Man (% by weight)					61.4	23	10	2.57	1.43	0.20	0.143	0.136

b) Tissue Equivalent Solution

Substance	Molecular Weight	Density (g cm^{-3})	Volume (cm^3)	Weight (g)	O 16.0	C 12.01	H 1.008	N 14.01	Ca 40.08	K 39.1	Na 22.99	Cl 35.45
Water H_2O	18.02	1	34997	34997	31074		3923					
Potassium Chloride KCl	74.55	1.984	101	201						105		95
Potassium Acetate KCH_3COO	98.14	1.8	48	87	28	21	3			35		
Sodium Acetate $NaCH_3COO$	82.04	1.528	234	357	139	104	13				101	
Glycerol $CH_2OHCHOHCH_2OH$	92.09	1.26	20703	26086	13597	10206	2284					
Calcium Acetate $Ca(CH_3COO)_2\ H_2O$	176.18	2.16	2043	4412	2003	1203	202		1004			
Urea NH_2CONH_2	60.06	1.335	2891	3859	1027	771	259	1801				
TOTAL			61017	70000	47869	12307	6684	1801	1004	140	101	95
% by weight					68.4	17.6	9.55	2.57	1.43	0.20	0.143	0.136
Reference Man (% by weight)					**61.4**	**23**	**10**	**2.57**	**1.43**	**0.20**	**0.143**	**0.136**

APPENDIX IX

THE EFFECT OF DEVIATIONS FROM REFERENCE MAN NITROGEN:HYDROGEN MASS RATIO ON THE CALIBRATION FACTOR, q

The calibration factor "q" relates the nitrogen:hydrogen mass ratio to the counts ratio by the relationship:-

$$\frac{M_N}{M_H} = \frac{N_c}{H_c} \; q\,(w,t,M_N/M_H) \qquad - (1)$$

where "q" is shown to be a function of width (w), thickness (t) and the nitrogen:hydrogen mass ratio (M_N/M_H).

The net nitrogen counts, N_c, arise entirely from the subject. However, a proportion (H_a) of the net hydrogen counts (H_c) arise from activation of hydrogen in the apparatus shielding materials, whilst the remainder (H_s) arises from the subject. The contribution H_a, from the apparatus cannot be measured as a function of subject size since hydrogen free phantoms cannot be constructed. Therefore, this contribution can only be corrected for indirectly by choice of a q-value corresponding to a given width and thickness. It is because this contribution to H_c cannot be directly determined that q might be expected to vary for different nitrogen:hydrogen mass ratios in the subject.

For a given subject size the q-value could vary with the hydrogen mass since H_s will be a changing proportion of H_c. In human subjects the hydrogen mass will vary with the degree of hydration and adiposity. Ignoring obese subjects then an indication of the change in the hydrogen mass can be derived by observation of the range of

hydration coefficients in disease states. Moore et. al. (74) reported the extremes of hydration coefficients to be 67% in dehydration and 85% in overhydration, i.e. -8.2% to +16.4% of Reference Man's 73%.

The effect of changes in the hydrogen mass on the q-value will depend on the magnitude of the contribution H_a to H_c. This will be greatest for small subjects. The worst case is taken to be a subject 20 cm wide by 10 cm thick. H_a was measured at 5% of H_s by irradiation wihout a phantom. This would be smaller in the presence of a subject, because of the shielding effect, and therefore represents the worst case.

Therefore $$H_a = 0.05H_s$$

and $$\frac{M_N}{M_H} = \frac{N_c}{1.05H_s}.q \qquad - (2)$$

for reference man nitrogen:hydrogen mass ratio.

Case 1 : Dehydration

Assume $$M_{H-d} = 0.8M_H$$

i.e. the hydrogen mass in the dehydrated subject (M_{H-d}) is 80% of that in a normal subject (M_H)

Therefore substituting into equation (1) yields:-

$$\frac{M_N}{0.8M_H} = \frac{N_c}{0.85H_s} \cdot q_d$$

Such that $$q_d = 1.0119q$$

i.e. an increase in q of just over 1% in extreme dehydration.

Case 2 : Overhydration

Assume $M_{H-o} = 1.2M_H$

i.e. the hydrogen mass in the overhydrated subject (M_{H-o}) is 120% that in a normal subject.

Substitution into equation (1) and comparison with equation (2) yields:-

$$q_o = 0.9921q$$

i.e. a decrease in q of less than 1% in extreme overhydration.

In practice subjects will be larger than the worst case assumed in these examples and the effect on q of changes in the nitrogen:hydrogen mass ratio reduced further.

BIBLIOGRAPHY

BIBLIOGRAPHY

1 Allen, H., Krzywicki, H.J., Roberts, J.E.. Density, Fat, Water and Solids in Freshly Isolated Tissue. J. Appl. Physiol., 14(6) : 1005-1008 , 1959.

2 Almond, D.J., King, R.F.G.J., Burkinshaw, L., Oxby, C.B., McMahon, M.J.. Measurement of Short Term Changes in the Fat Content of the Body : A Comparison of Three Methods in Patients Receiving Intravenous Nutrition. Br. J. Nutr., 52 : 215-225, 1984.

3 Anderson, E.C.. Three-Component Body Composition Analysis Based on Potassium and Water Determinations. Ann. N.Y. Acad. Sci., 110 : 189-212, 1963.

4 Beddoe, A.H, Zuidmeer, H., Hill, G.L.. A Prompt Gamma In-Vivo Neutron Activation Analysis Facility for Measurement of Total Body Nitrogen in the Critically Ill. Phys. Med. Biol., 29(4) : 371-383, 1984.

5 Beddoe, A.H., Streat, S.J., Hill, G.L.. Evaluation of an In-Vivo Prompt Gamma Neutron Activation Facility for Body Composition Studies in Critically Ill Intensive Care Patients : Results on 41 Normals. Metabolism, 33(3) : 270-280, 1984.

6 Beddoe, A.H., Streat, S.J., Hill, G.L.. A Quantitative Assessment of Protein Depletion and Increased Hydration in

Severely Ill Surgical Patients Using Prompt Gamma In-Vivo Neutron Activation Analysis. Australasian Physiol. & Eng. Sci. Med., 7(1) : 13-18, 1984.

7 Beddoe, A.H., Streat, S.J., Hill, G.L.. Hydration of Fat-Free Body in Protein Depleted Patients. Am. J. Physiol., 249 : E227-235, 1985.

8 Behnke, A.R.. Physiologic Studies Pertaining to Deep Sea Diving and Aviation, Especially in Relation to the Fat Content and Composition of the Body. Harvey Lect. Ser., 37 : 198, 1941-42.

9 Beisel, W.R.. Metabolic Balance Studies - Their Continuing Usefulness in Nutritional Research. Am. J. Clin. Nutr., 32 : 271-274, 1979.

10 Biggin, H.C., Chen, N.S., Ettinger, K.V., Fremlin, J.H., Morgan, W.D., Nowotny, R.. Determination of Nitrogen in Living Patients. Nature New. Biol., 236 : 187-188, 1972.

11 Bigler, R.E. & Woodard, H.Q.. Skeletal Distribution of Mineralized Bone Tissue in Humans. Health Physics, 31(3) : 213-218, 1976.

12 Birks, J.B.. The Theory and Practice of Scintillation Counting. International Series of Monographs on Electronics and Instrumentation, 27, 1964.

13 Boddy, K., King, P.C., Tothill, P., Strong, J.A.. Measurement of Total Body Potassium with a Shadow Shield Whole-Body Counter : Calibration and Errors. Phys. Med. Biol., 16(2) : 275-282, 1971.

14 Boddy, K., King, P.C., Hume, R., Weyers, E.. The Relation of Total Body Potassium to Height, Weight and Age in Normal Adults. J. Clin. Path., 25 : 512-517,1972.

15 Boddy, K., Holloway, I., Elliot, A.. A Simple Facility for Total Body In-Vivo Activation Analysis. Int. J. Appl. Radiat. Isotopes, 24 : 428-430, 1973.

16 Boddy, K., King, P.C., Womersley, J., Durnin, J.V.G.A.. Body Potassium and Fat Free Mass (Author's Reply). Clin. Sci., 44 : 621-625, 1973.

17 Boddy, K., Robertson, I., Mahaffy, M.E., Holloway, I.. A High Sensitivity Dual-Detector Shadow Shield Whole-Body Counter with an "Invariant" Response for Total Body In-Vivo Neutron Activation Analysis. Phys. Med. Biol., 20(2) : 296-304, 1975.

18 Brekhus, P.J., et al.. A Method for the Separation of Enamel, Dentin and Cementum. J. Dental Research, 15 : 23-29, 1935.

19 Brozek, J., Grande, F., Anderson, J.T., Keys, A.. Densitometric Analysis of Body Composition : Revision of Some Quantitative Assumptions. Ann. N.Y. Acad. Sci., 110 : 113-140, 1963.

20 Burkinshaw, L., Morgan, D.B., Silverton, N.P., Thomas, R.D.. Total Body Nitrogen and its Relation to Body Potassium and Fat-Free Mass in Healthy Subjects. Clin. Sci., 61 : 457-462, 1981.

21 Burkinshaw, L. & Morgan, D.B.. Mass and Composition of the Fat-Free Tissues of Patients with Weight-Loss. Clin. Sci., 68 : 455-462, 1985.

22 Cember. Introduction to Health Physics. Pergamon Press. 1983.

23 Chettle, D.R., Fletcher, J.G., Downey, S.P.M.J., Scott, M.C., James, H.M., Higgins, C.S.. Measurement of Nitrogen In-Vivo by Neutron Activation Analysis : Further Developments and Applications. J. Radioanal. Chem., 71(1-2) : 533-546, 1982.

24 Cohn, S.H. & Dombrowski, C.S.. Measurement of Total Body Calcium, Sodium, Chlorine, Nitrogen and Phosphorus in Man by In Vivo Neutron Activation Analysis. J. Nucl. Med., 12(7) : 499-505, 1971.

25 Cohn, S.H., Vaswani, A., Zanzi, I., Aloia, J.F., Roginsky, M.S., Ellis, K.J.. Changes in Body Chemical Composition with Age Measured by Total-Body Neutron Activation. Metabolism, 25 : 85-96, 1976.

26 Cohn, S.H., Sawitsky, A., Vartsky, D., Yasumura, S., Zanzi, I., Ellis, K.J.. Body Composition as Measured by In-Vivo Neutron Activation Analysis. The Second Ross Conference Sante Fe, New Mexico : 24-27, 1979.

27 Cohn, S.H., Vartsky, D., Yasumura, S., Sawitsky, A., Zanzi, I., Vaswani, A., Ellis, K.J.. Compartmental Body Composition Based on Total Body Nitrogen, Potassium and Calcium. Am. J. Physiol., 239 : E524-30, 1980.

28 Cohn, S.H., Sawitsky, A., Vartsky, D., Yasumura, S., Zanzi, I., Ellis, K.J.. In-Vivo Quantification of Body Nitrogen and Body Composition in Normal Subjects and in Cancer Patients for Cancer-Nutrition Studies. Nutrition and Cancer, 2(i) : 67-71, 1980.

29 Cohn, S.H., Gartenhaus, W., Sawitsky, A., Rai, K., Zanzi, I., Vaswani, A., Ellis, K.J., Yasumura, S., Cortes, E., Varsky, D.. Compartmental Body Composition of Cancer Patients by Measurement of Total Body Nitrogen, Potassium and Water. Metabolism, 30(3) : 222-229, 1981.

30 Cohn, S.H., Gartenhaus, W., Vartsky, D., Sawitsky, A., Zanzi, I., Vaswani, A., Yasumura, S., Cortes, E., Ellis, K.J.. Body Composition and Dietary Intake in Neoplastic Disease. Am. J. Clin. Nutr., 34 : 1997-2004, 1981.

31 Cohn, S.H., Ellis, K.J., Vartsky, D., Sawitsky, A., Gartenhaus, W., Yasumura, S., Vaswani, A.N.. Comparison of Methods of Estimating Body Fat in Normal Subjects and Cancer Patients. Am. J. Clin. Nutr., 34 : 2839-2847, 1981.

32 Cohn, S.H., Vaswani, A.N., Vartsky, D., Yasumura, S., Sawitsky, A., Gartenhaus, W., Ellis, K.J.. In Vivo Quantification of Body Nitrogen for Nutritional Assessment. Am. J. Clin. Nutr., 35 : 1186-1191, 1982.

33 Cohn, S.H., Brennan, B.L., Yasumura, S., Vartsky, D., Vaswani, A.N., Ellis, K.J.. Evaluation of Body Composition and Nitrogen Content of Renal Patients on Chronic Dialysis as Determined by Total Body Neutron Activation. Am. J. Clin. Nutr., 38 : 52-58, 1983.

34 Cohn, S.H., Vaswani, A.N., Yasumura, S., Yuen, K., Ellis, K.J.. Improved Models for Determination of Body Fat by In-Vivo Neutron Activation. Am. J. Clin. Nutr., 40 : 255-259, 1984.

35 Collins, J.P., Oxby, C.B., Hill, G.L.. Intravenous Amino Acids and Intravenous Hyperalimentation as Protein-Sparing Therapy After Major Surgery. Lancet, 788-791, 1978.

36 Culebras, J.M. & Moore, F.D.. Total Body Water and the Exchangeable Hydrogen. Theoretical Calculations of Nonaqueous Exchangeable Hydrogen in Man. Am. J. Physiol., 232(1) : R54-59, 1977.

37 Cunningham, J.J.. Review Article : New Approaches to the Noninvasive Assessment of Body Composition : Bioelectrical Impedance Analysis and Total Body Electrical Conductivity. Nutr. International, 3(1) : 6-10, 1987.

38 Diem, K. & Lentner, C.. Scientific Tables. Basle, Geigy, J.R., 1970.

38b Delwaide, P.A. & Crenier, E.J.. Body Potassium as Related to Lean Body Mass Measured by Total Water Determination and by Anthropometric Method. Human Biol., 45(3) : 509-526, 1973.

39 Duffey, D. & El-Kady, A.. Analytical Sensitivities and Energies of Thermal-Neutron-Capture Gamma Rays. Nucl. Instr. Meth., 80 : 149-171, 1970.

40 Durnin, J.V.G.A. & Womersley, J.. Body Fat Assessed from Total Body Density and its Estimation from Skinfold Thickness : Measurements on 481 Men and Women Aged from 16 to 72 Years. Br. J. Nutr., 32 : 77-97, 1974.

41 Elliot, A., Holloway, I., Boddy, K., Haywood, J.K., Williams, E.D.. Neutron Uniformity Studies Related to Clinical Total Body In-Vivo Neutron Activation Analysis. Phys. Med. Biol., 23(2) : 269-281, 1978.

42 Ellis, K.J., Yasumura, S., Vartsky, D., Vaswani, A.N., Cohn, S.H.. Total Body Nitrogen in Health and Disease : Effects of Age, Weight, Height and Sex. J. Lab. Clin. Med., 99(6) : 917-926, 1982.

43 Forbes, R.M., Cooper, A.R., Mitchell, H.H.. The Composition of the Adult Human Body as Determined by Chemical Analysis. J. Biol. Chem. 203 : 359-366, 1953.

44 Forbes, R.M., Mitchell, H.H., Cooper, A.R.. Further Studies on the Gross Composition and Mineral Elements of the Adult Human Body. J. Biol. Chem., 223 : 969-975, 1956.

45 Garrow, J.S.. New Approaches to Body Composition. Am. J. Clin. Nutr., 35 : 1152-1158, 1982.

46 Hackett, A.F., Yeung, C.K., Hill, G.L.. Eating Patterns in Patients Recovering From Major Surgery - A Study of Voluntary Food Intake and Energy Balance. Br. J. Surg., 66 : 415-418, 1979.

47 Harrison, J.E., McNeill, K.G., Strauss, A.L.. A Nitrogen Index - Total Body Protein Normalised for Body Size - For Diagnosis of Protein Status in Health and Disease. Nutr. Res., 4 : 209-224, 1984.

48 Haurowitz, F.. Chemistry and Biology of Proteins. N.Y. Academic Press, 1950.

49 Haywood, J.K., Williams, E.D., McArdle, F.J., Boddy, K.. Reliability of Absolute and Relative Measurement of Total Body Nitrogen by the $^{14}N(n,2n)^{13}N$ Reaction. Phys. Med. Biol., 26(4) : 591-602, 1981.

50 Heide, B., Pierratos, A., Khanna, R., Pettit, J., Ogilvie, R., Harrison, J.E., McNeill, K., Siccion, Z., Oreopoulos, D.. Nutritional Status of Patients Undergoing Continuous Ambulatory Peritoneal Dialysis (CAPD). Peritoneal Dial. Bull., 3 : 138-141, 1983.

51 Hill, G.L., McCarthy, I.D., Collins, J.P., Smith, A.H.. A New Method for the Rapid Measurement of Body Composition in Critically Ill Surgical Patients. Br. J. Surg., 65 : 732-735, 1978.

52 Hill, G.L., Bradley, J.A., Collins, J.P., McCarthy, I., Oxby, C.B., Burkinshaw, L.. Fat-Free Body Mass from Skinfold Thickness : A Close Relationship with Total Body Nitrogen. Br. J. Nutr., 39 : 403-405, 1978.

53 Hill, G.L.,King, R.F.G.J., Smith, R.C., Smith, A.H., Oxby, C.B., Sharafi, A., Burkinshaw, L.. Multi-Element Analysis of the Living Body by Neutron Activation Analysis - Application to Critically Ill Patients Receiving Intravenous Nutrition. Br. J. Surg., 66 : 868-872, 1979.

54 Hill, G.L., Bradley, J.A., Smith, R.C., Smith, A.H., McCarthy, I.D., Oxby, C.B., Burkinshaw, L., Morgan, D.B.. Changes in Body Weight and Body Protein with Intravenous Nutrition. J. Parenter. Enter. Nutr., 3(4) : 215-218, 1979.

55 ICRP. Reference Man : Anatomical Physiological and Metabolic Characteristics. Publication number 23 (Oxford : Pergamon), 1974.

56 James, H.M., Dabek, J.T., Chettle, D.R., Dykes, P.W., Fremlin, J.H., Hardwicke, J., Thomas, B.J., Vartsky, D.. Whole Body Cellular and Collagen Nitrogen in Healthy and Wasted Man. Clin. Sci., 67 : 73-82, 1984.

57 Jeejeebhoy, K.N., Baker, J.P., Woolman, S.L., Wesson, D.E., Langer, B., Harrison, J.E., McNeill, K.G.. Critical Evaluation of the Role of Clinical Assessment and Body Composition Studies in Patients with Malnutrition and After Total Parenteral Nutrition., Am. J. Clin. Nutr., 35 : 1117-1127, 1982.

58 Kennedy, A.C., Boddy, K., Williams, E.D., Elliot, A.T., Harvey, I., Holloway, I.,Haywood, J.K.. Whole Body Elemental Composition During Drug Treatment of Rheumatoid Arthritis : A Preliminary Study. Am. Rheumatic Diseases, 38 : 137-140, 1979.

59 Kennedy, N.S.J., Eastell, R., Ferrington, C.M., Simpson, J.D., Smith, M.A., Strong, J.A., Tothill, P.. Total Body Neutron Activation Analysis of Calcium : Calibration and Normalisation.

Phys. Med. Biol., 27(5) : 697-707, 1982.

60 Keys, A. & Brozek, J.. Body Fat in Adult Man. Physiol. Rev., 33 : 245-325, 1953.

61 Knight, G.S., Beddoe, A.H., Streat, S.J., Hill, G.L.. Body Composition of Two Human Cadavers by Neutron Activation and Chemical Analysis. Am. J. Physiol., 13 : E179-185, 1986.

62 Kyere, K., Oldroyd, B., Oxby, C.B., Burkinshaw, L., Ellis, R.E., Hill, G.L.. The Feasibility of Measuring Total Body Carbon by Counting Neutron Inelastic Scatter Gamma Rays. Phys. Med. Biol., 27(6) : 805-817, 1982.

63 Leach, M.O., Thomas, B.J., Vartsky, D.. Total Body Nitrogen Measured by the $^{14}N(n,2n)^{13}N$ Method : A Study of the Interfering Reactions and the Variation of Spatial Sensitivity with Depth. Int. J. Appl. Radiat. Isot., 28 : 263-269, 1977.

64 Lederer, C.M.. Table of Isotopes - 7th. Edition. Wiley. 1978.

65 Loeppky, J.A., Myhre, L.G., Venters, M.D., Luft, U.C.. Total Body Water and Lean Body mass Estimated by Ethanol Dilution. J. Appl. Physiol., 42(6) : 803-808, 1977.

66 Lukaski, H.C., Mendez, J., Buskirk, E.R., Cohn, S.H.. A Comparison of Methods of Assessment of Body Composition including Neutron Activation Analysis of Total Body Nitrogen.

Metabolism, 30 : 777-782, 1981.

67 MacFie, J., Smith, R.C., Hill, G.L.. Glucose or Fat as a Non-Protein Energy Source? Gastroenterology, 80 : 103-107, 1981.

68 MacFie, J., Yule, A.G., Hill, G.L.. Effect of Added Insulin on Body Composition of Gastroenterological Patients Receiving Intravenous Nutrition - A Controlled Clinical Trial. Gastroenterology, 81 : 285-289, 1981.

69 McCarthy, I.D., Sharafi, A., Oxby, C.B., Burkinshaw, L.. The Accuracy of Total Body Nitrogen Determined by Neutron Activation Analysis. Phys. Med. Biol., 25(5) : 849-863, 1980.

70 McNeill, K.G., Mernagh, J.R., Jeejeebhoy, K.N., Harrison, J.E.. In-Vivo Determination of Nitrogen in Wasting Disease. Reprint from "Nuclear Activation Techniques in the Life Sciences 1978". IAEA-SM-227/50, Vienna : 799-807, 1979.

71 McNeill, K.G., Harrison, J.E., Mernagh, J.R., Stewart, S., Jeejeebhoy, K.N.. Changes in Body Protein, Body Potassium, and Lean Body Mass During Total Parenteral Nutrition. J. Parent. Ent. Nutr., 6(2) : 106-108, 1982.

72 Mernagh, J.R., Harrison, J.E., McNeill, K.G.. In-Vivo Determination of Nitrogen Using Pu-Be Sources. Phys. Med. Biol., 22 : 831-835, 1977.

73 Mernagh, J.R., McNeill, K.G., Harrison, J.E., Jeejeebhoy, K.N.. Effect of Total Parenteral Nutrition in the Restitution of Body Nitrogen, Potassium and Weight. Nutr. Res., 1 : 149-157, 1981.

74 Moore, F.D., Olesen, K.H., McMurrey, J.D., Parker, H.V., Ball, M.R., Boyden, C.M.. The Body Cell Mass and its Supporting Environment : Body Composition in Health and Disease. Saunders, Philadelphia, 1963.

75 Moore, F.D. & Boyden, C.M.. Body Cell Mass and Limits of Hydration of the Fat-Free Body : Their Relation to Estimated Skeletal Weight. Ann. N.Y. Acad. Sci., 110 : 62-71, 1963.

76 Morgan, W.D., Vartsky, D., Ellis, K.J., Cohn, S.H.. A Comparison of ^{252}Cf and ^{238}Pu-Be Neutron Sources for Partial-Body In Vivo Activation Analysis. Phys. Med. Biol. 26(3) : 413-424, 1981.

77 Nelp, W.B., Denney, J.D., Murano, R.. Absolute Measurement of Total Body Calcium (Bone Mass) in Vivo. J. Lab. Clin. Med., 79 : 430-438, 1972.

78 Oxby, C.B., Appleby, D.B., Brooks, K., Burkinshaw, L., Krupowicz, D.W., McCarthy, I.D., Oldroyd, B., Ellis, R.E.. A Technique for Measuring Total Body Nitrogen in Clinical Investigations using the $^{14}N(n,2n)^{13}N$ Reaction. Int J. Appl. Radiat. Isotopes, 29 : 205-211, 1978.

79 Pace, H. & Rathbun, E.N.. Studies on Body Composition III. The Body Water and Chemically Combined Nitrogen Content in Relation to Fat Content. J. Biol. Chem., 158 : 685-691 , 1945.

80 Palmer, H.E., Nelp, W.B., Murano, R., Rich, C.. The Feasibility of In-Vivo Neutron Activation Analysis of Total Body Calcium and Other Elements of Body Composition. Phys. Med. Biol., 13(2) : 269-279, 1968.

81 Pauw, H.. Energy Spectra of Radioactive Neutron Sources. Ph.D. Thesis. University of Amsterdam, 1970.

82 Senftle, F.E., Moore, H.D., Leep, D.B., El-Kady, A., Duffey, D.. Analytical Sensitivities and Energies of Thermal Neutron Capture Gamma Rays II. Nucl. Instr. Meth., 93: 425-459, 1971.

83 Shike, M., Russel, D., Detsky, A.S., Harrison, J.E., McNeill, K.G., Shepherd, F.A., Field, R., Evans, W.K., Jeejeebhoy, K.N.. Changes in Body Composition in Patients with Small-Cell Lung Cancer : The Effect of Total Parenteral Nutrition as an Adjunct to Chemotherapy. Ann. Internal Med., 101 : 303-309, 1984.

84 Siri, W.E.. Body Composition from Fluid Spaces and Density : Analysis of Methods. University of California Radiation Laboratory Publication Number 3349, 1956.

85 Smith, M.A.. The Development and Clinical Application of Part Body Neutron Activation Analysis Using Californium-252. Ph.D. Thesis. University of Edinburgh, 1978.

86 Smith, R.C., Burkinshaw, L., Hill, G.L.. Optimal Energy and Nitrogen Intake for Gastroenterological Patients Requiring Intravenous Nutrition. Gastroenterology, 82 : 445-452, 1982.

87 Spinks, T.J.. Measurement of Body Nitrogen by Activation Analysis. Int. J. Appl. Radiat. Isot., 29 : 409-410, 1977.

88 Spinks, T.J., Goode, A.W., Ranicar, A.S.O., Steere, E.. Measurement of Total Body Nitrogen and Oxygen by Irradiation with Cyclotron Produced Neutrons and "Delayed" Gamma Ray Counting. Phys. Med. Biol., 29(4) : 385-394, 1984.

89 Streat, S.J., Beddoe, A.H., Hill, G.L.. Measurement of Body Fat and Hydration of the Fat-Free Body in Health and Disease. Metabolism, 34(6) : 509-518, 1985.

90 Streat, S.J., Beddoe, A.H., Hill, G.L.. Measurement of Total Body Water in Intensive Care Patients with Fluid Overload. Metabolism, 34(7) : 688-694, 1985.

91 Thorn EMI Electron Tubes, Photodetection Information Service. Voltage Divider Design. R/P 069.

92 Vartsky, D., Thomas, B.J., Prestwich, W.V.. Comparison of the Spatial Uniformity and Sensitivity of Neutron Activation Techniques for Whole Body Nitrogen Measurement. Kerntechnic, 18 : 304-307, 1976.

93 Vartsky, D.. Ph.D. Thesis. University of Birmingham, 1976.

94 Vartsky, D., Thomas, B.J., Prestwich, W.V.. Fractional Charge Collection Technique For Pile-Up Reduction - Counting Low Intensity Radiation In Presence Of Intense Gamma-Ray and Neutron Background. Nucl. Instr. Meth., 145 : 321-329, 1977.

95 Vartsky, D., Ellis, K.J., Cohn, S.H.. In Vivo Measurement of Body Nitrogen by Analysis of Prompt Gammas from Neutron Capture. J. Nucl. Med., 20(11) : 1158-1165, 1979.

96 Vartsky, D., Prestwich, W.V., Thomas, B.J., Dabek, J.T., Chettle, D.R., Fremlin, J.H., Stammers, K.. The Use of Body Hydrogen as an Internal Standard in the Measurement of Nitrogen In-Vivo by Prompt Neutron Capture Gamma-Ray Analysis. J. Radioanal. Chem., 48 : 243-252, 1979.

97 Vartsky, D., Ellis, K.J., Vaswani, A.N., Yasumura, S., Cohn, S.H.. An Improved Calibration for the In-Vivo Determination of Body Nitrogen, Hydrogen and Fat. Phys. Med. Biol., 29(3) : 209-218, 1984.

98 Widdowson, E.H., McCance, R.A., Spray, C.M.. The Chemical Composition of the Human Body. Clin. Sci., 10 : 113-129, 1951.

99 Williams, E.D., Boddy, K., Harvey, I., Haywood, J.K.. Calibration and Evaluation of a System for Total Body In Vivo Activation Analysis using 14MeV Neutrons. Phys. Med. Biol., 23(3) : 405-415, 1978.

100 Williams, E.D., Boddy, K., Brown, J.J., Cumming, A.M.M., Davies, D.L., Harvey, R., Haywood, J.K., Lever, A.F., Robertson, J.I.S.. Whole Body Elemental Composition in Patients with Essential Hypertension. Eur. J. Clin. Invest., 12 : 321-325, 1982.

101 Williams, P., Kay, R., Harrison, J.E., McNeill, K., Pettit, J., Kelman, B., Mendez, M., Klein, M., Ogilvie, R., Khonna, R., Carmichael, D., Oreopoulos, D.. Nutritional and Anthropometric Assessment of Patients on CAPD Over One Year : Contrasting Changes in Total Body Nitrogen and Potassium. Peritoneal Dial. Bull., 1 : 82-87, 1981.

102 Womersley, J., Boddy, K., King, P.C., Durnin, J.V.G.A.. A Comparison of the Fat Free Mass of Young Adults Estimated by Anthropometry, Body Density and Total Body Potassium Content. Cli. Sci., 43 : 469-475, 1972.

103 Woodard, H.Q.. Elementary Composition of Human Cortical Bone. Health Physics, 8 : 513-517, 1962.

104 Yeung, C.K. et al.. Comparison of Tissue Composition of Weight Changes Occuring in Patients Fed with an Elemental Diet and in Patients Fed Intravenously. Br. J. Surg., 65 : 816, 1978.

105 Yeung, C.K., Smith, R.C., Hill, G.L.. Effect of an Elemental Diet on Body Composition. Gastroenterology, 77 : 652-657, 1979.

106 Young, G.A., et al.. Effects of Intravenous Hyperalimentation or Amino Acid Infusion on Plasma Proteins After Major Surgery - A Controlled Clinical Trial. Br. J. Surg., 65 : 817, 1978.

107 Young, G.A., Hill, G.L.. A Controlled Study of Protein-Sparing Therapy After Excision of the Rectum. Ann. Surg., 192 : 183-191, 1980.

108 Young, G.A., Yule, A.G., Hill, G.L.. Effects of an Anabolic Steroid on Plasma Amino Acids, Proteins and Body Composition in Patients Receiving Intravenous Hyperalimentation. J. Parenter. Enter. Nutr., 7(3) : 221-225, 1983.

109 Yule, A.G., MacFie, J., Hill, G.L.. The Effect of an Anabolic Steroid on Body Composition in Patients Receiving Intravenous Nutrition. Aust. N. Z. J. Surg., 51(3) : 280-284, 1981.